UNITED STATES AIR FORCE

GRADUATE STUDENT RESEARCH PROGRAM

1989

PROGRAM TECHNICAL REPORT

UNIVERSAL ENERGY SYSTEMS, INC.

VOLUME 1 OF 3

PROGRAM DIRECTOR, U.E.S.

RODNEY C. DARRAH

PROGRAM ADMINISTRATOR, U.E.S.

SUSAN K. ESPY

PROGRAM MANAGER, A.F.O.S.R.

LT. COL. CLAUDE CAVENDER

SUBMITTED TO

AIR FORCE OFFICE OF SCIENTIFIC RESEARCH

BOLLING AIR FORCE BASE

WASHINGTON, DC

DECEMBER 1989

219

DISCLAIMER NOTICE

THIS DOCUMENT IS BEST QUALITY AVAILABLE. THE COPY FURNISHED TO DTIC CONTAINED A SIGNIFICANT NUMBER OF PAGES WHICH DO NOT REPRODUCE LEGIBLY.

UNITED STATES AIR FORCE
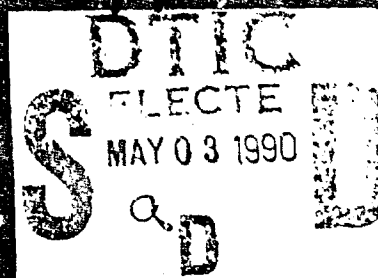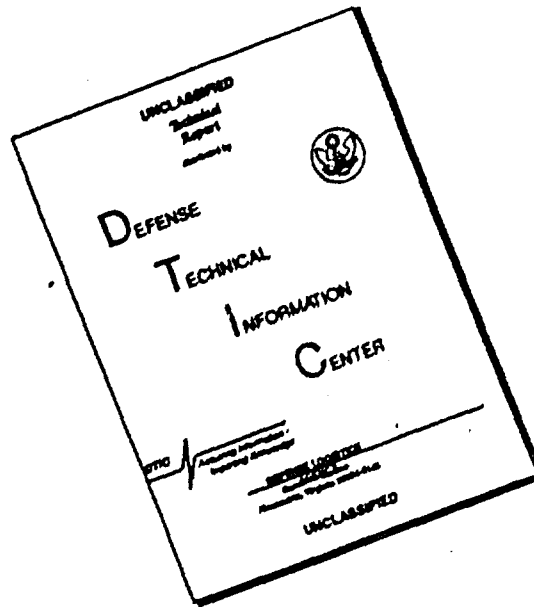
GRADUATE STUDENT RESEARCH PROGRAM

1989

PROGRAM TECHNICAL REPORT

UNIVERSAL ENERGY SYSTEMS, INC.

VOLUME I of III

Program Director, UES
Rodney C. Darrah

Program Manager, AFOSR
Lt. Col. Claude Cavender

Program Administrator, UES
Susan K. Espy

Submitted to

Air Force Office of Scientific Research

Bolling Air Force Base

Washington, DC

December 1989

TABLE OF CONTENTS

REPORT DOCUMENTATION PAGE

PORT SECURITY CLASSIFICATION	1b. RESTRICTIVE MARKINGS
UNCLASSIFIED	

CURITY CLASSIFICATION AUTHORITY	3. DISTRIBUTION/AVAILABILITY OF REPORT
CLASSIFICATION/DOWNGRADING SCHEDULE	APPROVED FOR PUBLIC RELEASE; Distribution Unlimited

FORMING ORGANIZATION REPORT NUMBER(S)	5 MONITORING ORGANIZATION REPORT NUMBER(S)
	AFOSR-TR-90-0372

ME OF PERFORMING ORGANIZATION	6b. OFFICE SYMBOL (If applicable)	7a. NAME OF MONITORING ORGANIZATION
versal Energy Systems Inc.		AFOSR/XOT

DDRESS (City, State and ZIP Code)	7b. ADDRESS (City, State and ZIP Code)
01 Dayton-Xenia Road yton, OH 45432	Building 410 Bolling AFB, DC 20332-6448

ME OF FUNDING/SPONSORING RGANIZATION	8b. OFFICE SYMBOL (If applicable)	9. PROCUREMENT INSTRUMENT IDENTIFICATION NUMBER
Same as #7		F49620-85-C-0013

DDRESS (City, State and ZIP Code)	10. SOURCE OF FUNDING NOS.			
	PROGRAM ELEMENT NO.	PROJECT NO.	TASK NO.	WORK UNIT NO.
Same as 7b	61102F	3396	D5	1

TLE (Include Security Classification)
AF Graduate Student Summer Support Program - Program Management Report- Vol A of B 3

ERSONAL AUTHOR(S)

dney C. Darrah, Susan K. Espy

TYPE OF REPORT	13b. TIME COVERED		14. DATE OF REPORT (Yr., Mo., Day)	15. PAGE COUNT
Annual	FROM _____	TO _____	Dec 89	

UPPLEMENTARY NOTATION

COSATI CODES			18. SUBJECT TERMS (Continue on reverse if necessary and identify by block number)
LD	GROUP	SUB. GR.	

BSTRACT (Continue on reverse if necessary and identify by block number)

See Attached

ISTRIBUTION/AVAILABILITY OF ABSTRACT	21. ABSTRACT SECURITY CLASSIFICATION
LASSIFIED/UNLIMITED ☒ SAME AS RPT. ☐ DTIC USERS ☐	IMC:ASSOFOED

NAME OF RESPONSIBLE INDIVIDUAL	22b. TELEPHONE NUMBER (Include Area Code)	22c. OFFICE SYMBOL
Lt Col Claude Cavender	202-767-4970	XOT

FORM 1473. 83 APR   EDITION OF 1 JAN 73 IS OBSOLETE.

PREFACE

The United States Air Force Graduate Student Resarch Program (USAF-GSRP) is conducted under the United Air Force Summer Faculty Research Program. The program provides funds for selected graduate students to work at an appropriate Air Force facility with a supervising professor who holds a concurrent Summer Faculty Research Program appointment or with a supervising Air Force Engineer/Scientist. This is accomplished by the students being selected on a nationally advertised competitive basis for a ten-week assignment during the summer intersession period to perfrom research at Air Force laboratories/centers. Each assignment is in a subject area and at an Air Force facility mutually agreed upon by the students and the Air Force. In addition to compensation, travel and cost of living allowances are also paid. The USAF-GSRP is sponsored by the Air Force Office of Scientific Research, Air Force Systems Command, United States Air Force, and is conducted by Universal Energy Systems, Inc.

The specific objectives of the 1989 USAF-GSRP are:

(1) To provide a productive means for the graduate students to participate in research at Air Force Laboratories/Centers;

(2) To stimulate continuing professional association among the graduate students and their professional peers in the Air Force;

(3) To further the research objectives of the United States Air Force;

(4) To enhance the research productivity and capabilities of the graduate students especially as these relate to Air Force technical interests.

During the summer of 1989, 102-graduate students participated. These researchers were assigned to 23 USAF laboratories/centers across the country. This three volume document is a compilation of the final reports written by the assigned students members about their summer research efforts.

i

PREFACE

The United States Air Force Graduate Student Research Program (USAF-GSRP) is conducted under the United Air Force Summer Faculty Research Program. The program provides funds for selected graduate students to work at an appropriate Air Force facility with a supervising professor who holds a concurrent Summer Faculty Research Program appointment or with a supervising Air Force Engineer/Scientist. This is accomplished by the students being selected on a nationally advertised competitive basis for a ten-week assignment during the summer intersession period to perfrom research at Air Force laboratories/centers. Each assignment is in a subject area and at an Air Force facility mutually agreed upon by the students and the Air Force. In addition to compensation, travel and cost of living allowances are also paid. The USAF-GSRP is sponsored by the Air Force Office of Scientific Research, Air Force Systems Command, United States Air Force, and is conducted by Universal Energy Systems, Inc.

The specific objectives of the 1989 USAF-GSRP are:

(1)   To provide a productive means for the graduate students to participate in research at Air Force Laboratories/Centers;

(2)   To stimulate continuing professional association among the graduate students and their professional peers in the Air Force;

(3)   To further the research objectives of the United States Air Force;

(4)   To enhance the research productivity and capabilities of the graduate students especially as these relate to Air Force technical interests.

During the summer of 1989, 102-graduate students participated. These researchers were assigned to 23 USAF laboratories/centers across the country. This three volume document is a compilation of the final reports written by the assigned students members about their summer research efforts.

i

LIST OF 1989 PARTICIPANTS

NAME/ADDRESS   **DEGREE, SPECIALTY, LABORATORY ASSIGNED**

Ben Abbott
Vanderbilt Univ.
Electrical Eng. Dept.
Nashville, TN 37240
(615) 322-6588

Degree: BS
Specialty: Computer Science
Assigned: Arnold Engineering Development Center

Sudarkodi Alagarsamy
Trinity University
715 Stadium
San Antonio, TX 78284
(512) 736-7011

Degree: BS
Specialty: Biochemistry
Assigned: School of Aerospace Medicine

Julie Albertson
Washington State Univ.
Sloan 201
Pullman, WA 99164
(509) 335-8654

Degree: MS
Specialty: Mechanical Eng.
Assigned: Frank J. Seiler Research Lab.

David Alden
Cincinnati, Univ. of
408A Rhodes Hall
Cincinnati, OH 45221
(513) 556-3701

Degree: MS
Specialty: Metal. Engineering
Assigned: Materials Laboratory

Darren Allen
Middle Tennessee State Univ.
Dept. of Mathematics
Murfreesboro, TN 37132
(615) 898-2669

Degree: MS
Specialty: Mathematics
Assigned: Arnold Engineering Development Center

Mojdeh Anderson
Cornell University
Phillips Hall
Ithaca, NY 14853
(607) 255-1445

Degree: BS
Specialty: Physics
Assigned: Frank J. Seiler Research Lab.

David Andreshak
Illinois, Univ. of
101 Transportation Bldg.
Urbana, IL 61801
(217) 333-2651

Degree: BS
Specialty: Aerospace Engineering
Assigned: Weapons Laboratory

Fred Arnold
Michigan, University of
Rackman Graduate School
Ann Arbor, MI   48109
(318) 764-4437

Degree: BS
Specialty: Physics
Assigned: Aero Propulsion Laboratory

John Baker
Kentucky, Univ. of
3200 Lochness Dr.
Lexington, KY   40503
(606) 439-1296

Degree: BS
Specialty: Mechanical Eng.
Assigned: Flight Dynamics Laboratory

John Bambery
Indiana Univ. at Penn.
Rm. 25 Weyanot Hall
Indiana, PA   15705
(412) 357-2611

Degree: BS
Specialty: Physics
Assigned: Avionics Laboratory

Rosemary Barbaro
Dayton, Univ. of
300 College Park Drive
Dayton, OH   45432
(513) 254-4444

Degree: BS
Specialty: Biology
Assigned: Harry G. Armstrong Aerospace
            Medical Research Laboratory

Brian Bennett
Middle Tennessee State Univ.
Computer Sci. Dept.
Murphreesboro, TN   37132
(615) 898-2397

Degree: BS
Specialty: Electrical Eng.
Assigned: Arnold Engineering Development
            Center

Robert Bolton
Texas A&M Univ.
EDG Area
College Station, TX   77843
(409) 845-0588

Degree: MS
Specialty: Civil Eng.
Assigned: Weapons Laboratory

Darwin Boyd
Kent State Univ.
Smith Laboratory of Physics
Kent, OH   44242
(216/) 672-2880

Degree: MS
Specialty: Physics
Assigned: Materials Laboratory

Marcia Boyle
New Hampshire, Univ. of
PO Box LL
Durham, NH   03824
(603) 868-3107

Degree: BS
Specialty: Mechanical Eng.
Assigned: Materials Laboratory

John Butemeyer
Texas A&M Univ.
Dept. of Psychology
College Station, TX 77843
(409) 845-0483

Degree: MS
Specialty: Psychology
Assigned: Human Resources Laboratory:
Manpower & Personnel Division

Eric Byrne
Kansas State Univ.
1225 Claflin Rd. #6
Manhattan, KS 66502
(913) 537-8647

Degree: MS
Specialty: Computer Sci.
Assigned: Avionics Laboratory

Paul Calvo
Scranton, Univ. of
Biology Dept.
Loyola Hall
Scranton, PA 18510
(717) 961-6117

Degree: BS
Specialty: Biology
Assigned: School of Aerospace Medicine

Keith Carroll
Oregon Instit. of Tech.
3201 Campus Dr.
Klamath Falls, OR 97601
(503) 882-6321

Degree: BS
Specialty: Electronical Eng.
Assigned: Electronic Systems Division

Kerry Christopher
West Florida, Univ. of
11000 University Parkway
Pensacola, FL 32514
(904) 474-2150

Degree: BS
Specialty: Physical Science
Assigned: Flight Dynamics Laboratory

J. Clemens
Wright State Univ.
Chemistry Dept.
Dayton, OH 45431
(513) 873-2855

Degree: BS
Specialty: Chemistry
Assigned: Harry G. Armstrong Aerospace
Medical Research Laboratory

Scott Coffin
Oklahoma, Univ. of
5530 Willowcliff
Oklahoma City, OK 73122
(405) 325-4721

Degree: BS
Specialty: Physics
Assigned: Rome Air Development Center

Bradley Combs
Wichita State Univ.
1845 Fairmont
Wichita, KS 67208
(316) 689-3120

Degree: BS
Specialty: Biochemistry
Assigned: Frank J. Seiler Research Lab.

Michael Costarella
Wright State Univ.
Dept. of Computer Sci.
Dayton, OH 45435
(513) 879-2491

Degree:	BS
Specialty:	Computer Science
Assigned:	Avionics Laboratory

Duane Daddis
Buffalo, Univ. of
PO Box 554
Buffalo, NY 14209
(716) 884-1993

Degree:	BS
Specialty:	Mechanical Engineering
Assigned:	Aero Propulsion Laboratory

Brian Davis
Meharry Medical College
1005 D.B. Todd Blvd.
Nashville, TN 37212
(615) 297-2763

Degree:	BS
Specialty:	Biology
Assigned:	School of Aerospace Medicine

Vincent Dimiceli
Texas A&M Univ.
407 A Tauber St.
College Station, TX 77840
(409) 846-5874

Degree:	MS
Specialty:	Applied Mathematics
Assigned:	Harry G. Armstrong Aerospace Medical Research Laboratory

Judy Dye
Alabama, Univ. of
Box 870350
Tuscaloosa, AL 35487
(205) 348-1970

Degree:	MS
Specialty:	Applied Mathematics
Assigned:	Arnold Engineering Development Center

Nancy Faulkner
Central State Univ.
110 Jenkins Tech. Bldg.
Wilberforce, OH 45384
(513) 376-6435

Degree:	BS
Specialty:	Manufacturing Eng.
Assigned:	Flight Dynamics Laboratory

Dagmar Fertl
Texas A&M Univ.
Wildlife & Fisheries Sci.
College Station, TX 77843
(409) 845-1261

Degree:	BS
Specialty:	Biology
Assigned:	School of Aerospace Medicine

Michael Findler
Arizona State Univ.
Dept. of Computer Sci.
Tempe, AZ 85287
(602) 965-3190

Degree:	MS
Specialty:	Computer Science
Assigned:	Avionics Laboratory

Patrick Fitzpatrick Texas A&M Univ. Heaton Hall College Station, TX 77843 (409) 845-1003	Degree: Specialty: Assigned:	BS Meteorology Geophysics Laboratory
Lawrence Fleischer Texas A&M University 347 Zachry Eng. Center College Station, TX 77843 (409) 845-5531	Degree: Specialty: Assigned:	MS Industrial Engineering Harry G. Armstrong Aerospace Medical Research Laboratory
Bryan Foos Ohio State Univ. 2070 Neil Ave. Columbus, OH 43201 (614) 292-2771	Degree: Specialty: Assigned:	BS Civil Engineering Flight Dynamics Laboratory
Robert Gabruk Virginia Poly. Instit. 400 A Houston St. Blacksburg, VA 24061 (703) 552-3434	Degree: Specialty: Assigned:	BS Mechanical Engineering Aero Propulsion Laboratory
Ellen Goldey Miami Univ. Dept. of Zoology Oxford, OH 45056 (513) 529-3184	Degree: Specialty: Assigned:	MS Zoology Harry G. Armstrong Aerospace Medical Research Laboratory
Charles Gray Wright State Univ. Dept. of Chemistry Dayton, OH 45435 (513) 873-2855	Degree: Specialty: Assigned:	BS Chemistry Materials Laboratory
Stuart Harbert Texas A&M Univ. 2500 A Tabor Rd. Bryan, TX 77803 (409) 845-1251	Degree: Specialty: Assigned:	MS Mechanical Engineering Weapons Laboratory
David Harper Bowling Green State Univ. Dept. of Psychology Bowling Green, OH 43402 (419) 372-2301	Degree: Specialty: Assigned:	BS Psychology Harry G. Armstrong Aerospace Medical Research Laboratory

Bradley Herman	Degree:	BS
Tennessee Tech. Univ.	Specialty:	Electrical Engineering
201 West 13th Apt. 2	Assigned:	Electronic Systems Division
Cookeville, TN 38501		
(615) 528-5032		

Randall Hodgson	Degree:	BS
Alabama-Huntsville, Univ. of	Specialty:	Applied Physics
44\2-A Myrtlewood Cir.	Assigned:	Armament Laboratory
Huntsville, AL 35816		
(205) 895-6276		

Dean Hofmann	Degree:	BS
Dayton, Univ. of	Specialty:	Chemical Engineering
Dept. of Materials and	Assigned:	Materials Laboratory
Chemical Engineering		
Dayton, OH 45469		
(513) 229-2627		

Deborah Hollenbach	Degree:	MS
Ohio State Univ.	Specialty:	Biology
1803 Gerrard Ave.	Assigned:	Harry G. Armstrong Aerospace
Columbus, OH 43212		Medical Research Laboratory
(614) 481-0986		

Alice Horton	Degree:	BS
Northern Colorado, Univ. of	Specialty:	Mathematics
2725-20th St. #1	Assigned:	Human Resources Laboratory:
Greeley, CO 80631		Manpower & Personnel Division
(303) 351-8344		

Genevieve Huston	Degree:	BS
Ohio Univ.	Specialty:	Electrical Engineering
9 S. Congress St.	Assigned:	Flight Dynamics Laboratory
Athens, OH 45701		
(614) 594-7315		

Matthew Jacobson-Carroll	Degree:	BS
Boston College	Specialty:	Geology
Devlin Hall Rm. 209	Assigned:	Geophysics Laboratory
Chestnut Hill, MA 02167		
(617) 552-3640		

Neal Jahren	Degree:	BS
Minnesota-Duluth, Univ. of	Specialty:	Philosophy
371 Marshall W. Alworth Hall	Assigned:	Materials Laboratory
Duluth, MN 55812		
(212) 726-8568		

William Jefferson
South Carolina, Univ. of
Marine Science Program
Columbia, SC 29208
(803) 777-3943

Degree: BS
Specialty: Biology
Assigned: Occupational and Environmental
           Health Laboratory

Terrance Jorden
Meharry Medical College
944 21st Ave. N. #515
Nashville, TN 37208
(615) 321-5657

Degree: BS
Specialty: Biology
Assigned: Wilford Hall Medical Center

George Kim
Trinity Univ.
715 Stadium Dr.
San Antonio, TX 78284
(512) 736-7231

Degree: BS
Specialty: Biology
Assigned: School of Aerospace Medicine

Christopher Kocher
Southern Illinois Univ.
Carbondale, IL 62901
(618) 536-7525

Degree: BS
Specialty: Engineering
Assigned: Astronautics Laboratory

John Lafferty
Miami, Univ. of
Dept. of Chemistry
Coral Gables, FL
(305) 284-5842

Degree: BS
Specialty: Mathematics
Assigned: Wilford Hall Medical Center

David Lapioli
Penn State Univ.
51A Hammond Bldg.
University Park, PA 16802
(814) 865-0396

Degree: BS
Specialty: Aerospace Engineering
Assigned: Astronautics Laboratory

Teresa Lee
Western Illinois Univ.
Dept. of Sociology
Macomb, IL 61455
(309) 298-1056

Degree: BS
Specialty: Western Literature
Assigned: School of Aerospace Medicine

Patricia Liu
California, Univ. of
2404 Cedar St.
Berkeley, CA 94708
(415) 644-8394

Degree: BS
Specialty: Materials Engineering
Assigned: Astronautics Laboratory

Jon Longtin
Cincinnati, University of
Mechanical Eng. Dept.
Cincinnati, OH 45238
(513) 451-4136

Degree: BS
Specialty: Mechanical Engineering
Assigned: Aero Propulsion Laboratory

Lester Lynd
Vanderbilt Univ.
612 Watts Circle
Nashville, TN 37209
(615) 356-3632

Degree: BS
Specialty: Electrical Engineering
Assigned: Arnold Engineering Development
           Center

Diana Major
Southwestern Louisiana,
 University of
PO Box 70504
Lafayette, LA 70504
(318) 231-6702

Degree: MS
Specialty: Physics
Assigned: Avionics Laboratory

Randal Mandock
Georgia Instit. of Tech.
PO Box 37122
Atlanta, GA 30332
(404) 894-3503

Degree: MS
Specialty: Atmospheric Science
Assigned: Rome Air Development Center

Toby Martin
Illinois, Univ. of
1010 W. Illinois St.
 URH 126 TW
Urbana, IL 61801
(217) 332-4006

Degree: BS
Specialty: Aerospace Engineering
Assigned: Weapons Laboratory

Timothy Mavor
Worcester Poly. Instit.
100 Institute Rd.
Worcester, MA 01609
(508) 831-5730

Degree: BS
Specialty: Mathematics
Assigned: Rome Air Development Center

Walter McCarter
North Carolina State Univ.
2501 Kilgore Ave.
Raleigh, NC 27607
(919) 755-1541

Degree: MS
Specialty: Physics
Assigned: Weapons Laboratory

Stephen McClain
Cornell Univ.
Phillips Hall
Ithaca, NY 14853
(607) 255-1445

Degree:	MS
Specialty:	Physics
Assigned:	Frank J. Seiler Research Lab.

John McCord
Murray State Univ.
Dept. of Chemistry
Murray, KY 42071
(502) 762-4490

Degree:	BS
Specialty:	Chemical Engineering
Assigned:	Aero Propulsion Laboratory

Paula Mellon
New York University
Washington Square East
New York, NY 10003
(212) 998-4730

Degree:	PhD
Specialty:	Psychology
Assigned:	Wilford Hall Medical Center

Douglas Melton
Ohio State Univ.
205 Dreese Lab
Columbus, OH 43210
(614) 292-2906

Degree:	MS
Specialty:	Electrical Engineering
Assigned:	Avionics Laboratory

Cynthia Moorhead
Texas A&M Univ.
1907 Dartmouth #206
College Station, TX 77843
(409) 845-3381

Degree:	BS
Specialty:	Economics
Assigned:	School of Aerospace Medicine

Lisa Newberg
Eastern Washington Univ.
Mathematics Dept.
Cheney, WA 99004
(509) 458-6200

Degree:	BS
Specialty:	Mathematics
Assigned:	Occupational and Environmental Health Laboratory

William Newbold
Florida, Univ. of
231 Aerospace Bldg.
Gainesville, FL 32611
(904) 392-0961

Degree:	BS
Specialty:	Aerospace Engineering
Assigned:	Armament Laboratory

Randy Nguyen
San Jose State University
San Jose, CA 95117
(408) 244-9743

Degree:	BS
Specialty:	Mechanical Engineering
Assigned:	Astronautics Laboratory

Mary Nickels
New Mexico, Univ. of
Clark Hall
Albuquerque, NM 87131
(505) 277-6655

Degree: BS
Specialty: Chemistry
Assigned: Weapons Laboratory

William Patience
Ohio Univ.
21 1/2 S. Court St.
Athens, OH 45701
(614) 594-2468

Degree: BS
Specialty: Electrical Engineering
Assigned: Rome Air Development Center

Douglas Pederson
Oregon Instit. of Tech.
Electronics Dept.
Klamath Falls, OR 97601
(503) 882-6321

Degree: BS
Specialty: Electrical Engineering
Assigned: Electronic Systems Division

Hao Pham
California State Univ.
1250 Bellflower Blvd.
Long Beach, CA 90840
(213) 985-1524

Degree: BS
Specialty: Mechanical Engineering
Assigned: Frank J. Seiler Research Lab.

Betty Pipes
Middle Tennessee State Univ.
Computer Science Dept.
Murfreesboro, TN 37132
(615) 898-2397

Degree: BS
Specialty: Mathematics
Assigned: Arnold Engineering Development Center

Laura Pytel
Ohio University
428 Sargent Hall
Athens, OH 45701
(614) 597-5663

Degree: BS
Specialty: Mechanical Engineering
Assigned: Harry G. Armstrong Aerospace Medical Research Laboratory

George Ramlow
Oregon Instit. of Tech.
PO Box 2297
Klamath Falls, OR 97601
(503) 882-6524

Degree: BS
Specialty: Electrical Engineering
Assigned: Electronic Systems Division

Lionel Ramos
Texas-San Antonio, Univ. of
Div. of Engineering
San Antonio, TX
(512) 691-5518

Degree: BS
Specialty: Electrical Engineering
Assigned: School of Aerospace Medicine

Rex Ramsier	Degree:	BS
Akron, Univ. of	Specialty:	Physics
Dept. of Physics	Assigned:	Materials Laboratory
Akron, OH 44325		
(216) 375-6054		

Joseph Rea	Degree:	BS
Texas-San Antonio, Univ. of	Specialty:	Electrical Engineering
Dept. of Electrical Eng.	Assigned:	School of Aerospace Medicine
San Antonio, TX 78285		
(512) 691-4011		

Ernest Rho	Degree:	BS
Illinois Instit. of Tech.	Specialty:	Electrical Engineering
3300 S. Federal	Assigned:	Rome Air Development Center
Chicago, IL 60616		
(312) 567-3400		

James Sago	Degree:	BS
Missouri-Rolla, Univ. of	Specialty:	Metal. Engineering
B-19 McNutt Hall	Assigned:	Materials Laboratory
Rolla, MO 65401		
(314) 341-6461		

John Salinas	Degree:	MS
Meharry Medical College	Specialty:	Biochemistry
1005 D.B. Todd Blvd.	Assigned:	Wilford Hall Medical Center
Nashville, TN 37208		
(615) 327-6204		

David Sanborn	Degree:	MS
Lowell, Univ. of	Specialty:	Electrical Engineering
Box 2559N	Assigned:	Geophysics Laboratory
Lowell, MA 01854		
(508) 452-5000		

Sonja Schillmoeller	Degree:	BS
Illinois Univ. of	Specialty:	Aero. Engineering
Urbana, IL 61801	Assigned:	Astronautics Laboratory
(217) 328-6638		

Royce Simpson	Degree:	BS
Alabama, Univ. of	Specialty:	Psychology
Box 870348	Assigned:	Human Resources Laboratory:
Tuscaloosa, AL 35487		Operations Training Division
(205) 343-1934		

Janet Slifka
Dayton, Univ. of
300 College Park Ave.
Dayton, OH 45469
(513) 229-3611

Degree: MS
Specialty: Electrical Engineering
Assigned: Harry G. Armstrong Aerospace
           Medical Research Laboratory

Richard Souder
Vanderbilt Univ.
612 Watts Circle
Nashville, TN 37209
(615) 356-3632

Degree: BS
Specialty: Electrical Engineering
Assigned: Arnold Engineering Development
           Center

Richard Swift
Notre Dame, Univ. of
Dept. of Aero. and Mech. Eng.
Notre Dame, IN 46556
(219) 239-7666

Degree: BS
Specialty: Aeronautical Engineering
Assigned: Flight Dynamics Laboratory

Lynda Tomlinson
Syracuse Univ.
111 Link Hall
Syracuse, NY 13244
(315) 443-4415

Degree: MS
Specialty: Electrical Engineering
Assigned: Rome Air Development Center

George Tompkins
Kansas State Univ.
M-27 Jardine Terrace
Manhattan, KS 66502
(913) 776-5691

Degree: BS
Specialty: Industrial Engineering
Assigned: Materials Laboratory

Mona Toms
Wright State Univ.
Applied Behavior Sci.
Dayton, OH 45435
(513) 873-2310

Degree: BS
Specialty: Psychology
Assigned: Human Resources Laboratory:
           Logistics & Human Factors

Robert Tramel
Tennessee Space Instit.
Dept. of Mathematics
Tullahoma, TN 37388
(615) 455-0631

Degree: BS
Specialty: Physics
Assigned: Arnold Engineering Development
           Center

Scott VanDam
Central Florida, Univ. of
PO Box 2500
Orlando, FL 32816
(407) 275-2416

Degree: MS
Specialty: Electrical Engineering
Assigned: Aero Propulsion Laboratory

Ronald VanEtten
Illinois State Univ.
Normal, IL 61761
(309) 452-6529

Degree: BS
Specialty: Education
Assigned: Human Resources Laboratory:
Manpower & Personnel Division

John Wagnon
Oklahoma State Univ.
2001 N. Perkins #M135
Stillwater, OK 74075
(405) 743-3750

Degree: BS
Specialty: Electrical Engineering
Assigned: Rome Air Development Center

Glenn Waguespack
Louisana State Univ.
736 Dentation Dr.
Baton Rouge, LA 70808
(504) 766-1271

Degree: BS
Specialty: Mechanical Engineering
Assigned: Armament Laboratory

Matthew Westerheide
Missouri-Rolla, Univ. of
Thomas Jefferson Hall
  Room 729
Rolla, MO 63138
(314) 341-5740

Degree: BS
Specialty: Electrical Engineering
Assigned: Astronautics Laboratory

John Williamson
Texas A&M Univ.
Dept. of Psychology
College Station, TX 77843
(409) 845-2581

Degree: BS
Specialty: Psychology
Assigned: Human Resources Laboratory:
Training Systems

Raymond Wolfe
Scranton, Univ. of
423 Madison Ave.
Scranton, PA 18510
(717) 342-3402

Degree: BS
Specialty: Biology
Assigned: School of Aerospace Medicine

Jon Zern
Florida, Univ. of
Box J-125
Gainesville, FL 32610
(904) 392-2381

Degree: BS
Specialty: Biology
Assigned: Engineering Services Center

Joseph Ziegler
Florida, Univ. of
Dept. of Civil Eng.
Gainesville,FL 32611
(904) 392-3261

Degree: BS
Specialty: Civil Engineering
Assigned: Engineering Services Center

PARTICIPANT LABORATORY ASSIGNMENT

1989 USAF/UES GRADUATE STUDENT RESEARCH PROGRAM

AERO PROPULSION LABORATORY (WRDC/APL)
(Wright-Patterson Air Force Base)

1.	Fred Arnold	4.	Jon Longtin
2.	Duane Daddis	5.	John McCord
3.	Robert Gabruk	6.	Scott VanDam

ARMAMENT LABORATORY (ATL)
(Eglin Air Force Base)

1. Randall Hodgson
2. William Newbold
3. Glenn Waguespack

HARRY G. ARMSTRONG AEROSPACE MEDICAL RESEARCH LABORATORY (AAMRL)
(Wright-Patterson Air Force Base)

1.	Rosemary Barbaro	6.	David Harper
2.	J. Matthew Clemens	7.	Deborah Hollenbach
3.	Vincent Dimiceli	8.	Laura Pytel
4.	Lawrence Fleischer	9.	Janet Slifka
5.	Ellen Goldey		

ARNOLD ENGINEERING DEVELOPMENT CENTER (AEDC)
(Arnold Air Force Base)

1.	Ben Abbott	5.	Lester Lynd
2.	Darren Allen	6.	Betty Pipes
3.	Brian Bennett	7.	Richard Souder
4.	Judy Dye	8.	Robert Tramel

ASTRONAUTICS LABORATORY (AL)
(Edwards Air Force Base)

1.	Christopher Kocher	4.	Randy Nguyen
2.	David Lapioli	5.	Sonja Schillmoeller
3.	Patricia Liu	6.	Matthew Westerheide

AVIONICS LABORATORY (Avionics Laboratory)
(Wright-Patterson Air Force Base)

1.	John Bambery	4.	Michael Findler
2.	Eric Byrne	5.	Diana Major
3.	Michael Costarella	6.	Douglas Melton

ELECTRONIC SYSTEMS DIVISION (ESD)
(Hanscom Air Force Base)

1.	Keith Carroll	3.	Douglas Pederson
2.	Bradley Herman	4.	George Ramlow

ENGINEERING AND SERVICES CENTER (ESC)
(Tyndall Air Force Base)

1. Jon Zern
2. Joseph Ziegler

FLIGHT DYNAMICS LABORATORY (FDL)
(Wright-Patterson Air Force Base)
1. John Baker
2. Kerry Christopher
3. Nancy Faulkner
4. Bryan Foos
5. Genevieve Huston
6. Richard Swift

FRANK J. SEILER RESEARCH LABORATORY (Frank J. Seiler Research Lab.)
(USAF Academy)
1. Julie Albertson
2. Mojdeh Anderson
3. Bradley Combs
4. Stephen McClain
5. Hao Pham

GEOPHYSICS LABORATORY (Geophysics Laboratory)
(Hansom Air Force Base)
1. Patrick Fitzpatrick
2. Matthew Jacobson-Carroll
3. David Sanborn

HUMAN RESOURCES LABORATORY
(Brooks, Williams and Wright-Patterson Air Force Bases)
1. John Butemeyer
2. Alice Horton
3. Royce Simpson
6. Mona Toms
7. Ronald Van Etten
8. John Williamson

MATERIALS LABORATORY (ML)
(Wright-Patterson Air Force Base)
1. David Alden
2. Darwin Boyd
3. Marcia Boyle
4. Charles Gray
5. Dean Hofmann
6. Neal Jahren
7. Rex Ramsier
8. James Sago
9. George Tompkins

OCCUPATIONAL AND ENVIRONMENT HEALTH LABORATORY (OEHL)
(Brooks Air Force Base)
1. William Jefferson
2. Lisa Newberg

C. PARTICIPANT LABORATORY ASSIGNMENT (Page 3)

ROME AIR DEVELOPMENT CENTER (Rome Air Development Center)
  (Griffiss Air Force Base)
  1. Scott Coffin
  2. Randal Mandock
  3. Timothy Mavor
  4. William Patience
  5. Ernest Rho
  6. Lynda Tomlinson
  7. John Wagnon

SCHOOL OF AEROSPACE MEDICINE (School of Aerospace Medicine)
  (Brooks Air Force Base)
  1. Sudarkodi Alagarsamy
  2. Paul Calvo
  3. Brian Davis
  4. Dagmar Fertl
  5. George Kim
  6. Teresa Lee
  7. Cynthia Moorhead
  8. Lional Ramos
  9. Joseph Rea
  10. Raymond Wolfe

WEAPONS LABORATORY (Weapons Laboratory)
  (Kirtland Air Force Base)
  1. David Andreshak
  2. Robert Bolton
  3. Stuart Harbert
  4. Toby Martin
  5. Walter McCarter
  6. Mary Nickels

WILFORD HALL MEDICAL CENTER (Wilford Hall Medical Center)
  (Lackland Air Force Base)
  1. Terrance Jorden
  2. John Lafferty
  3. Paula Mellon
  4. John Salinas

RESEARCH REPORTS

RESEARCH REPORTS

1989 GRADUATE STUDENT RESEARCH PROGRAM

Technical Report Number	Title	Graduate Researcher

Volume I

Armament Laboratory

1	Laser Polarimeter Development	Randall Hodgson
2	Euler Solutions to Transonic Flow Past an Ogive-Cylinder Body with Wraparound Fins	William Newbold
3	Observations and Improvements of Ballistic Stress Analysis Techniques	Glenn Waguespack

Arnold Engineering Development Center

4	Distributed and Parallel Image and Signal Processing *** Same Report as Dr. Wilkes ***	Ben Abbott
5	Latin Hyper-Cube Sampling with Regression Analysis for Prediction of Engine Infrared Observables	Darren Allen
6	A General Purpose Two Dimensional Plotting Program	Brian Bennett
7	Matrix Inversions of Candidate Geometries for Application of CT Emission Techniques to Broad Band Radiative Transfer	Judy Dye
8	Distributed and Parallel Image and Signal Processing *** Same Report as Dr. Wilkes ***	Lester Lynd
9	A Survey of the Personal Computer Environment at Arnold Engineering Development Center	Betty Pipes
10	Distributed and Parallel Image and Signal Processing *** Same Report as Dr. Wilkes ***	Richard Souder
11	A Nonlinear Filter and an Odd/Even Iteration for Inviscid Fluid Flow Equations	Robert Tramel

Astronautics Laboratory

Electronic Systems Division

Engineering and Services Center

Frank J. Seiler Research Laboratory

Frank J. Seiler Research Laboratory (continued)

25	Second Harmonic Generation in Optical Fibers *** Same Report as Dr. Hillman **	Mojdeh Anderson
26	Transition State Analysis: Gluconolactone by MOPAC	Bradley Combs
27	Second Harmonic Generation in Optical Fibers *** Same Report as Dr. Hillman ***	Stephen McClain
28	Modeling of a Structure-Actuator System with Structure-Borne Reaction-Mass Actuators with Optimal Design of Passive Vibration Absorbers *** Same Report as Dr. Hung Vu ***	Hao Pham

Geophysics Laboratory

29	Adaptation of the Axisymmetric TASS Model for Hurricane Simulations	Pat Fitzpatrick
30	Estimating Characteristics of Chemical Explosions in New England and Eastern Kazakhstan Using Local and Regional Seismic Data *** Same Report as Dr. Alan Kafka ***	Matt Jacobson-Carroll
31	Final Summary of Research Effort *** 1988 Participant ***	Thomas Kimble
32	Comparative Analysis of Various Atmospheric Modelling Techniques	David Sanborn

Rome Air Development Center

33	Characterization of a Spatial Light Modulator for Optical Filtering	Scott Coffin
34	Adaptive Beamforming Software for the Digital Beam Steering Antenna	Randal Mandock
35	A Study of Interacting Tunneling Units with Possible Application to High Temperature Superconductors *** Same Report as Dr. Klein ***	Timothy Mavor
36	A Simplified Method of Determining Noise Parameters of High Frequency MESFET's	William Patience

Flight Dynamics Laboratory (continued)

62   Strain Distribution in Composite   Bryan Foos
                       Coupons in Tension
                       *** Same Report as Dr. W. Wolfe ***

63   Control System Design Modeling   Genevieve Huston

64   Accessing the Computer Automated   Richard Swift
                       Design Database (CADDB) Through
                       CADS- A Computer Aided Design System

Materials Laboratory

65   Dislocations in Rene' N4+ with Respect   David Alden
                       to Orientation and Temperature

66   An Approximate Analytical Solution   Darwin Boyd
                       of the Nonlinear Diffusion Equation
                       and a Preliminary Investigation of
                       Nonlinear Optics

67   Investigation of the Thermomechanical   Marcia Boyle
                       Response of a Titanium Aluminide Metal
                       Matrix Composite Using a Viscoplastic
                       Constitutive Theory
                       *** Same Report as Dr. James Sherwood ***

68   Synthesis of Model Benzothiazoles   Charles Gray

69   State of the Art Sensors for In-Situ   Dean Hofmann
                       Monitoring of Composite Cure

70   Data Reduction of Photoreflectance   Neal Jahren
                       from Capped Aluminum Gallium
                       Arsenide Structures

71   Scanning Tunneling Microscopy and   Rex Ramsier
                       and Ballistic-Electron-Emission
                       Spectroscopy

72   Evaluation of CR-SI Alloys for   James Sago
                       Aerospace Structural Applications
                       *** Same Report as Dr. Joseph Newkirk ***

73   An Intelligent Neural Model for   George Tompkins
                       Recognition of Input/Output Patterns
                       for a Molecular Beam Epitaxy Process

74   High Resolution Scanning Electron   Deborah Vezie
                       Microscopy of Pitch-Based Carbon
                       Fiber
                       (1988 Participant)

School of Aerospace Medicine (continued)

Wilford Hall Medical Center

1989 USAF-UES SUMMER FACULTY RESEARCH PROGRAM/
GRADUATE STUDENT RESEARCH PROGRAM

Sponsored by the
AIR FORCE OFFICE OF SCIENTIFIC RESEARCH
Conducted by the
Universal Energy Systems, Inc.
Final Report

Laser Polarimeter Development

Prepared by: Randall R. Hodgson
Academic Rank: Graduate Student
Department and   Department of Physics
 University: University of Alabama in Huntsville
Research Location: USAF AFATL/AGA
                      Eglin AFB, Florida 32542
USAF Researcher: Dennis Goldstein
Date: 17 Aug 1989
Contract No: F49620-88-0053

Laser Polarimeter Development

by

Randall R. Hodgson

Abstract

Steps were taken to reduce measurement and data processing errors asso-
ciated with the laser polarimeter developed last year. An automatic
alignment procedure was coded into the lab computer as well as error
checking and compensation code. The measurement-taking programs were
altered to allow averaging the intensities over 2 or 4 sets of 180
degrees. Beam wander error with a period of 360 degrees was reduced by
the averaging process. Changes were made in the equipment configuration
which resulted in reduced mechanical vibration of the optical system.
Documentation for each of the software modules is provided.

ACKNOWLEDGMENTS

I wish to acknowledge the Air Force Office of Scientific Research for sponsoring this program. Universal Energy Systems was effective in administering the summer effort in a helpful and efficient manner.

I enjoyed working under the supervision of Mr. Dennis Goldstein. He has provided opportunities for some fascinating research and has given sound direction and assistance. Danielle Walker must be given credit for her valuable work in running simulations, making measurements, and preparing drawings. Michael VanTassel, Howard McCormick, and Voncile Houston of the Special Projects Laboratory provided outstanding support in the optics laboratory. I would also like to thank the members of the AGA group for their friendship and help.

I. INTRODUCTION:

The infrared laser polarimeter at the Air Force Armament Laboratory
(AFATL) was assembled in the summer of 1988 by Mr. Dennis Goldstein and
Mr. David Chenault. This work was described in the report submitted in
August of 1988 by David Chenault and in Mr. Goldstein's dissertation
proposal.[1,2] These reports include the operating principles of the
laser polarimeter and the first measurements made with the instrument.

The laser polarimeter measures the optical polarizing properties of
materials at infrared wavelengths. This instrument directly supports
the development of optical systems in which polarization is important.
Any device which depends on optical interference, such as laser radar,
will suffer a loss in signal-to-noise ratio when the system polarization
is not well controlled. This is due to the fact that waves of orthogo-
nal polarization states do not form interference fringes. Therefore,
the sharpness of beat patterns will be reduced when the polarization
states of the interfering waves are not the same. Systems which depend
on modulating the polarization state of light with modulator crystals or
liquid crystal light valves constitute a second category of need for
polarization control in Air Force hardware.

Prior to this summer's work under Mr. Dennis Goldstein, I worked as a
graduate student researcher at the University of Alabama in Huntsville
(UAH). Under the direction of Dr. Russell Chipman, I investigated
instrumental polarization in the spectropolarimeter at UAH and co-
authored a report on the work submitted to the Armament Laboratory. In
a separate effort, I performed a Jones matrix polarization analysis of a
Doppler interferometer system. Before beginning graduate work at UAH, I
worked in an optical thin films laboratory and developed measurement and
computer modeling techniques for thin film coatings. These experiences
have helped me to more fully understand and perform laser polarimeter
research at AFATL.

II. OBJECTIVES:

The overall objective of this summer's laser polarimeter development is
to find ways to measure, and if possible, reduce the errors involved in
finding the polarizing properties of the sample under test. Under this
objective are two main sub-objectives -- 1) reducing errors due to the
physical configuration and 2) reducing errors introduced by the computer
analysis of the measured values.

a. A number of steps were planned to eliminate errors caused by instru-
mental errors. One objective was to validate and then implement a set
of equations which compensate for error in alignment of the components
and error in the retardance values. After testing the equations with
MathCad software, they were to be integrated into the computer system
used to measure Mueller matrices with the laser polarimeter.   Other
objectives were to automate the initial alignment of the polarizers,
reduce laser fluctuations, and increase the mechanical stability of the
optical system.

b. Computer code was to be written to check the accuracy of the Fourier
series coefficients.

III. ALIGNMENT CODES

To meet the objectives above, several software modules were created
and/or modified. Figure 1 contains a diagram which shows the relation-
ship among these programs. This section documents the software with
flowcharts and descriptions.

Two programs were written for alignment. The first program, entitled
ALIGNP, is used to align the two polarizers in the laser polarimeter
before the retarders are installed. The flow chart describing this
program is shown in Figure 2. Using the blackbody as the radiation
source, the wire grid polarizer is rotated while the prism polarizer
(with greater beam wander) stays fixed. The HP computer automatically

Laser Polarimeter Procedure

Alignment Codes
ALIGNP, RETALIGN

Sample Measurement

Rotate Retarders
Yields Intensity Values
vs. Angle

Computer finds Fourier
Series Coefficients
MMM180, MMM360,
MMM720

Re-create Intensity
Function
Enter Errors,
Error Compensation
INVERSION

Mueller Matrix
16 elements

Adjusted
Mueller Matrix

Figure 1 Laser Polarimeter Computer Codes
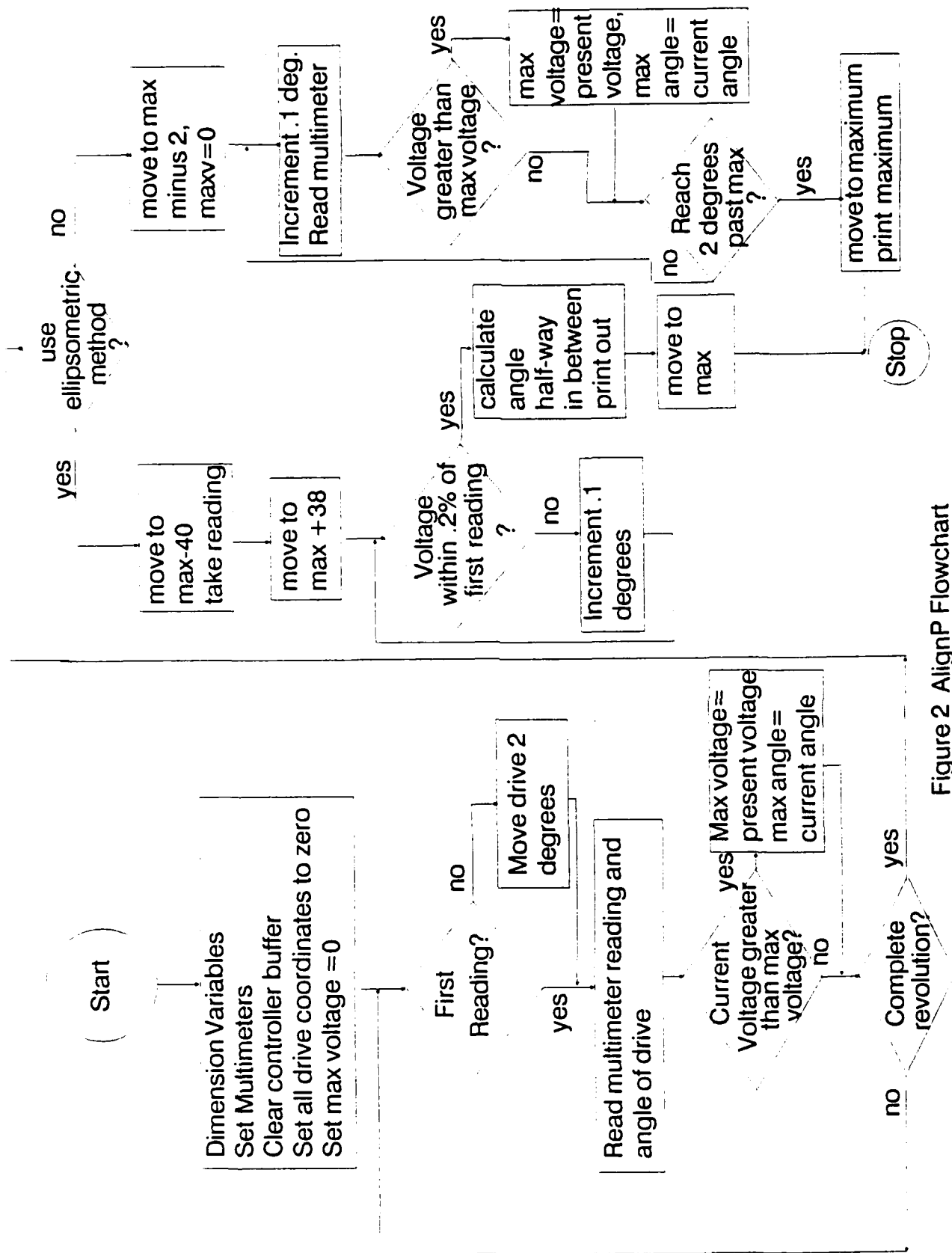
Figure 2 AlignP Flowchart

Start

Dimension Variables
Set Multimeters
Clear controller buffer
Set all drive coordinates to zero
Set max voltage = 0

First Reading? — no → Move drive 2 degrees
yes ↓

Read multimeter reading and angle of drive

Current Voltage greater than max voltage? — yes → Max voltage = present voltage, max angle = current angle
no ↓

Complete revolution? — no → / yes

use ellipsometric method?

no ↓

move to max minus 2, maxv=0

Increment .1 deg. Read multimeter

Voltage greater than max voltage? — yes → max voltage = present voltage, max angle = current angle
no ↓

Reach 2 degrees past max? — yes → move to maximum print maximum
no

yes (ellipsometric):
move to max-40 take reading

move to max +38

Voltage within .2% of first reading? — no → Increment .1 degrees
yes ↓

calculate angle half-way in between print out

move to max

Stop

records the intensity readings over one full revolution of the wire grid polarizer. During this rotation, the polarizers cause two intensity maxima to be read with the detector. Either one of these maxima are acceptable to use for alignment. The computer chooses one of the two maxima and then uses an ellipsometric technique to execute the alignment.

First, the polarizer is moved 40 degrees to one side of the maximum and records the multimeter output. It then moves 38 degrees to the other side of the maximum and begins making 0.1 degree steps. The multimeter voltage reading is compared with the reading made on the other side of the maximum. When this difference is less than a set percentage of the original reading, the voltage and angle are recorded. The alignment angle corresponding to the maxima is then taken to be the angle exactly half way in between the angles located on either side of the maximum. The reason for using this method to align with the intensity maximum is that the slope of the intensity curve is 0 or close to zero near the maximum, but the slope is much steeper 40 degrees before or after the maximum. This allows for a more accurate location of angles using the voltage readings.

Once the polarizers are aligned, the retarder fast axes are aligned one at a time with the polarizer transmission axes. The program which performs this task is named RETALIGN and is similar to the ALIGNP program described above. One revolution of a retarder between aligned polarizers yields four intensity maxima, two from the crystal slow axis and two from the fast axis. After the computer records the coarse locations of the maxima, the user must tell the computer which of the maxima is from the fast axis (there is no way for the computer to distinguish this). The computer then uses the same ellipsometric technique to align to the maximum as used in the polarizer alignment program.

IV. MUELLER MATRIX CODE WITH AVERAGING AND ERROR COMPENSATION

The Mueller matrix of the measured sample is obtained using the code
entitled MMM180 which is diagrammed in Figure 3. The computer rotates
the retarders, records intensity values of the two detectors, finds the
Fourier series coefficients for the series which describes this func-
tion, and finds the Mueller matrix using these coefficients in expres-
sions derived by Azzam and Hauge[3,4]. The code contains utilities for
printing and plotting all pertinent data, such as the intensity values
as a function of angle, the Fourier series coefficients, the Mueller
matrix, the laser stability measurements, and the measurement time and
date.

Figure 4 contains diagrams of changes made to MMM180 incorporated into
the program MMM360, which takes readings over 360 degrees. The first
change was made in the portion of the main program which reads in the
measured intensity values as the retarders are rotated. The second
change was made in the routine which plots the graph of the intensities.
The reason for measuring over two sets of 180 degrees is to compensate
for beam wander of the retarders. Beam wander can be caused by either a
slight wedge shape of an element or a slight misalignment of the optic
in its mount. In the current laser polarimeter configuration, the laser
is focused onto a small detector. Beam wander causes the beam to move
off the edges of the detector. This causes a roughly sinusoidal modu-
lation with a frequency of 1 period per retarder revolution. Averaging
the intensities over two sets of 180 degrees will compensate in part for
beam wander due to the first retarder. The second retarder rotates 5
times for each rotation of the first retarder. The averaging over two
sets of 180 degrees also helps compensate for beam wander of the second
retarder. A 180 degree rotation of the first retarder corresponds to
2.5 complete rotations of the second retarder. Thus, intensities in the
first 180 degrees are averaged with values 2.5 periods of the second
retarder away, averaging to zero in the case of a perfect sinusoid.

```
                        ┌─────────┐
                        │  Start  │
                        └────┬────┘
                             │
                             ▼
        ┌─────────────────────────────────┐
        │ Set dump device to printer      │
        │ Clear Soft Keys                 │
        │ Define Soft Keys                │
        └─────────────────────────────────┘
        Lb19             │
        ┌────────────────┴────────────────────┐
        │   Clear Screen                       │
        │ "Menu Available on Soft Keys"        │
        │ "Press Run to make measurements"     │
        └──────────────────────────────────────┘
        No Key depressed │
                         │  Key 3
        ┌────────────────┴─────────────┐
        │ Wait for Input by looping    │
        └──────────────────────────────┘
        Lb10             │
        ┌────────────────┴─────────────────────────┐
        │ Declare Variables                         │
        │ Initialize Variables                      │
        │ Enter angle increment                     │
        │ Print increment and number measurements   │
        └───────────────────────────────────────────┘
                         │          Sub Init
        ┌────────────────┴─────────────┐
        │ Clear Controller Buffer       │
        │ Take Control                  │
        │ Set Velocities of drives      │
        │ Print current coordinates     │
        │ Option to reset drives        │
        │ Set all coordinates to zero   │
        │ Initialize multimeters        │
        └───────────────────────────────┘
                         │
                         ▼
                    ╱─────────╲                ┌──────────────────────┐
                   ╱ Subtract  ╲     yes       │ Enter value or       │
                  ╱   min.      ╲──────────────│ return to use        │
                   ╲ intensity ?╱              │ measured value       │
                    ╲─────────╱                └──────────────────────┘
                         │ no
                         ▼
        ┌──────────────────────────────┐
        │ Record Start time            │
        └──────────────────────────────┘
```

Figure 3 MMM180 Flowchart page 1/4

Record PC detector - Stab 1, Stab(T)
Read Retarder angles - P1$
Read PV detector - L1, I(T)
Print readings
Move Retarders to next angle

no   Done?

yes

Record end time
Calculate Elapsed time
Reset second retarder coordinate to angle under 360
Send both drives home
Subtract minimum intensity reading from all intensity values

SUB REDDAT

Compute Fourier Series Coefficients
Print Fourier Series Coefficients
Calculate Mueller Matrix
Normalize matrix to largest element

Calculate Power Fluctuation

Lb15

Prints Angle Increment, Power Fluctuation,
Minimum intensity, Total time,
end time.
Prints Mueller matrix

Figure 3 MMM180 Flowchart page 2/4

Figure 3 MMM180 Flowchart page 3/4

Sub program "Filesub"

Key Select

Key 1	Key 2	Key 3	Key 4	Key 5	Key 6	Key 7	Key 8
Retrieve File	Save File	List Files	Purge File	CD Hard Disk	CD Floppy	not used	Return

Lb11 Enter Filename

Blank? — no / yes

Read in
Data points
Angle Increments
End time
Minimum Intensity
PV Intensity values
PC Intensity values

Lb12 Enter Filename

Blank? — no / yes

Create file

Save
Data points
Angle Increments
End time
Minimum Intensity
Intensity values PV
Intensity values PC

Lb13 Display Directory

Lb14 Enter Filename

Blank? — no / yes

Print Filename

are you sure? — no / yes

Purge file

Lb15 Change directories to Hard Disk /MMDATA/

Lb16 Change directories to Floppy Disk

Figure 3 MMM180 page 4/4

1-13

Count 1=0
Count 2=0

Read PC detector-Stab(T)
Read retarder angles
Read PV detector- Q(T)
Print Readings

First retarder angle >=180?

yes → Average intensities with this angle-180, Store in I(θ-180)

no

Store Intensity value in I(θ)

Second Retarder angle greater than 720 and count1 =0?

yes → Reset second retarder controller coordinate to θ-720, count 1=1

no

Second Retarder angle greater than 1440 and count2 =0?

yes → Reset second retarder coordinate to θ-1080, count 2=1

no

Repeat for # of datapoints

Done?

yes

Figure 4 Data Taking Loop of MMM360 Altered from MMM180

1-14

Figure 4   MMM360   Plot Graph Procedure (When Plot Graph Key is pressed)

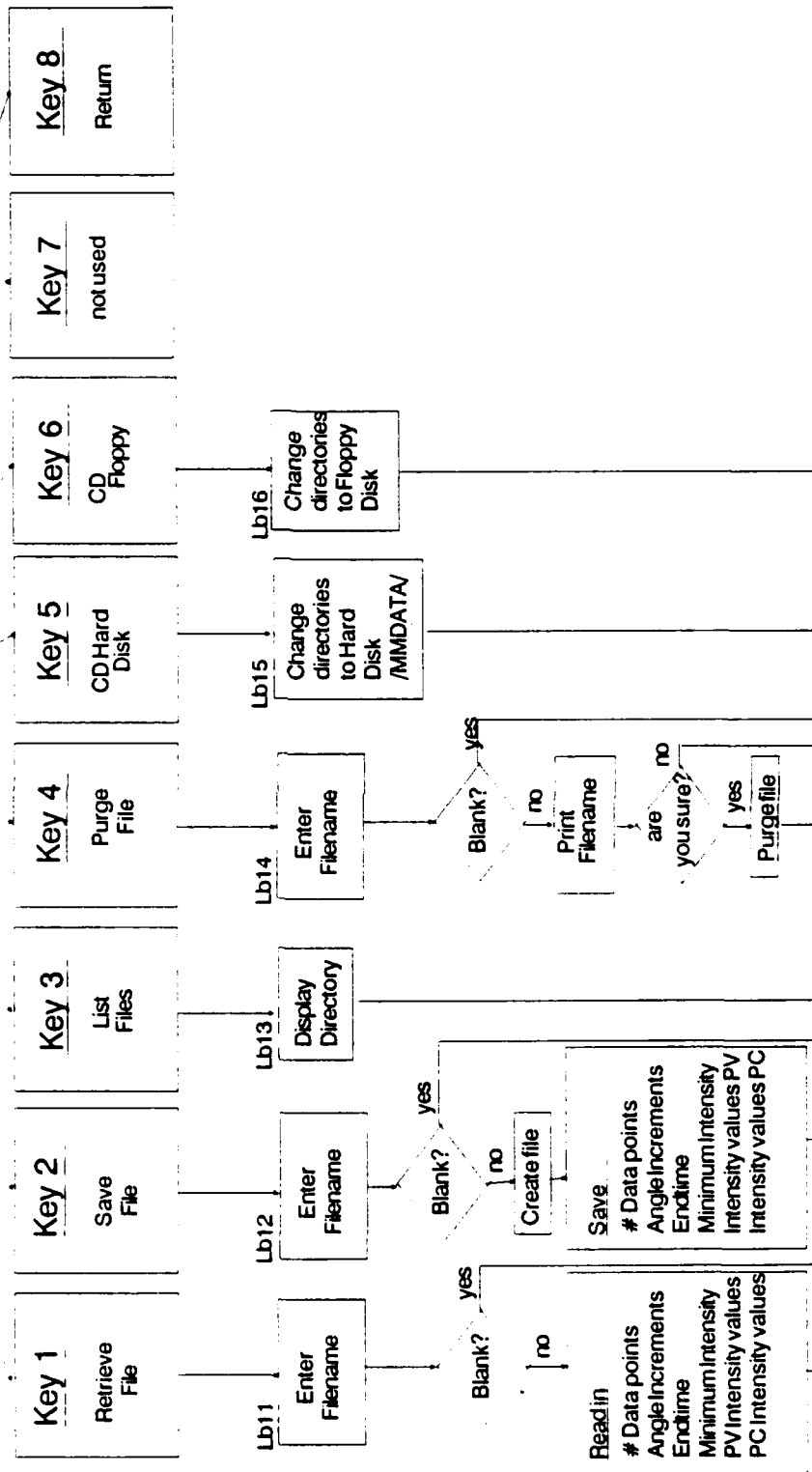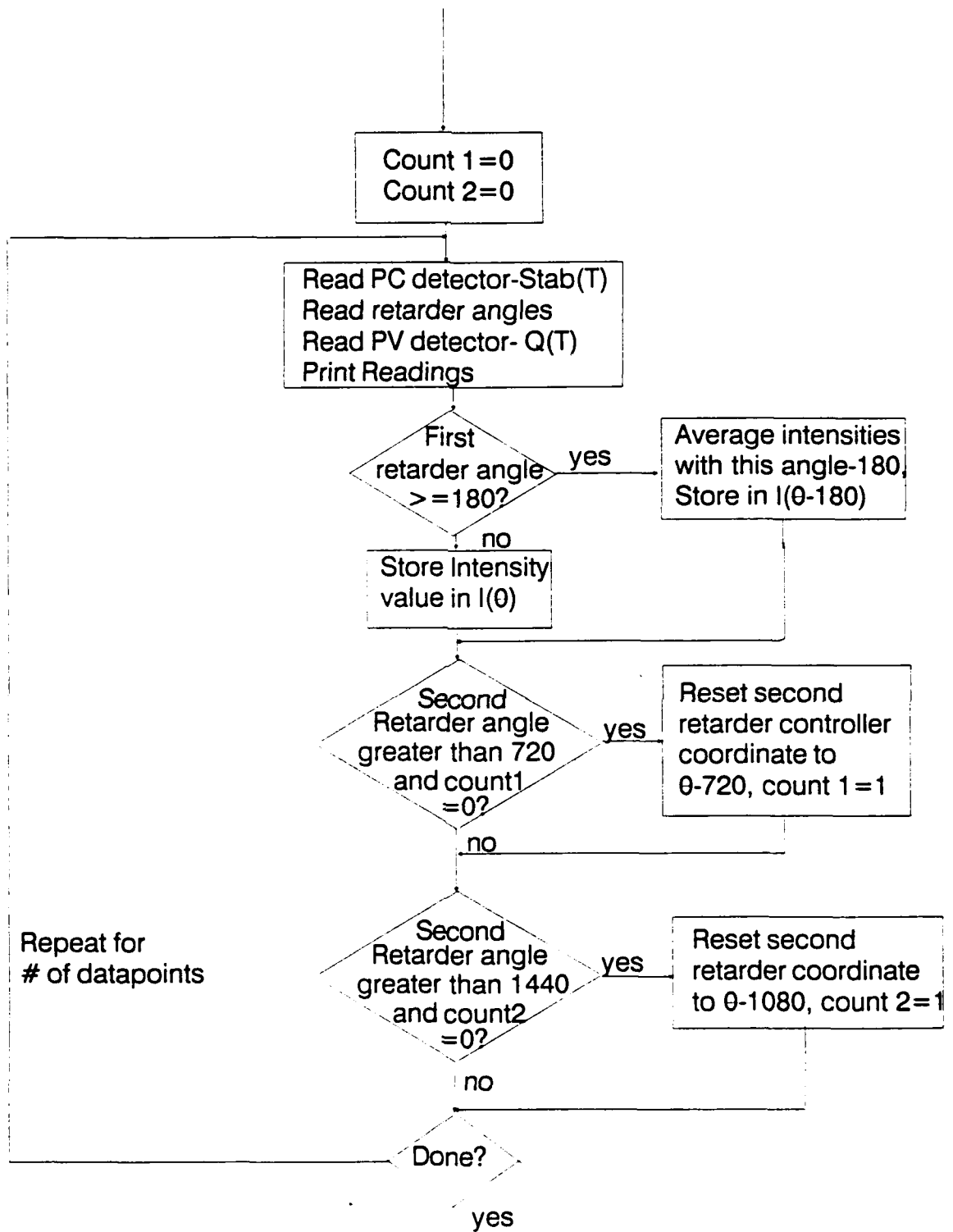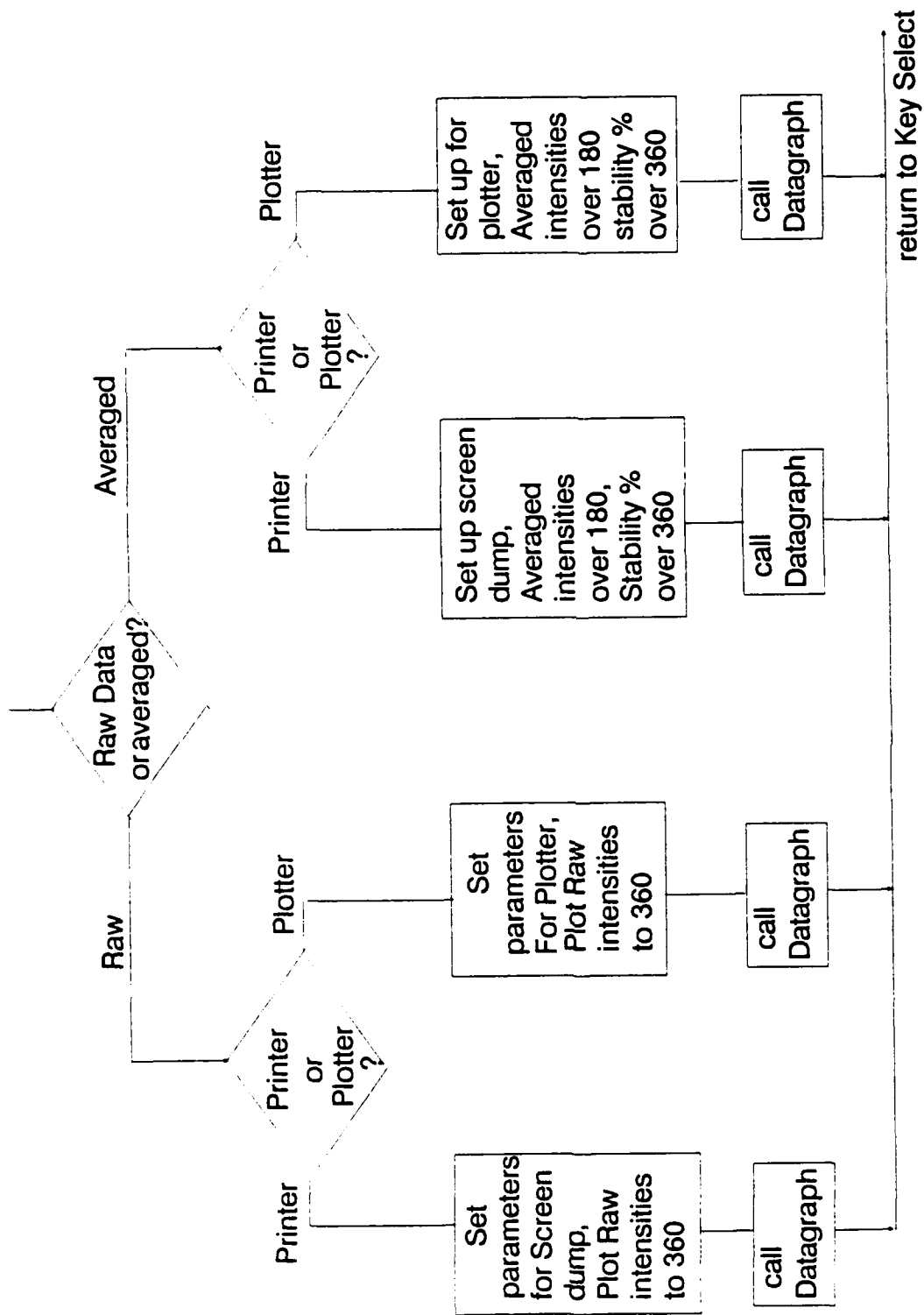Averaging four sets of 180 degrees is accomplished with MMM720, which is very similar to MMM360 except for a more streamlined algorithm for reseting the second retarder's drive coordinates. Another possible approach to reducing beam wander effects is to use an integrating sphere; this is discussed in the recommendations section.

A different type of error compensation is used in the INVERSION routine shown in Figure 5. Mr. Goldstein has derived a set of equations which compensate for alignment error of the polarizers and retarders as well as deviation of the retardance values from 90 degrees[2]. Before exiting any one of the MMM programs, the Fourier series coefficients can be saved as a file for use by the INVERSION program. Five error values are entered by the user. The first error value is the deviation of the retardance of the first retarder from quarter-wave at 10.6 microns wavelength. The second parameter is the deviation of the second retarder from quarter-wave. Using the first polarizer's orientation as the reference point, the third value is the angle between the first polarizer's transmission axis and the first retarder's fast axis (they should be parallel). The fourth value is the alignment error of the second retarder, and the fifth value is the alignmemt error of the last polarizer. INVERSION uses these values and the Fourier series coefficients to produce an adjusted Mueller matrix. This matrix is closer to the real characteristics of the sample when the real errors are known and employed in the program.

A short part of the INVERSION code takes the Fourier series coefficients and sums up the series to re-create the original intensity function measured by the polarimeter. This serves as a check to observe how accurately the Fourier series coefficients were computed by the MMM programs.

V. CONFIGURATION CHANGES

A few changes have been made to the laser polarimeter hardware which should result in reduction of measurement error:
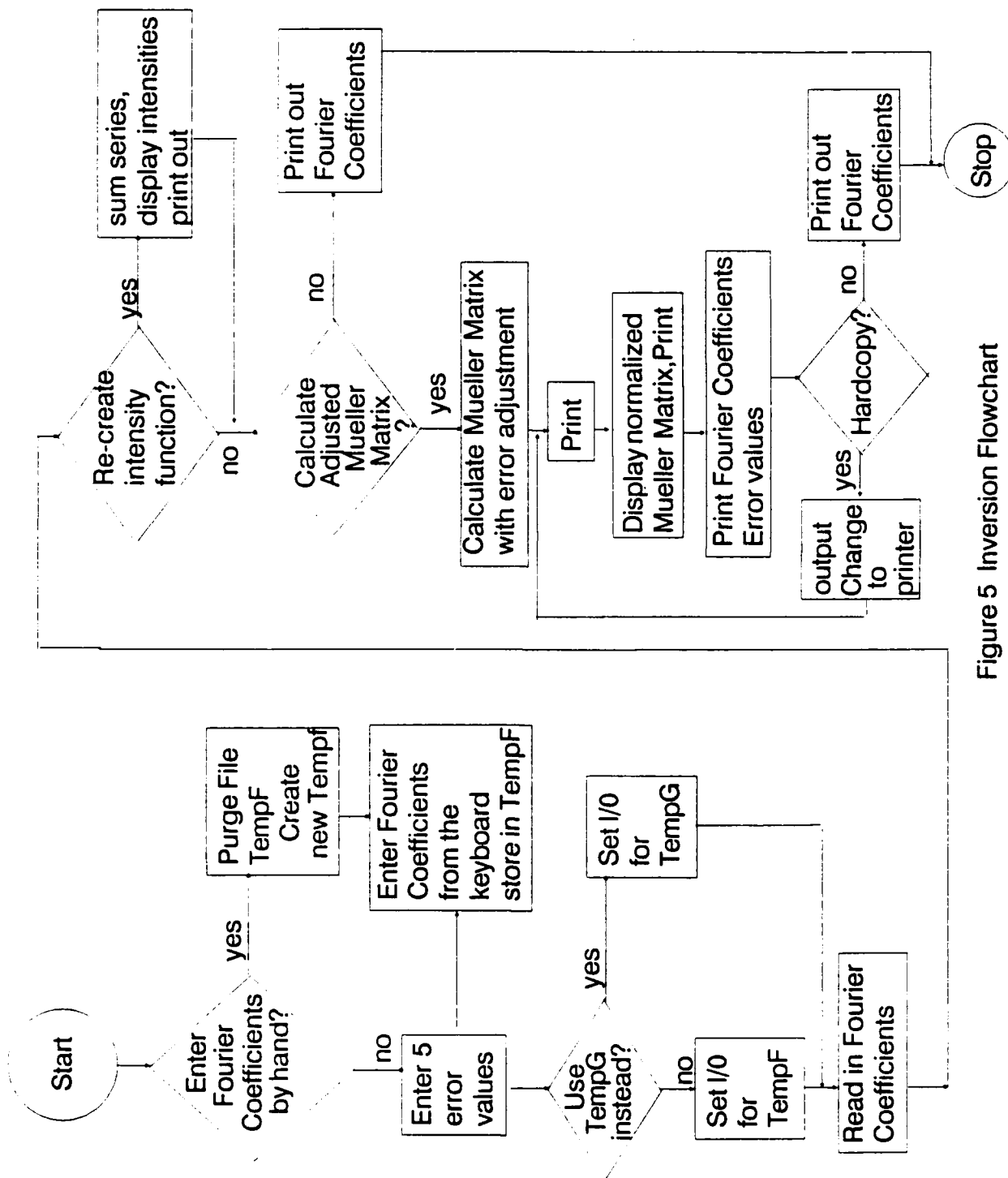
Figure 5 Inversion Flowchart

1) A photoconductive HgCdTe detector replaced the pyroelectric detector previously used for monitoring laser power. The photoconductive detector has much more immediate response to power fluctuations than the pyroelectric detector.

2) All of the optical components in the laser polarimeter have been re-mounted on magnetic bases which were lower to the table. This reduced the mechanical vibration which was present with the post mounts. The post-mounts had a significant amount of freedom to vibrate in the bracket which connected them to the rail. Mechanical vibration of the components adds noise to the detected intensity.

3) New multimeters have been introduced which allow integration over a set number of power-line cycles. This may help in reducing error by averaging over the noise above 2 Hz.

VI.   RECOMMENDATIONS

As mentioned in section IV, the beam wander error of the retarders can be partially averaged out by making measurements over more than one set of 180 degrees. This did help the test Mueller matrix to come closer to the target form of the identity matrix. However, the function describing the beam wander may only approximate a sinusoid, and thus the averaging would not fully compensate for this error. One alternative would be to use an integrating sphere. Due to scattering within the sphere, beam wander on the order of a few millimeters does not change the detected signal level. Using the integrating sphere would require more laser power, but this can be provided with the current equipment. The beam wander due to both retarders would be compensated for, except for one circumstance. If the sample to be measured has a transmission which is extremely dependent on angle of incidence, then beam wander from the first retarder would cause an intensity modulation even with an integrating sphere. In this case, the 180 degree averaging technique mentioned above would still be helpful.

During the summer, a photoconductive HgCdTe detector was used to monitor laser power fluctuations during the measurement period. When the fluctuation is relatively high during a measurement, the measurement is declared invalid. We noticed, however, that often the largest changes during the measurement period were due to the detector itself changing in temperature and thus in sensitivity. This problem is obviously more pronounced when longer measurement periods are used. Care must be taken to make sure the detectors are well cooled and not in a state of flux. A possible of way of improving this situation is with some type of continuously replenished cooling system or a different detector which has this feature.

If the power fluctuations recorded by the PC detector during a series of measurements are due to the laser, the intensities measured through the sample arm of the polarimeter could be ratioed with those measured by the PC detector. However, during a series of stability measurements made with no polarizing elements in the optical path, it was apparent that the noise was occasionally due to the laser, but was often due to detector changes.

Another approach to the detector problem would be to use only one detector. A chopper with mirrors on the fins would be used to divide the laser into two paths, one through the polarimeter and the other with nothing in the path but a mirror to steer it toward the detector. The signals from the two paths would alternate reaching the detector. The measurement electronics would be set to read from one path, then read from the other a set time later. This would facilitate dividing out the slow fluctuation due to both the laser and the detector itself. The fin spacing and rotation speed of the chopper would be chosen to produce the frequencies which are within the bandwidth of the detector.

REFERENCES

1. Chenault, David B., "Mueller Matrix Infrared Polarimetry", Final Report for the 1988 USAF-UES Graduate Student Research Program, 22 August 1988.

2. Goldstein, Dennis H., "Polarization Modulation in Infrared Electroopotical Materials", dissertation proposal submitted to Department of Physics, University of Alabama in Huntsville, 1989.

3. Azzam, R. M. A., "Photopolarimetric measurement of the Mueller matrix by Fourier analysis of a single detected signal", Optics Letters, 2, 6 (1978).

4. Hauge, P. S., "Mueller matrix ellipsometry with imperfect compensators", Journal of the Optical Society of America, 68, 11 (1978).

1989 USAF-UES SUMMER FACULTY RESEARCH PROGRAM/

GRADUATE STUDENT RESEARCH PROGRAM

Sponsored by the

AIR FORCE OFFICE OF SCIENTIFIC RESEARCH

Conducted by the

Universal Energy Systems, Inc.

FINAL REPORT

Euler Solutions to Transonic Flow

Past an Ogive-Cylinder Body

With Wraparound Fins

Prepared by: William D. Newbold

Academic Rank: Graduate Student

Department and   Aerospace Engineering, Mechanics,

  University: and Engineering Sciences

                    University of Florida

Research Location: AFATL/FXA

                    Eglin AFB, FL   32542-5434

USAF Researcher: L. Bruce Simpson, Ph.D.

Date: 21 July 1989

Contract No: F49620-88-C-0053

Euler Solutions to Transonic Flow

Past an Ogive-Cylinder Body

With Wraparound Fins

by

William D. Newbold

ABSTRACT

Euler solutions for transonic flow past a tangent-ogive
cylinder projectile with wraparound fin stabilizers have
been computed at two angles of attack using multiblock grid
networks. Two flow problems with a Mach number of 0.95 were
considered at zero degree and two degrees angle of attack.
These flow problems were also used in a grid refinement
study to investigate the sensitivity of the flow field to
grid resolution and the relative accuracy of the computed
solutions. Results for both flow problems show good
agreement between the computed results and the physics of
the flow field. At zero degree angle of attack a weak shock
is formed behind the nose of the projectile, and there is no
flow field disturbance produced by the infinitely thin fins.
A second shock wave spans between the fins on the top
surface of the projectile when at two degrees angle of
attack. Smaller shocks are also captured on the sides of
the projectile, extending from the lower fins. The flow
field solutions for the two degree angle of attack problem,
using two different grids, show no perceivable difference,
indicating relatively grid independent results.

ACKNOWLEDGEMENTS

I.   INTRODUCTION:

The wraparound fin stabilizer has become an increasingly
attractive design for unguided projectile configurations.
One of the most prominent advantages of this type of
stabilizer is its significant reduction of space
requirements as compared to the more conventional rigid
planar stabilizer configuration.

Space requirements are reduced by having the fin stabilizers
wrap around the body of a projectile while being stored.
Upon deployment, the fins are rotated outward using a hinge
mechanism and remain rigid during flight to provide
stability. For example, in multiple store configurations,
such as on aircraft weapon pylons, the use of wraparound
fins increase the weapon packing density thus providing the
aircraft greater defense and strike capability. This
reduction of space also enables launch from a tube whose
inside diameter need only be slightly greater than the
maximum body diameter of the weapon. With these and other
advantages, increasing attention has been given to
wraparound fin stabilizer configurations.

One of the primary missions of the Air Force Armament
Laboratory is to research, develop, and simulate
conventional armament for air-to-air and air-to-ground
tactical and strategic defense missions. Within the

Aerodynamics Branch of the Aeromechanics Division, researchers and experimentalists focus on predicting and measuring the aerodynamic properties of various existing and proposed weapon configurations. The Computational Fluid Dynamics (CFD) Section of the Aerodynamics Branch, in which I was assigned during the Graduate Student Research Program, centers on the numerical simulation of airflow past arbitrary weapon configurations. A recent set of CFD codes, EAGLE, were jointly developed by the CFD Section and the Department of Aerospace Engineering at Mississippi State University. The EAGLE[1,2] code is a multiblock grid generation and steady-state flow solver system which combines a boundary conforming surface generation scheme, a composite block structure grid generation scheme and a multiblock, implicit Euler flow solver algorithm.

My past research has included the application of a self adaptive computational method to transonic flow problems, and the development of various multiblock grids about arbitrary geometries using the EAGLE code. Having this previous experience with the EAGLE code, along with undergraduate and graduate research in CFD, contributed to my assignment to the CFD section of the Aeromechanics Division.

II.   OBJECTIVES OF THE RESEARCH EFFORT:

Considering the space requirement advantages of the
wraparound fin configuration, greater attention has been
given to this design in the development of weapons and
submunitions. Thus the need for aerodynamic data and flow
field characteristics about such configurations is also
rising. As a highly cost effective complement to wind
tunnel testing and laboratory testing, CFD has become an
increasingly popular engineering tool for the researcher and
designer.

Under the support of the 1989 USAF-UES Summer Faculty
Research Program/ Graduate Student Research Program, and the
interests of the CFD section, my research effort as a
graduate student researcher was to computationally model the
flow field about a generic projectile with wraparound fins
to determine the aerodynamic properties and the flow
characteristics generated by the wraparound fin stabilizer.

To computationally obtain accurate results to a well posed
flow problem, the grid structure developed about a given
geometry must be properly suited to the flow problem
considered. In fact, poor grid generation in the physical
domain can often be detrimental to both solution accuracy
and stability. Consequently, a major emphasis in this
research was to generate a suitable grid(s) for the flow

problems considered. Two transonic inviscid flow problems were investigated in an effort to determine the aerodynamic characteristics produced by the wraparound fin stabilizer. In the course of this work, a grid refinement study was also carried out with one of the flow problems to investigate the effects of grid structure on the numerical solution. The computations for this research were completed using the CRAY-2 supercomputer at the Air Force SuperComputer Center (AFSCC) at Kirtland AFB.

III.   GRID GENERATION:

The projectile modeled in this research is a 10-caliber tangent ogive projectile with wraparound fins. This configuration, shown in figure 1, was chosen to model an actual projectile of this geometry which is to be tested later this year at the Aeroballistics Research Facility, Eglin AFB. The projectile geometry is computationally modelled with a sting, the diameter of the projectile body, attached to the base of the projectile.

In order to effectively compute the flow field characteristics about a given geometry, one must not only have an accurate and robust flow solver but also a 'suitable' grid on which to numerically solve the governing equations of motion. To this effect, the concept of multiblock grids has gained widespread attention. This

technique has two primary advantages over single block grids. One is the ability to construct suitable grids about highly complex geometries by subdividing the entire grid into smaller subgrids, or blocks, which themselves are easier to construct and handle computationally. The other advantage is based on computer memory limitations. By dividing a single grid into multiple blocks one is able to significantly increase the number of grid points in each block and treat the blocks separately, one at a time during computations.

The grid developed for this study is an eight block algebraic grid. Blocks 1-4 are centered between the four fins. These blocks stretch the entire length of the projectile with sting, and extend to the top of the fins. The remaining four blocks are then centered on top of blocks 1-4. Figure 2 shows the transformation between the physical and computational domains for any of the four lower blocks. The shaded planes in the computational domain indicate their respective solid surfaces of the projectile. The front plane of all these blocks, as well as from blocks 5-8, degenerate to the stagnation line in the physical domain.

For the grid refinement study, two grids were constructed which contained different grid point densities and spacing near the solid surfaces. The first of these two grids contains 140 grid points along the axis of the body and 32

points normal to the body, figure 3a, and 10 circumferential planes between each fin, shown in figure 3b. Figure 4 shows the second grid studied which contains nearly 100,000 more grid points than the first. There are 134 points along the body axis and six additional circumferential planes between each fin. The grid point spacing near all solid surfaces has also been reduced in this grid.

IV.   FLOW PROBLEM:

The EAGLE flow solver was used to solve the equations of motion for transonic inviscid flow at a Mach number of 0.95 and with the projectile at zero and two degrees angle of attack. The flux difference split[3] algorithm with Roe[4] averaging was utilized. In order to accelerate convergence, local time stepping was used with a Courant number, CFL=5.0. Convergence of the iterative solution algorithm is based on the maximum residual of both density and energy, the L2-norm and the number of supersonic points in the flow field after each iteration.

For transonic flow at Mach 0.95 and zero degree angle of attack, figure 5 shows the surface pressure coefficient plot along the body of the projectile. This data is taken from the first circumferential plane off the fin, and is computed using the relatively coarse grid containing 10 circumferential planes. For this flow problem, a converged

solution was obtained after 500 iterations, at which the
magnitude of the density residual was on the order of 10^{-3}
and the number of supersonic points remained constant for
some 40 iterations. This plot clearly shows the
acceleration of the flow to supersonic around the nose of
the projectile and then forming a weak shock near the ogive-
cylinder intersection. This condition agrees well with the
physics of the flow and previous computations of unfinned
ogive-cylinder bodies[3]. It should be noted in these
computations, that the fins are modeled as infinitely thin
plates for which no flow boundary conditions are prescribed.
Therefore at zero degree angle of attack the flow would
actually not detect the fins in the absence of
circumferential flow. This is further supported in the
pressure coefficient plot of figure 5.

Results for the flow conditions at Mach 0.95 and two degrees
angle of attack also conform reasonably well to the physics
of the flow field. This flow problem was solved using the
two grids previously discussed in an effort to determine the
sensitivity of the computed flow field, if any, to the
various grids. Figures 6 and 7 indicate that there is no
appreciable difference between the two grids in effectively
modelling the flow problem, and that both grids are able to
capture the shock formation over the nose and in the fin
area equally well. Based on this data and the convergence
history of the two iterative solution processes, it is

reasonable to expect that for the inviscid flow problem
considered, the coarser grid can be used to accurately
predict the flow field characteristics at a significant cost
savings. However, in the absence of experimental data it is
preferred to use the grid containing the greater number of
points and higher resolution near the body in order to have
a 'base model' to study the entire flow field.

Using the relatively coarse grid, a converged solution was
again reached in 500 iterations. However, the number of
supersonic points in the flow field did not remain as
constant when compared to the flow problem at zero degree
angle of attack. Similar convergence was also obtained with
the finer grid for the two degree angle of attack problem.

The Mach contour plot in figure 8 explicitly shows the two
shock waves on the upper surface of the projectile along
with the single shock wave on the lower surface. This
solution and that shown in figure 9 are from computations
using the relatively dense grid. The shock wave between the
fins on the upper side of the body is anticipated due to the
circumferential flow around the body at an angle of attack.
In addition, the location of the side fins, also at two
degree angle of attack, will accelerate the flow over the
leading edge while producing lift, which will consequently
add to the strength of the shock wave formed between the
fins. The span of this shock wave on the top surface of the

body, figure 9a, reaches entirely between the two upper fins. In contrast, there is no shock wave on the bottom surface, figure 9b, and the shock waves off the fins on the lower sides of the body reach just over half the span between adjacent fins as shown in figures 9c and 9d. In particular we see a difference in the size and strength of these two shocks due to the asymmetry of the fin curvature relative to the vertical plane. A review of the projectile geometry and fin locations shows that near the root of the right lower fin (looking forward along the body axis), the surface is nearly a horizontal plane as opposed to a nearly vertical plane on the left lower fin. Therefore a greater acceleration of the flow and consequently a stronger shock is produced near the root of the right fin.

A review of the forces and moments exerted on the body and fins alone (excluding sting) at both zero and two degrees angle of attack show that there is no significant rolling moment. At two degrees angle of attack both the body and the fin set are contributing to the lift coefficient, whereas at zero degrees, there is no lift as expected.

In general, the results produced by the inviscid flow computations shown here, agree reasonably well with the physics of the problem. However when trying to investigate in detail the effects of the wraparound fin stabilizer, viscous flow problems must be considered.

V.   RECOMMENDATIONS:

It is anticipated that later this year several ballistics tests will be conducted at the Aeroballistics Facility using the projectile that was studied in this research. Tentative plans are to test over a Mach range and various angles of attack which may include those reported here. Such tests could validate the numerical solutions already obtained and also generate additional research areas for computationally modelling this configuration.

To better understand the effects of the wraparound fin stabilizers, solutions to the viscous problem is desired. Future research efforts will perhaps concentrate on obtaining such viscous solutions. In solving this problem, a new grid would need to be generated about the geometry which is suitable for viscous problems. This viscous grid would demand highly refined grid point spacing near the solid surfaces on the order of 10^{-4} or 10^{-5}, as opposed to the current spacing of 10^{-2}. Additional modifications may be required to smooth the transition between the lower and upper blocks in the fin area. Currently there is a slope discontinuity between the curvature of the fins in the lower blocks and the radial lines of the outer blocks. Adding thickness to the fins may also be required with the above modifications.

REFERENCES

1. Thompson, J. F., and Gatlin, B., "Program EAGLE User's Manual," U.S. Air Force Armament Laboratory, Eglin AFB, Fl., AFATL-TR-88-117, Vol. II and Vol. III, Sep. 1988.

2. Mounts, J. S., Belk, D. M., and Whitfield, D. L., "Program EAGLE User's Manual," U.S. Air Force Armament Laboratory, Eglin AFB, Fl., AFATL-TR-88-117, Vol. IV, Sep. 1988.

3. Whitfield, D. L., Janus, J. M., and Simpson, L. B., "Implicit Finite Volume High Resolution Wave-Split Scheme for Solving the Unsteady Three-Dimensional Euler and Navier-Stokes Equations on Stationary or Dynamic Grids," Mississippi State University Report, MSSU-EIRS-ASE-88-2, Feb. 1988.

4. Roe, P. L., "Approximate Rieman Solvers, Parameter Vector, and Difference Schemes," _Journal of Computational Physics_, Vol. 43, pp. 357-372, 1981.

5. Cottrell, C. J., Martinez, A., Chapman, G. T., "Study of Multibody Aerodynamic Interference at Transonic Mach Numbers," _AIAA Journal_, Vol. 26, May 1988, pp. 553-560.
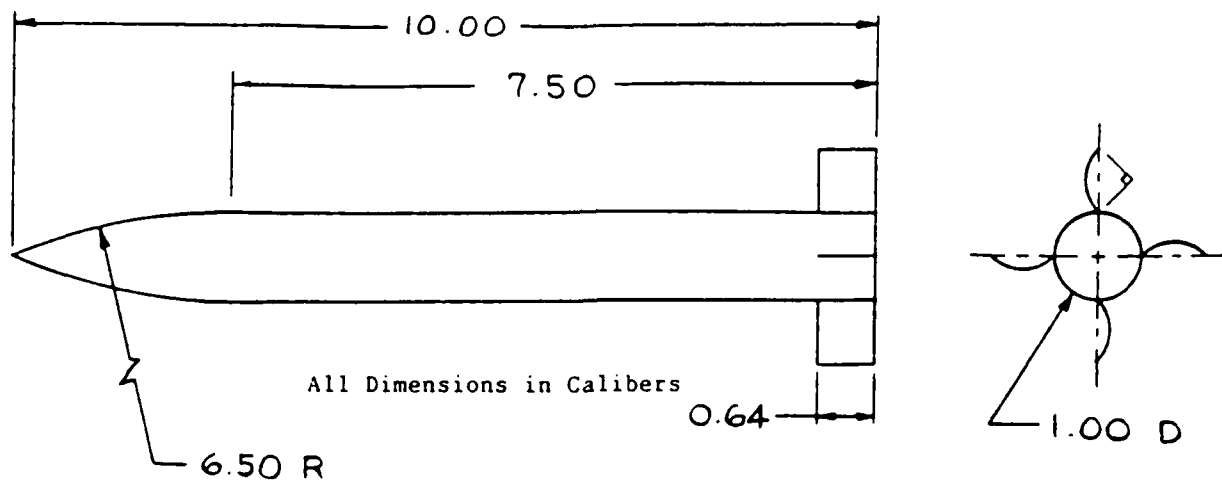
FIGURE 1. Tangent Ogive Cylinder Body
With Wraparound Fins.
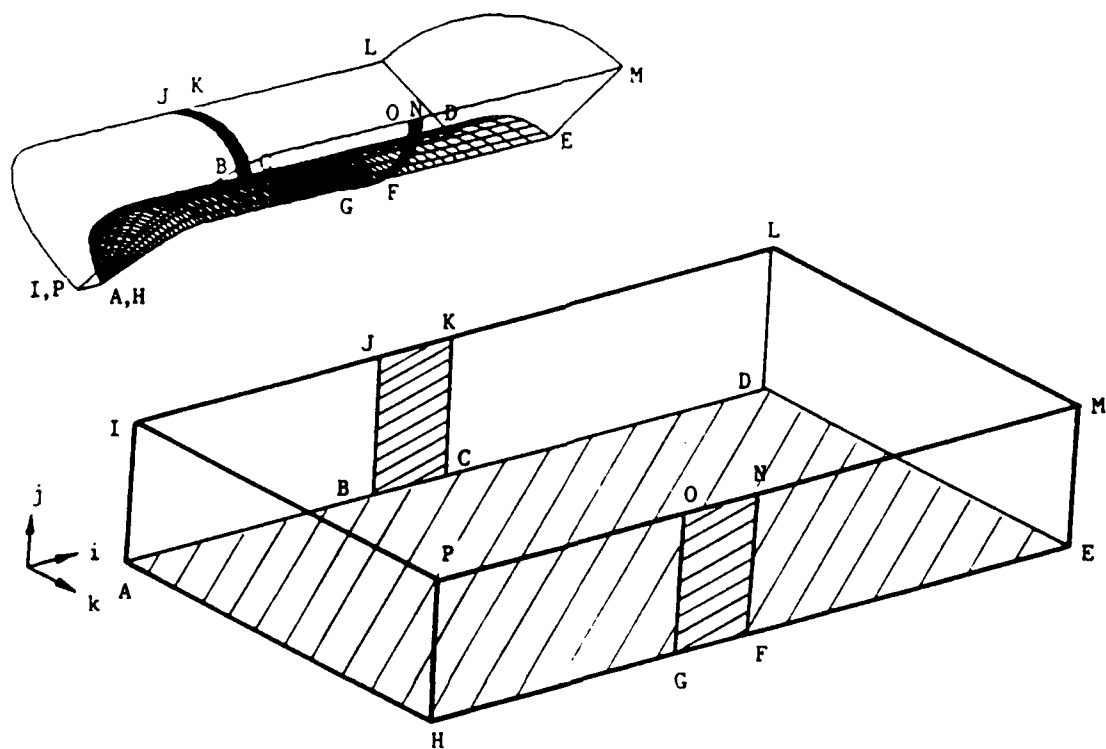
FIGURE 2. Grid Transformation
Blocks 1-4, Typical.

2-15
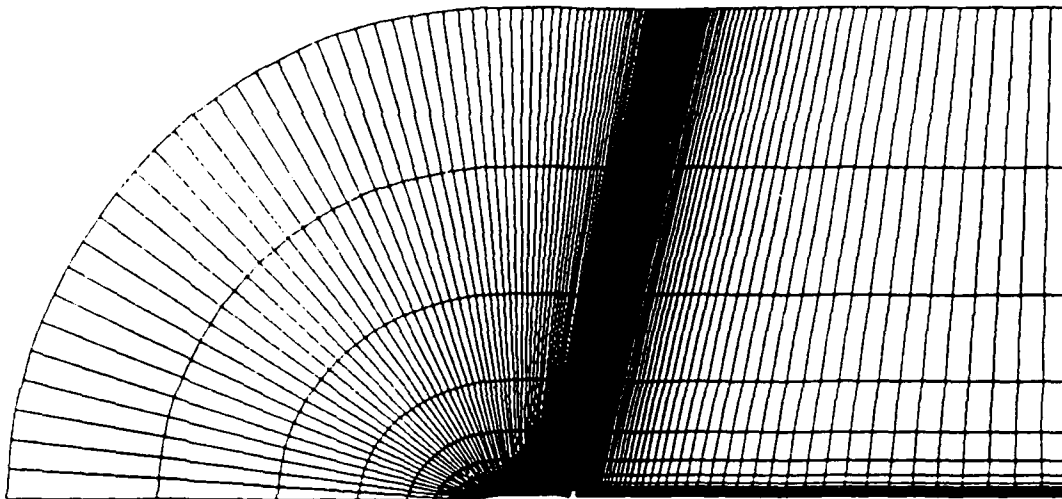
8 Block Grid :   140 x 21 x 10 x 4
                   140 x 12 x 10 x 4

(a)   complete circumferential plane
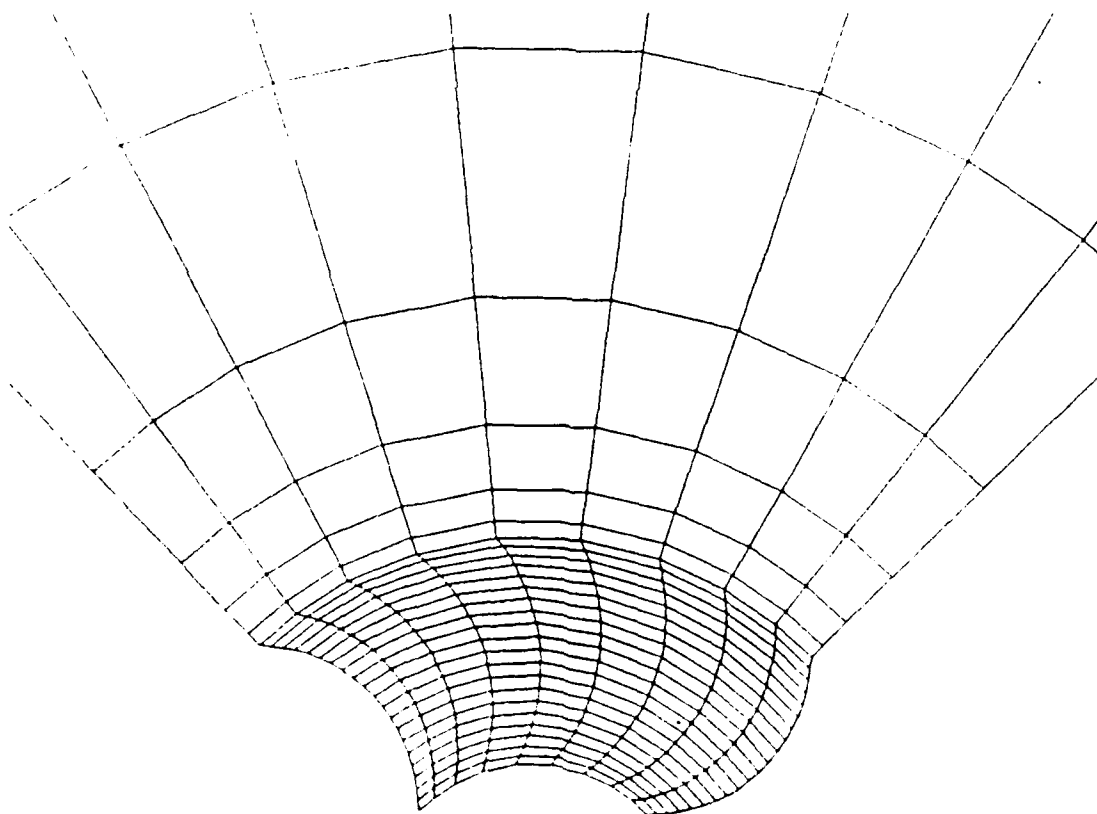
(b)   domain between adjacent fins

FIGURE 3.   Grid Network - Coarse.

2-16
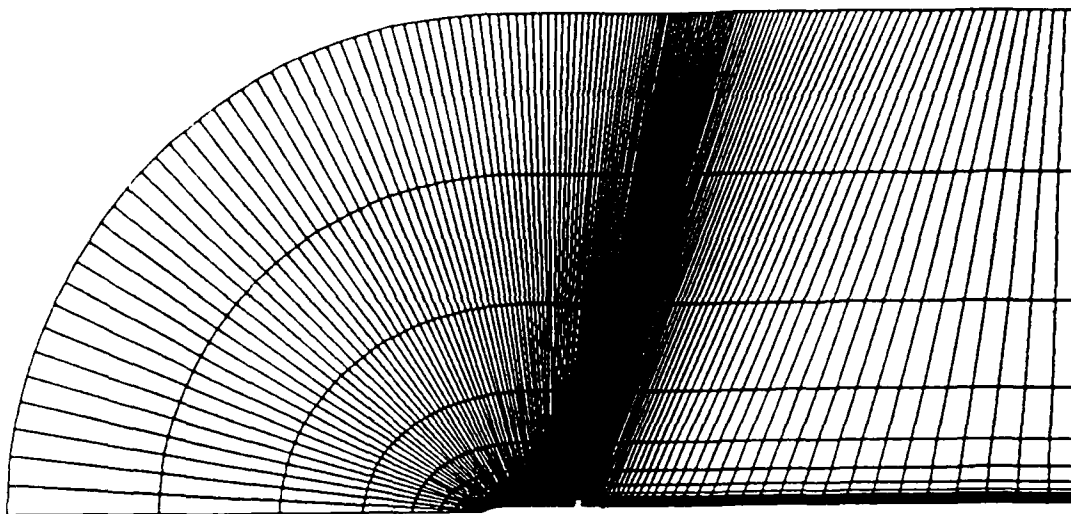
8 Block Grid :   134 x 21 x 16 x 4

134 x 12 x 16 x 4

(a) complete circumferential plane
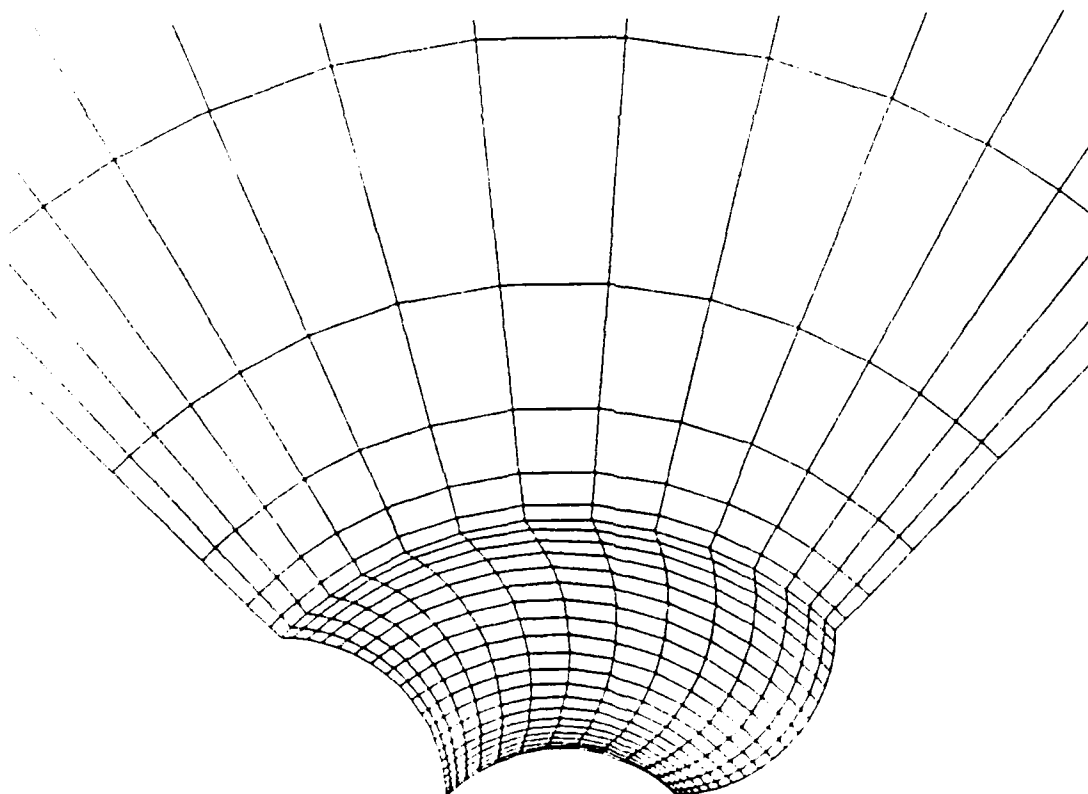
(b) domain between adjacent fins

FIGURE 4.   Grid Network - Fine.
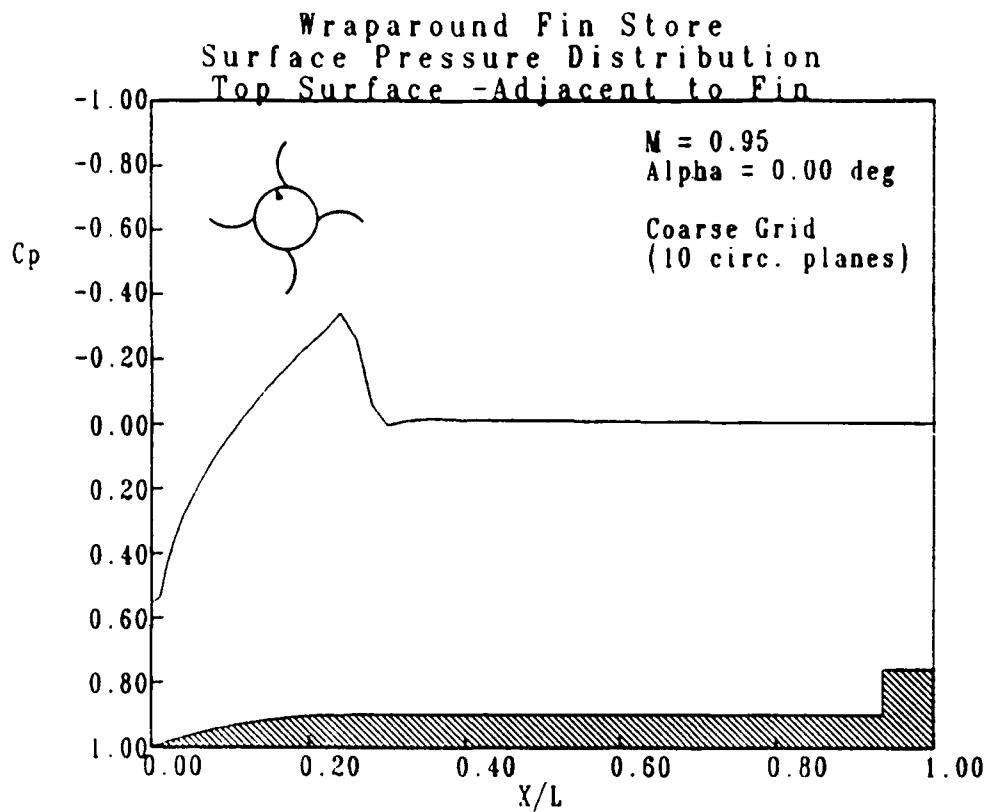
FIGURE 5.   Pressure Coefficient Plot,   Alpha = 0.00 deg.
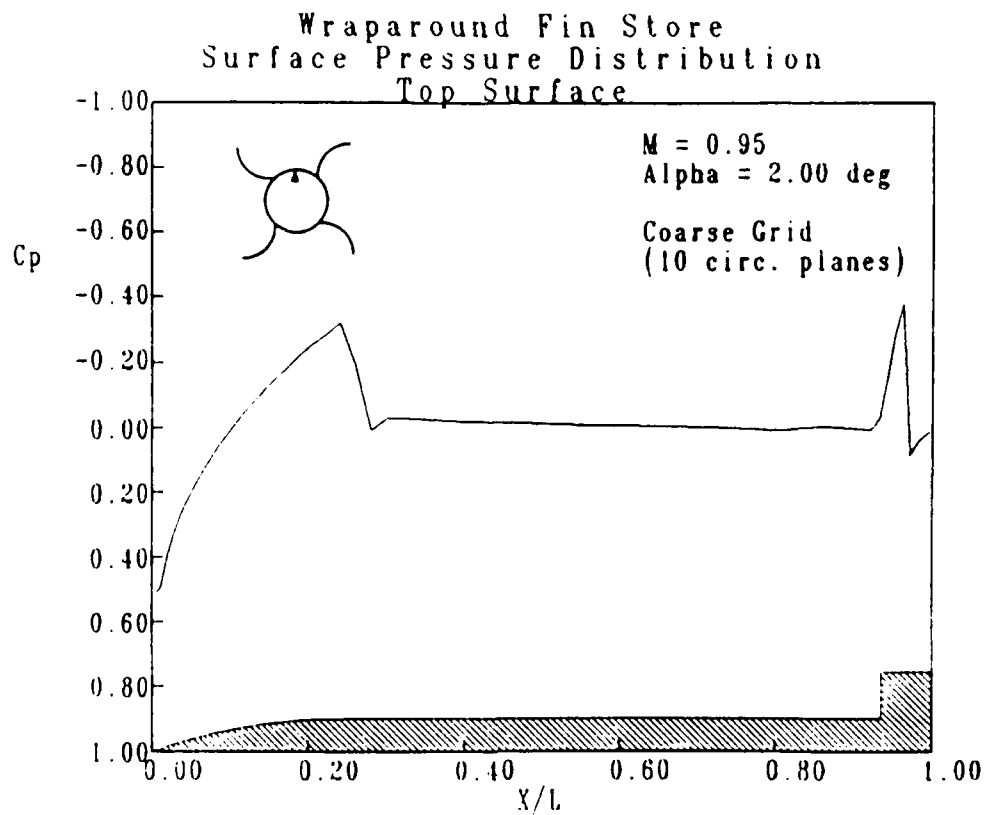
FIGURE 6.   Pressure Coefficient Plot,   Alpha = 2.00 deg.
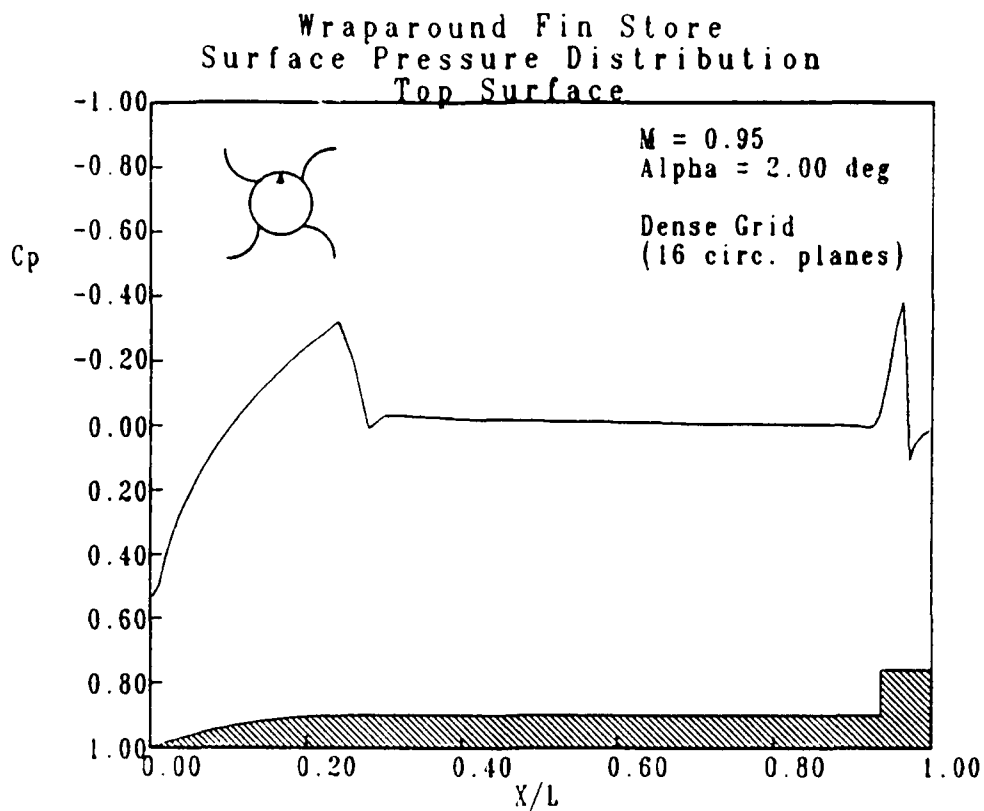
FIGURE 7. Pressure Coefficient Plot
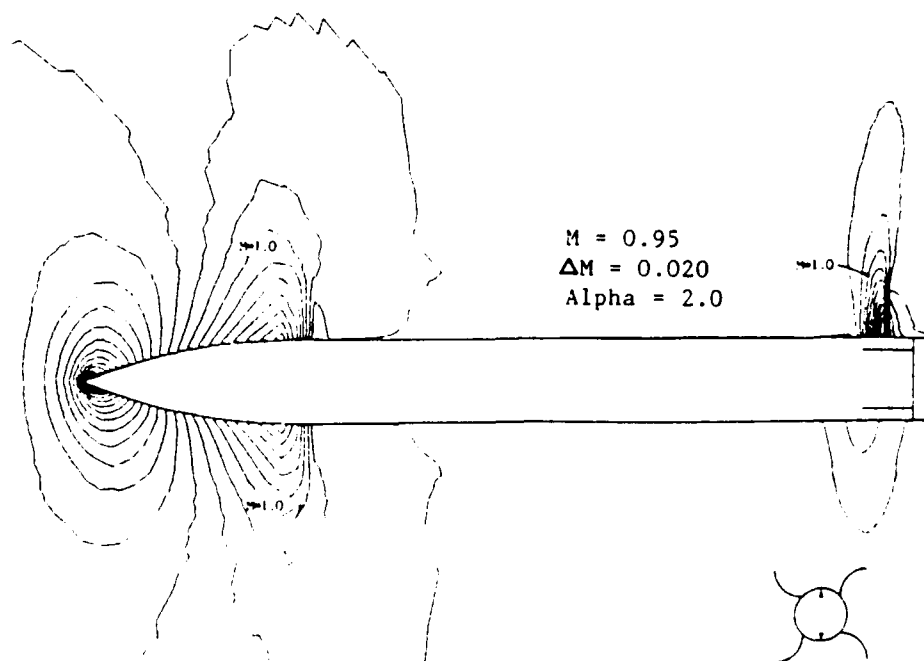
FIGURE 8. Mach Contour Plot
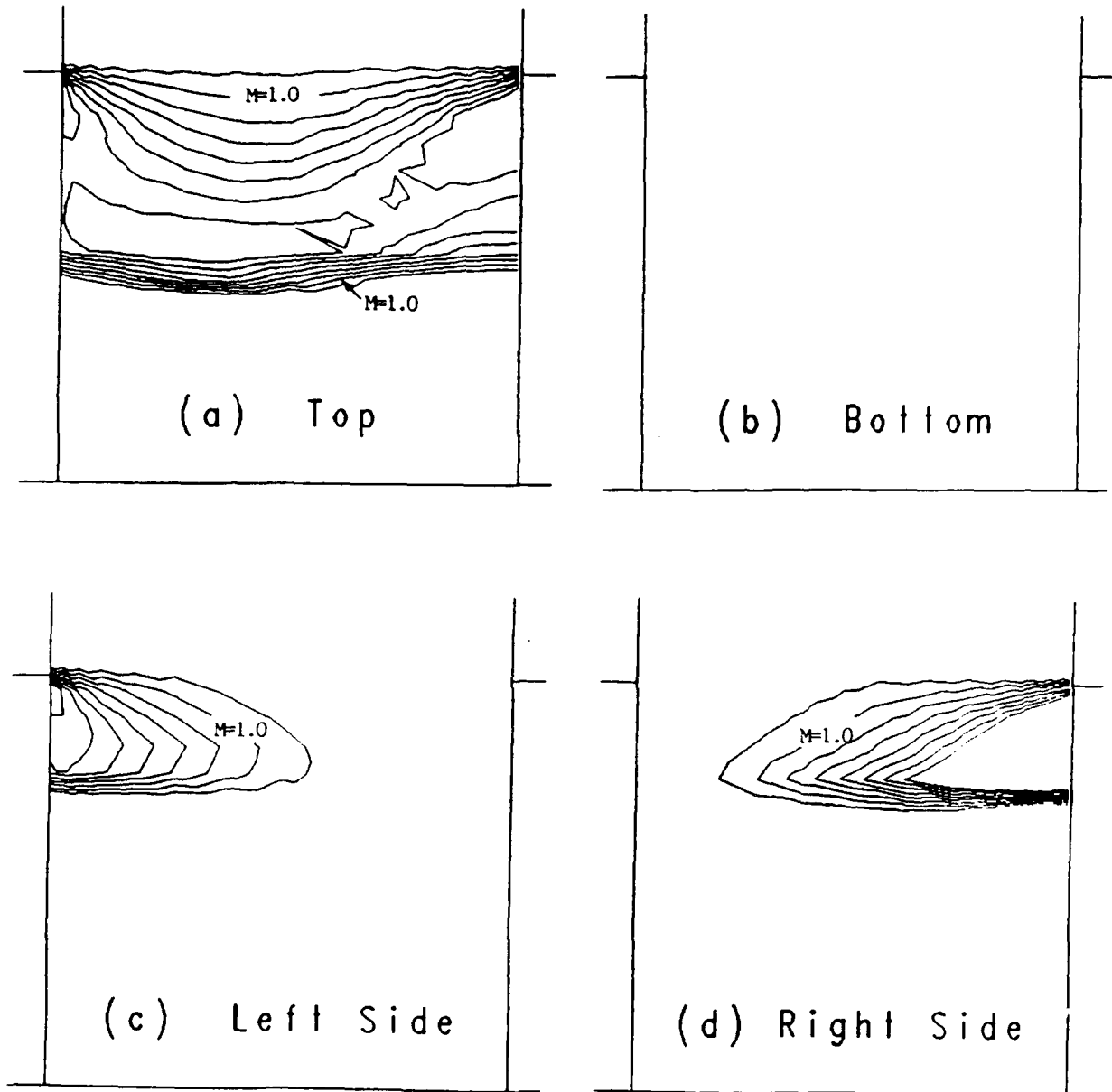
FIGURE 9. Mach Contour Plot
M = 0.95, Alpha = 2.0 Degrees,
ΔM = 0.025
Contours Between Adjacent Fins
Near Projectile Body (Fin Root).
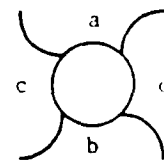
1989 USAF-UES SUMMER FACULTY RESEARCH PROGRAM/

GRADUATE STUDENT RESEARCH PROGRAM

Sponsored by the

AIR FORCE OFFICE OF SCIENTIFIC RESEARCH

Conducted by the

Universal Energy Systems, Inc.

OBSERVATIONS AND IMPROVEMENTS OF BALLISTIC

STRESS ANALYSIS TECHNIQUES

Prepared by: Glenn M. Waguespack

Academic Rank: Graduate Student

Department and   Department of Mechanical Engineering

  University: Louisiana State University

Research Location: AFATL/FXA
                          Eglin AFB. FL   32542

USAF Researcher: Mr. Gerald L. Winchenbach

Date: August 4, 1989

Contract No: F49620-88-C-0053

OBSERVATIONS AND IMPROVEMENTS OF BALLISTIC

STRESS ANALYSIS TECHNIQUES

by

Glenn M. Waguespack

ABSTRACT

In an attempt to predict and prevent structural failures in experimental projectiles during their initial accelerations, the Air Force Armament Laboratory at Eglin Air Force Base, Florida is incorporating various stress analysis programs into the Projectile Design Analysis System (PRODAS), a software package that performs various analyses to aid projectile designers. The main objective of this research was to incorporate a finite element stress analysis routine by Mr. Wafa Yazigi into PRODAS. While waiting for the completion of this proposed group of subroutines, I spent the first portion of this research period learning about PRODAS by modifying and debugging a conventional stress analysis routine written by Kurt Gothe. The FE routine was never written, so the objective shifted to studying and recommending different modeling and analysis techniques for performing an FE analysis on projectiles. The findings suggest that projectiles can be easily modeled by AXISYMMETRIC or 3-D elements, and a quasistatic analysis is sufficient to perform the analysis without solving the dynamic equations of motion.

ACKNOWLEDGMENTS

I. INTRODUCTION:

The Aeroballistics Division of the Aerodynamics Branch at Eglin Air Force Base, Florida continually designs, tests and performs research on projectiles for military use. As part of their procedure for testing projectiles, they often design and shoot prototype models in a ballistics range to study its characteristics. Structural failures sometimes occur in these prototypes from the high stresses induced by the projectile's initial acceleration. In an attempt to eliminate the additional time and cost caused by structural failures, the engineers at the Aeroballistics Branch are having several stress analysis routines incorporated into the software system currently used for aiding projectile design, the Projectile Design and Analysis System (PRODAS). PRODAS already contains two stress analysis routines: one that analyzes only high explosive incendiary (HEI) rounds (it cannot analyze sabot models) and one that uses a conventional stress analysis method to analyze sabot-fired models. In order to obtain more accurate stress analysis results, the engineers at AFATL/FXA wish to incorporate a finite element program into PRODAS.

A finite element stress analysis program suitable for incorporation into PRODAS was supposedly under development by Mr. Wafa Yazigi of Richland College in Richland, Washington. As part of the Graduate Student Research Program, a graduate student was to be assigned the task of incorporating Yazigi's resulting subroutines into PRODAS by appropriately modifying the subroutines' input/output structure.

As a graduate student who recently obtained a bachelor of science degree in mechanical engineering, my coursework as an undergraduate involved training in computer programming (FORTRAN), strengths of materials, dynamics and vibrations, and other related subjects. My

experience from programming assignments as an undergraduate, along with my familiarity with dynamics and strengths of materials, gives me enough qualifications to be able to manipulate and modify stress analysis programs and recognize possible sources of error.

II. OBJECTIVES OF THE RESEARCH EFFORT

As mentioned in the introduction, my main objective this summer was to obtain a set of subroutines from Wafa Yazigi and make the necessary modifications to incorporate them into PRODAS. Therefore, upon arriving at Eglin, my first goal was to learn as much as possible about the structure and algorithm of PRODAS before Yazigi's subroutines arrived. As an aid and incentive to learning about PRODAS, I spent several weeks modifying the conventional stress analysis routines recently developed by Kurt Gothe for sabot-fired projectiles. These modifications mainly consisted of correcting spelling in the comment and output statements, adding additional I/O options, and debugging several branches of the algorithm.

When Wafa Yazigi's information was received, it was discovered that he wrote no finite element program. Instead, due to an apparent misunderstanding between Yazigi and AFATL/FXA, he used two commercial FE software packages to analyze a sample projectile and compare the two results. The information sent to AFATL/FXA consisted of a report describing the modeling technique and boundary conditions, computer printouts listing the input data files and the results of the analyses, and a floppy disk containing data files and binary output files that can only be read by MCS/PAL2, one of the commercial software packages used. Thus, no FE subroutines were available to be incorporated into PRODAS, and no commercial FE package could be obtained within the ten week research period. Once we realized that the main objective of this research effort

will not be fulfilled within the research period. I set an alternate goal to learn as much as possible about the methodology and theory of finite element stress analysis and its associated modeling techniques relating to the actual physical phenomena occurring in an accelerating projectile, compare this information with the modeling and analysis techniques used by Yazigi, and make recommendations and conclusions about alternate methods of performing the FE analysis. This study was performed to meet two objectives: 1) to provide enough information about different analysis and modeling techniques for facilitating a decision on the most desirable technique for accuracy and efficiency, and 2) to correct previous modeling errors and provide a specific modeling technique that can be immediately used to analyze axisymmetric projectiles once an FE program becomes available.

III. BRIEF DESCRIPTION OF FINITE ELEMENT METHOD

Finite element analysis is a numerical method for approximating the solution of a series of differential equations. The finite element method functions by breaking the model into discrete elements and assigning an approximation (usually a polynomial) of the solution within each element in the form of a linear combination of shape functions multiplied by values representing the nodal solutions. (Nodes are the points that define the size and shape of each element.) These nodal solutions are determined using an optimizing criterion such as the commonly used method of weighted residuals. The optimizing criterion essentially transforms the given differential equations into a system of linear algebraic equations that evaluate the nodal solution values to provide the closest fit between the functional solution approximations and the true solution.

In FE stress analysis problems, the displacement field is usually treated as the unknown. Once the numerical displacement solutions are obtained, they are substituted first into the definitions of strain from the theory of elasticity and then into Hooke's law to determine the corresponding stresses. For a single element, the trial solution is defined as follows:

$$\{U\}^{(e)} = [\phi]^{(e)}\{a\} \tag{1}$$

where $\{U\}^{(e)}$ is a vector of elemental displacement functions, $[\phi]^{(e)}$ is a matrix of shape functions, and $\{a\}$ is the vector of nodal displacements. These trial functions are then substituted into the the following formulas from the theory of elasticity to define a vector of strains:

Rectangular coordinates:

$$\epsilon_x = \frac{\partial u}{\partial x} \qquad\qquad \epsilon_y = \frac{\partial v}{\partial y} \qquad\qquad \epsilon_z = \frac{\partial w}{\partial z}$$

$$\gamma_{xy} = \frac{\partial v}{\partial x} + \frac{\partial u}{\partial y} \qquad \gamma_{yz} = \frac{\partial w}{\partial y} + \frac{\partial v}{\partial z} \qquad \gamma_{zx} = \frac{\partial w}{\partial x} + \frac{\partial u}{\partial z} \tag{2a}$$

Cylindrical coordinates:

$$\epsilon_r = \frac{\partial u}{\partial r} \qquad\qquad \epsilon_\theta = \frac{u}{r} + \frac{1}{r}\frac{\partial v}{\partial \theta} \qquad\qquad \epsilon_z = \frac{\partial w}{\partial z}$$

$$\gamma_{r\theta} = \frac{1}{r}\frac{\partial u}{\partial \theta} - \frac{v}{r} + \frac{\partial v}{\partial r} \qquad \gamma_{\theta z} = \frac{\partial v}{\partial z} + \frac{1}{r}\frac{\partial w}{\partial \theta} \qquad \gamma_{zr} = \frac{\partial u}{\partial z} + \frac{\partial w}{\partial r} \tag{2b}$$

The resulting expressions for the strain can be represented as follows:

$$\{\epsilon\} = [B]^{(e)}\{a\} \tag{3}$$

where $\{\epsilon\}$ is the vector of strains and $[B]^{(e)}$ is a matrix of functions obtained by substituting equations (1) into equations (2). By applying Hooke's law to the strains in equation (3), the stresses are obtained:

$$\{\sigma\} = [C]\{\epsilon\} = [C]([B]^{(e)}\{a\}) \tag{4}$$

where $\{\sigma\}$ is a vector of strains and $[C]$ is the matrix of proportionality constants defined by Hooke's law.

Using the nomenclature of equations (1) through (4), the following equations relate the nodal displacements to the element geometry, shape functions, material properties, constraints, and loading conditions. These

are derived using the Galerkin criterion in (Burnett, 1987) and Lagrange's equations in (Rao, 1982):

$$[M]^{(e)}\{\ddot{a}\} + [K]^{(e)}\{a\} = \{Ft\} + \{Fb\} \tag{5}$$

where

$$[M]^{(e)} = \iiint_V \rho[\phi]^{(e)T}[\phi]^{(e)}dV,$$

$$[K] = \iiint_V [B]^{(e)T}[C][B]^{(e)}dV,$$

$$\{Ft\} = \iint_A [\phi]^{(e)T}\{t\}dA,$$

and

$$\{Fb\} = \iiint_V [\phi]^{(e)T}\{f\}dV$$

where $[K]^{(e)}$ is the elemental stiffness matrix, $\{Ft\}$ is a vector of surface forces, $\{Fb\}$ is a vector of body forces, $\{t\}$ is a vector of surface tractions, and $\{f\}$ is the vector of body forces per unit volume. Note that $[M]^{(e)}$, $[K]^{(e)}$ and $\{Fb\}$ are volume integrals while $\{Ft\}$ is a surface integral. By noting that the force at each node is the sum of the forces exerted by each adjacent element containing the node, the equations for all elements can be assembled into a large system of equations

$$[M]\{\ddot{a}\} + [K]\{a\} = \{Ft\} + \{Fb\} = \{F\} \tag{6}$$

by summing the equations representing the forces exerted at each node by each element. In static problems, where $\{\ddot{a}\} = 0$, equation (10) reduces to:

$$[K]\{a\} = \{Ft\} + \{Fb\} = \{F\} \tag{7}$$

Once $\{a\}$ is determined, the stress at each node can be calculated using equation (4) and appropriate averaging and smoothing functions. These stresses can then be compared to the allowable strength of the material using an appropriate failure theory.

IV. PROJECTILE MODELING FOR FE STRESS ANALYSIS

In any analysis technique, the accuracy of the results depends significantly on how close the mathematical model represents the actual

object. In the most general case, finite element models are specified as an assembly of three-dimensional elements, such as BRICK elements. In such specifications, each node exhibits three degrees of freedom; and a 3-D element which can contain no fewer than four nodes, must contain at least twelve degrees of freedom. Because the number of equations required to analyze the nodal displacements equals the total number of degrees of freedom, computational time increases as the number of degrees of freedom increases. Fortunately, the modeling effort and computational time can be significantly decreased for axisymmetric projectiles because these stress analysis problems can be reduced to essentially 2-D problems.

The necessary criteria for this DOF reduction of axisymmetric projectiles is that 1) the projectile must have a rotational axis of symmetry and 2) all loads applied to the projectile must have no tangential components and must also be symmetric about the projectile's axis of symmetry. If a cylindrical coordinate system is defined with the z axis lying on the projectile's axis of symmetry, all quantities and properties used in the stress analysis are independent of the θ coordinate; therefore, the nodal locations can be defined on an r-z plane and rotated about the z axis to form ring elements consisting of nodal circles, as shown in Figure 1.
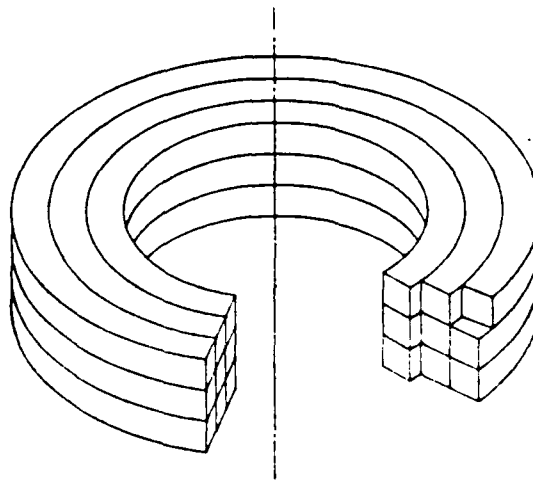
Figure 1: Illustration of the geometric concept of AXISYMMETRIC elements.

Since no significant quantities are θ-dependent, the problem is effectively reduced from 3-D to 2-D, thus eliminating one degree of freedom from each node and simplifying the FE model. Therefore, a projectile can be modeled in two dimensions as an assembly of triangular and quadrilateral AXISYMMETRIC elements, as shown in Figure 2.
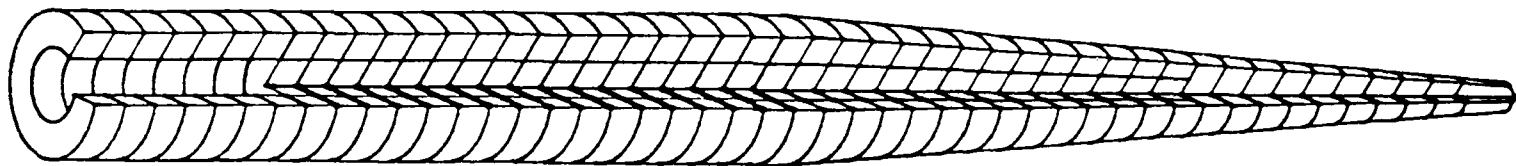
Figure 2: Illustration of an AXISYMMETRIC FE model of a projectile.

V. A REVIEW OF TWO POSSIBLE ANALYSIS TECHNIQUES

Once the geometric specifications and appropriate boundary conditions are known for a given model, the mass [M], stiffness [K], and load {F} matrices are evaluated. These matrices, along with [B] and [G], provide sufficient information to analyze the state of stress within each element. This analysis can be performed by either solving the dynamic equations (equation (6)) for {a} as a function of time, or using a quasistatic approximation (equation (7)), in which {a} is a vector of constants. The dynamic analysis accounts for the propagation of vibrational compression waves in the projectile materials that result from the rapidly varying base pressure. The quasistatic analysis neglects the vibrational effects by assuming that the acceleration of every point in the body is the same. Thus, the inertia load is treated a distributed body force and equation (6) reduces to equation (7).

Since the dynamic analysis includes both static and vibrational effects, it is the most accurate of the two techniques. In order to perform the dynamic analysis, a system of differential equations (equation (6)) must be solved using a numerical technique such as Runge-Kutta. In the quasistatic analysis, however, only linear algebraic equations must be solved. Therefore, the quasistatic analysis requires much less computer time than the dynamic analysis. The dynamic analysis thus presents the greatest advantage only when the application of the base pressure is rapid enough to create vibrations with an amplitude large enough to significantly affect the stress state within the projectile.

According to (Avallone and Baumeister, 1986), the dynamic effects of shock loads are significant only when the time of application of the load is less than half the member's fundamental natural period. If a projectile is approximated as a bimetallic rod vibrating only in the axial direction, the natural period τ is given by the following transcendental equation:

$$\sqrt{E_1 \rho_1}\ \tan\left(\frac{2\pi L_1}{\tau}\sqrt{\frac{\rho_1}{E_1}}\right) + \sqrt{E_2 \rho_2}\ \tan\left(\frac{2\pi L_2}{\tau}\sqrt{\frac{\rho_2}{E_2}}\right) = 0 \tag{8}$$

where E_1, ρ_1, and L_1 are the elastic modulus, density and length of the first material, and E_2, ρ_2, and L_2 are the elastic modulus, density, and length of the second material. For a unimetallic rod ($E_1 = E_2 = E$, $\rho_1 = \rho_2 = \rho$), equation (8) gives the following expression for the natural period:

$$\tau = \frac{2L}{n}\sqrt{\frac{\rho}{E}} \qquad n = 1, 2, 3, \ldots \tag{9}$$

where L is the rod's length. When the physical properties of aluminum and brass are substituted into equation (9) and compared with a time of application of one millisecond, an order of magnitude approximation for the application time of a projectile's base pressure, the results indicate that the aluminum and brass rods must each be longer than 201 inches and 139 inches, respectively, to meet the above criterion for shock loading.

To test the validity of this criterion, a one-dimensional three-

element finite element model of a 6 in. long 1 in. diameter aluminum rod (see Figure 3) was analyzed using both the quasistatic and dynamic techniques. The base pressure was specified as a spike function (see Figure 4) that would cause a peak acceleration of 40,000 G's one millisecond after the initiation of the load. The resulting stress histories are shown in Figures 5 through 7.
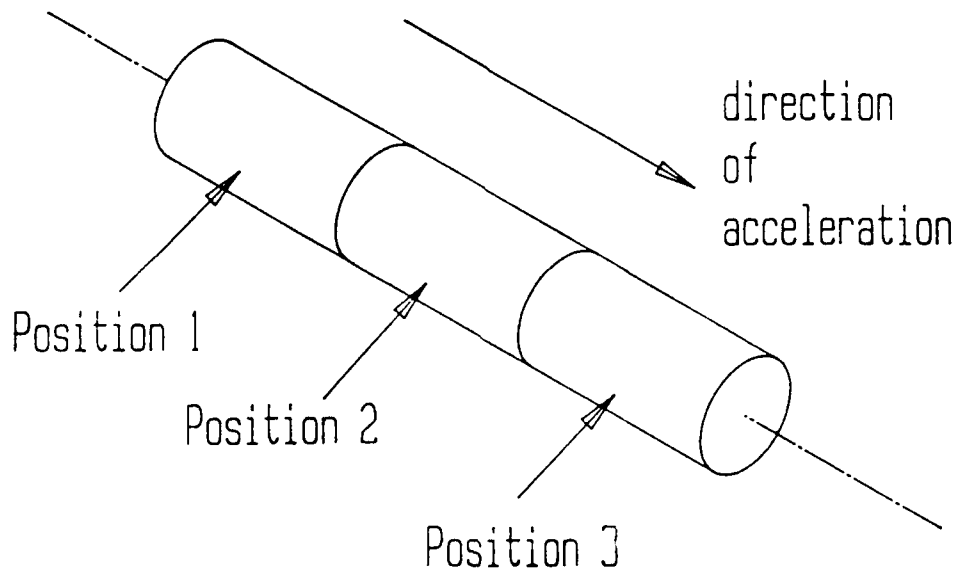
Figure 3: Illustration of the three element 1-D FE model of an aluminum rod used to compare the dynamic and quasistatic analysis techniques.
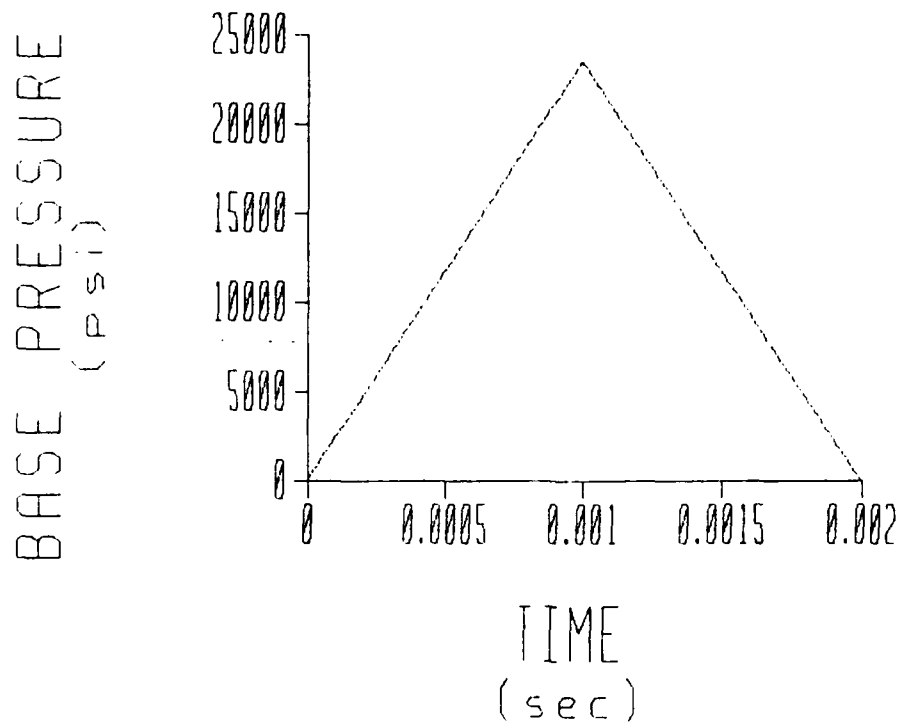
Figure 4: Plot of the base pressure input used in the 1-D analysis.
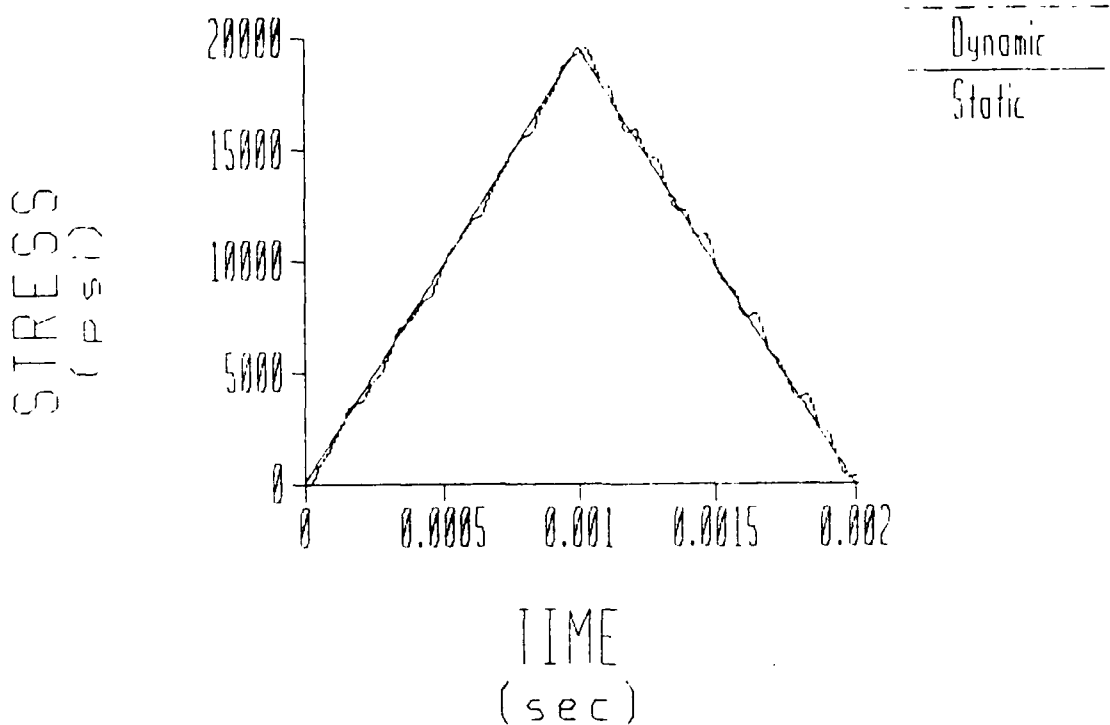
Figure 5: Comparison of the stress history of the aluminum rod at position 1, as determined by the quasistatic (straight line) and dynamic (oscillating line) analysis techniques.
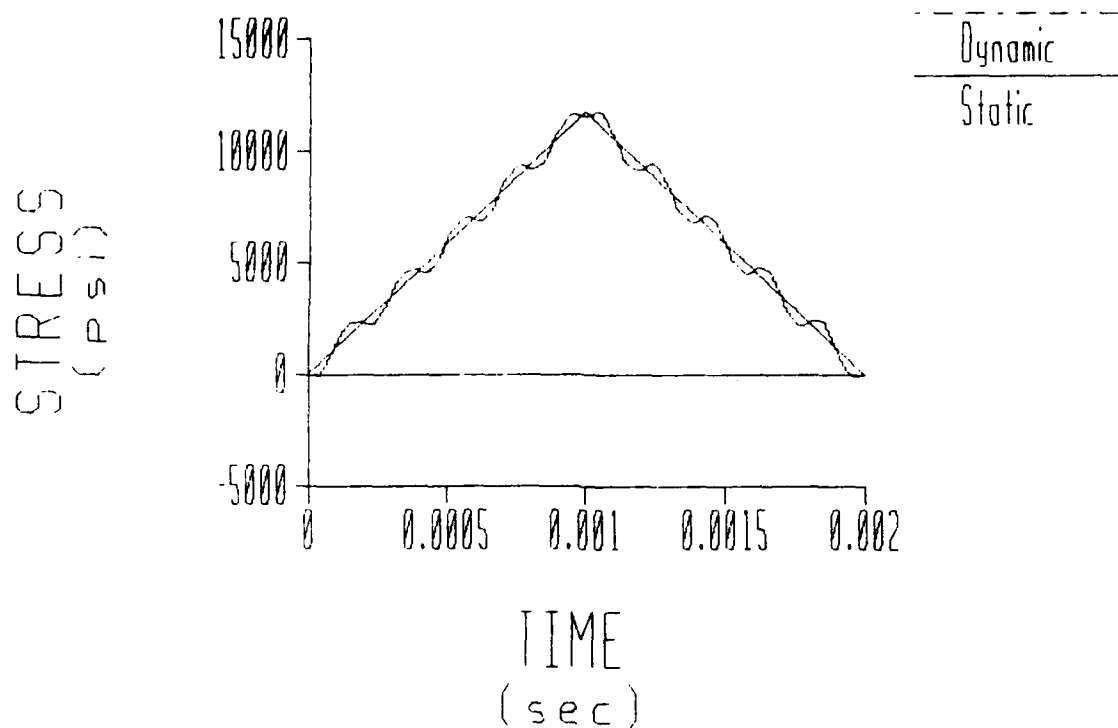
Figure 6: Comparison of the stress history of the aluminum rod at position 2, as determined by the quasistatic (straight line) and dynamic (oscillating line) analysis techniques.
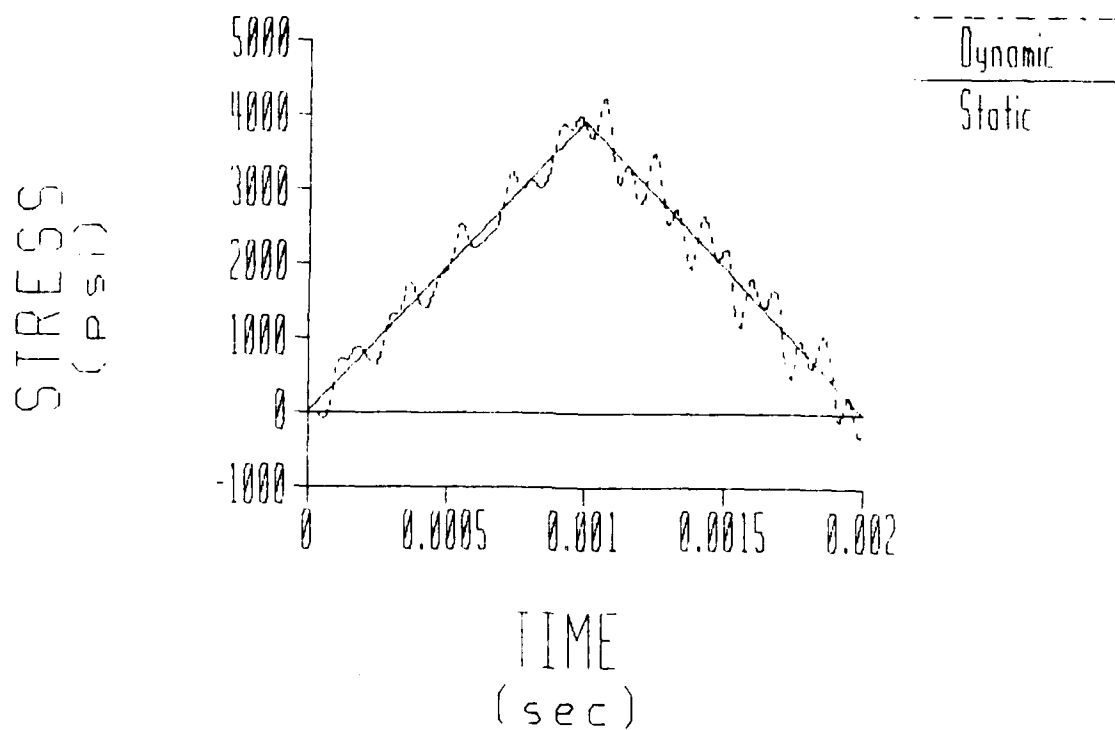
Figure 7: Comparison of the stress history of the aluminum rod at position 3, as determined by the quasistatic (straight line) and dynamic (oscillating line) analysis techniques.

According to the analytical results, as presented in Figures 5 through 7, the percent error of the quasistatic approximation increases as the distance from the base increases. The quasistatic curves, however, fit the dynamic curves so closely that any error in determining the maximum stresses using the quasistatic approximation is probably negligible in comparison with the descretization error in the finite element analysis and the uncertainties in the base pressure specifications. This result confirms the results obtained from the shock criterion in (Avallone and Baumeister, 1986). Therefore, the quasistatic approximation is probably the best analysis technique for projectiles because it requires less computer time and it produces results having acceptable accuracy.

VI. BOUNDARY CONDITIONS AND LOADING

In order to perform a proper stress analysis on any object, the object must first be modeled. Then the necessary loading and boundary conditions must be specified. Both the model and the boundary conditions should resemble the real situation as much as possible. Since modeling techniques were reviewed earlier in this report, this section will concentrate on suggesting loading and boundary conditions to be used in FEM, particularly for axisymmetric models.

Proper loading conditions for any stress analysis can be determined by first examining Newton's second law of motion:

$$\Sigma \vec{F}_{ext} = \iiint_V \rho \vec{a} \, dv \qquad (14)$$

or

$$\iint_S \vec{t} \, dA + \iiint_V \vec{f} \, dv = \iiint_V \rho \frac{d^2 \vec{u}}{dt^2} \, dv$$

where

$$\vec{u} = \text{displacement field} = u\vec{i} + v\vec{j} + w\vec{k}$$

3-15

$$\vec{t} = \text{surface traction} = t_x\vec{i} + t_y\vec{j} + t_z\vec{k}$$

and

$$\vec{f} = \text{body force (per unit volume)} = f_x\vec{i} + f_y\vec{j} + f_z\vec{k}$$

Also. ρ, V, and A respectively refer to the density, volume, and surface area. Since the acceleration and body force integrals have the same form (i.e. these "forces" affect every point inside the projectile), the density times the acceleration at each point within the projectile can be interpreted as a negative body force.

In performing an FE stress analysis on any object. the three necessary requirements of boundary and loading conditions are as follows:

1) All known loads must be applied either as surface tractions or body forces.

2. All known constraints must be applied.

3) If a quasistatic analysis is to be performed on a moving object. a body force equal to the local inertial force per unit volume should first be applied to each element in a manner that creates "static" equilibrium in the direction of the acceleration. Then, additional constraints should be applied to the minimum number of nodes necessary to prevent rigid body motion (to avoid singularities in the stiffness matrix). (Note that if a dynamic analysis is to be performed, neither the inertial body force nor the additional constraints should be added.)

Applying these requirements to an axisymmetric projectile for a quasistatic analysis. the following loading and boundary conditions result:

1. Apply a uniform pressure of magnitude $P = ma/A$ to the base of the projectile as a surface traction. In the above equation. m is the total projectile mass. a is the maximum acceleration. and A is the area of the base projected on a plane perpendicular to the projectile's axis.

2. Apply an axial body force of magnitude $-\rho a$ to all elements. Remember that all force components should balance in the axial direction.

3. Constrain all nodes on the axis of symmetry from radial motion.

4. To prevent rigid body motion. constrain one point on the axis of symmetry from axial motion. Since all specified axial loads balance. this constraint will not induce an axial force at this node.

5. (Optional) If the projectile is spinning. one may wish to apply a body force equal to $\rho r \omega^2$ to each element. where r is the radial distance from

the axis and w is the projectile's angular velocity about the axis of symmetry.

6. (Optional) One may also wish to apply an axial surface traction to the projectile's outer surface to account for friction. Frictional effects are probably negligible when compared to the inertial stresses. If these stresses are added, the base pressure must be increased to maintain axial force equilibrium.

The boundary conditions listed above (except the optional ones) are schematically represented in Figures 8 and 9. Also, if a dynamic analysis is to be performed to the model, boundary conditions 2 and 4 should be omitted.
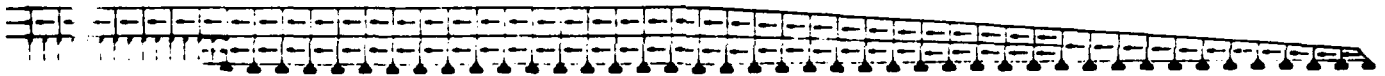
Figure 8: Schematic of a FE model of an axisymmetric projectile with loading and boundary conditions applied.
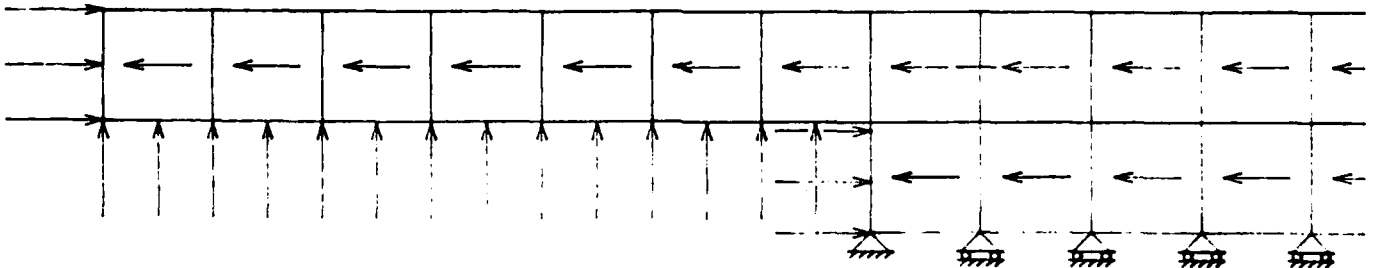
Figure 9: Detail from the schematic in Figure 8 emphasizing the axially constrained node and the base pressure.

3-17

VII. RECOMMENDATIONS

In the original report "Stress Analysis of a Penetrator Using Finite Element Method," Wafa Yazigi described a finite element model of an axisymmetric projectile that was constructed of 2-D PLATE elements. On the projectile's base, one node was completely constrained from motion while the others were constrained from axial motion. A force equal in magnitude to the projectile's maximum acceleration was then applied to the projectile's tip, giving boundary conditions simulating a projectile being compressed between two walls. A static analysis was then performed on the model.

In order to obtain an accurate representation of the state of stress in an accelerating projectile, I recommend that both the type of modeling elements and the loading and boundary conditions, as presented in Yazigi's report, be changed to the ones described in this report. Two-dimensional PLATE elements are not valid for axisymmetric problems. Instead, AXISYMMETRIC elements, which are specially formulated for axisymmetric problems, should be used. Also, Mr. Yazigi's loading and boundary conditions would give a very conservative stress estimate if applied on an appropriate model. By applying the base pressure at the base and a balancing inertial body force to each element, a more realistic stress distribution can be obtained. For projectiles that are not axisymmetric, I suggest the use of a 3-D finite element program.

In comparing dynamic analysis with quasistatic analysis for a projectile, both analyses gave very similar results because the base pressure's time of application, though very rapid, is not quick enough to cause significantly large vibrational effects in the projectile. Therefore, because the quasistatic analysis requires less computer time and is easier to perform than a dynamic analysis, I suggest that the

3-18

quasistatic FE analysis be used to analyze projectiles unless the base pressure's time of application is less than half the projectile's fundamental natural period.

Also, in order to obtain maximum usability and practicality of the finite element stress analysis, I recommend that 1) an interior ballistics program be obtained or developed that can analyze more diverse projectiles than the interior ballistics program in PRODAS; 2) a literature search be performed to determine the effects of shock loading on the effective yield strength of materials (so that a proper failure analysis can be performed using the FE results); and 3) all projectile material failures not predicted by the stress analysis be recorded so that an effective safety factor can be determined for design purposes.

REFERENCES

Avallone, Eugene A. and Theodore Baumeister III (ed). Mark's Standard Handbook for Mechanical Engineers. 9th ed. New York: McGraw-Hill Book Company. 1986. p. 5-47.

Burnett, David S. Finite Element Analysis: From Concept to Applications. Reading, Massachusetts: Addison-Wesley Publishing Company. 1987.

Gothe, Kurt G. "A New Stress Routine for the Projectile Design Analysis System (PRODAS)." Air Force Armament Laboratory. 1989.

Rao, S. S. The Finite Element Method in Engineering. Oxford: Pergamon Press. 1982.

Vitogi, Sofa. "Stress Analysis of a Penetrator Using Finite Element Method." June 14, 1989.

1989 USAF-UES SUMMER FACULTY RESEARCH PROGRAM

GRADUATE STUDENT RESEARCH PROGRAM

Sponsored by the

AIR FORCE OFFICE OF SCIENTIFIC RESEARCH

Conducted by the

Universal Energy Systems, Inc.

<u>FINAL REPORT</u>

<u>DISTRIBUTED AND PARALLEL IMAGE AND SIGNAL PROCESSING</u>

Prepared by:	D. Mitchell Wilkes, Ph.D. <u>Ben A. Abbott</u> Lester E. Lynd, Jr. Richard S. Souder
Academic Rank:	Professor and Graduate Students
Department and	Electrical Engineering Department
University:	Vanderbilt University
Research Location:	AEDC Arnold AFB, TN 37389
USAF Researcher:	Capt. Ted Bapty
Date:	16 Aug 89
Contract No:	F49620-88-C-0053

Same Report As
Dr. Mitchell Wilkes
(Report # 19)

1989 USAF-UES SUMMER FACULTY RESEARCH PROGRAM/

GRADUATE STUDENT RESEARCH PROGRAM

Sponsored by the

AIR FORCE OFFICE OF SCIENTIFIC RESEARCH

Conducted by the

Universal Energy Systems, Inc.

<u>FINAL REPORT</u>

<u>Latin Hyper-Cube Sampling with Regression Analysis for</u>

<u>Prediction of Engine Infrared Observables</u>

Prepared by:	Darren Michael Allen, M.S.
Academic Rank:	Graduate Teaching Assistant
Department and	Mathematics Department
University:	Middle Tennessee State University
Research Location:	AEDC
	Arnold AFB, TN 37389
USAF Researcher:	Tom Bentley, III
Date:	20 Sep 89
Contract No:	F49620-88-C-0053

Latin Hyper-Cube Sampling with Regression Analysis for

Prediction of Engine Infrared Observables

by

Darren Michael Allen

ABSTRACT

The Latin Hypercube Sampling (LHS) and Rank Regression codes from Sandia National Laboratories were ported to the IBM-PC to facilitate model development of jet turbine engine IR (Infrared) observables. A sample model was developed to illustrate the use of both programs and a step by step method developed for application to the actual engine data and/or model simulations produced by super-computer.

I. INTRODUCTION:

Mathematical models are often used to predict the behavior of physical phenomena, especially when the phenomenon in question is difficult to simulate in the laboratory or, for reasons of time and/or cost, is deemed unfeasible. Unfortunately, the mathematical models (and their associated computer codes) are often so complicated that the simulation of a particular input situation may require an inordinate amount of computer resources and it may thus be deemed unfeasible to evaluate all the needed possible inputs (McKay et al., A Comparison 239).

The goal with such difficult simulations is to construct a response surface (i.e. predict the model's behavior) after evaluating a predetermined set of input variables. The difficulty lies in choosing the set of input vectors to run to best predict behavior. Many methods of selection exist, the most commonly used (or not so widely as the case may be) methods are Monte Carlo (or random sampling), stratified sampling, and the method used on this project, Latin hypercube sampling (LHS). Clearly, even random sampling with work sufficiently well if the sample size is large enough. In the case at hand, the simulation of IR observables, the computational complexity of the modelling codes used (PARC, etc.) dictated the LHS method, since for a model of N variables, $1.25N$ is the minimum

Acknowledgements

I wish to thank the Air Force Systems Command and the Air Force Office of Scientific Research for sponsorship of this research. Universal Energy Systems must be mentioned for their concern and help administering the program and especially Sue Espy, for her efforts above and beyond the call of duty.

I would also like to thank the many people at AEDC who helped, including Keely Beale, Tom Bentley, III, Janice Denny, Brenda McDonald, and last but certainly not least, Dr. Steve Cobb, who kept me amused with his many stories of growing up in Missouri.

number of trials needed to build the response surface. For an in-depth discussion of the justification for choosing the LHS method, the reader is encouraged to read McKay, Beckman, and Conover (1978).

II. OBJECTIVES OF THE RESEARCH EFFORT:

At the time of my appointment, Tom Bentley, III, and others of Sverdrup Technology, Inc., at Arnold AFB had selected the LHS method and procured the LHS FORTRAN77 code from Ron Iman at Sandia Laboratories. The original code was written to run on a wide spectrum of mini- and mainframe computers, and a port for the IBM-PC was desired.

Upon completion of the IBM-PC port of the LHS code (designated LHSpc), developed with Lahey's FORTRAN77 compiler, F77L v2.22, an initial set of input vectors were created and a psuedo-engine model (and predicting equation) was developed. As the initial regression analysis was begun with Lotus Development Corporation's Lotus 1-2-3, it became apparent that a more useful statistical tool was needed. The STEP (Stepwise Regression with PRESS and Rank Regression) code by V.J. McDonough, K.E. Kemp, and Javier Rojo, was procured from Sandia Laboratories and ported to the IBM-PC (resulting in the STEPpc program) again utilizing the Lahey F77L compiler. Compatibility with the Microsoft FORTRAN 77 version 4.10 compiler was tested and the needed

routines developed to allow either language development system to be used. The IBM-PC ports of both codes, LHSpc and STEPpc, were shipped back to Sandia for further improvements, distribution, and use.

III.

The "psuedo-engine" (hereafter abbreviated PE) model developed to provide a demonstration of both programs and methods is defined $E(x)=10^{x_1} + \pi x_2 x_3 + rnd*10$, where rnd provides a random number in (0..1). The use of the random term is to give the illusion of experimental error, without it, the model and associated data analysis would be too "perfect". To begin the simulation process, a command file was created as input to LHSpc. Since the distribution of input parameters for our PE was not known, it was assumed to be uniform for all three variables, x_1, x_2, and x_3. The following command file was created with a word processor (any will do as long as they are capable of writing an ASCII text file) and used as input to LHSpc.

```
TITLE Sample Mock Engine Input File For LHSpc Demonstration
RANDOM SEED    -3527346
NOBS   15
UNIFORM   The 1st input parameter.
     0 1
UNIFORM   The 2nd input parameter.
     0 10
UNIFORM   The 3rd input parameter.
     0 25
OUTPUT CORR DATA
```

The run file above, ENGINE.LHS, was executed by LHSpc by the following command "C>LHSPC ENGINE.LHS". Note that LHSpc was located in the current directory when executed. This is not necessary, but it would be good computer management practice to have LHSpc, and STEPpc, as well as the command files for both programs in their own directory on a fixed disk.

An in-depth explanation of all commands for the LHSpc program may be found in the Latin Hypercube Sampling Program User's Guide by Iman, Davenport, and Zeigler. An explanation of the commands used for our PE follows.

TITLE	Title line for each page of program output.
RANDOM SEED	Initializes the random seed generator.
NOBS	Number of run vectors to generate.
UNIFORM	x_n: Generate a uniformly distributed random variable.
OUTPUT CORR DATA	Output an NV by NV (number of variables) correlation matrix for raw data as well as the ranks of the data. Print the complete sample (N observations by NV variables) followed by a complete listing of the ranks of each variable.

The output run vectors were written by LHSpc to a file on the default drive called VECTORS.OUT. This file was then imported to Lotus 1-2-3 to have the model calculations performed. It is at this point that the PARC code (or whatever IR model is being utilized) would be run if an actual engine were begin profiled. For the PE, $y = E(x_1, x_2, x_3)$ was calculated as well as x_1^2, x_2^2, x_3^2, $x_1 x_2$, $x_1 x_3$, $x_2 x_3$. These combinations were included because it was

determined that the model had a significant dependence upon them (obvious in the PE case, but not necessarily obvious in the real world). The generation of complete STEPpc input vectors (i.e., the run vectors output by LHSpc, appended with any combinations of independent variables thought by the user to be significant as well as the model-calculated dependent variables) must be done by someone with a thorough knowledge of the physical processes being modelled. If, for example, the input temperature is variable x_1 and the model is dependent upon the cube of the temperature, then x_1^3 should be calculated and included (as, say, $x_1 x_2$ was included in the PE model). The use of both the LHSpc and STEPpc programs <u>require</u> a solid understanding of the simulation. This is not a black-box approach but one which requires continual work and fine-tuning.

The file used for the statistical analysis of the engine model (i.e. input to STEPpc), ENGINE.STP, is printed in full below.

```
TITLE, "Mock" Engine Run - LHSpc (STEPWISE Regression)
DATA,10,0,1.
LABEL(1)=X1,X2,X3,X1~2,X2~2,X3~2,X1*X2,X1*X3,X2*X3,Y
MODEL,10=1+2+3+4+5+6+7+8+9.
STEPWISE,SIGIN=.05,SIGOUT=.10
PRESS
OUTPUT,CORR,STEPS,RESIDUALS
END OF PARAMETERS
(10(E10.4,1X))
1.626e-1 5.9664e0 9.4079e0 2.644e-2 3.5598e1 8.8508e1 9.702e-1 1.5298e0 5.6131e1 3.1081e1
2.092e-1 6.6492e0 2.1198e1 4.377e-2 4.4212e1 4.4937e2 1.3911e0 4.4351e0 1.4095e2 4.7847e1
5.229e-1 7.6298e0 1.6607e1 2.734e-1 5.8214e1 2.7578e2 3.9895e0 8.6833e0 1.2671e2 5.0815e1
```

```
7.687e-1 4.6006e0 1.309e1  5.908e-1 2.1166e1 1.7135e2 3.5363e0 1.0062e1 6.0223e1 4.2365e1
4.575e-1 7.484e-1 1.7448e1 2.093e-1 5.601e-1 3.0444e2 3.424e-1 7.9816e0 1.3058e1 2.2731e1
6.591e-1 8.0763e0 6.4943e0 4.344e-1 6.5227e1 4.2175e1 5.323e0  4.2803e0 5.245e1  4.0973e1
6.683e-1 1.661e0  7.7752e0 4.466e-1 2.7588e0 6.0454e1 1.1099e0 5.1958e0 1.2914e1 2.5135e1
1.380e-2 2.947e-1 1.006e1  1.905e-4 8.687e-2 1.0121e2 4.068e-3 1.389e-1 2.9651e0 1.8573e1
3.448e-1 7.1584e0 4.4538e0 1.189e-1 5.1243e1 1.9837e1 2.4683e0 1.5358e0 3.1883e1 3.7853e1
5.755e-1 5.1777e0 1.9887e1 3.312e-1 2.6809e1 3.955e2  2.9798e0 1.1445e1 1.0297e2 4.1218e1
9.156e-1 2.4331e0 2.4781e1 8.384e-1 5.9198e0 6.1412e2 2.2278e0 2.269e1  6.0295e1 4.4412e1
8.586e-2 9.0676e0 2.6339e0 7.371e-3 8.2222e1 6.9373e0 7.785e-1 2.261e-1 2.3883e1 3.9221e1
2.734e-1 3.0105e0 1.3416e1 7.474e-2 9.0629e0 1.7999e2 8.23e-1  3.6676e0 4.0388e1 2.5377e1
8.159e-1 9.6861e0 2.3307e1 6.657e-1 9.3821e1 5.432e2  7.9028e0 1.9016e1 2.2575e2 6.2067e1
9.920e-1 3.7526e0 7.586e-1 9.841e-1 1.4082e1 5.755e-1 3.7225e0 7.526e-1 2.8469e0 2.9409e1
END OF DATA
TITLE, "Mock" Engine Run - LHSpc (BACKWARD Regression)
DATA,10,0,2.
LABEL(1)=X1,X2,X3,X1^2,X2^2,X3^2,X1*X2,X1*X3,X2*X3,Y
MODEL,10=1+2+3+4+5+6+7+8+9.
BACKWARD,SIG=.05
OUTPUT,CORR,STEPS,RESIDUALS
PRESS
END OF PARAMETERS
TITLE, "Mock" Engine Run - LHSpc (STEPWISE RANK Regression)
DATA,10,0,2.
LABEL(1)=X1,X2,X3,X1^2,X2^2,X3^2,X1*X2,X1*X3,X2*X3,Y
MODEL,10=1+2+3+4+5+6+7+8+9.
STEPWISE,SIGIN=.05,SIGOUT=.10
PRESS
RANK REGRESSION
OUTPUT,CORR,STEPS,RESIDUALS
END OF PARAMETERS
```

As with LHSpc, the STEPpc input file commands are documented completely in Stepwise Regression with PRESS and Rank Regression, Program User's Guide by Iman, Davenport, Frost, and Shortencarier. The command used to execute the ENGINE.STP file (which, like the LHSpc input file, may be created with any ASCII editor) is "C> STEPPC ENGINE.STP".

Although the output is too lengthy to include in full, the most significant information can be seen on the pages titled **CORRELATION MATRIX** and **AOV**. Selected pages of the

actual STEPpc output are reproduced below to show the significant parts which the user should be concerned with.

          SANDIA LABORATORIES <><> STEPWISE REGRESSION <><> FROM KANSAS STATE UNIVERSITY

                                    CORRELATION MATRIX

X1	1	1.0000								
X2	2	-.0162	1.0000							
X3	3	.1954	-.0461	1.0000						
X1^2	4	.9654	-.0625	.1249	1.0000					
X2^2	5	-.0672	.9671	-.0312	-.0983	1.0000				
X3^2	6	.3011	.0227	.9686	.2630	.0389	1.0000			
X1*X2	7	.6483	.6116	.2043	.5938	.6073	.2797	1.0000		
X1*X3	8	.6152	.0405	.8120	.5619	.0588	.8614	.4880	1.0000	
X2*X3	9	.1927	.6098	.6813	.1210	.6091	.6950	.6701	.5786	1.0000
Y	10	.2036	.6058	.6853	.1335	.6063	.7013	.6737	.5898	.9998	1.0000
	NO.	1	2	3	4	5	6	7	8	9	10
	NAME	X1	X2	X3	X1^2	X2^2	X3^2	X1*X2	X1*X3	X2*X3	Y

          SANDIA LABORATORIES <><> STEPWISE REGRESSION <><> FROM KANSAS STATE UNIVERSITY
                                       AOV TABLE
                        ANALYSIS OF REGRESSION FOR VARIABLE 10---Y
                                       (TABLE 1)

SOURCE	D.F.	SS	MS	F	SIGNIFICANCE
REGRESSION	5	530995.70	106199.10	24665.610	.0000
RESIDUAL	9	38.750000	4.3055550		
TOTAL	14	531034.40			

$R^{**}2$ IS   .99993
INTERCEPT IS   7.9029620
STANDARD ERROR OF INTERCEPT IS   1.68828

VARIABLE NUMBER	VARIABLE NAME	REGRESSION COEFFICIENTS	STANDARDIZED REGRESSION COEFFICIENTS	PARTIAL SSQ	T-TEST VALUES	R**2 DELETES	ALPHA HATS
2	X2	-1.7486290	-.027021	24.5275	-2.3868	.9999	.0408
4	X1^2	15.030270	.024450	88.1103	4.5238	.9998	.0014
5	X2^2	.21457760	.033750	33.8988	2.8059	.9999	.0205
7	X1*X2	-1.6591940	-.018274	25.7235	-2.4443	.9999	.0371
9	X2*X3	3.1627520	1.005042	230682.1000	231.4688	.5655	.0000

UNIQUE SEQUENCE NUMBER FOR THIS ANOVA =   107
PRESS IS   120.61

              SANDIA LABORATORIES <><> STEPWISE REGRESSION <><> FROM KANSAS STATE UNIVERSITY
                            TABLE OF RESIDUALS FOR VARIABLES 10----Y

TIME	OBSERVED	PREDICTED	RESIDUAL	95 PER CENT CONF INT (MEAN)		95 PER CENT CONF INT (INDIV)	
1	180.890	181.425	-.534637	179.166	183.683	176.216	186.634
2	447.380	449.903	-2.52261	446.663	453.142	444.199	455.606
3	407.970	405.295	2.67508	403.387	407.202	400.228	410.362
4	199.710	197.883	1.82684	195.762	200.004	192.732	203.034
5	49.2870	50.5909	-1.30387	47.9562	53.2256	45.2080	55.9737
6	169.450	171.360	-1.91037	168.106	174.615	165.649	177.072
7	50.7790	51.3046	-.525623	49.2945	53.3147	46.1984	56.4108
8	17.9350	16.7702	1.15478	13.3092	20.2512	10.9423	22.6181
9	106.970	104.911	2.05909	102.488	107.334	99.6287	110.193
10	330.470	330.304	.165741	328.063	332.546	325.103	335.506
11	206.630	204.521	2.10896	201.231	207.811	198.789	210.253
12	84.3610	84.0452	.315826	79.7518	88.3385	77.6839	90.4065
13	131.120	132.078	-.958450	129.839	134.318	126.878	137.279
14	721.470	721.982	-.511841	717.701	726.262	715.629	728.335"
15	19.9420	21.9810	-2.03897	18.6115	25.3505	16.2028	27.7591

Page 3 of the output contains the correlation matrix. It should be of no surprise that x_1 has a high correlation with x_1^2 (and less so with $x_1 x_2$ and $x_1 x_3$). If the regression analysis had to be done by hand, this would be the place to start. Only those variables with a marked significance would make good predictors and would be the ones added to the model until a satisfactory fit was found. Thankfully, STEPpc does all the work.

Page 8 of the output contains, among other things, the set of variables chosen for the model along with their respective regression coefficients. The next printed page, page 10 shows the predictions of the model as well as the observed values (those supplied by experiment or simulation). We see that the predicted values closely match

those observed and seems to satisfy our requirements. It should be noted that occasionally one method of regression (or one determination of significant variables) may yield a seemingly better fit for the observed values (or simulated values) than another, but spurious ridges and valleys may have created in the response surface to minimize the sum of the squares of residuals. It is to alleviate this problem that the **PRESS** value is used. The simplest way to determine the best model is to use STEPpc to do both forward and backward regressions, along with calculating the **PRESS** value for each regression. The set of regression coefficients which yield the lowest **PRESS** value is probably the best fit. This, however, is not an absolute. Any choice of regression method and result should be made based on a solid understanding of the physical processes being modelled as well as the intuition of the user.

> "All of these procedures are merely aids in the decision making process. They should be considered in addition to expert advice, not instead of expert advice. Amateur statisticians often make the mistake of having either too little or too much faith in the methods of regression analysis. Professional statisticians often make the same mistake, but to a lesser extent. The better these regression methods are understood, the more likely it is that the results of a regression analysis will be given its proper weight in the final decision process (Iman and Conover, Sensitivity-Analysis 99)

IV. RECOMMENDATIONS:

a. Tom Bentley, III, or another in the EL1 Group who is intuitively familiar with the IR behavior of the engine being modelled should determine the distributions of the input parameters (i.e., altitudes, Mach numbers, etc.). If this is not possible, then a uniform distribution may be used for all variables.

b. When input distributions have been determined, the appropriate LHSpc run file can be created (with any editor capable of writing ASCII text files) and then this file executed.

c. Once a satisfactory set of run vectors has been output from LHSpc (i.e., no unwanted correlations between random variables), the model must be evaluated for each of the sets of input vectors, either in the laboratory or by the PARC (or other) code on the super-computer.

d. The model-calculated dependent variables should then be appended (column-wise) to the run-vectors created by LHSpc along with any combinations thought to be significant, for instance, the square of the temperature. This should then be used as input to STEPpc (with the appropriate commands).

e.   STEPpc should then be executed and the results interpreted by Tom or someone else suitably acquainted with the engine so a determination can be made of the "best" set of regression coefficients. The model is then complete.

REFERENCES

Iman, Ronald L. et al. "An Approach to Sensitivity Analysis of Computer Models: Part II - Ranking of Input Variables, Response Surface Validation, Distribution Effect and Technique Synopsis." _Journal of Quality Technology_ Vol. 13, No. 4 (1981): 232-239.

Iman, Ronald L. and Michael Shortencarier. _A FORTRAN 77 Program and User's Guide for the Generation of Latin Hypercube and Random Samples for Use With Computer Models_. SAND83-2365. Sandia National Laboratories (1984).

Iman, Ronald L. et al. _Stepwise Regression With PRESS and Rank Regression (Program User's Guide)_. SAND79-1472. Sandia National Laboratories (1980).

Iman, Ronald L. et al. _Sensitivity-Analysis Techniques: Self Teaching Curriculum_. NUREG/CR-2350. U.S. Nuclear Regulatory Commission (1982).

Iman, Ronald L. et al. _Latin Hypercube Sampling (Program User's Guide)_. SAND79-1473. Sandia National Laboratories (1980).

McKay, M.D. et al. "A Comparison of Three Methods for Selecting Values of Input Variables in the Analysis of Output from a Computer Code." _Technometrics_ Vol. 121, No. 2 (1979): 239-246.

1989 USAF-UES SUMMER FACULTY RESEARCH PROGRAM/

GRADUATE STUDENT RESEARCH PROGRAM

Sponsored by the

AIR FORCE OFFICE OF SCIENTIFIC RESEARCH

Conducted by the

Universal Energy Systems, Inc.

FINAL REPORT

PLOTTER:

A GENERAL PURPOSE TWO DIMENSIONAL PLOTTING PROGRAM

Prepared by: Brian W. Bennett

Academic Rank: Graduate Student

Department and   Department of Computer Science

University: Middle Tennessee State University

Research Location: AEDC
                      Calspan Corp.
                      CFD Group
                      Arnold AFB, Tennessee   37389

USAF Researcher: Frederick L. Shope

Date: 25 Aug 89

Contract No: F49620-88-C-0053

A New User Friendly Two Dimensional Plotting Program
for the Cray Time Sharing System

by

Brian W. Bennett

ABSTRACT

The program was designed to make quick two
dimensional plots using the graphics package DISSPLA.
The program that was currently in use was not easily
modified if anything other than a linear plot was
desired. After talking with the group members about
what changes they would like to see, these suggestions
were incorporated into the new program. The program was
written in FORTRAN 77 using structured programming
techniques. A semi menu driven format was also
employed. A final summary page of all parameters
entered by the user is presented for a final
confirmation before the plot is actually drawn. This
allows for correction of any typographical errors.

Acknowledgments

I would like to thank the Air Force Systems Command
and the air Force Office of scientific Research for
their sponsorship of this program. I would also like to
thank Universal Energy Systems for their administration
and especially Barbara Vincent for her patience and help
with my security clearance.

I would like to thank Jim Curtis and Mouphid
Aboulmona for their insights into the workings of AEDC
and Calspan and their input into the project. Thanks go
to Fred Shope for getting me into the project. And
finally big thanks to Ged Gasperas for the use of his
terminal without which the program would never have been
written.

I. INTRODUCTION

Before 1983, there was not a general purpose
plotting program for the Cray Time Sharing System. The
ability to graphically see the results of computed data
is a great help in the prediction of flow fields
surrounding aerodynamic bodies. In September of 1983 an
inhouse written program named PLOTTER was made
available. This program would quickly draw two
dimensional plots using either linear, polar, or
logarithmic scaling.

The program PLOTTER has been used to generate two
dimensional plot. However, the problem with this
program was that if the automatic scaling function was
not used and a mistake was made in the input of
parameters, there was no way to make a correction
without going back through the program again. This was
very time consuming which resulted in the program not
being utilized to its fullest potential.

My interests have been in computer graphics and
user interfaces with graphics programs. Having just
completed a one year sequence in compiler theory and
computer graphics, the programming techniques

plots. So another objective was to make the logarithmic
and polar plotting options easier to use.

Also, for future modifications the program was to
be documented fully internally. This would allow future
modifications to the program to be made easily.

III.

From talking with the other group members, the
biggest complaint about the program currently in use at
AEDC was the inability to correct inputs. This became
the primary objective of the project. After examining
the old program, it was discovered that every input that
was given to the program, including the yes and no
answers, was stored in the output file. This was a very
inefficient method of storage and made making
corrections impossible. A new means of data storage had
to be developed. This meant coding separate subroutines
to write inputs to the data file for each of the three
types of plots which can be produced by the program
(polar, logarithmic, and linear). In each of these
subroutines, only the actual data inputs are stored.
This allows for easier access to the data from the
program and facilitates ease of corrections and/or

demonstrated in these classes were of great help in the design of the new program.

II. OBJECTIVES

The current program in use at AEDC was written in FORTRAN IV which did not use structured programming techniques. It was determined that the new program should be written in FORTRAN 77 which does make use of structured programming. Also the old program did not allow for correction to numeric inputs before the graph was plotted.

My task was to create a program that was partially menu driven and allow for correction to the numeric inputs before the plotting took place. Also, the program was very cumbersome to use if the automatic scaling option was not employed. The automatic scaling option only allowed for the production of a linear plot, so if either a logarithmic or polar plot was needed the process to produce such a plot became somewhat difficult. From talking with other group members, it was determined that the program was not used very much for anything other than production of simple linear

changes before the plot is drawn.

Also to assist in making corrections, before each
plot is drawn a summary page is presented with all of
the inputs displayed (Figure 1). This is the point at
which any corrections to the inputs must be made. The
numbers before each entry are used for the correction
process. If a previous run is being used there is an
option of turning off the summary page.

The next major objective was to internally document
the program. This is a necessity for any good program.
This allows anyone who wishes to modify the code to make
use of future additions or modifications to DISSPLA or
make changes in the program to customize it for his or
her own use, to do so easily. For each subroutine every
variable used in that particular subroutine is defined.
For the main program every variable used in the program
is defined. Also inside each subroutine there are
comments which describe what each part of the code is
doing. This is invaluable in finding the appropriate
part of the program whenever bugs occur.

Finally, the program was designed to be partially
menu driven. That is, the user is presented with a list
of choices and is asked to pick one. His choice directs

6-7

the program to prompt him for the appropriate inputs for the particular graph he has chosen.

This program is a more efficient and easier method of doing general two dimensional plotting. This will increase the productivity of those who use it.

IV. RECOMMENDATIONS

One of the problems with any graphics plotting using a mainframe computer as a host is the time required for the data transmission to and from the host. Since the program was written and debugged on a personal computer before being loaded onto the mainframe, it would be advantageous to acquire a site license from Computer Associates for DISSPLA to be run on some of the personal computers. The ideal situation would be to have DISSPLA on every PC but realistically at least one computer per office should have it and be connected to a printer that would produce the proper graph. This would take a great burden off of the Cray and get result to the staff quickly.

From observations of the work in the CFD group, it appears that quick three dimensional plotting is also a

major aid in their work. An extension of PLOTTER to
three dimensions would be of great help.

```
------------------------------------------------------------

            ***   PLOT SUMMARY   ***

1) Plot type:              Linear
2) Page size:              9.00000" x     7.00000"
3) Axis Labels - X: X - AXIS
                 Y: Y - AXIS
4) Heading: PLOT HEADING
   Character Height:         .2800"
5) Grid:                   Solid
   Grid lines/division - X: 2
                         Y: 2
6) Axis Lengths - X:          5.50000      10) Border: No
                  Y:          3.50000
7) X-axis - Start:           -20.000       11) Supress points: Yes
            End:              60.000
     Increment:               10.000
8) Y-axis - Start:          -100.00        12) Frame: Yes
            End:             100.00
     Increment:               50.000
9) Symbols: Connected
   Every  10 points a symbol.


            FIGURE  1.   Summary page
```

REFERENCES

Display Integrated Software System and Plotting Language Users Manual. Version 10.0. Computer Associates International, Inc. 1987.

Microsoft Fortran Compiler User's Guide. Zenith Data Systems. 1984.

Program PLOTTER User's Guide. Arnold Engineering Development Center. 1983.

1989 USAF-UES SUMMER FACULTY RESEARCH PROGRAM/

GRADUATE STUDENT RESEARCH PROGRAM

Sponsored by the

AIR FORCE OFFICE OF SCIENTIFIC RESEARCH

Conducted by the

Universal Energy Systems, Inc.

FINAL REPORT

MATRIX INVERSIONS ON CANDIDATE GEOMETRIES
FOR APPLICATION OF CT EMISSION TECHNIQUES
TO BROAD BAND RADIATIVE TRANSFER

Prepared by:	Judy E. Dye
Academic Rank:	Graduate Student
Department and	Department of Mathematics
University:	University of Alabama
Research Location:	AEDC Arnold AFB, TN 37389-5000
USAF Researcher:	Charles Limbaugh
Date:	August 7, 1989
Contract No:	F49620-88-C-0053

MATRIX INVERSIONS ON CANDIDATE GEOMETRIES FOR APPLICATION OF CT EMISSION TECHNIQUES TO BROAD BAND RADIATIVE TRANSFER

by

Judy E. Dye

Abstract

This reports the effort undertaken to lay the groundwork for the application of the emission techniques of computed tomology to broad band radiative transfer for the determination of gas properties (temperature, pressure) of hot radiating gases at the interior of combustion flames and burners. Matrix inversion was done on several geometries with a first-order examination of sensitivity.

Acknowledgments

I have enjoyed my participation in the GSRP and sincerely thank the Air Force Systems Command and the Air Force Office of Scientific Research for their sponsorship. I commend Universal Energy Systems for their efficient administration of this program.

Working with the men and women at Sverdrup was a pleasant and rewarding experience. I found support there from many whose names I never learned. I hope they know their kindness was appreciated. Special thanks go to Charles Limbaugh who spent valuable time inspiring and guiding this effort. Thanks also go to Bill Phillips who was a first-class supervisor. Jim Sirbaugh and Mike Stokes provided considerable help in learning to use the Apollo work stations. Robert Hiers, Jr. helped time and again with applications needing access to the main frame computer. Carlos Tirres was in every way supportive and has done a fine job supervising the summer faculty program.

Finally, I thank Dr. Richard Tipping, my supervising professor, for helping me to enter the program and for assisting me in every aspect of the work. His clarity of thought and presentation are an inspiration.

I. INTRODUCTION

A recent observation, inspired by and shared with Chad Limbaugh, is that english composition (in particular, the preparation of this final report) is an iterative procedure. It occurs that the development of the diagnostics for combustion flames and plumes is also an iterative procedure. Data collection methods have improved with the advent of increasingly sensitive detectors and high-resolution spectrometers. A vast database of spectroscopic parameters for reacting gases is in the process of expansion (Rothman, et.al.). If diagnostic procedures are to reflect this advance in data quality, a corresponding improvement must be made in the mathematical models used for emission inversion.

The current method of choice for modelling broad band radiative transfer is the Abel inversion or "onion peel" (Limbaugh, 1985) which is limited by an assumption of cylindrical symmetry of the spatial distribution of properties (e.g. species temperature, pressure) considered important for the diagnostics. The success of computed tomology techniques (CT) in medical and industrial diagnostics suggests similar methods might be used to model more accurately the densities in a cross-section of combustion flames and plumes.

CT methods have been defined as "the reconstruction of a clean image of the density from digital computational operations on measurements of emanations that have passed through the body". More specifically, a "clean image of the density is one for which the value reconstructed at any spatial point is (ideally) uncontaminated by values of the true density outside the

neighborhood of the point". (Bates, et.al.) An Abel inversion may be loosely classified as a CT method, failing to qualify only in that the reconstructed image is not "clean" (the neighborhood of possible contamination is the entire "body").

In medical diagnostics, the familiar CAT scan uses low-level x-ray to obtain a "clean" image of internal organs of the body. In some applications of x-ray remote-probing, there may be as many as 100,000 scans across the "body". (Herman, 1975) The damage done by this radiation precludes its use for some applications, for instance the imaging of a developing fetus. The need for improved diagnostics in Obstetrics led to the development of CT methods using Ultra-Sound. Similarly, research suggests that probing a rocket plume with standard x-ray CT methods would require the use of unacceptably high levels of radiation to obtain acceptable resolution of the image.

Without disregard for the possibilities of remote-probing, we consider here the potential of remote-sensing emission CT for plume diagnostics. Although there has been no known application of the emission techniques to broad band radiative transfer for the determination of gas properties, emission inversion techniques for single line radiative emission preceded the x-ray based medical and industrial applications by several years. These earlier single line inversion techniques were applied to an optically thin media, a characteristic often met by broad band molecular emission. This observation led to the present effort to investigate the use of a simple matrix inversion on various

plume geometries with known solutions and slightly perturbed data as a first-order examination of the sensitivity of the inversion. This reports the results of that effort in order to provide guidance as to the efficacy of the approach and to focus on areas for future research.

II. PLUME CROSS-SECTION GEOMETRIES

I will not attempt to summarize here the theory of Infrared Emission-Absorption and its defining equations. For these I refer to the work of Limbaugh(1985), Monnig, et.al(1988), and Wang(1977). The problem is presented in the broader terminology of CT methods (Bates et.al.,1983). A detector scanning a circular cross-section of a plume receives a signal $s(r',a')$ produced by the cumulative emissions along a line of sight intersecting the circle at points A and B. The variables r' and a' are the radial and angular position of the detector. If emission from the region outside the plume is considered negligible, the signal can be represented by the integral along chord AB

$$s(r',a') = \int_{l(A)}^{l(B)} e(r,a) \, dl \qquad (1)$$

The unknown densities $e(r,a)$ along the line of sight are a function of the radial and angular position (r,a) and therefore a function of l, the distance from point A on the chord. If the plume is divided into a number of regions or elements small enough so that e may be considered constant within each element, the signal (eqn. 1) may be approximated by the Riemann sum

$$s(i) = \sum_{j}^{nel} l(i,j)*e(j) \qquad (2)$$

7-6

where nel is the total number of elements in the circle and $l(i,j)$ is the length of intersection of sight line i with element j. If there are at least nel measured signals, if each element is traversed by at least one sight line, and if all lines are linearly independent, the unknown emissions may be found by inversion of the system of linear equations

$$Le=S. \tag{3}$$

The process of choosing among an infinite number of possible plume geometries is constrained to a certain extent by the need to minimize the cost of the detectors and, more particularly, the number of angles of projection. Consequently, the first geometry investigated (Fig. 1) uses only two angles of projection.

A. Geometry 1: The "Chair-Weave"

A sample case of the first geometry (Fig.1) uses two perpendicular projections with 29 parallel lines of sight intersecting 29 elements of the circle. It was assumed that a cross-section of a plume with 4 cm radius has cylindrical symmetry in the measured radiance. The values of signals vector S are taken from a simulated data curve (Fig. 2). Sight line j is the line passing through the long dimension of element j. With this ordering, lengths matrix L is nearly upper-triangular and (3) is easily solved. The values of vector S and the computed solutions of the unknown emissions vector e are as follows:

```
s(1)          =  56.8D-5,  e(1)          =  .1261236743784E-03
s( 2, 3, 4, 5) =  51.6D-5,  e( 2, 3, 4, 5) =  .1030517098763E-03
s( 6, 7, 8, 9) =  44.2D-5,  e( 6, 7, 8, 9) =  .6372872410345E-04
s(10,11,12,13) =  36.0D-5,  e(10,11,12,13) =  .5236847992430E-04
s(14,15,16,17) =  30.5D-5,  e(14,15,16,17) =  .4422045482845E-04
s(18,19,20,21) =  28.0D-5,  e(18,19,20,21) =  .4819712608614E-04
s(22,23,24,25) =  27.1D-5,  e(22,23,24,25) =  .5810849938821E-04
s(26,27,28,29) =  20.1D-5,  e(26,27,28,29) =  .7220133141476E-04
```

If data vector S is taken to be exact, the solution is correct to the extent that it reflects the cylindrical symmetry to be modeled. Using this geometry, it is possible to increase (to the limits of optical resolution of the signals) the number of lines of sight used from each angle of projection and thereby reduce the width of each element. However, the outer elements remain long and narrow, the neighborhood of possible contamination of the image is greater than 1/2 the diameter, and increasing the number of lines of sight will not result in a cleaner image (in CT, a problem called aliasing).

Monnig, et.al.(1988) offer the following criterion for bandlimiting resolution:

$$m=(pi/2)n \qquad . \qquad (4)$$

Here n is the number of data points in a single lateral projection and m is the number of projection angles which must be equally spaced over at least 180 degrees. The sample case in Figure 1 has 15 lines of sight at each projection angle (n=15). By criterion (4), standard CT methods would require 24 projection angles for this problem. To explain this, the model equation (3) can be replaced by the model

$$Le + V = S \qquad (5)$$

which includes a noise vector V. There are at least two components of vector V. The first, called N-measurement noise, results from error in the measured signal. The least-squares spline methods described by Limbaugh (1985) or the Kalman filter of Wood, et.al. (1979) could be used to minimize the size of this

noise. In many CT applications, data smoothing cannot reduce the size of the second component of the noise vector, the "model noise" (Wood, Macovski, and Morf: comments of G. Herman, 1979), which results from the failure of the arrangement of elements in the geometry to match sharp changes in density of the object to be reconstructed. To minimize aliasing, a high number of projection angles is required. However, it can be argued that while there may be steep temperature and pressure gradients in the cross-section of a plume, there should be no boundaries or discontinuities of the densities which need to be brought into focus. If this argument is valid, then the model noise for this application is actually a discretization error and will be of order max(l), the largest value in the lengths matrix L. This aspect of the problem deserves further investigation.

B. Geometry 2

Two criteria were considered in developing the software to configure the elements in the second geometry (Fig. 3). First, by entering an integer called RES, the operator can control the size of the elements of the lengths matrix L. If RAD is the radius of the cross-section, we have

$$\max(l) = RAD/RES \quad . \quad (6)$$

To meet this criterion, the circle is first divided into RES concentric rings. Each ring is divided into NREL elements of equal size by the formula

$$NREL = (2*RES-1)*4 \quad . \quad (7)$$

With RES=3 (Fig. 3), there are 20 elements in each of 3 concentric rings.

As a second criterion, the code allows for variation in the number of scanners (projection angles), their radial and angular position, the number of lines of sight at each angle, and the size of the angle separating these lines of sight. A parallel-line scan can be modeled by sufficiently increasing the radial position of the scanner and reducing the angle between lines of sight.

Using this geometry with RAD=4, RES=4, and 14 scanners spaced evenly over 180 degrees, the values of S below were taken from the simulated data set (Fig.2) to compare solutions with those obtained in Geometry 1 above. As in Geometry 1, the solutions have cylindrical symmetry to the 7th decimal, giving the following emission coefficients from center to outer ring:

```
Radiance from Fig.2            Emission Coefficients
s(ring 1) = 54.0D-5            e(ring 1) = 0.1168819E-03
s(ring 2) = 40.0D-5            e(ring 2) = 0.6767451E-04
s(ring 3) = 29.0D-5            e(ring 3) = 0.3044490E-04
s(ring 4) = 25.0D-5            e(ring 4) = 0.6454972E-04
```

The data sets were for RAD=1 and RES=3. Data set D has 10 projection angles (# scans=10) each having 6 lines of sight. All other data sets are for 3 projection angles having 20 lines of sight each, with the 3 centerlines being included in sets A and C.

Gaussian elimination with row pivoting was used to compute $\|L^{-1}\|_{\infty}$ by back substitution. The relative error for (5) can be bounded by the following

$$\frac{\|e - \tilde{e}\|}{\|e\|} \leq \frac{K(L)}{1 - K(L)*(\|dL\|/\|L\|)} \cdot \left[\frac{\|dS\|}{\|S\|} + \frac{\|dL\|}{\|L\|} \right] \quad (8)$$

The last term on the right is a measure of numeric or roundoff error. Since all computations were done in double precision, the

roundoff error can be considered negligible. In the Data Sets recorded here, the geometry was fixed and therefore $\|L\|_\infty$ is close to the diameter (2 units). The condition number K(L) is a constant multiple of $\|L^{-1}\|_\infty$ and (8) can be simplified as

$$\frac{\|e - \tilde{e}\|}{\|e\|} \leq \frac{2\|L^{-1}\|\cdot\|v\|}{\|S\|} \qquad . \qquad (9)$$

To observe how solutions varied with the size of $\|L^{-1}\|_\infty$, vector e was assumed known to be the step function e(i,j)=i where i is the ring number. The actual vector S was computed, perturbed uniformly, and the corresponding solution vector e was computed. While this shows how well the model handled a perturbed case having cylindrical symmetry (as for instance when there is calibration error), random perturbations are suggested for further research.

III. CONCLUSIONS

The following are some observations based on the results given in the data sets:

1. Decreasing the number of projection angles increases the number of lines passing through each ring and consequently the probability of singularities like the one in data set AA at scanr=4. This singularity is removed by using the centerlines as in set A. In selecting the sightlines to be used for the rows of L, a set should be chosen with the smallest angle of incidence between lines.

2. The "best" solutions to the perturbed problem were obtained in Data Set D (10 Scanners). The solutions had cylindrical

symmetry and varied from the step function by about twice the
size of the perturbation in S. This is a particular case of the
geometry suggested by Wang (1977) in which scanners are equally
spaced over 180 degrees. Solutions may be obtained ring-by-ring,
as in the Abel inversion, the matrices used are nearly band-type,
and storage requirements and computation times can be reduced
dramatically allowing for much smaller elements.

3. With only 3 scanners, the best solutions were obtained when
the angle between scanners was equal. Using this arrangement it
is necessary to avoid the periodic singularities evidenced in
Data Set L. Strong singularities occur at 6 degree intervals of
rotation of the scanners, suggesting this arrangement has
close to the largest number of elements which may be used with 3
scanners spaced symmetrically. It should be noted that even with
the largest norms, solutions for this particular perturbation
were feasible (non-negative) and more accurate (closer to the
step function values) than when scanners were not equally spaced.
In the latter case, non-feasible solutions and huge error can
occur even when the norm is very low, suggesting the source
of error is model noise which can be reduced only by increasing
the number of scanners to reduce the size of the elements.

4. Using this fixed geometry (Fig.3) , there is a lower bound on
the norm near 1500. This baseline level is probably the result
of the increasingly smaller size of the inner elements. Future
effort should address uniformity of element size.

5. Two geometries are suggested for future efforts. The first

geometry is one used by Wood, et.al. (1979) (Fig. 4). This
configuration has the advantages of the geometry of Wang
discussed in 2 above and is designed for applications with a
limited number of projection angles. The second geometry, called
the "H Grid" (Fig. 5), was created by Robert Hiers, Jr. at AEDC
to enable the use of existing contouring packages on circular
geometries. I thank Robert for permitting me to include a
version of it here.

6. Perhaps the most attractive feature of the matrix inversion
is that the geometry can be chosen and refined, the matrix
inverted, and a sensitivity analysis completed on mock data, all
prior to actual test firing.

IV. A BRIEF REPORT OF OTHER WORK
Reference was made in the introduction to HITRAN, the database of
spectroscopic parameters for reacting gases now in the process of
expansion. (Rothman, et.al.) I had the privilege of working with
Dr. Richard Tipping in generating data for several of the
reaction gases. Dr. Tipping has prepared a separate report fully
detailing this work. I present here (Fig. 6) one graphic that is
designed to show the temperature dependence of a series of
spectral lines for these gases, in this case for water vapor.

DATA SETS

To determine the effect on the norm of L Inverse due to:
1. Change in scanner Radial Position
2. Use of scanner centerlines (an overdetermined set)
3. Increase in number of scanners

------------------ ----------------- ----------------------

Data Set: A	Data Set: AA	Data Set: D
Radius: 1.0	Radius: 1.0	Radius: 1.0
Res: 3	Res: 3	Res: 3
Frac: 0.5	Frac: 0.5	Frac: 0.5
# Scans: 3	# Scans: 3	# Scans: 10
a(1): 3pi/10	a(1): 3pi/10	a(1): pi/20
a(2): 17pi/24	a(2): 17pi/24	a(i): pi/20+
a(3): 29pi/20	a(3): 29pi/20	a(i-1)*pi/10
		(scans at element ctrs)
RowXCol: 63X60	RowXCol: 60X60	RowXCol: 60X60

	With C/L	Without C/L	Without C/L
Scanr(1,2,3)	Norm(LInv)	Norm(LInv)	Norm(LInv)
1	10,698	13,527	3,711,497
2	2,673	49,615	7,653
3	11,213	12,898	6,720
3.9	-	17,988	-
3.994	-	2,094,477	-
3.994994994994	-	219,835,695	-
3.994994994994994	-	219,835,693	-
3.995	-	143,497,178	-
4	1,354	416,370	2,081
5	1,392	2,656	2,367
6	1,708	2,406	2,903
6.5	-	1,913	3,761
6.6	-	1,905	-
6.61	-	1,905	-
6.7	-	1,916	-
7	1,192	2,066	5,409 (See Set I)
8	2,022	3,316	7,877
9	1,927	5,806	10,353
10	3,644	15,399	13,860
20	8,007	10,269	6,056
100	9,101	113,723	2,392
1.0E03	199,261	325,780	2,218
1.0E04	2,047,208	2,288,152	2,213
1.0E05	20,572,759	14,244,232	2,213
1.0E10	117,054	336,810	2,213
1.0E15	15,020	100,456	26,344*
1.0E16	fails*	fails*	
1.0E20	fails*	fails*	

* Failure Attributed to method employed to compute
  intersection lengths

To determine the effect of eqi-angular spacing between
scanners:

1. When the scanner radial position is varied
2. When centerlines are used (to find degree of singularity)

Note: The solutions obtained using eqi-angular spacing are
      feasible (i.e. no negative values), even in the cases
      having high norms.

-------------------- ------------------- --------------------

Data Set: E	Data Set: B	Data Set: C
Radius: 1.0	Radius: 1.0	Radius: 1.0
Res: 3	Res: 3	Res: 3
Frac: 0.5	Frac: 0.5	Frac: 0.5
# Scans: 3	# Scans: 3	# Scans: 3
a(1): 0	a(1): pi/40	a(1): pi/40
a(2): 2pi/3	a(2): pi/40+2pi/3	a(2): pi/40+2pi/3
a(3): 4pi/3	a(3): pi/40+4pi/3	a(3): pi/40+4pi/3
RowXCol: 60X60	RowXCol: 60X60	RowXCol: 63X60

Scanr(1,2,3)	Without C/L Norm(LInv)	Without C/L Norm(LInv)	With C/L Norm(LInv)
1	478,307	176,080,147,834	4,648,002,259
2	12,514	10,310,470,452	3,042,381,258
3	17,462	3,059,363,933	-
4	-	99,239,017,070	-
5	18,409	1,589,017,799	- (See L)
6	-	27,152,048,445	-
7	20,900	-	-
8	1,146,484	-	-
9	5,464	-	-
9.3	4,789	-	-
9.4	4,666	-	-
9.5	4,601	-	-
10	4,645	1,980,506,084	1,018,178,376
10.5	5,492	-	-
11	7,286	-	-
15	11,046	-	-
100	274,459	18,227,053,257	4,521,080,595
1.0E05	-	fails*	59,691,766
1.0E10	-	-	359,819,479

To determine the effect of eqi-angular spacing between
scanners when scanner positions are rotated by "Ang" degrees.
Geometry is 3 rings with 20 elements per ring. Each element
spans 18 degrees and has radial thickness of 1/3.
(Scanner radial position is fixed.   See sets E and B
for change in radial position):

Note: 1.   The solutions obtained using eqi-angular spacing are
           feasible (i.e. no negative values), even in the cases
           having high norms.
      2.   The calculated norms repeat at 6 degrees intervals.

        Data Set: L
          Radius: 1.0
             Res: 3
            Frac: 0.5
         # Dets: 3
Scanr(1,2,3): 5.0
            a(1): 0+Ang degrees
            a(2): 120+Ang degrees
            a(3): 240+Ang degrees
         RowXCol: 60X60

	Without C/L
Ang	Norm(LInv)
0	18,409
9	1,589,017,799
10	12,835
11	13,354
12	18,408
13	13,355
13.5	12,757
13.99999	12,835
14	12,835
14.00001	12,835
14.5	19,345
15	3,998,743,902
15.00001	376,257,961
15.5	19,345
16	12,839
17	13,355
18	18,408
19	13,355
20	12,835
21	1,344,179,321
27	784,325,344
28	12,835
29	13,354
30	18,408
33	734,325,344
39	6,347,781,672
369	1,500,384,611

To show the effect of sightline placement across the plume:
The geometry has 3 scanners, each having 20 lines of sight
(not including the center line). The outer line is arbitrarily
chosen to pass through the scanner and a point some fraction
(Frac) of the radial width of a ring inside the circle (measured
along the line bisecting the circle perpendicular to the
centerline). The angle between the outer line and the centerline
is divided into 10 equal parts for placement of the remaining
lines.

Data Set: I
Radius: 1.0
Res: 3
Scans: 3
a(1): 3pi/10
a(2): 17pi/24
a(3): 29pi/20
RowXCol: 60X60
Without C/L

		Norm(LInv)		
Frac	Scanr=1.0	Scanr=2.0	Scanr=7.0	Scanr=1.0E05
0.1	6,454	fails	fails	fails
0.2	6,829	fails	fails	fails
0.3	8,888	fails	fails	fails
0.4	4,980	76,424	fails	fails
0.5	13,527	49,615	2,066	14,244,232
0.6	172,291	46,098	9,562	6,778
0.7	13,652	7,885	1,773*	3,082
0.8	11,919	63,216	3,833	6,944
0.9	26,920	2,627,163	11,209	3,262

* Although the norm is low, the solution set was not feasible
(negative values).
===

Data Set: J (Geometry same as Data Set I above)

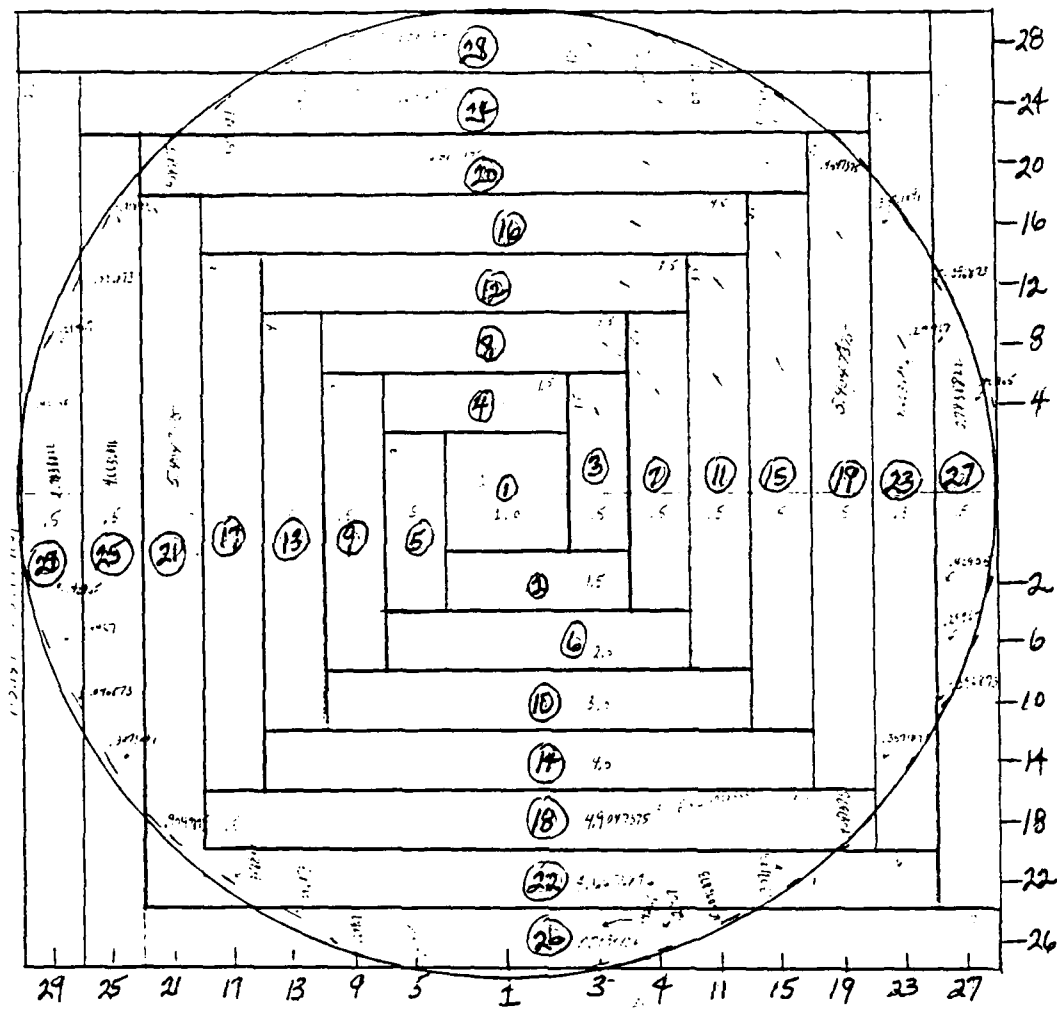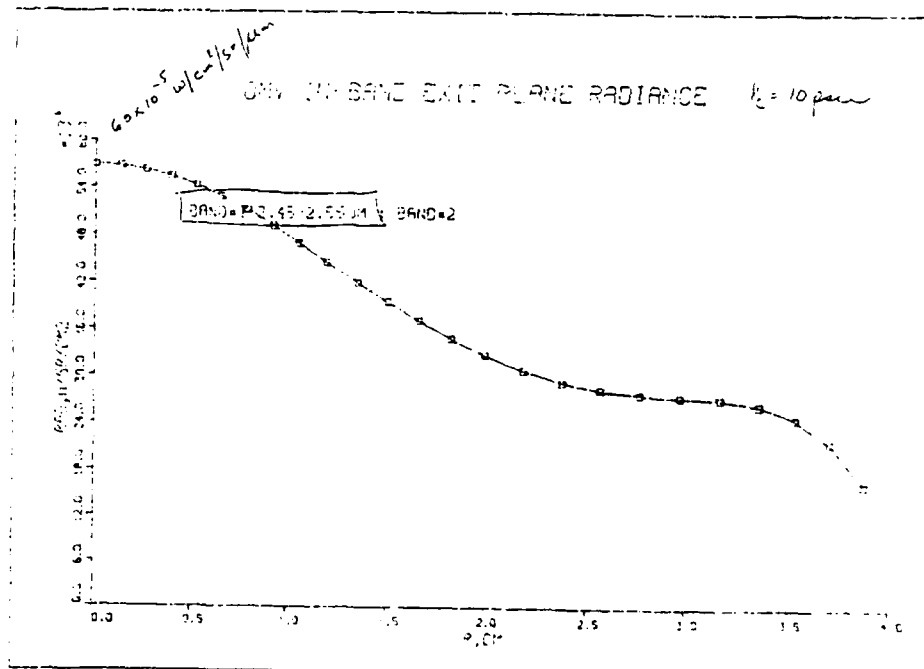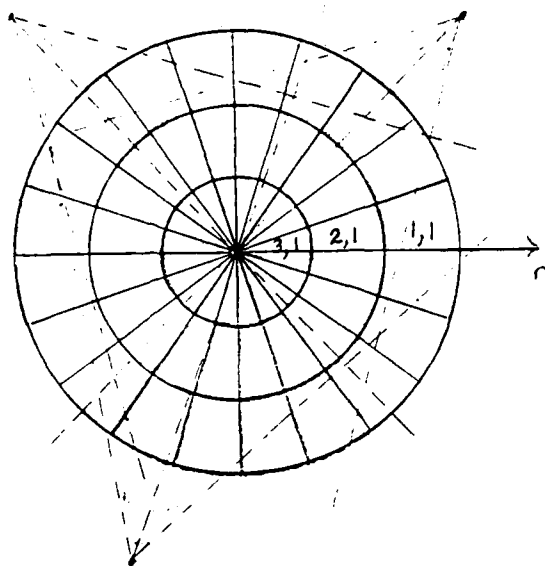|			Norm(LInv)			
Frac	Scanr=3.0	4.0	5.0	6.0	8.0	9.0
0.7	17,658,505	9,906	4,060	25,898	1,645	1,929

Figure 1
Geometry 1
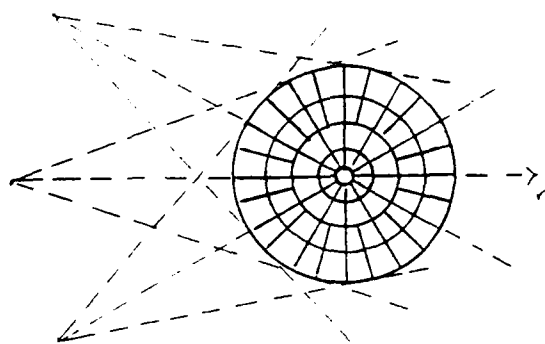

Figure 2

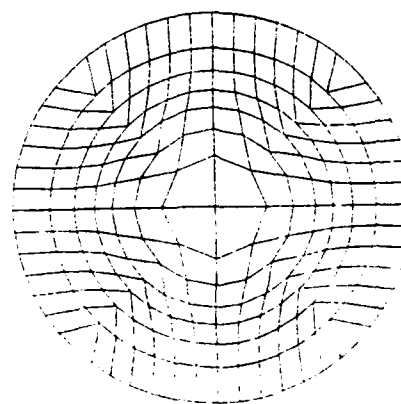Figure 3.
Geometry 2

Figure 4.
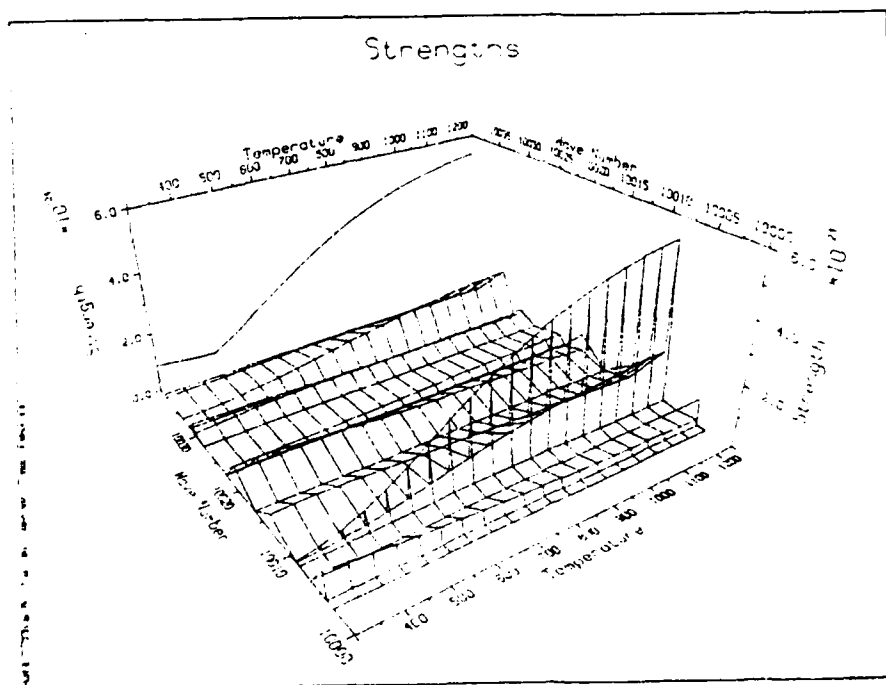

Figure 5. "H Grid"

Figure 6.

REFERENCES

Bates, R.H.T., et. al, "Overview of Computerized Tomography with Emphasis on Future Developments", Proc.IEEE, Vol 71, No.3, March, 1983, pp.356-372.

Herman, G. T., "A Relaxation Method For Reconstructing Objects From Noisy X-Rays", Mathematical Programming, 8, 1975, pp.1-19.

Limbaugh, Charles C., "The Infrared Emission-Absorption Method for Temperature and Species Partial Pressure Determination in Flames and Plumes", Infrared Methods for Gaseous Measurements, Joda Wormhoudt, Ed., Marcel Dekker, Inc. New York, N. Y., 1985, pp.197-245.

Monnig, C. A., et. al., "Tomographic Image Reconstruction Techniques for Spectroscopic Sources: Theory and Computer Simulations", Prep. for pub. in Spectrochimica Acta, Part B, Tech. Report No. 36, Office of Naval Research, (distribution unlimited), July 11, 1988.

Rothman, L. S., et. al., "The HITRAN Database: 1986 Edition", Applied Optics, Vol. 26, No. 19, Oct.1, 1987, p. 4058-.

Wang, J. Y., "Passive Optical Diagnostics of Combustion Flows", Applied Optics, Vol. 16, No. 3, Mar., 1977, pp.627-634.

Wood, Sally L., et. al., "Reconstruction with Limited Data Using Estimation Theory", Computer Aided Tomography and Ultrasonics in Medicine, Raviv et. al.,eds., 1979, pp.219-233.

1989 USAF-UES SUMMER FACULTY RESEARCH PROGRAM

GRADUATE STUDENT RESEARCH PROGRAM

Sponsored by the

AIR FORCE OFFICE OF SCIENTIFIC RESEARCH

Conducted by the

Universal Energy Systems, Inc.

<u>FINAL REPORT</u>

<u>DISTRIBUTED AND PARALLEL IMAGE AND SIGNAL PROCESSING</u>

Prepared by: D. Mitchell Wilkes, Ph.D.
                      Ben A. Abbott
                      <u>Lester E. Lynd</u>, Jr.
                      Richard S. Souder

Academic Rank: Professor and Graduate Students

Department and   Electrical Engineering Department

  University: Vanderbilt University

Research Location: AEDC
                      Arnold AFB, TN   37389

USAF Researcher: Capt. Ted Bapty

Date: 16 Aug 89

Contract No: F49620-88-C-0053

Same Report As
Dr. Mitchell Wilkes
(Report # 19)

1989 USAF-UES SUMMER FACULTY RESEARCH PROGRAM

GRADUATE STUDENT RESEARCH PROGRAM

Sponsored by the

AIR FORCE OFFICE OF SCIENTIFIC RESEARCH

Conducted by the

Universal Energy Systems, Inc.

FINAL REPORT

A SURVEY OF THE PERSONAL COMPUTER ENVIRONMENT

AT ARNOLD ENGINEERING DEVELOPMENT CENTER

Prepared by:	Betty A. Pipes, B.S.
Academic Rank:	Graduate Student
Department and	Computer Science Department
University:	Middle Tennessee State University
Research Location:	Arnold Engineering Development Center Tullahoma TN 37389
USAF Researcher:	Marshall Kingery
Date:	14 July 89
Contract No:	F49620-88-C-0053

DISCLAIMER

References to named commercial products in this report are not to be considered in any sense as an endorsement of the product by the US Air Force or the government.

A SURVEY OF THE PERSONAL COMPUTER ENVIRONMENT

AT ARNOLD ENGINEERING DEVELOPMENT CENTER

by

Betty A. Pipes

ABSTRACT

There are approximately 700 personal computers (PC's) at AEDC. They are purchased by different companies for varying purposes and function with a variety of software. With the advent of more PC's in the workplace and a larger range of usages, their requirements become more visible and the nature of their strengths and weaknesses manifests itself in wider arenas. As a response to the needs of the PC community at AEDC, a Small Computer Support Committee is being formed. This committee will be an advocate for users' needs and concerns. Its mission will require a knowledge of the areas wherein resources can be constructively applied.

This report details my efforts to survey AEDC personal computer users and to define their environment with special attention toward the areas in which support can be best directed.

ACKNOWLEDGMENTS

I would like to express my appreciation to the Air Force Systems Command

and the Air Force Office of Scientific Research for their maintenance of

this effort. My gratitude is also extended to Universal Energy Systems

for their consideration and support.

This summer's tenure at AEDC has been informative and interesting. My

experience has been guided and supported by Mr. Kingery and his staff,

especially Anita Bates who helped in entering the data into the database.

Friendly assistance was always available from Mr. Benshoof and his Small

Computer Group, notably Betty Jernigan and Angela Raby. My reception was

always pleasant and I would like to thank OAO Corp. for the courtesies

and helping hand which it extended to me.

I.   INTRODUCTION:

Arnold Engineering Development Center is an Air Force Systems Command Test Center managed by the Air Force and operated by three prime contractors: Calspan Corporation, Sverdrup Technology, Inc., and Schneider Services International. Among the sub-contractors pertinent to this effort is OAO Corp., specifically the Small Computer Group headed by Mr. Bill Benshoof. These companies all contribute to the center's mission of testing space systems and maintaining research and development of relevant techniques and instrumentation. Each company has its own methods and procedures; this has resulted in a variety of PC's in operation as well as an even larger variety of software. With such a diversity of hardware and software, some confusion will occur, as well as those concerns attendant with new equipment; e.g., installation, training, etc.

In an effort to address these concerns and provide small computer support, Marshall Kingery, AF/SC (Communications-Computer Systems), SSI and OAO have initiated the establishment of a Small Computer Working Group and a study of the PC's at AEDC. As a graduate student in computer science at Middle Tennessee State University, I approach this project with an objective viewpoint. My generalized background provides me with a familiarity towards personal computers while my non-affiliation with any specific employer exempts me from bias.

II.   OBJECTIVES OF THE RESEARCH EFFORT:

In an effort to gather information regarding the manner and method of PC

utilization at AEDC, I have spent approximately half my time in constructing a

questionnaire which was distributed broadly across the center. With the help

of Miss Angela Raby, a database was created to hold the results of the

questionnaire so that the data could be analyzed as well as maintained and

updated at the discretion of the committee.

In addition to the questionnaire as a source of input, I spoke with engineers

and other users around the center to get a more immediate sense of their

impressions and criticisms. They were all generous with their time and

opinions; some were content and undemanding, other vociferously outspoken

about discrepancies and/or needs they recognized.

My aims were threefold:

      1)   determine how PC's are being used at AEDC

      2)   accentuate positive procedures and help extend their range

      3)   define similarities/differences among different user-catagories

My ultimate objective was to establish a base of information upon which the

committee could draw to formulate support functions for PC users. Therefore,

the results of my analysis were only a partial conclusion to my effort: the

larger result was the database containing PC data.

III.

a.   My major appoach to collecting data was the creation of a questionnaire.

Please note attachmments Q1-Q3: the questionnaire which was distributed at

AEDC. Approximately 400 responses were returned to me and have been entered

into five related databases. I feel that this is a favorable response and a

large enough portion of the users to determine some obvious trends. Also

please note attachments S1-S2 which contain the attendant database structures.

The questions were grouped to address specific areas:

Area 1:   (1) and (3) identify the user   (QUEST_MA.DBF)

Area 2:   (2) list hardware   (HARDWARE.DBF)

Area 3:   (3)-(7)   evaluate Ethernet services   (QUEST_MA.DBF)

Area 4:   (8)-(12) evaluate DOS services   ("   "   )

Area 5:   (13)-(15) evaluate personal procedures ("   "   )

Area 6:   (15) length of usage at AEDC   ("   "   )

Area 7:   (16)-(26) identify software usage   (SOFTWARE.DBF)

Area 8:   (27) and (29) education history   (QUEST_MA.DBF)

Area 9:   (28) list courses at Training Center   (QUEST_CO.DBF)

Area 10:   (29)-(31) evaluate local facilities   (QUEST_MA.DBF)

Area 11:   (32)-(34) list group proclivities   (QUEST_US.DBF)

Area 12:   (35) general comments   (QUEST_MA.DBF)

b.   The following explanations detail some of the statistics

      which the questionnaire revealed.

Area 1:   TOTAL RESPONDANTS......402

              engineering/scientific.........196
              management/administrative......209
              firmware/hardware intensive.... 9
              report/publishing intensive.... 78
              executive...................... 15

As the numbers show, the two main catagories are engineering/scientific

and management/administrative. Within these groupings, there is further

classification where respondants wrote in their areas of interest. These

entries are many and diversified (e.g., specific engineering disciplines,

artificial intelligence, spreadsheets, CAD, data management, fluid dynamics,

stress management, word processing). Some users refer to specific software;

others allude to generic needs. These catagories can be utilized to define

the users into more specific groupings and will only require querying the

database and viewing the pertinent field (Field 14: INT_COM of QUEST_MA).

Area 2:   The database which holds this information, HARDWARE.DBF,

               is related to the information in the other databases through the

               ID_NO which is affixed to each questionnaire.

               The results show the preponderance of Zenith units:

                         Zenith 248's............347
                         IBM XT's & AT's.........35
                         other...................46

          Some printer statistics:
                         Alps....................115
                         HP Laserjet............. 61
                         Epson................... 50

          Modems, mice and plotters were nominally mentioned.

Area 3:   Ethernet users: 154

Less than 20% of the above count used the facilities more than once a day.

The comments in this area were many and mostly negative although respondants

were positive about the possible benefits of a network. A great deal of

frustration resulted from delays in installing connections and many saw the

software as cumbersome and unfriendly. The greatest number of aspersions

occured in this area due to slow and awkward file manipulation and the

inability, via the network or otherwise, to transfer files from PC's to the

STAR workstations which are prevalent for administrative processing. Another

common complaint: the proliferation of copies and junk mail.

Area 4:

> Use several DOS commands daily.......243
> Write own batch files...............209
> Desire more knowledge...............240

Here the statistics reveal that half the users feel they could benefit from

more information on operational procedures. A majority of users said that

they find help on their own with DOS problems - mainly through the aid

of the manual, occasionally with the help of co-workers.

Area 5:   Customized features of the computer were indicated here:

> have office/secretarial aids on PC.........125
> write software for own use.................175

The comment field in this area describes what type of programs the user

wrote or would like to write. Some of the engineering applications were very

specific, while others were quite general, e.g. computational fluid dynamics

and tracking procedures. Most all agreed to share.

Area 6:   The minimum usage exposure at AEDC........1 month (11 users)
             The maximum usage exposure at AEDC........36 months (4 users)
             The average time of exposure at AEDC......26 months

YEARS OF USE	1	2	3	4	5	6	7	8
NUMBER OF USERS	122	112	91	47	19	5	1	5

This data shows the number of PC's increasing steadily in the preceding years.

Area 7:   This information is in the database SOFTWARE.DBF and is related

to the other databases through the ID_NO field. The most pragmatic feature

of this database is its ability to identify specific types of software in use

or desired to be used. Lotus 123 predominates among the software presently

employed. Among the most highly desired facilities are C, UNIX, and

Ethernet.   This database also provides a listing of local experts on

various software contained in the ADV (advisor/helper) field.

Area 8:   These fields indicate the training history of users. Question

#27 asking if the user had Software Engineering training was unclear to many;

answers were ambiguous. Question #28 asked for comments about the training

sessions offered through the Computer Learning Center where 222 respondants

had taken one or more courses. The majority of responses were positive,

although a common complaint was the time differential between class and the

actual application of the material. Several users found it frustrating to

wait for courses, so began by themselves on a self-teaching odyssey. Some

common suggestions were:

        1) better promotion of courses

        2) tailoring course content to specific applications

        3) shorter (perhaps more) training sessions

Area 9:   This information is in another database, QUEST_CO.DBF, again

related to other databases through the ID_NO. This base contains a listing

of courses taken by respective users through the Computer Learning Center.

Area 10:   Question #29 asks for user comments regarding the Network

Control Center (and indirectly, the Small Computer Group who receive distress

calls via the NCC). Comments were very laudatory; it is a tribute to

the employees who work in this area that they engender such praise - they

received glowing reports. The follow-up checking that they do was pointedly

mentioned as a favorable feature.

        The two succeeding questions deal with the receptivity of users

toward a laboratory and/or information clearinghouse. The lab was not defined;

the concept was merely presented. Some respondants were admonitory in

cautioning that they would not promote any resource which would take them

from their local work area. Others eagerly included a list of software and

hardware they would be interested in trying, or using on a limited basis.

The clearinghouse idea received little advocacy - except in cases of specific

application or generally as a bulletin board of troubles and shortcuts.

Area 11:   As a forum for new ideas, troubles and remedies, the concept

of a users' groups has merit. This topic asked in which group(s) the

user would be interested. The data was collected in the fifth and final

database, QUEST_US.DBF, again related through the ID_NO to respective users.

The following numbers reflect those who expressed interest in the listed user groups:

General PC...167   MS-DOS...104   C...36

UNIX...28   spreadsheet...82   networking...45

Next, comments were invited regarding seminars the user would be either interested in giving or attending. Few admitted to enough knowledge to deliver a presentation, but many were interested in attending where the topics covered were pertinent to their work.

Area 12:   The final area covered the general comment statement. I had hoped it would be an overview of the user's perspective. Many chose not to comment but those who did were enlightening. Generally, it can be said that comments fell into two broad catagories: optimistic and pessimistic. Happily, the former outweighed the latter. It seems that where users were required to tie into or follow foreign dictums, there was dissension and strife; where users were free to go their own way, they were satisfied with their lot, with the exception of cases where there were too many users on one PC or there was no responsive process for purchasing software or additional hardware.

There were many expressions of encouragement accompanied with some valid

suggestions, especially with regard to a PC newsletter. There were also

factual reports of methods used in other locations that were condusive to

an alert and efficient user community. Moreover, many users were desirous of

improving their skills and presented further avenues for consideration: local

community college, at-home computer experience, work-area oriented user group,

critiques of current software from fellow workers, and sharing of short-cuts

and peccadillos of familiar packages.

A recurring contention was the problem of (or solution through) standardiza-

tion. It would behoove communications to have one standard word processor,

spreadsheet, database, graphics package; however, this uniformity flaunts the

engineer's individuality - a trait which most engineers valiantly defend.

However, some consideration should be directed toward this recurring issue of

escalating diversification.

IV.

a.   My second mode of approach toward collecting data was through

interviews with the users at the center. This method was more revealing than

the questionnaires, and more fun! Engineers tend to be uniquely-configured

individuals and are quite self-reliant and outspoken - especially when they

are discussing their "personal" computers.

b.   The interviews clearly defined two main user catagories: engineer

and non-engineer. The engineering group contained independent users who were

mainly concerned with the functionality of different application methods

and the efficacy of their hardware. The other catagory, in which PC's were

used for report production and administration, required printing, filing and

information facilities. Users readily agreed that the complexity of the

situation made it difficult to formulate a simple solution; however, they had

definite ideas about how to approach solutions and were eager to share them.

The historical attitude of positioning PC's in the work area appears to have

been pragmatic, if not well-considered: get them out there and then contend

with the problems that follow. This situation is not unique and has been

recently detailed by commentators :

>   "As divisions, departments, and business units continue to increase
>   PC spending and to build more company-critical applications around
>   PC's, most companies are looking for a new and better way to manage
>   the development and support of those systems. They are putting an
>   end to the often ad hoc, disjointed approach to PC's that evolved
>   in the early to mid-1980's."
>
>   "End users are being asked to take more responsibility for seeing
>   to it that the applications they are demanding conform to company-
>   wide architectural and business goals. And they are becoming
>   active partners in team approaches to PC-based application
>   development."   (Moad, 1989)

V. RECOMMENDATIONS:

a.   To better orient PC users: publish an AEDC PC User's Guide to

be distributed (and kept) attendant with each PC. Within each guide

provide an area where the specifics of each PC can be enumerated and

recorded, e.g. different configurations and Ethernet pecularities. Include

the Network Control Center phone and and a description of their services,

the Training Center phone and description of courses and schedules,

the Small Computer Group phone and detail their services and facilities.

List the software resident on each unit with instructions about where to

procure help (human or manual).

b.   Supplement the library with new text relevant to computer topics.

c.   Provide resources: shareware - software in the public domain; a

          resource person familiar with new software (or new versions) who

          could offer advice; a software library where packages could

          be tested and evaluated before purchasing; a lab stocked with

          facilities that can be tried or occasionally used for unique

          tasks.

d.   Formulate and publish information about procedures which will allow

          Wordstar/Volkswriter/Enable conversion to Xerox STARS.

e.   Publish and distribute a PC Newsletter with current training courses,

          reviews of new software, seminar announcements, feature PC users

and their successful adventures, progress reports about relevant programs/changing situations, e.g., AIMS, Ethernet.

f. Sponsor the revitalization of user groups: this structure provides a dynamic forum for users to commiserate, congratulate and determine similar concerns. Together users can provide much of their own support: there is a large fund of expertise at the center, it only needs be tapped.

REFERENCES

Bringing Power to the Desktop, Machine Design/Applied Technology for Design Engineering, June 18, 1987.

Bryant, S.F., Spreading the User-Group Gospel, Computer Decisions, April 23, 1985, Vol. 17 No. 8, pp. 40-44.

Moad, J., The Second Wave, Datamation, Feb. 1, 1989, Vol. 35, No. 3, pp. 14-20.

Seybold, P., Foundations for the Next Decade, Computer Decisions, April, 1989, p. 11.

1989 USAF-UES SUMMER FACULTY RESEARCH PROGRAM

GRADUATE STUDENT RESEARCH PROGRAM

Sponsored by the

AIR FORCE OFFICE OF SCIENTIFIC RESEARCH

Conducted by the

Universal Energy Systems, Inc.

<u>FINAL REPORT</u>

<u>DISTRIBUTED AND PARALLEL IMAGE AND SIGNAL PROCESSING</u>

Prepared by: D. Mitchell Wilkes, Ph.D.
                      Ben A. Abbott
                      Lester E. Lynd, Jr.
                      <u>Richard S. Souder</u>

Academic Rank: Professor and Graduate Students

Department and   Electrical Engineering Department

  University: Vanderbilt University

Research Location: AEDC
                      Arnold AFB, TN   37389

USAF Researcher: Capt. Ted Bapty

Date: 16 Aug 89

Contract No: F49620-88-C-0053

Same Report As
Dr. Mitchell Wilkes
(Report # 19)

1989 USAF–UES SUMMER FACULTY RESEARCH PROGRAM/

GRADUATE STUDENT RESEARCH PROGRAM

Sponsored by the

AIR FORCE OFFICE OF SCIENTIFIC RESEARCH

Conducted by the

Universal Energy Systems, Inc.

FINAL REPORT

A NONLINEAR FILTER AND AN ODD/EVEN ITERATION

FOR INVISCID FLUID FLOW EQUATIONS

Prepared by:	Robert W. Tramel
Academic Rank:	Graduate Research Assistant
Department and	Mathematics
University:	The University of Tennessee, Tullahoma
Research Location:	Arnold Air Force Base Tullahoma, TN 37389
USAF Researcher:	K. C. Reddy
Date:	06 SEPT 89
Contract No:	F49620–88–C–0053

A NONLINEAR FILTER AND AN ODD/EVEN ITERATION
FOR INVISCID FLUID FLOW EQUATIONS

by

Robert W. Tramel

ABSTRACT

A nonlinear filter based on artificial dissipation is tested and shown to produce an effective shock capturing scheme for hyperbolic systems of conservation laws. In order to control spurious oscillations, the filter is applied after every time step to the difference solution from a locally implicit scheme for the Euler equation. The method is tested on both unsteady and steady test problems in order to demonstrate the efficacy of the technique. On steady flow problems, an odd/even grid ordering is considered. This ordering is shown to be robust and also well suited for implementation on vector computers.

ACKNOWLEDGEMENTS

I. INTRODUCTION:

The scope and magnitude of the problems that the working engineer wishes to solve using the methods of computational fluid dynamics grow constantly. Thus, there is a very important need for more efficient methods for solving large scale problems.

The computational fluid dynamics group of Calspan Corporation, Arnold Engineering Development Center Branch is actively engaged in this effort. They need efficient, robust algorithms for the solution of fluid flow problems about bodies of various configurations. These algorithms must also be suited to the current computer architectures such as vector processors if they are to be implemented effectively.

My own research interests include the development of new algorithms for the solution of the equations of fluid motion and the use of these methods in the elucidation of the behavior of fluid systems.

II. OBJECTIVE OF THE RESEARCH EFFORT:

In the past, many methods have been developed to produce shock capturing schemes for hyperbolic systems of conservation laws. Practical experience has shown that central difference schemes when supplemented with a well chosen blend of second and fourth order artificial dissipation terms have proven useful for the prediction of shock waves in steady flow situations. However, the cost of the computation of these terms is as much or more than the cost of the corresponding conservation quantities and fluxes. If the equations are solved by an iterative technique, then the costly dissipation terms must be computed many times per time step.

On the other hand, Engquist, Lötstedt, and Sjögreen (1989) have shown recently that the oscillations associated with central difference schemes can be checked by applying a nonlinear filter to the difference scheme at each time step. This filter searches for

unwanted maxima and minima in the flow field. These unwanted extrema are then removed in a manner consistent with the governing conservation laws (i.e., conserved variables are neither created nor destroyed).

The main objective of my research effort for the 1989 Summer Faculty Research Program (SFRP) is to develop a nonlinear filter similar to those proposed by Engquist, Lötstedt, and Sjögreen but based on adaptive artificial dissipation techniques as developed by Antony Jameson (1985A), (1985B) and modified by Pulliam (1985) and others. This filter should control oscillations in all parts of the flow field on both steady and unsteady test problems. The filter will reduce the computational cost of the artificial dissipation terms when used with an iterative technique.

The filter will be used with a locally implicit scheme for the Euler equations as developed by Reddy and Jacocks (1987). It has been found that Reddy and Jacocks' scheme works well with a modified Gauss–Seidel iteration, but numerical evidence and linearized stability analysis of model scalar equations indicate that when a modified Jacobi iteration is applied the method tends to amplify medium wavelength disturbances. Unfortunately, a Gauss–Seidel type iteration is a recursive process, and a recursive process is not suitable for implementation on vector computers. (See Ortega and Voigt (1982) for a general discussion of the solution of partial differential equations on vector computers.) My second objective for the SFRP is to test an odd/even ordering of the grid points. This ordering will allow Gauss–Seidel type iteration to be carried out in a Jacobi like manner. This will remove the instability inherent with the modified Jacobi method while maintaining the desirable feature of compatibility with vector computers.

III.

We take the Euler equations as our example of a hyperbolic system of conservation laws. The Euler equations in one dimension can be written in the form (1)

$$\frac{\partial Q}{\partial t} + \frac{\partial F}{\partial x} = 0, \tag{1}$$

where Q is the vector $(\rho, \rho u, e)$ and F is the vector $(\rho u, \rho u^2 + P, u(e + P))$. Here ρ is the density, u is the velocity, e is the energy per unit volume, and P is the pressure. The pressure is related to the other variables for a perfect gas by the relation $P = (\gamma - 1)\left(e - \frac{1}{2}\rho u^2\right)$.

The implicit scheme based on central difference spatial approximations is written at each grid point I as follows.

$$\frac{1}{\Delta t}\left(Q_I^{n+1} - Q_I^n\right) + \frac{1}{2\Delta x}\left(F_{I+1}^{n+1} - F_{I-1}^{n+1}\right) = 0 \tag{2}$$

Q_I^{n+1} is the value of the vector Q at the Ith lattice point at time step $n+1$, while F_I^{n+1} is the value of the vector F evaluated using Q_I^{n+1}. Δt is the lattice spacing in the time direction, and Δx is the lattice spacing in the spatial direction. From one time step to the next, the system of equations (2) is solved by the following iterative method. An iteration sweep is made from the initial lattice point to the final point. The process is then repeated with the sweep going from the final lattice point to the initial point. Several such symmetric iteration sweeps are made at each time step. Let $Q_I^{(m)}$ be the latest approximation to Q_I^{n+1} after m sweeps. $Q_I^{(0)}$ is set equal to $Q_I^{(n)}$ for all values of I. Also, let $F_I^{(m)}$ be the value of the vector F evaluated using $Q_I^{(m)}$. At each lattice point I during the iterative sweeps, the value of $Q_I^{(m)}$ is updated as follows

$$Q_I^{(m+1)} = Q_I^{(m)} + Res_I/c_I, \tag{3}$$

where c_I is given by the formula $c_i = \frac{1}{\Delta t} + \frac{1}{2\Delta x}\left(|u_I^n| + a_I^n\right)$ where a_I^n is the local speed of sound computed using Q_I^n. Res_I is the so called residue. For a modified Gauss–Seidel

iteration Res_I is defined to be

$$Res_I = -\left[\frac{1}{\Delta t}\left(Q_I^{(m)} - Q_I^n\right) + \frac{1}{2\Delta x}\left(F_{I+1}^{(*)} - F_{I-1}^{(*)}\right)\right], \qquad (4)$$

where $F^{(*)}$ is the value of the vector F evaluated using $Q_I^{(*)}$. Here, $Q_I^{(*)}$ will always be taken to be the most recently computed approximation to Q_I^{n+1} (i.e., $Q_I^{(m+1)}$ is used where available). A modified Jacobi iteration can also be defined for which

$$Res_I = -\left[\frac{1}{\Delta t}\left(Q_I^{(m)} - Q_I^n\right) + \frac{1}{2\Delta x}\left(F_{I+1}^{(m)} - F_{I-1}^{(m)}\right)\right]. \qquad (5)$$

After 2–3 sweeps for unsteady problems and 1–2 sweeps for steady problems, the value of Q_I^{n+1} and $Q_I^{(0)}$ are both set equal to $Q_I^{(*)}$ at all grid points. The process is then repeated for the next time step. More details on the locally implicit scheme can be found in Reddy and Jacocks (1987).

IV.

The locally implicit scheme as described above is not sufficient for performing fluid flow calculations. The central difference scheme is known to produce spurious oscillations and suffer form pressure undershoots (i.e., negative pressures) in rarefaction regions and in the vicinity of moderate to strong shocks. The traditional method of controlling these problems is to add additional artificial dissipation terms to the Euler equations and then solving the augmented equations (Jameson (1985A), Reddy and Jacocks (1987)). In the present approach the artificial dissipation is applied as a filter. This filter is consistent with the definition of a filter as given by Engquist, et al. (1987) but is implemented quite differently.

Denote by Q_I^* the numerically computed approximation to Q_I^{n+1}. The value of Q_I^{n+1} is computed to be

$$Q_I^{n+1} = Q_I^* + S(Q^*)_I, \qquad (6)$$

where $S(Q^*)_I$ is a nonlinear filter defined by

$$S(Q^*)_I = (\psi 2_I * S1_I - \psi 2_{I-1} * S1_{I-1}) - (\psi 4_I * S3_I - \psi 4_{I-1} * S3_{I-1}). \qquad (7)$$

Here

$$S1_I = Q_{I+1}^* - Q_I^* \quad ; \quad S3_I = S1_{I+1} - 2*S1_I + S1_{I-1}. \tag{8}$$

The dissipation coefficients $\psi 2$ and $\psi 4$ are chosen such that the second order dissipation term is significant only near shocks while the fourth order term is used to damp oscillations in smooth flow regions and is turned off near shocks. This is accomplished by the use of a pressure sensor. Following Jameson define

$$\nu_I = \frac{|P_{I+1} - 2*P_I + P_{I-1}|}{|P_{I+1} + 2*P_I + P_{I-1}|} \quad ; \quad \nu\,\mathrm{max}_I = \max(\nu_{I+1}, \nu_I). \tag{9}$$

$\psi 2_I$ and $\psi 4_I$ are then defined to be

$$\psi 2_I = K2*\psi_I*\nu\,\mathrm{max}_I \quad ; \quad \psi 4_I = K4*\psi_I*\max(0.0, 1.0 - K*\nu\,\mathrm{max}_I) \tag{10}$$

where $K2, K4$, and K are adjustable parameters and ψ_I is defined to be

$$\psi_I = \frac{1}{2}(\lambda_{I+1} + \lambda_I), \tag{11}$$

where

$$\lambda_I = (|u_I| + a_I) = \text{ spectral radius of } \frac{\partial F}{\partial Q}. \tag{12}$$

The $S3$ terms can also be modeled after Jameson's (1985B) flux limited artificial dissipation. In this approach the $S3_I$ term becomes

$$S3_I = B\left(S1_{I+1}, S1_I\right) - 2*S1_I + B\left(S1_I, S1_{I-1}\right), \tag{13}$$

where $B(p, q)$ is Roe's MINMOD function defined for scalars by the equation

$$B(p, q) = ((S(p) + S(q)) * \min(|p|, |q|);$$
$$S(p) = \begin{cases} \dfrac{1}{2} & ; p \geq 0 \\ -\dfrac{1}{2} & ; p < 0 \end{cases} . \tag{14}$$

The function is applied component by component to vectors.

11-8

V.

a. As a test of the technique, we apply the modified Gauss–Seidel scheme with the flux limited artificial dissipation filter to Sod's (1978) shock tube problem. For all the test cases reported below, the values of $K2, K4$, and K are held fixed at the values 0.3, 0.03, and 12.0. A CFL number of 0.9 is used in all cases. At $t = 0$, the initial conditions are

$$Q_L = (1.0, 0.0, 2.5) \quad ; \quad Q_R = (0.125, 0.0, 0.25), \tag{15}$$

with the initial discontinuity located at $x = 0.0$.

In figures 1–2, the velocity, and energy per unit mass are shown for a 40 time step run made with $\Delta x = 0.1$. The true solution is plotted as a solid line and computed values are shown as circles centered at the computed point. The scheme maintains it's spatial order of accuracy in smooth regions, but it smears the shocks somewhat and the contact discontinuity even more so.

In figures 3–4 the velocity and energy are shown for the same test problem, but the artificial dissipation is included as part of the equation rather than applied as a filter. Comparison of the graphs show that the filter is superior to the traditional method in suppressing overshoots and spurious oscillations. Also, in this case the filter required only a third of the computational work.

b. Engquist, et al. (1989) have shown that for scalar conservation laws a consistent finite difference scheme with a filter will converge to the correct weak solution in the limit $\Delta t, \Delta x \to 0$ provided that the difference solution converges as this limit is taken. As a test of these ideas for systems of equations, the density and velocity from a 400 time step run with $\Delta x = 0.01$ are presented in figures 5–6. In this case the shocks are not smeared at all by the artificial dissipation and the contact discontinuity is only slightly smeared. In this limit very sharp nonoscillatory solutions are obtained.

VI.

We consider the nozzle flow problem of Shubin, Glaz, and Stephen (1981) as our test case for steady flow problems. The governing equations are

$$\frac{\partial Q}{\partial t} + \frac{\partial F}{\partial x} = H(Q), \tag{16}$$

where Q is the vector $A(x) * (\rho, \rho u, e)$, F is the vector $A(x) * (\rho u, \rho u^2 + P, u(e + P))$, and H is the vector $(0, P\frac{dA}{dx}, 0)$. $A(x)$ is the area variation of the nozzle given by relation $A(x) = 1.398 + 0.347 * TANH(0.8 * x - 4)$, $x \in [0.0, 10.0]$.

For these equations the locally implicit scheme still has the form of equation (3). c_I is as defined before, but for the modified Jacobi method Res_I is defined to be

$$Res_I = -\left[\frac{1}{\Delta t}\left(Q_I^{(m)} - Q_I^n\right) + \frac{1}{2\Delta x}\left(F_{I+1}^{(m)} - F_{I-1}^{(m)}\right) - H\left(Q_I^{(m)}\right)\right]. \tag{17}$$

As mentioned previously, the Jacobi method tends to amplify medium wavelength disturbances. This inevitably causes the method to compute negative pressures. The method produces good results when a Gauss–Seidel type iteration is applied, but this method will not vectorize. In order to remedy this situation, an odd/even grid ordering is considered. In this method, all the values of $Q_I^{(m+1)}$ when I is even are computed. The values of $Q_I^{(m+1)}$ when I is odd are then computed making use of the previously updated even I terms.

The boundaries are treated as follows. The boundary at $x = 0.0$ is a supersonic inflow, and thus the independent variables are held fixed at the free stream conditions. The boundary at $x = 10.0$ is subsonic outflow. This is handled by fixing the exit pressure at Pexit = 1.40844. The density and momentum are interpolated from the interior by the formula

$$Q(1,2)_{I\text{end}} = 2 * Q(1,2)_{I\text{end}-1} - Q(1,2)_{I\text{end}-2} \tag{18}$$

The energy is computed from the exit pressure and the interpolated density and momentum.

For initial conditions the variables are all set equal to the free stream conditions, $Q_I^0 = A(I) * (1.0, 1.26, 3.29)$. The modified Jacobi method with odd/even grid ordering is used to advance the solution as many time steps as necessary to reach a converged solution.

In order to demonstrate the spatial accuracy of the method, the solution is computed with 21 grid points. The solution ran 75 time steps with a CFL number of 10.0. The computed density normalized by the total density is shown in figure 7. The solution is compared with a 251 grid point solution which is displayed as a solid line. In all test cases, the flux limited dissipation filter is used with $K = 12.0$, $K3 = 0.3$, and $K4 = 0.03$. In figure 8 the density computed for the same test problem by a Beam and Warming (1976) code with standard artificial dissipation is shown. Comparison of figures 7 and 8 indicate that the iterative method produces results that agree well with those produced by the Beam and Warming method without the need for time consuming Jacobian calculations and block matrix reductions. On a Sun–4 computer, the run time ratio per time step of the two methods is greater than 2 to 1. On a vector computer the difference should be even more pronounced.

In figure 9 a convergence history for the modified Gauss–Seidel, modified Jacobi, and Beam and Warming methods are displayed. The base 10 log of the $L2$ norm of $(Q^{n+1} - Q^n)$ is plotted vs. the iteration count n. Local time stepping is used in all cases. Both the iterative methods ran with a CFL number of 10.0. The Beam and Warming code ran with an CFL number of 4.0. This value was experimentally determined to produce the greatest convergence rate. The results show that all methods have similar convergence rates. The odd/even modified Jacobi method converges almost as well as the modified Gauss–Seidel method while maintaining its ability to be implemented on vector computers.

VII. RECOMMENDATIONS:

a. The filter and odd/even grid point iteration have been shown to produce an effective shock capturing scheme for the Euler equation. The odd/even grid ordering is also successful in combining the advantages of Jacobi and Gauss–Seidel type iterations. It is recommended that these ideas be extended to two– and three–dimensional systems. It is also recommended that these ideas be extended to other areas of fluid dynamical interest such as the Navier–Stokes equations.

b. On steady state problems the artificial dissipation filter does a good job of dissipating high frequency errors rapidly but is slower in reducing long and medium wavelength errors. Therefore, it is recommended that this method be used with a multi-grid scheme. On a coarse grid, the long and medium wavelength errors will become short wavelength errors and be dissipated away. This should enhance the convergence properties of the scheme.

REFERENCES

Beam, R.M., Warming, R.F., (1976), An Implicit Finite–Difference Algorithm for Hyperbolic Systems in Conservation Law Form. *J. Comp. Phys.*, **22**, pp. 87–110.

Engquist, B., Lötstedt, P., Sjögreen, B., (1989), Nonlinear Filters for Efficient Shock Computation. *Math. Comp.*, 52, pp. 509–537.

Jameson, A., (1985A), Numerical Solution of the Euler Equations for Compressible Inviscid Fluids. *Numerical Methods for the Euler Equations of Fluid Dynamics, Ed. Angrand, et al.*, SIAM, 1985, pp. 199–245.

Jameson, A., (1985B), A Nonoscillatory Shock Capturing Scheme Using Flux Limited Dissipation, in: B.E. Enguist, S. Osher, and R.C.J. Somerville, Eds., *Large Scale Computations in Fluid Mechanics, Lectures in Appl. Math.*, **22**, part 1 (American Mathematical Society, Providence, RI, 1985), pp. 345–370.

Ortega, J.M., Voigt, R.G., (1985), Solution of Partial Differential Equations on Vector and Parallel Computers. *SIAM Rev.* **27**, pp. 149–240.

Pulliam, T.H., (1985), Artificial Dissipation Models for the Euler Equations. AIAA PAPER 85–0438 presented at the AIAA 23rd Aerospace Sciences Meeting, Reno, Nevada, 1985.

Reddy, K.C., J.L. Jacocks., (1987), A Locally Implicit Scheme for the Euler Equations. *Proceedings of the AIAA 8th Computational Fluid Dynamics Conference, Honolulu, 1987.* pp. 470–477.

Sod, G.A., (1987) A Survey of Several Finite Difference Methods for Systems of Hyperbolic Conversation Laws. *J. Comp. Phys.*, **27**, pp. 1–31.

Shubin, G.R., Stephens, A.B., Glaz, H.M., (1981), Steady Shock Tracking and Newtons Method Applied to a One–Dimensional Duct Flow. *J. Comp. Phys.*, **39**, pp. 364-374.
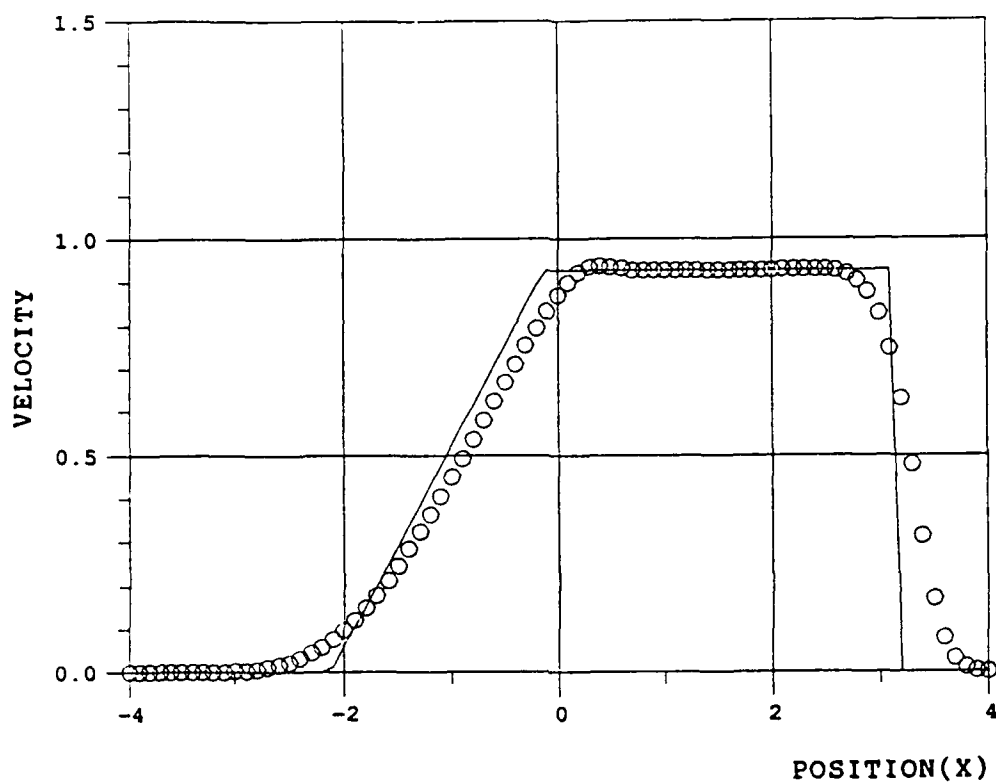
Fig. 1 Velocity computed by the modified Gauss-Seidel method
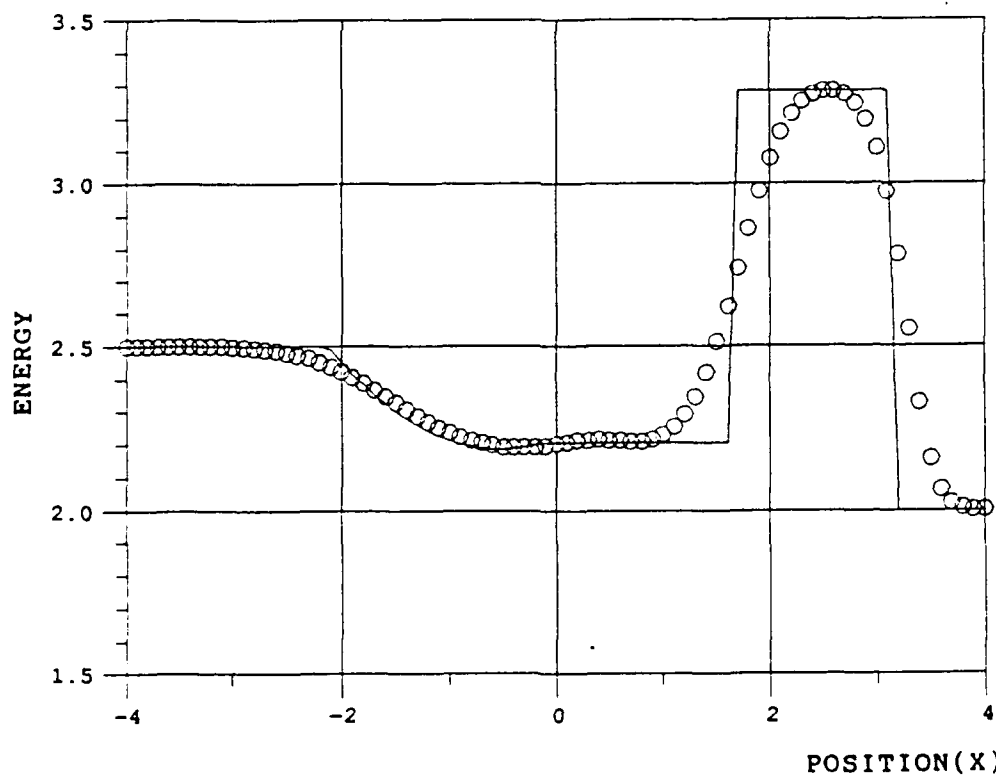with artificial dissipation filter for Sod's shock tube.

Fig. 2 Energy computed by the modified Gauss-Seidel method
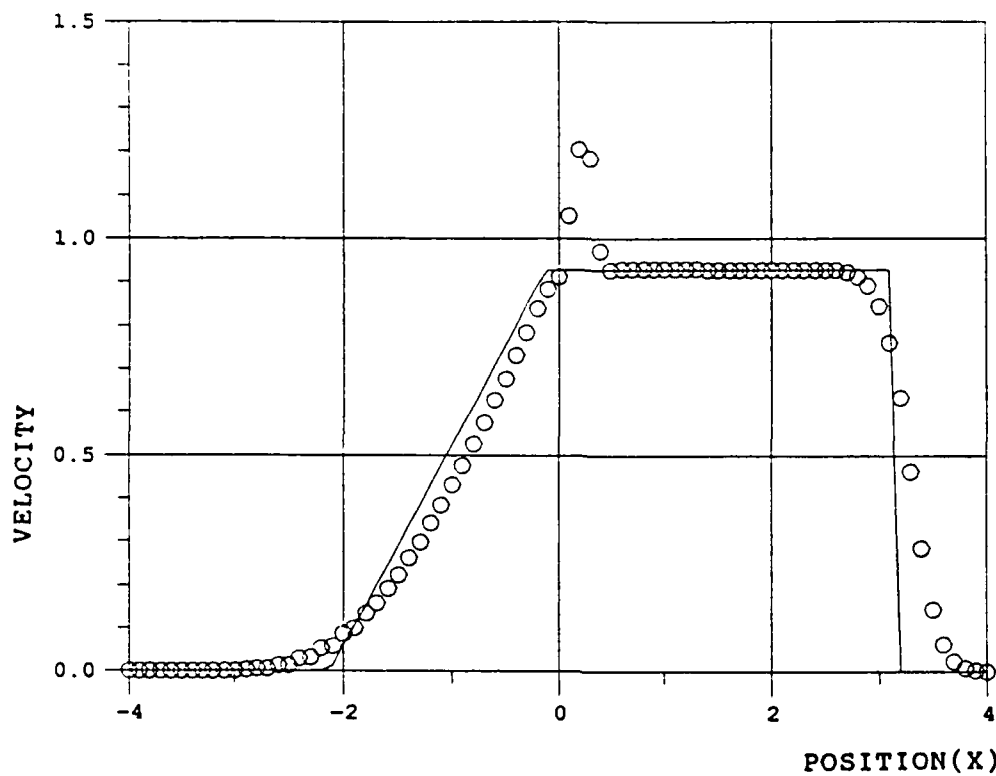with artificial dissipation filter for Sod's shock tube.

11-14

Fig. 3 Velocity computed by the modified Gauss-Seidel method with standard artificial dissipation for Sod's shock tube.
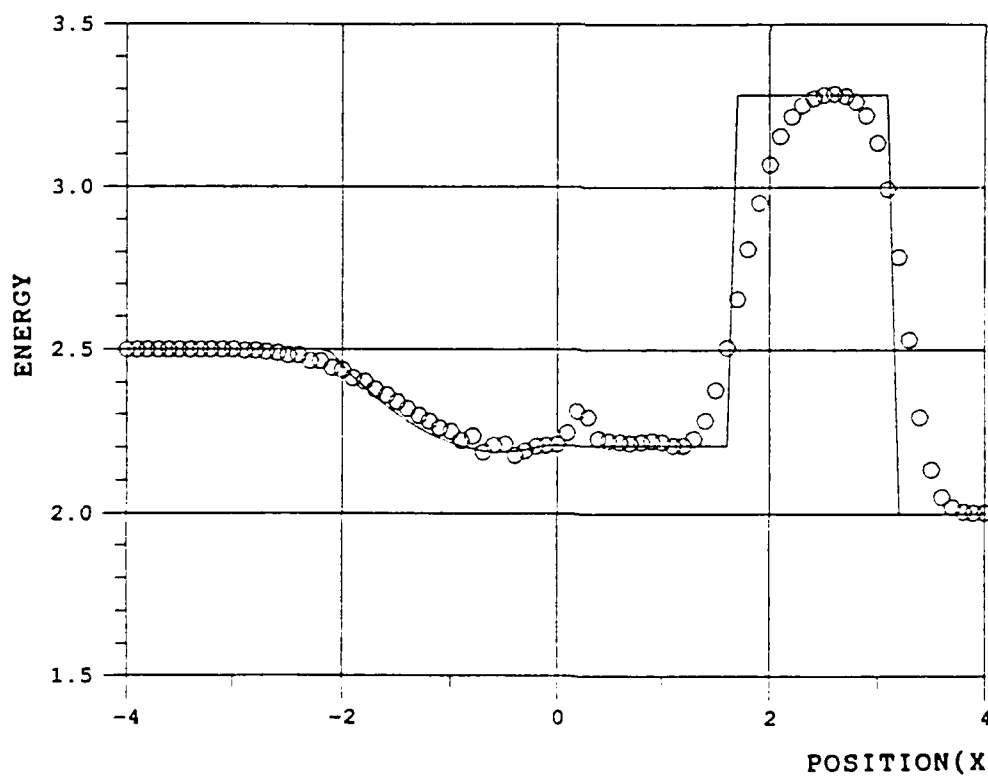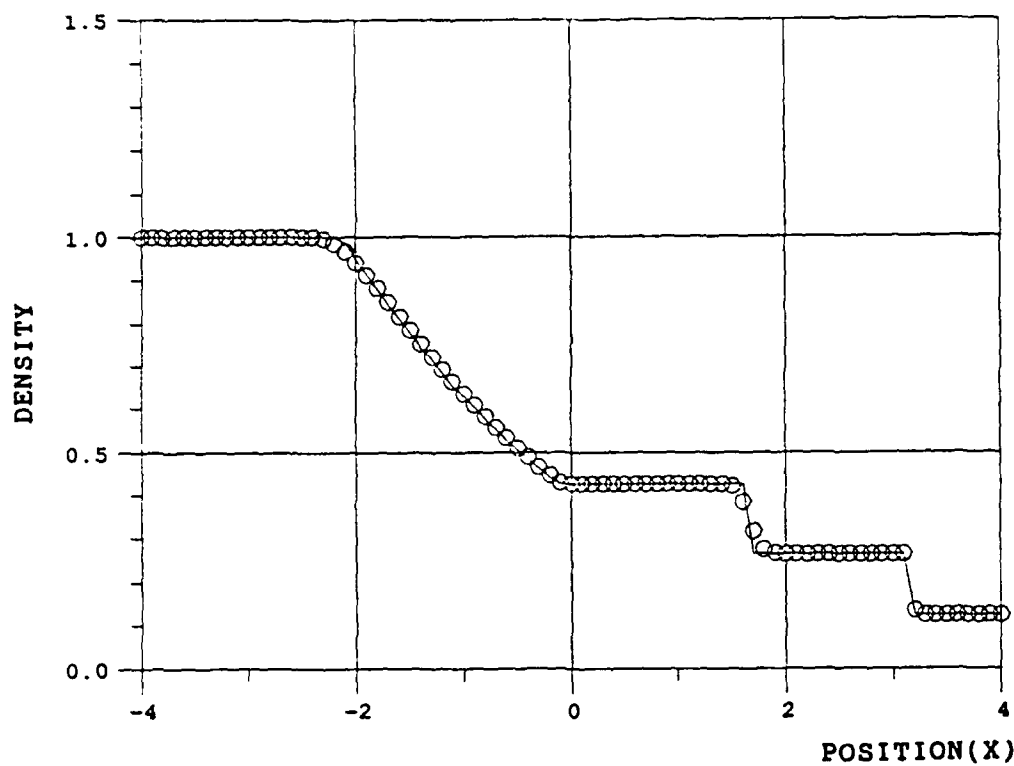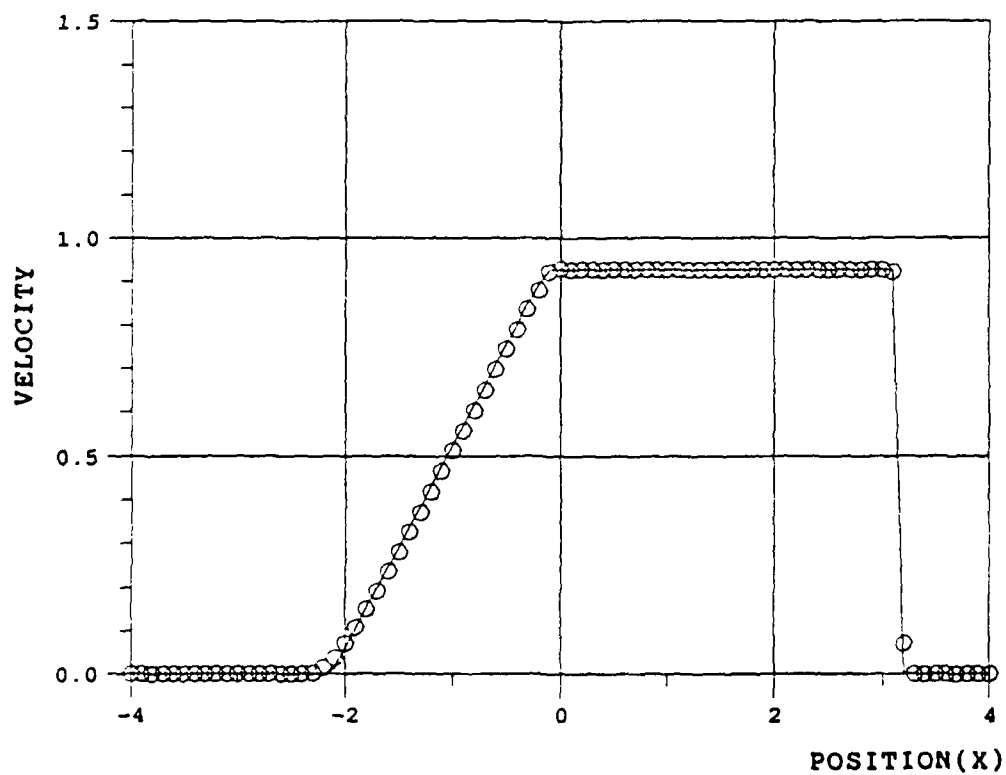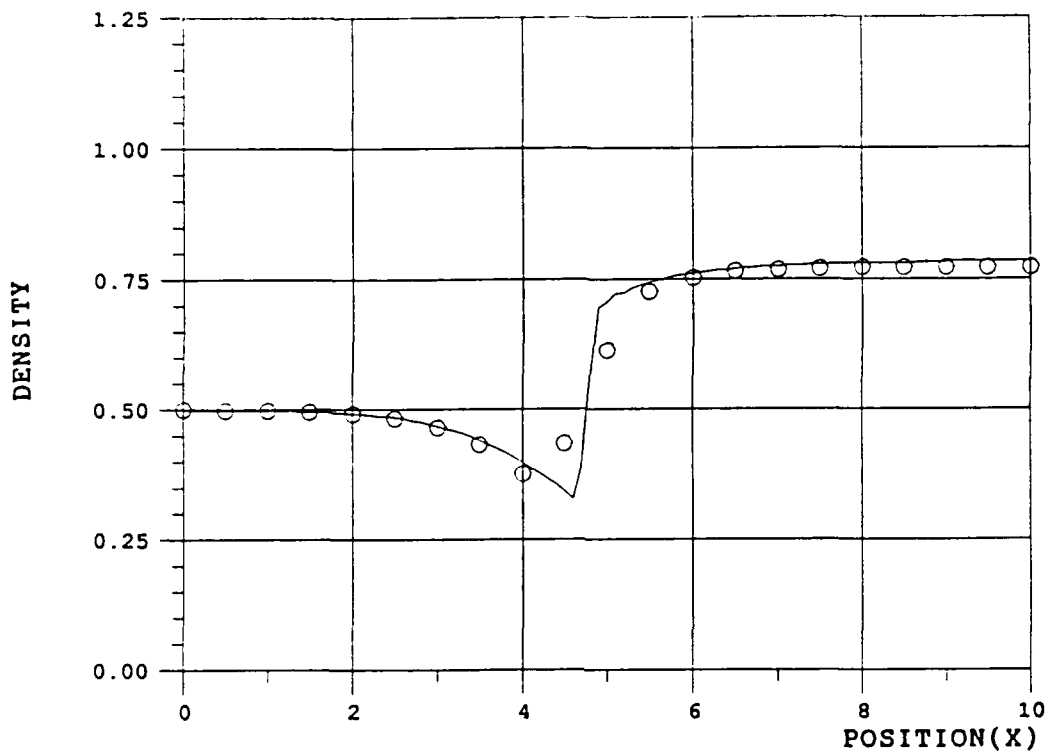

Fig. 4 Energy computed by the modified Gauss-Seidel method with standard artificial dissipation for Sod's shock tube.

Fig. 5 Density computed by the modified Gauss-Seidel method with artifical dissipation filter for Sod's shock tube.

Fig. 6 Velocity computed by the modified Gauss-Seidel method with artificial dissipation filter for Sod's shock tube.

11-16

Fig. 7 Density computed by the modified odd-even Jacobi method with dissipation filter for Shubin's nozzle.
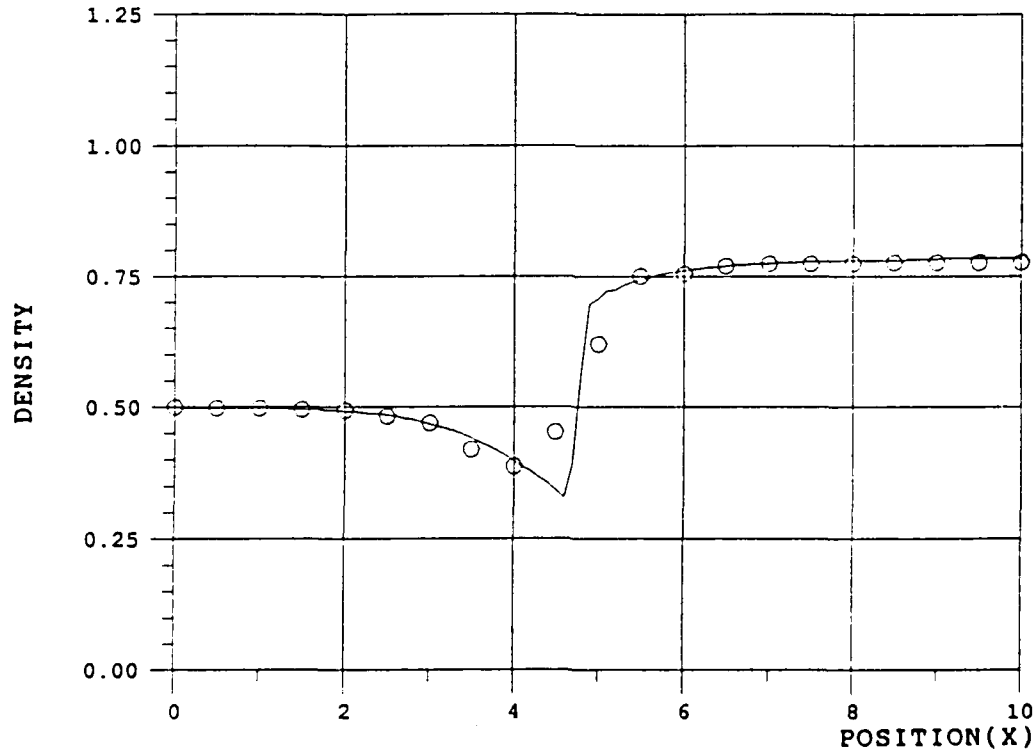
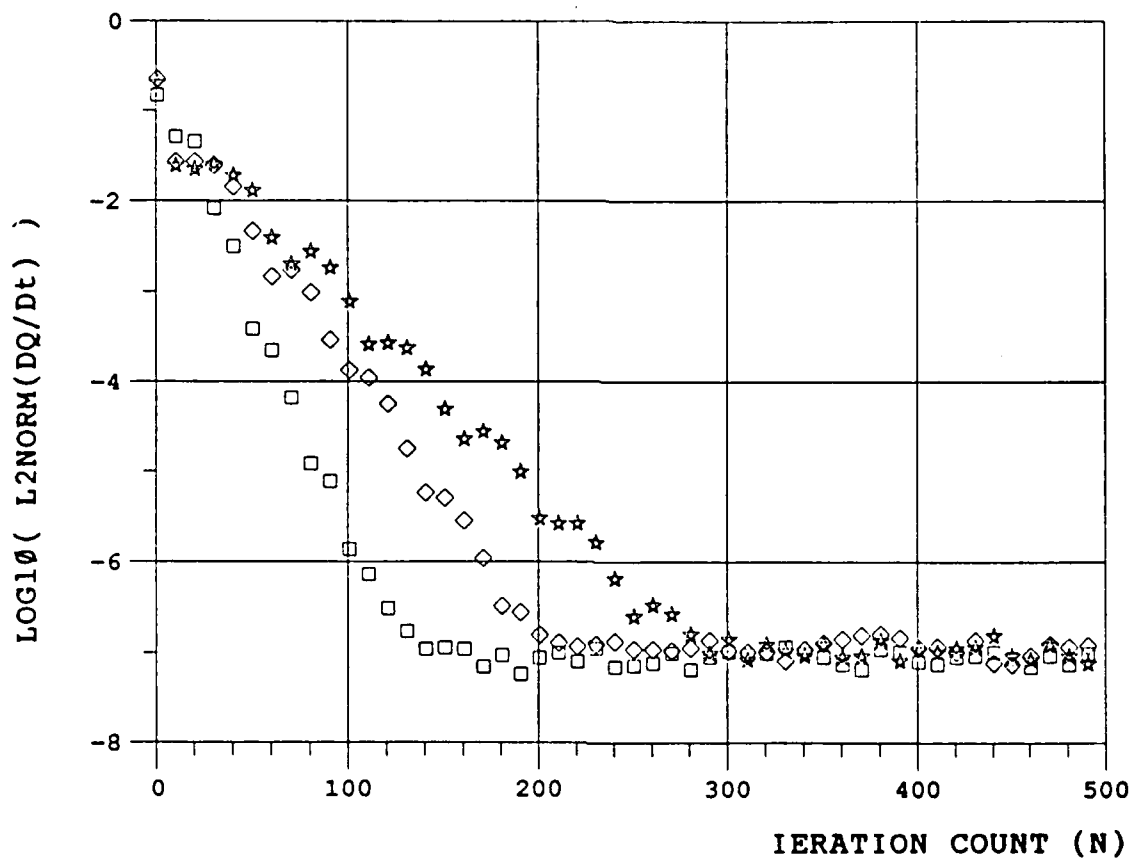Fig. 8 Density computed by Beam and Warming implicit scheme with standard artificial dissipation for Shubin's nozzle.

Fig. 9 Convergence history for the modified Gauss-Seidel, modified odd-even Jacobi, and Beam and Warming implicit methods. The modified Gauss-Seidel method is shown as a square, the modified Jacobi is shown as a star, and the Beam and Warming is shown as a diamond.

1989 USAF-UES SUMMER FACULTY RESEARCH PROGRAM/

GRADUATE STUDENT RESEARCH PROGRAM

Sponsored by the

AIR FORCE OFFICE OF SCIENTIFIC RESEARCH

Conducted by the

Universal Energy Systems, Inc.

<u>FINAL REPORT</u>

<u>THE EFFECTS OF ELEVATED TEMPERATURE EXPOSURE</u>

<u>ON THE STRENGTH AND MICROSTRUCTURE</u>

<u>OF 2-D CARBON-CARBON</u>

Prepared by:	Christopher G. Kocher
Academic Rank:	Graduate Student
Department and	Civil Engineering and Mechanics
University:	Southern Illinois University at Carbondale
Research Location:	AL/VSSC
	Edwards AFB, CA 93523
USAF Researcher:	Dr. Peter B. Pollock
Date:	September 19, 1989
Contract No:	F49620-88-C-0053

THE EFFECTS OF ELEVATED TEMPERATURE EXPOSURE

ON THE STRENGTH AND MICROSTRUCTURE

OF 2-D CARBON-CARBON

by

Christopher G. Kocher

ABSTRACT

Results of an investigation into the effects of heat treatment on the strength and microstructure of 2-D CVD-matrix carbon-carbon are presented. Test specimens were heat treated to 1800°F, 2700°F, 3500°F, and 4500°F in an inert atmosphere. Tension, shear, and compression tests were performed to ascertain the effect of heat treatment on the strengths and moduli of the material. Microscopic evaluation was performed using optical microscopy to determine microstructural changes. Periodic edge replication was performed during some tests to examine the cumulative development of damage. Exposure to the highest temperature was shown to produce an approximately 25% decrease in tensile and shear strength. The compression data showed wide scatter and is inconclusive, though edge replication gave evidence as to the failure process in compression as well as in tension. It is determined that characteristic damage states are created that are dependent on the temperature of exposure but appear to be independent of the heating rate.

I. INTRODUCTION:

The range of applications of carbon-carbon composite materials (composite materials consisting of carbon fibers suspended in a carbon matrix) is steadily increasing. Current uses lie primarily in aerospace, where carbon-carbon is utilized due to its low coefficient of thermal expansion (CTE), high strength-to-weight ratio, resistance to ablative and corrosive environments, and its high temperature stability. Such applications include space radiators, mirrors, rocket nozzles, and high-temperature surfaces of advanced aerospace vehicles. However, other fields are beginning to see applications of the material as well. In medicine, for instance, carbon-carbon artificial hip joints and bone plates have been successfully tested. In the automotive industry, carbon-carbon is used for high-performance race car brakes and clutches (tribological applications).

As carbon-carbon receives increasing consideration as a candidate for primary structural elements, it is important that the mechanical response of the material be understood in detail. Designers of advanced aerospace vehicles must have certain knowledge of both the strength and moduli of a material in order to achieve efficient designs which minimize weight while optimizing strength. Not only are the standard properties of the as-received material important, but any effects induced by the service environment must be known as well.

Most applications of carbon-carbon involve subjecting the material to extreme heat on the order of several thousand degrees F. Certain behavioral changes from such an environment are well known, qualitatively. It is common knowledge, for instance, that exposure to elevated temperatures will

increase the crack density in the material and therefore cause an associated degradation of material properties. One must, however, have information about the quantitative changes in material response from such an operating environment.

To this end, the Composites Lab at the Edwards Air Force Base Astronautics Lab is interested in determining the environmental effects on structural carbon materials for applications to space structures.

This research dealt with the effects of thermal exposure on the mechanical properties and microstructural characteristics of a 2-D carbon-carbon composite material consisting of carbon fibers with a matrix deposited by chemical vapor deposition (CVD). Although very little work is available in the open literature regarding this type of material, information about the constituents is abundant.

The structure of pyrolitic carbon is generally classified according to its appearance under an optical microscope using crossed polarizers. Such lighting will then reflect colors particular to the orientation of the crystallites relative to the light source. These structures are dependent on the deposition conditions within the CVD reactor, but local variations of the deposition parameters within the component may produce varying optical textures, regardless of the conditions exterior to the component within the furnace.

It is known that heating carbon-carbon introduces microcracks within the structure due to the differences in CTE in the longitudinal and transverse directions. This CTE mismatch produces a network of cracks which lie in planes normal to the midplane of the laminate and traverse the bundles from one bundle interface to another. A second type of microcracking can occur. This is crack formation at the fiber/matrix interface. Interfacial cracks can propagate completely or only partially around a fiber. These microcracks

degrade the performance of the composite. The processing temperatures involved in the manufacture of structural carbons is sufficiently high (2000°F) to induce microcracking, so a carbon-carbon component after manufacturing is considerably weaker than the theoretical maximum strength predicted from the constituent ideal properties.. If the carbon material is then graphitized (4500°F), then additional cracking will occur. Typical operating temperatures for carbons may be as high as 3500-4000°F.

The transverse cracks (or "straight cracks") are believed to be caused by a shear lag phenomenon through which the large shear stresses induced by the CTE mismatch between the orthogonal bundles are redistributed creating high normal stresses. As the matrix is a brittle material, it will fail on a plane of maximum normal stress.

A Bachelor's and Master's degree in Engineering Mechanics with an emphasis on the mechanics of composite materials coupled with several years of experience performing microstructural studies of carbon-carbon composites provide me with an excellent background to study these materials, for which both microscopic and macroscopic studies are essential for a complete description of material behavior.

II. OBJECTIVES OF THE RESEARCH EFFORT:

Several objectives were specified at the onset of this work:

(i)   determine how heat treatment in an inert atmosphere affects the mechanical properties (strengths and moduli) of CVD-matrix carbon-carbon via a comprehensive experimental program,

(ii)   determine any microstructural changes in terms of crack spacing and fiber or matrix crystal structure,

(iii)   correlate the microstructural changes with the experimental observations,

(iv)   develop an analytical model to complement the observations.

All of these objectives were satisfied at least in part. Nearly all of the mechanical testing was completed and some observations about the direct effects of thermal exposure on the mechanical properties as well as the failure process of the material under tensile and compressive loading were determined. Microstructural analysis using optical microscopy revealed the presence of characteristic damage states particular to the temperature history received by the material, and these damage states were seen to affect the mechanical properties in the anticipated manner. Most of the analysis portion of this project was left to another summer student.

Some new objectives were specified as the project became underway. It was decided to devise a method for the observation of the development of damage during testing so that the damage induced by mechanical loading could be separated from the pre-existing damage induced by the heat treatment. This, too, became the responsibility of another summer student. It was at first desired to obtain data on the fracture toughness of material, but circumstances beyond our control caused us to obtain data on the compressive behavior of the material instead.

These objectives were reached.

III. PREVIOUS STUDIES:

Pyrolitic carbons have been classified according to their appearance under polarized light. The deposition conditions (gas concentrations, temperature) in the CVD reactor dictate the resulting microstructure, whether the deposition is dominated by the nucleation or growth of the crystallites. Low temperatures and high gas concentrations favor crystallite growth over nucleation, resulting in a coarse, columnar structure with distinct growth cones and high optical activity, while high temperatures and low concentrations favor nucleation, resulting in the formation of small, fine crystallites possessing low optical activity. The structures of pyrolitic carbon are classified under four categories: Rough laminar (or columnar), smooth laminar, transition, or isotropic. The rough laminar structure results from low temperatures ($1000-1200^\circ$C) and is characterized by high optical activity with a grainy (or "rough") appearance overall, and prominent growth features. This structure possesses a low density and is mechanically weak. The

smooth laminar structure is characterized by high optical activity as well, but the surface appears smooth. It is formed in intermediate-to-high temperatures and low-to medium gas concentrations. This structure is more dense than the rough laminar structure. The fourth category, the isotropic structure, is deposited at high temperatures and low gas concentrations. Isotropic structures have very small crystallite sizes and as a consequence appear amorphous or isotropic under polarized light. In fact, these structures are still anisotropic, but the crystallite size can be smaller than the wavelength of the light used for viewing, hence the crystallites are not discernable. Such a structure possesses the highest density and is mechanically superior to the other structures. The third structure, the transition structure, is deposited at middle-to-low gas concentrations and middle-to-high temperatures. It represents a transition from the fine-grained isotropic structure to the more coarse-grained laminar structures, hence it appears to have some optical activity, though it is not pronounced.

Kaae (1970) deposited pyrolitic carbon on graphite discs in a fluidized bed at 1200°-2000°C, then determined the elastic modulus and fracture strength from 3-point bending specimens. The modulus and fracture strength increased significantly with density at constant crystallite size.

Oh and Lee (1988) examined the mechanical behavior of pyrolitic carbons deposited within carbon mats at 1100°-1400°C and for propane concentrations of 10% to 70%. The resulting composites had fiber volume fractions of approximately 12%, so the contribution of the fibers to the overall composite properties would be negligible. It was found that at 10% propane, the matrix density and crystallite size decreased significantly over the temperature range, while the macroporosity increased. At 70% propane, however, the matrix density and crystallite size remained constant over the

temperature range while the macroporosity still increased. The mechanical properties were affected significantly as well. For the 10% propane samples, the modulus and fracture stress decreased over the temperature range, but for the 70% propane samples the modulus and fracture stress increased over the temperature range. For both groups, the fracture strain remained constant.

Oh and Lee (1988) then examined the tensile failure behavior of 2-D carbon-carbon laminates with CVD matrices. A propane concentration of 30% at a flow rate of 0.5 to 4 l/min and a temperature of 1000°C were used for all samples, however two different cooling rates were used. Material A was cooled at a rate of approximately 4°C/min while material B was cooled at a rate of approximately 80°C/min. Although the specimens had similar bulk densities, large differences in the mechanical properties were seen. Specimens of material A had more distinct circumferential microcracks around the fibers compared to material B. The cracks in material A are wider and almost extend completely around the fibers, in contrast to material B which exhibited more, shorter, narrower microcracks. This is attributed to the cooling rates. As material B is cooled rapidly, the material is forced to suddenly accommodate the thermal stresses resulting in the instantaneous formation of a series of short microcracks. Having been cooled more slowly, material a could relieve its stresses more gradually through the formation of fewer cracks which are then extended further and/or linked to other cracks; therefore, more crack opening and growth occurs. The crack patterns were thought to be the source of the differences in tensile failure modes observed between the two materials. Material A exhibited a terraced fracture surface while the failure plane for material B was comparatively smooth. It was explained that the tensile cracks advancing through the laminate during loading are deflected by the circumferential microcracks, which are more pronounced in material A,

resulting in a terraced fracture surface around each fiber. For material B, however, the existing circumferential microcracks are not effective in absorbing the energy of the tensile cracks, thus the tensile cracks propagate freely across the laminate resulting in the flat fracture surface.

The transverse cracks observed in 2-D carbon-carbons are similar in many ways to transverse cracks seen in the 90° layers of cross-plied graphite-epoxy laminates fabricated from unidirectional material. Riefsnider and Highsmith (1982) observed the formation of uniformly-spaced transverse cracks in orthotropic lamina under tension. The crack density (spacing) was dependent on, among other things, the load level experienced by the laminate. For a given load level, laminates attained a saturation crack density . The higher the load, the narrower the crack spacing giving a higher crack density and a correspondingly greater reduction in laminate stiffness. The behavior was attributed to a shear lag phenomenon, and an accurate model was developed to predict the saturation crack densities.

Extending this work, Groves, Highsmith, et al (1987) observed in similar laminates that not only were the straight transverse cracks formed, but under certain conditions curved cracks were formed as well. These curved cracks initiated at the interface of the 0° and 90° plies and angled inwards symmetrically towards the existing straight cracks. If the load was increased, the angle cracks would curve such that they ran parallel to the straight cracks. Often two or four angle cracks would develop near a straight crack. They would initiate at either interface and on either side of the transverse crack. Cracks opposite each other with respect to the midplane of the laminate would link as the load was increased. a shear lag phenomenon was again believed to be responsible for angle crack formation.

Similar angle cracks were observed in the material that is the subject of this work. These cracks are also believed to be caused by a similar shear lag phenomenon.

Work done by Jortner (1988) and Pollock (1988) has linked the tensile strength of 2-D carbon-carbon to the crimp angle of the woven bundles in the material. Pollock has postulated that the shear component of the applied stress is responsible for bundle failure.

IV. MATERIAL DESCRIPTION

The 2-D carbon carbon laminates used in this study were manufactured by HITCO using their industrial CVD reactors. The cloth used consists of T-300 PAN fiber bundles with 3000 filaments per bundle woven into an 8-harness satin weave. The weave is balanced, i.e. the same number of ends per inch exist in both the warp and fill directions. The carbon cloth was first heat set at 4500°F. This was done so that the effects of any further heat treatment of the finished composites (up to this temperature) could be attributed to changes in the matrix only. Thirty-two dry plies were stacked, warp aligned, to fabricate each of three laminates. The stacked cloth was then sandwiched between graphite plates with a regular array of holes drilled through. The assemblies were then infiltrated with a pyrolitic carbon matrix through five 125 hr densification cycles. Although most of the particulars of the process were proprietary, it was revealed that the deposition temperature was approximately 1800°F. Intermittently between some of the CVD runs, the plates wer' removed from the furnace, weighed, and measured to calculate the bulk

densities. Prior to the final CVD infiltration, the plates were removed and machined to their final dimensions: 10" x 12" x 0.33 ".

V. EXPERIMENTAL PROGRAM

To investigate the changes in material properties and microstructure of the material induced from high temperature exposure, a comprehensive testing plan was devised through which all of the moduli and strengths of the material subjected to various temperature ranges could be determined. It was decided that tension in the warp, fill, and 30° off-axis directions would give all of the in-plane moduli. The Iosipescu shear test was used to give the shear strength data, and the compact tension fracture test would give the fracture toughness of the material.

An appropriate specimen cutting plan was implemented to maximize the number of specimens. The specimen net shapes were cut from the panels using a diamond-impregnated band saw blade. The tension specimens were ground to final dimensions using a high-speed diamond-impregnated router bit and a template to give uniformity of dimensions. The compact tension specimens were machined on a conventional milling machine using carbide tooling. The Iosipescu shear specimens blanks were sent to Ultracarbon for final machining. To double the number of tensile specimens, all of them were sent to the Permag Corporation where they were sliced along the midplane of the laminate and ground to no more than 0.0005" deviation in thickness along the length of each specimen.

The material was divided into groups for four temperature histories. One group remained as-received, while the remaining groups were subjected to 2700°F, 3500°F, and 4500°F, respectively.

Heat treatment was done in an Astrofurnace manufactured by Astro Industries. Prior to each run the chamber was evacuated to 10^{-5} torr and backfilled with 10-15 psi of helium. Two runs were made to 4500°F. For one run, the heating rate was very fast; the final temperature was reached within 2.5 hrs. A second group of specimens was heated to the same temperature at a slower rate of 200°F per hour. For both runs, the material was allowed to soak at the maximum temperature, then the temperature was decreased to ambient within 3 hrs.

Due to nonlinearities in the response of the system, the initial temperature ramp could not be accurately controlled. Hence the chamber reached 2000°F in a shorter time than was anticipated. This was expected not to cause undue thermal shock to the material, since it had already seen a similar temperature during processing.

Ramp rates of approximately 200°F per hour were used for the remaining temperature runs.

Tests were performed using an MTS tension-torsion materials testing machine with a 50,000 lb capacity. Displacement data from the tension tests was taken with a clip-on extensometer. Displacement data was channelled through an amplifier into a data aquisition system. Load output was fed directly into the computer from the MTS machine.

During the tension tests, a clevis joint was used between the upper grip and the crosshead to prohibit the influence of bending or twisting induced by misalignment of the grips. Wedge-type mechanical grips were used to grip the specimens. Great care was taken to insure alignment of the specimens in

12-13

the grips for all tests. Only 1 or 2 of approximately 30 tension specimens failed near the grips. The gage section dimensions were 0.75" x 0.125 " and 4" long. Aluminum end tabs were bonded to the ends of the specimens.

Edge replications were made periodically on some of the tension specimens during the loading. Prior to loading, the specimens were polished along one edge down to 0.3 μm alumina. During testing, the load was held fixed and a replication was made. During this time displacement data was not taken. The process involved the application of acetate tape softened with acetone to the edge of the specimen. The replica took a half hour or more to dry, so the material had to be kept under load for that time until the finished replica could be removed. As the test was resumed and extensional data taken again, a drop in load was seen on the stress-strain curve. This particular type of material may be susceptible to creep relaxation over relatively short periods of time. This has not been studied yet.

Iosipescu shear tests were performed in a special fixture manufactured at the University of Wyoming. Each specimen had a notch radius of 0.1875" and a gage width of 0.400". The thickness of the specimens was 0.33". Due to the difficulty of obtaining strain or displacement data at the highly localized net section, only load and crosshead displacement data were obtained.

In performing the fracture tests, it was discovered that the compression strength of the material was lower than anticipated. Extension of the initial crack did not occur, but rather the material failed in compression at the rear of the specimen. This caused all of the fracture specimens to be converted into compression specimens.

The dimensions of the compression specimens were approximately 0.7" x 1.0" x 1.5". The low area to length ratio was assumed to be adequate to prohibit global buckling of the specimens.

Edge replications were made of some of the compression specimens as well.

VI. MICROSTRUCTURAL OBSERVATIONS

Samples of the as-received and heat treated material were examined using optical microscopy. Considerable variation in the microstructure of the pyrolitic carbon matrix was seen in a given sample. Within the bundles, the matrix carbon appeared to have an isotropic texture derived from deposition at high temperatures (<1250°C) and low gas concentrations (>30%), according to Oh and Lee (1988). This is in contradiction to what would be expected from the "known" process temperature. Such a low temperature (980°C), according to Oh and Lee, would produce a smooth laminar structure, regardless of the concentration of the gas. The interbundle matrix, however, possessed the expected smooth laminar structure. A number of boundaries between distinctly different structures were seen within the matrix. It was thought that these boundaries corresponded to the end of one deposition and the beginning of another. This was later found to be false. The optical texture of CVD carbon can change abruptly within a continuous deposit. The explanation for this phenomena is unknown as of this writing.

No textural changes in the nature of the CVD coatings was observed with respect to the heat treatment temperature sen by the material, as graphitization does not alter the optical texture of CVI carbon. Hence other microscopic methods are necessary to determine the qualities of the matrix material. Several techniques, transmission electron microscopy and laser ramann microprobe analysis are currently being investigated for the

determination of the crystallite parameters l_c and d_{002}. Knowing these parameters will enable the quantification of microstructural changes brought about by heat treatment and the estimation of the mechanical properties of the matrix material.

Photographic montages of all materials were made using an optical microscope at low magnification (50x). From these montages, the crack densities could be determined. The distance between two adjacent cracks was measured with a ruler, and this measurement was repeated 100 times over each specimen taking a random distribution of transverse cracks. For the material heat treated to the highest temperature, high magnification (1000x) photographs of transverse cracks from both rapidly heated and slowly heated material were taken to measure the crack widths.

In addition to the straight transverse cracks, a number of angle cracks were observed. The study of these cracks using a shear lag model has been undertaken.

It is anticipated that porosity measurements will be made. Porosity has been shown to play an important role in the response of carbon-carbon composites.

VII. RESULTS

Although not all of the data has been processed, some preliminary results are given. The heat treatment to the highest temperature produced a 25% decrease in both shear and tensile strength. The tensile strength in the warp direction was, on the average, higher than the fill tensile strength by 5% or so. This is attributed to the differences in curvature of the warp and fill

bundles due to the weaving process. In the weaving of 2-D cloth, the warp bundles are kept stretched tight and the fill bundles are woven in with less tension being kept on them. Thus the fill bundles exhibit more curvature than the warp bundles. Only the shear strength across the warp bundles was tested, as they are the strongest. The shear data showed little scatter, while considerable scatter was seen in the tension tests. The data has not been normalized to the porosity, and it is believed that doing this would decrease the scatter. It is well established that porosity decreases the strength of materials.

The compression tests have not all been completed. Wide variations in both the modulus and strength of initial tests were cause for concern. No correlation could be made with the data and the density of the material, variation of the fiber alignment from axial, or dimensional accuracy. Since porosity measurements have not been made as of this writing, no correlation of porosity with the observed behavior could be made. The remaining compression experiments have been delayed until a satisfactory explanation for the observed behavior has been found.

Edge replication has proven to be a valuable tool in the visualization of progressive damage in carbon-carbon materials. The replicas taken of the tension specimens revealed the formation of "s-cracks" within the fiber bundles. It appears that the transverse cracks reach a saturation crack density as the load increases, then s-cracks form. One possible mechanism for the formation of the s-cracks is that partial delamination results in the separation of adjacent bundles. When this occurs, uneven load distribution within the laminate results and a series of s-cracks are formed to redistribute the stresses. The s-cracks each extend to the nearest longitudinal bundle and initiate local delamination. The localized delaminations quickly link and cause

catastrophic failure of the specimen. The uneven load distribution among the fiber bundles explains the observed "brooming" of the tensile specimens.

Examination of the failed compression specimens gave clues as to their failure process. The specimens failed by way of diagonal "slip planes" in the material as local microbuckling of the fiber bundles introduced shearing planes in the material. The interlaminar strength of carbon-carbon is extremely low, so tensile poisson stresses generated normal to the direction of the applied load may easily contribute to delamination. Delamination cracks were observed to run parallel to a fiber bundle along its straight section (a bundle in an 8-harness satin weave has considerably long straight sections) until reaching a point of curvature. The crack then jumped across diagonally to the next longitudinal bundle along which it proceeded to the next point of curvature, and so on. The point of crossing of the crack took the form of a straight crack indicative of a possible dependence on the crimp angle (shear strength of the bundle). In other places, the crack traversed the bundle where microbuckling occurred. This microbuckling occurred at the position of maximum crimp angle. This is not surprising, as the larger the angle of the bundle relative to the loading axis, the lower the resistance of the bundle to axial loading and eventual buckling. Bending moments are introduced in these angled sections.

No study of the failure of the shear specimens was done, though it would be of interest to examine the failure surfaces. Indeed, it is planned to examine the failure surfaces of all types of specimens in detail using both optical and electron microscopy.

VIII. RECOMMENDATIONS

Examination of the results gathered thus far has indicated areas requiring further exploration. Although a general hypothesis is presented for the tensile failure mode of this 2-D material, additional testing combined with periodic edge replication is needed. The dependence of the crimp angle on the failure modes should also be investigated. Further experiments are also needed to more accurately describe the failure processes in compression and shear as well. Analysis is required to supplement the experimental observations, which requires the formulation of a realistic model of the physical problem. Extensive microscopic analysis of the material is required so that accurate estimates of the constituent properties can be used in the analysis, and a more complete idea of the effects of heat traement on the material can be determined. Also, the correlations between crack density and mechanical properties bears further study.

IX. ACKNOWLEDGEMENTS

I would also like to thank Mr. James Wanchek and the entire staff of the Composites Lab at Edwards AFB for their helpful guidance and accommodation. They couldn't have provided a better atmosphere in which to work, learn, and have fun. In particular, Dr. Peter Pollock of the University of Dayton Research Institute, with whom this work was performed, is to be commended for providing me and a host of other students with such an outstanding opportunity to learn about the business of doing science.

I must also extend my sincere appreciation to Universal Energy Systems for providing the excellent program allowing myself and many other students and faculty around the country to gain experience at such highly regarded research institutions.

1989 USAF-UES GRADUATE STUDENT RESEARCH PROGRAM

Sponsored by the

AIR FORCE OFFICE OF SCIENTIFIC RESEARCH

Conducted by

Universal Energy Systems, Inc.

FINAL REPORT

Vibration Control of a Cantilevered Beam Using a Distributed Actuator

Prepared by:	David A. Lapioli
Academic Rank:	Graduate Student (MS Program)
Department and University:	Aerospace Engineering Department The Pennsylvania State University
Research Location:	Vehicle Systems Division Air Force Astronautics Laboratory Edwards AFB, CA 93523
USAF Researcher:	Dr. Alok Das
Date:	September 1989
Contract No.:	F49620-88-C-0053

<u>Vibration Control of a Cantilevered Beam Using a Distributed Actuator</u>

by

David A. Lapioli

ABSTRACT

The dynamics and control aspects of a long, thin cantilevered beam were studied to model a component of a large flexible space structure. Experiments using piezoelectric film as a distributed actuator were conducted and the results were compared to computer simulation and to previous work done at the Charles Stark Draper Laboratory (CSDL). In the experiments, tip acceleration for a cantilevered beam with an initial tip deflection was measured. Various control laws (mainly "bang-bang" type) were applied to actuate the piezo-film, to try to find the vibration settling time. The partial differential equation and boundary conditions are presented for the cantilevered beam configuration and a solution is shown which results in the shape functions for the beam and the system model. The experimental methods and techniques for film application, data acquisition, etc. are described.

ACKNOWLEDGEMENTS

I. INTRODUCTION

Many of the designs for future space platforms can be described as large space structures (LSS). A large space structure will be defined as a structure in space which consists of a large number of structural elements configured in such a way to provide a space platform for ongoing scientific experiments or defense missions. The structure is constructed of many elements and may be highly flexible. Structures with special mission requirements, such as pointing accuracy, orientation control, shape control and target tracking may be classified as large space structures if the structure has a large number of controlled structural modes. Typical configurations are football field size or larger structures envisioned for communications antennas, astronomical observations, solar power stations, space defense platforms, and manned laboratories (Ref. 1). Many LSS components are made of aluminum or composite materials which have low inherent natural damping. The low damping and high flexibility make the structures susceptible to environmental disturbance (Ref. 2). To conform to certain mission requirements, such as fine pointing and targeting/tracking, active vibration control is required to damp out, say, residual oscillations due to a slewing maneuver or attitude/orbit adjustment.

One possible actuator for this type of low authority vibration control is piezoelectric polymer film. In this study, the piezo- film is bonded to an aluminum cantilevered beam which represents a typical LSS component. When a voltage is applied to the film the electric field induces a stress in the beam which can be used to control the vibrational modes of the beam.

The distributed nature of this problem coincides with the author's research interest in the field of structural dynamics. All real world dynamical systems are distributed systems which may be described by partial differential equations (PDE) and the appropriate boundary/initial conditions. In many cases, the system can be discretized such that a system model would now contain simultaneous ordinary differential equations (ODE) with boundary/initial conditions.

Examples of discrete control systems include proof mass actuators, torque wheels, thrusters,

and discrete piezoelectric elements. Some distributed active control systems are piezoelectric film and NITNOL material.

There are several advantages to implementing a distributed control scheme. First, as the current designs for space structures grow increasingly flexible, the difference between ground tests of these structures in a strong gravitational field and their actual on-orbit behavior increases, and determining discrete actuator placement becomes more difficult. This can be avoided using distributed actuators and sensors. Distributed control schemes are less sensitive to individual actuator and sensor failure. Some distributed control schemes can control all modes for certain boundary conditions (Ref. 3). This study is concerned only with the first mode vibrations and control of an aluminum cantilevered beam.

II. OBJECTIVES OF THE RESEARCH EFFORT

There were two main objectives of the research effort. The first was to reproduce the experiments done at the Charles Stark Draper Laboratory (although on a smaller scale) and experiment with the techniques used for beam specimen preparation and data acquisition. Piezo-film application was an important step in the preparation process. Mechanical work is done on the beam by the film induced stress, so the adhesives, electrical leads, and film size must be properly considered. Data acquisition techniques, such as sensor selection, electronic noise levels, and computer/transducer matching must also be taken into account.

The second objective was to utilize a "bang-bang" type control law in simulations. The control voltage used in the CSDL study was on the order of 100 to 500 volts. The available voltage for controlling the beam at the AFAL was 5 volts. Since the CSDL voltage could not be reproduced, various control laws were implemented in simulation to attempt to increase controller performance.

III. SIMULATION RESULTS

The partial differential equation describing the cantilevered beam in Figure 1 can be written as

$$\frac{\partial^2 w}{\partial t^2} + \frac{EI}{\rho A}\frac{\partial^4 w}{\partial x^4} = p(x,t) \qquad \text{Equation (1)}$$

where
$w = w(x,t) = $ displacement

$p = p(x,t) = $ forcing function

$E = $ Young's modulus

$I = $ cross section moment of inertia

$\rho = $ density

$A = $ cross section area

Equation (1) can be transformed to two simultaneous ODE's in x and t respectively by separation of variables. The result is:

$$\Phi^{IV}(x) - \beta^4 \Phi(x) = 0 \qquad \text{Equation (2)}$$

$$\ddot{W}(t) + \beta^4 c^2 W(t) = P(t) \qquad \text{Equation (3)}$$

The solution of Equation (2) represents the eigenfunctions or mode shapes of the beam equation and is a function of x only. Equation (3) provides the state space system model, and is a function of t only.

For this analysis, only the first mode vibrations are considered. Also, it is assumed that the eigenfunctions, $\Phi(x)$, contribute to $p(x,t)$, the piezo-film forcing function, such that:

$$p_i(x,t) = \gamma_i P(t) \qquad \text{Equation (4)}$$
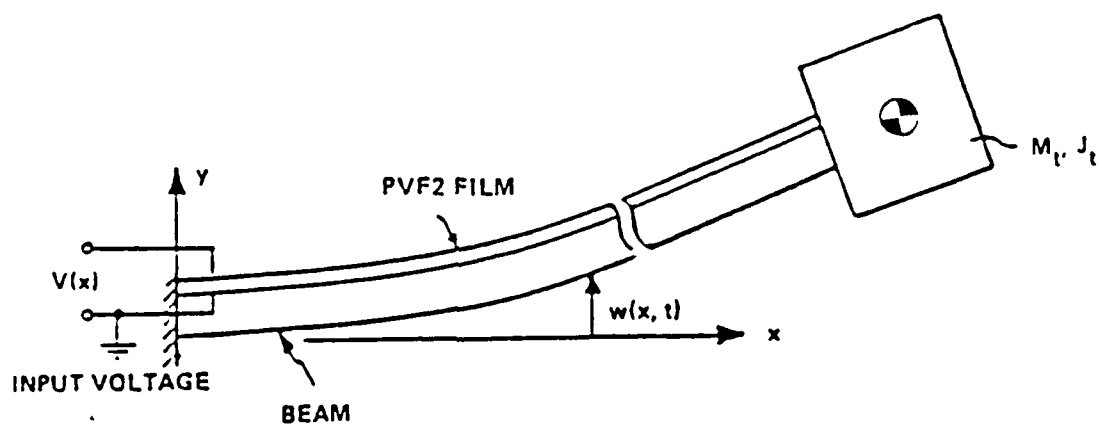
Figure 1.   Piezo-film damper on cantilevered beam
with tip mass (from Reference 2)

where, for the ith mode,

$$\gamma_i = \int_{x_1}^{x_2} \Phi_i(x)dx \qquad \text{Equation (5)}$$

$P(t)$ = constant force per unit length that is calculated from film properties and geometry

For the <u>first</u> <u>mode</u> oscillations:

$$\gamma_1 = \int_{x_1}^{x_2} \Phi_1(x)dx = 0.8826$$

$$P(t) = \frac{V_c b}{g_s L} \qquad \text{Equation (6)}$$

V_c = control voltage

b = beam width

L = beam length

g_s = piezoelectric film stress constant

The initial concept for controlling the beam was to use a "bang-bang" type control where the sign of the control voltage (+ or -) is determined by the acceleration feedback, that is, the control law is:

$$V(t) = SGN(\ddot{W}) \quad V_{control} \qquad \text{Equation (7)}$$

This configuration "matches" the actual experimental set up since a linear accelerometer is placed at the beam tip, and the small angle assumption is made such that angular acceleration is approximately equal to linear acceleration at the tip.

If the coefficients of Equation (3) are combined and the forcing function is substituted into the control law parameter $V_{control}$, an equation of the following form can be derived:

$$\left(1 + \frac{\gamma}{|\dot{W}|}\right)\ddot{W} + \omega^2 W = 0 \qquad\qquad \text{Equation 8}$$

where $\left(1 + \frac{\gamma}{|\dot{W}|}\right)$ can be described as an effective mass "m_{eff}" of the classic spring-mass dynamical system. By increasing the control voltage (contained in γ), not only is the vibration settling time reduced, but "m_{eff}" is also increased and the frequency of the damped system oscillation is reduced. This is seen in the simulation outputs shown in Figure 2.

A finite element analysis was performed using a NASTRAN model and the same properties and dimensions as the experimental aluminum beam. The first mode frequency of the NASTRAN output matched experimental data (from a spectrum analyzer) very closely. This value (10.4 Hz) was used in the state space model to determine the coefficients of the state equation matrix A.
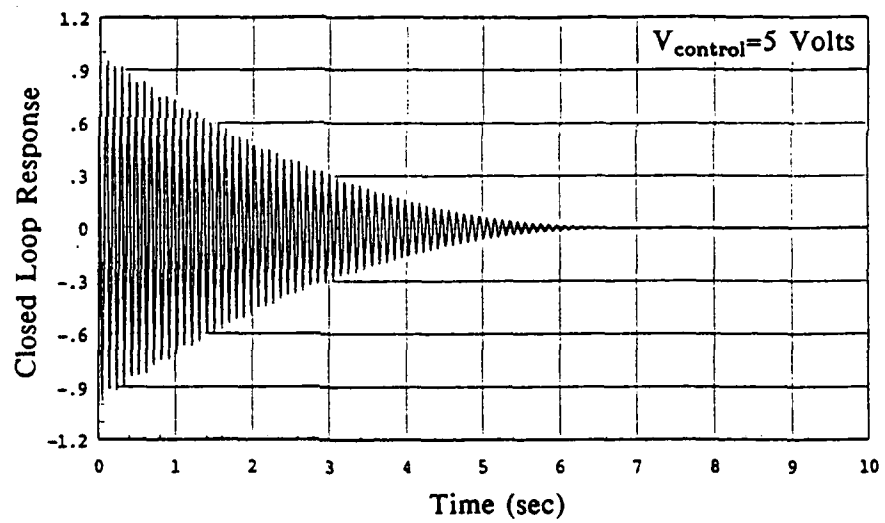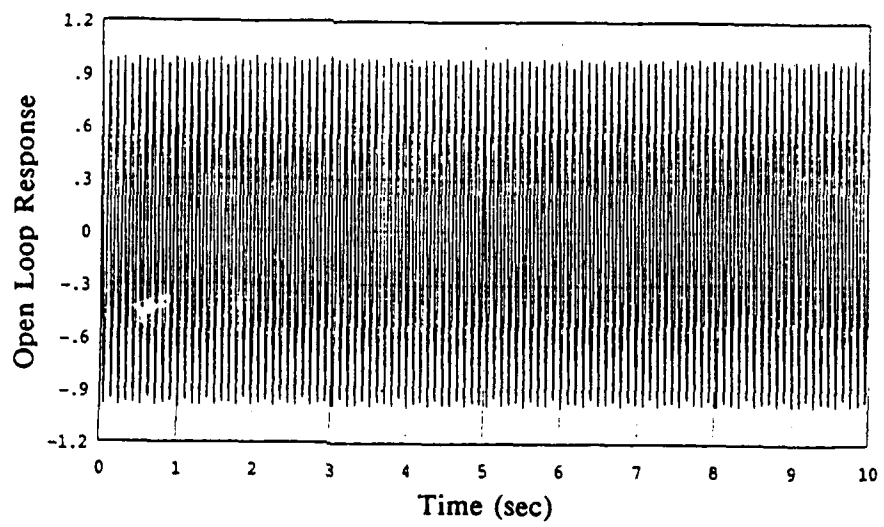
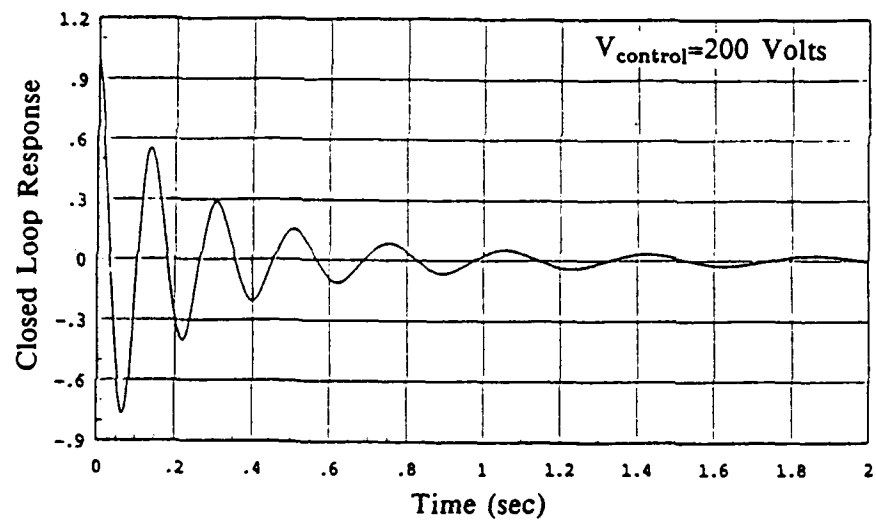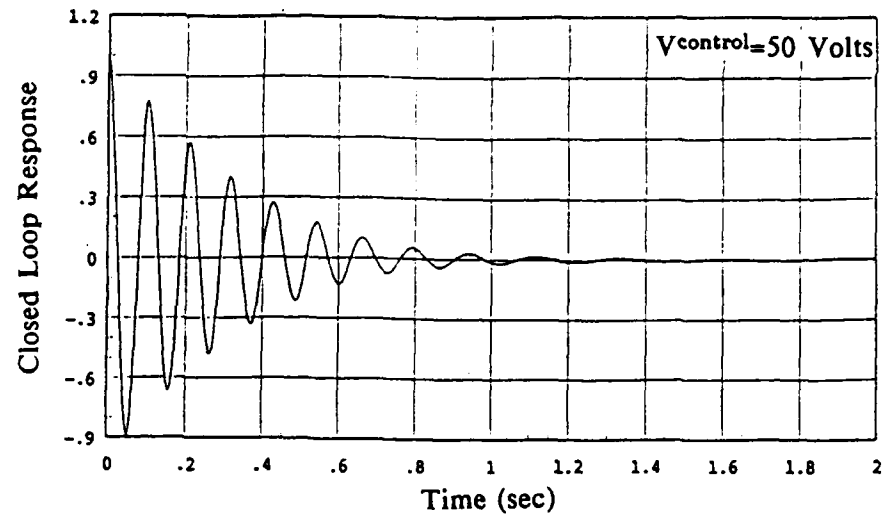Figure 2.   Simulation results for increasing control voltages

Figure 2.   Simulation results for increasing control voltages
(cont.)

IV. EXPERIMENTAL RESULTS

A. Specimen Preparation

Care must be taken in mounting the piezo-film to the aluminum beam. Any bubbles or wrinkles in the film surface may cause a non-uniform control over the beam span. The following procedure was used to apply the piezo-film to the beam:

1. Using alcohol and Kim-wipes, clean one side of the beam until no dirt appears on the Kim-wipe.

2. Cut the piezo-film to a size slightly larger than the beam area. It is important to note the electrical polarity and positive stress direction of the film.

3. Clean the side of the film that is glued to the beam. This is done by wiping the film lightly with an alcohol-dampened Kim-wipe.

4. Apply a thin uniform layer of epoxy to the cantilever (clean side). Using a razor blade, start at the base and "pull" the glue towards the tip. Be aware of the hardening time of the epoxy.

5. With the piezo-film direction and polarity correctly aligned, apply the film to the beam. Start at the base while holding the film taut and "roll" out any bubbles with the thumbs.

6. Let the specimen dry (until adhesive cures) and trim excess with a razor blade.

The electrical lead was connected by soldering the wire to a brass tab. This tab was then mounted to the film using an electrically conductive epoxy.

B. Experimental Apparatus and Procedure

The apparatus is shown in Figure 3. A tool vise is used as the cantilever support. The beam and film properties are given as follows:

	Beam	Film
Material	Aluminum (6061-T6)	Kynar piezo-film
Length (in)	12	11.75
Width (in)	1	1
Thickness (in)	0.05	9.06E-4
Modulus, E	9.9E6 psi	2E09 N/sq. m
Density	0.098 lb/cu. in.	1.78E03 kg/cu. m

An accelerometer (Endevco 2250A-10) is fixed at the tip of the beam. Its mass is 0.4 g and the sensitivity of the accelerometer is 10.39 mV/g. The accelerometer signal is the input for the MAX100 computer system which applies the control law (determined in Section III) and outputs the control voltage (5 volts) to the piezo-film.

Both beam tip response (input) and control voltage (output) are collected as data. The specimen tip is initially deflected 0.25 inches and released from rest. The data acquisition is started before the beam is released and continues for thirty seconds (nominal) at a sampling rate of 100 Hz.

C. Experimental Results

The piezo-film actuator was tested on a beam vibrating in a single mode (primarily). The first bending mode was chosen for study to duplicate the CSDL effort and, as stated in Reference 2, the first mode was easiest to isolate and visually identify. The results of the tests
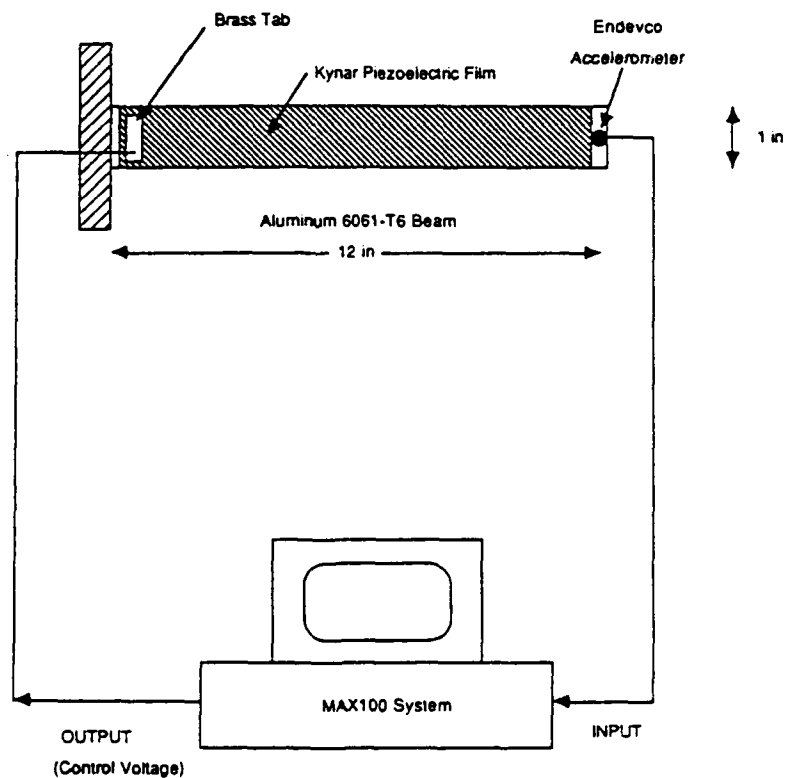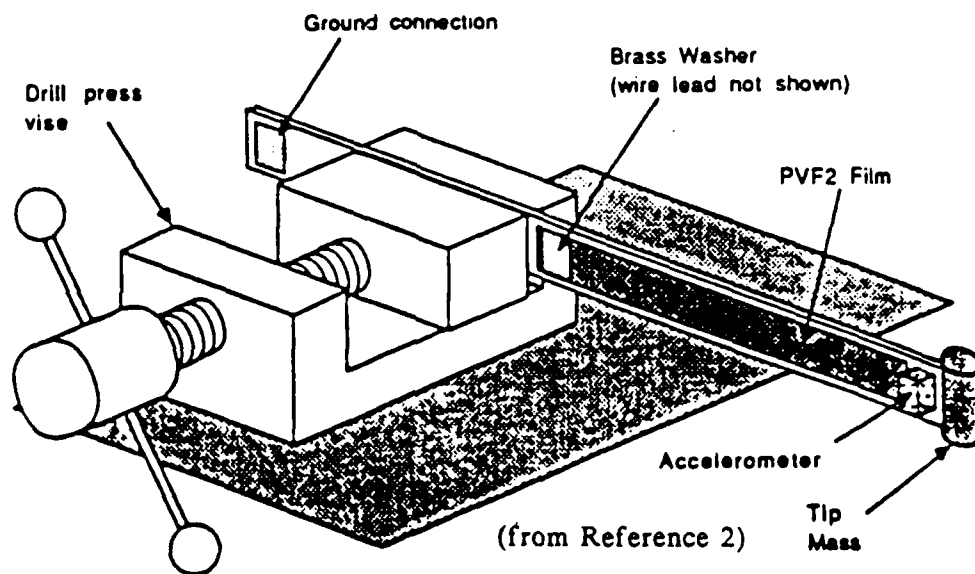
Figure 3.   Schematic of experimental apparatus and controller

are shown in Figure 4. The first trace shows the free decay time with no control applied. Since the control voltage was limited to 5 volts, some variations on the "bang-bang" control were tried, but these control laws were not as effective during testing as they were in simulation.

The variation on the "bang-bang" type control is also a function of the input acceleration. The control law is:

$$V(t) = SGN(\ddot{W}) \cdot \sqrt{\ddot{W}} \cdot V_{control}$$

<div align="right">Equation (9)</div>

In simulation, this control law produced faster settling times than "bang-bang" type control. It has the effect of smoothing the square wave produced by Equation (7) proportionally with the square root of the input acceleration.

In comparison to simulation, the settling time for the free vibration is not greatly reduced when the active control is applied. The "bang-bang" control had a settling time of 23 seconds, whereas the open-loop response resulted in a 30 second settling time. This result is primarily due to the inability of the control system to output a sufficient voltage for increased vibration suppression.
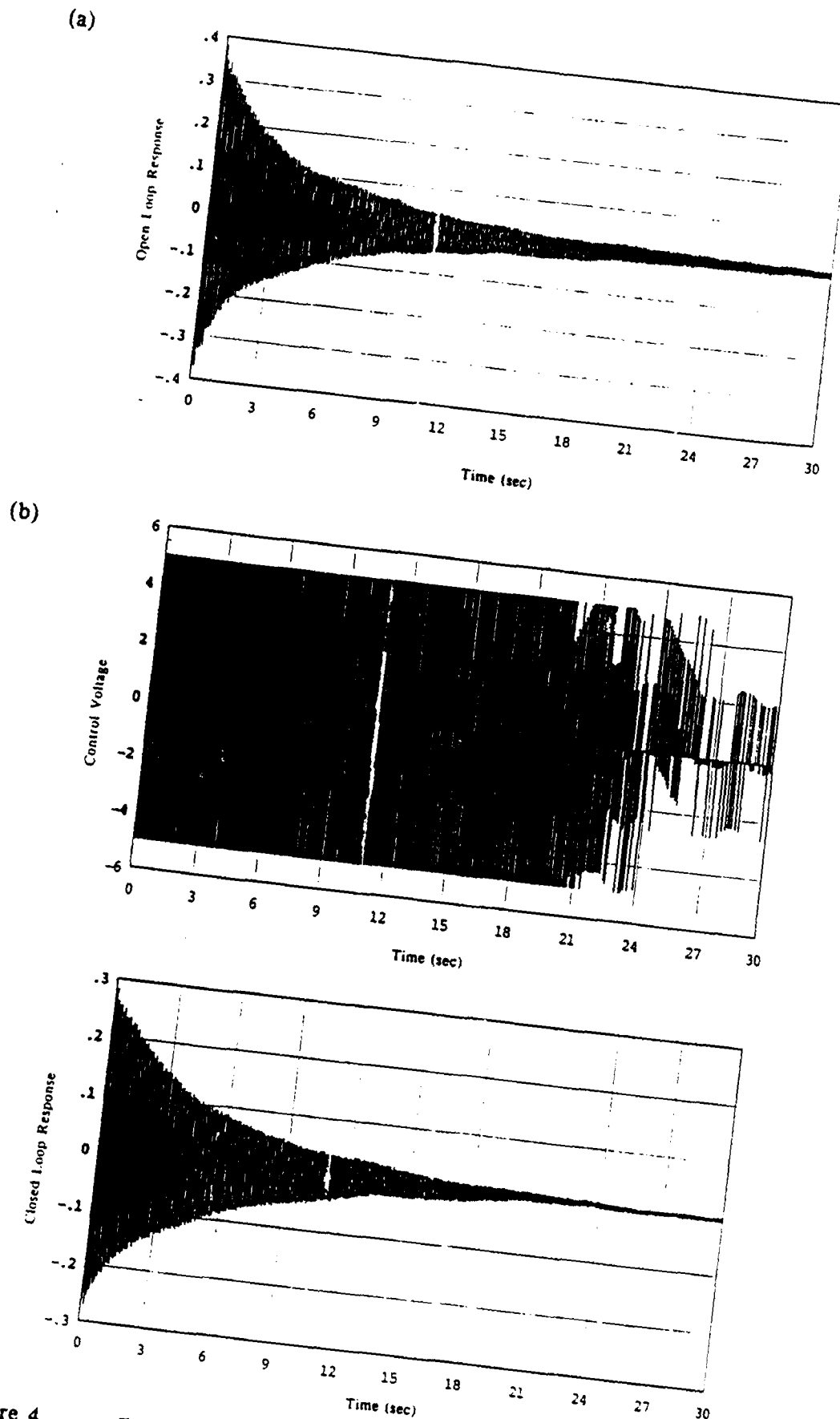
(a)

(b)

Figure 4.   Experimental data: (a) open-loop response,
(b) bang-bang control, (c) "smoothed" control as
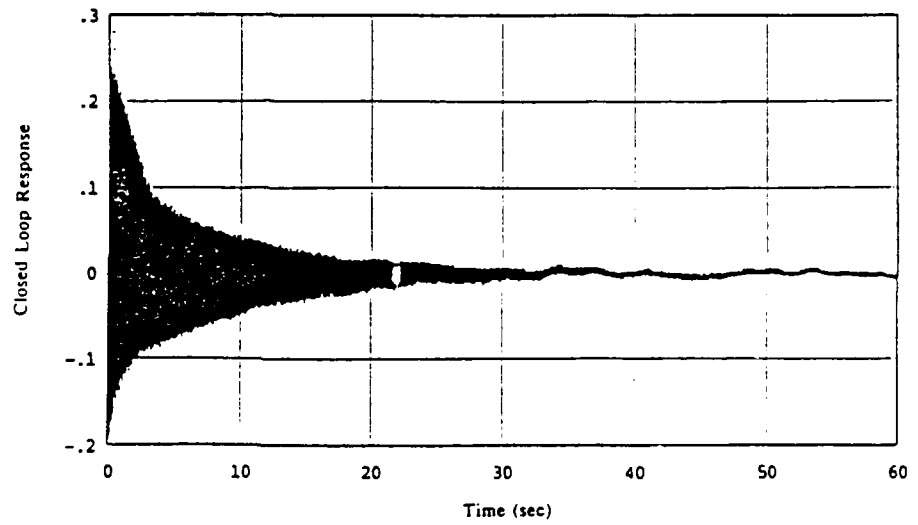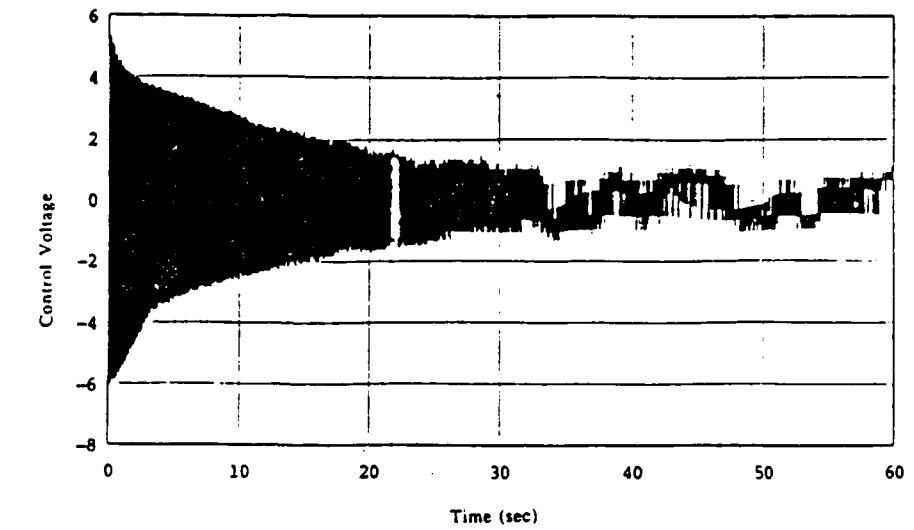expressed in Equation (9)

13-17

(c)

Figure 4.   Experimental data: (a) open-loop response,
(cont.)   (b) bang-bang control, (c) "smoothed" control as
              expressed in Equation (9)

13-18

V. RECOMMENDATIONS

Although the MAX100 data acquisition system performed well for sensing beam vibration, it was limited to 5 volts output for the film control voltage. To see any marked change in beam vibration settling time, higher voltages (on the order of 100-500 volts) are needed. The low authority nature of the piezoelectric film actuator requires the larger output voltages. One possible solution would br to connect a transformer to the controller output leads to increase the voltage seen by the piezo-film.

Another recommendation for the experimental work is to use an accelerometer that is matched to the frequencies under study. Since the sensitivity of the accelerometer used was 10 mV/g, and the MAX100 "noise" is calculated to be about 2 mV, there is a definite need for a better MAX100/transducer combination. Accelerometers intended for use in relatively low frequency vibrations (about 10 Hz for first mode) would have been acceptable in this case. However, when choosing and accelerometer it is important to consider its mass. The greater mass of some transducers usually modifies the dynamic response of lightweight specimens like the aluminum beam under study.

In addition to acceleration feedback control, rate feedback should also be considered for the piezo-film actuator. The system model used does not include any structural damping term, so rate feedback may add a damping factor and reduce the vibration settling time.

Some investigation should be made to determine the "correctness" of the equation used to determine the linear force due to the control voltage. This equation was derived by analyzing the dimensions of the piezo-film stress constant g_r. If the actual performance of the film cannot be simplified to an equation like Equation (6), then a better representation of the film properties must be used in the force equation.

REFERENCES

1. Denman, E., Et Al., "Identification of Large Space Structures on Orbit," American Society of Civil Engineers, Final Report Prepared for the Air Force Rocket Propulsion Laboratory, September 1986.

2. Baily, T., Et Al., "RCS/Piezoelectric Distributed Actuator Study," The Charles Stark Draper Laboratory, Final Report Prepared for the Air Force Astronautics Laboratory, August 1988.

3. Cudney, H.H., Et al.,"Distributed Parameter Actuators for Structural Control," Presented at the Seventh VPI&SU Symposium on Dynamics and Control of Large Structures, Virginia Polytechnic Institute and State University, May 8-10, 1989, pp. 1-2.

1989 USAF-UES SUMMER FACULTY RESEARCH PROGRAM/

GRADUATE STUDENT RESEARCH PROGRAM

Sponsored by the

AIR FORCE OFFICE OF SCIENTIFIC RESEARCH

Conducted by the

Universal Energy Systems, Inc.

<u>FINAL REPORT</u>

<u>USING THE STM TO CHARACTERIZE THE EFFECTS</u>

<u>OF SURFACE TREATMENTS ON THE</u>

<u>SURFACE MORPHOLOGY OF CARBON FIBERS</u>

Prepared by:	Patricia Liu
Academic Rank:	Student
Department and	Materials Science and Engineering
University:	University of California, Berkeley
Research Location:	Astronautics Laboratory AL/RKBA Edwards AFB Edwards, CA 93523-5000
USAF Researcher:	Dr. Wesley P. Hoffman
Date:	August 25, 1989
Contract No:	F49620-88-C-0053

Patricia Liu

Using the STM to Characterize the Effects of Surface
Treatments on the Surface Morphology of Carbon Fibers
Abstract

Proper adhesion between the fiber and the matrix is a necessary factor in achieving optimum performance of composite materials. Thus, a fundamental understanding of the microstructural changes at the fiber surface will provide guidance in developing a strong adhesion at the fiber-matrix interface . In order to achieve this goal, the microstructural changes that resulted from different fiber surface treatments were investigated by using a scanning tunnelling microscope.

Acknowledgements

I. Introduction:

Graphite fibers are the preferred reinforcement in many composite applications. Their high strength and modulus are derived from the orientation of the graphite lamellas. Graphite consists mainly of stacked hexagonal layers of carbon atoms: the high strength covalent bonds between carbon atoms lying in the plane results in an extremely high modulus while the weak van der Waals bonds between the neighboring layers results in a lower modulus in that direction. As a result of fiber processing, these graphitic layers are oriented toward the fiber axis. The overall properties, especially the modulus, are affected by the varying degrees of orientation of the layers. To have a high modulus fiber, the orientation of graphitic crystals must be improved. This is achieved by different types of thermal and stretching techniques involving rigorous controls. The composition of the graphite fibers also plays a role in their properties: the higher the carbon content, the higher the modulus; the lower the carbon content, the lower the modulus.

Graphite fibers provide superior vibration damping and fatigue limits far in excess of steel or aluminum. In addition, as the modulus of the graphite fibers is increased, their thermal expansion coefficients become increasingly negative. This property is particularly critical to many spacecraft, electronics, and instrumentation applications because structures made of these composites experience almost no thermal expansion or contraction across widely ranging thermal cycles.

The aerospace and astronautics industry has shown considerable interest in the use of graphite fibers as a structural component because of their unique properties of high specific strength and modulus to 3000° C. To form a composite material, these fibers are oriented in a preform and a matrix material

is used to bind the fibers together. Since the matrix has the function of transferring the applied load to the fibers, the bond between the fiber and the matrix will affect the mechanical properties of the composite. It follows that, if the surface morphology of the fiber is modified, the interfacial bond and thus the mechanical properties of the composite will change as well.

Dr. Hoffman of the Engineering Design Evaluation Section in the Propulsion Division of the Astronautics Laboratory at Edwards Air Force Base is currently conducting research on different surface treatments on carbon fibers in an attempt to increase the degree of bonding between the fiber and the matrix in carbon-carbon composites.

Through course work at the undergraduate and graduate levels, I developed a strong interest in composite materials research, in particular the role of fiber surface treatment in promoting adhesion between the fibers and the matrix. I further developed my skills and expanded my knowledge in this area by working for my professor. I feel my background in Materials Science and my research experience contributed to my assignment to the Propulsion Division.

II. Objective of Research Effort

My project as a summer fellow was to investigate the effects of various surface treatments on the surface morphology of carbon fibers. In the past, the scanning electron microscope (SEM) and the transmission electron microscope (TEM) have been used to conduct extensive studies on carbon surface morphology. However, using the SEM and TEM requires viewing the sample in a vacuum as well as special specimen preparation, both of which are destructive to the sample's surface or adsorbed surface groups. In addition, the SEM only operates down to the micron scale. Thus, to examine the fiber

surface, I used a scanning tunnelling microscope (STM), an electron microscope which allowed the carbon fiber surface to be viewed nondestructively from the micron scale down to the angstrom scale for the first time.

III. The Theory Behind the STM

The STM was developed by Gerd Binnig and Heinrich Rohrer in 1981 at the IBM Research Lab in Zurich, Switzerland. They were rapidly recognized for their fundamental work on electron microscopy with a Nobel prize in physics in 1986. The STM was a revolutionary development in that it allowed scientists to view surface atomic structure non-destructively for the first time in history.

The operation of the STM is simple in theory. A sharp, metallic tip (Figure 1), whose position is controlled by a piezoelectric scanner, is brought to about 10 angstroms above the sample's surface. A bias voltage, typically tens to hundreds of millivolts, is applied between the tip and sample. When the electron clouds of the tip and sample overlap, quantum mechanical tunnelling occurs. This tunnelling creates an electrical current, whose magnitude varies exponentially with the distance between the tip and sample.

A feedback loop, which is connected to the piezoelectric scanner, senses the current and regulates the vertical position of the tip by maintaining the tunnelling current at a constant value. A constant tunnelling current keeps the tip at a constant height above the sample's surface.

The tip is scanned in an x-y raster fashion across the sample while the feedback loop raises and lowers the tip accordingly. By recording the x,y, and z voltages in the piezoelectric scanner, the three dimensional topography of the surface can be constructed.

IV. Approach and Results

To view the carbon fibers with the STM, they were mounted on a piece of copper and held down with strips of Scotch tape. The copper, being a conductor, made it easier for a tunnelling current to be established between the tip and sample surface. The mounted fibers were placed on an x-y stage to facilitate the alignment of the fiber with the tip. The images included in this report were captured while viewing the fibers with a 9 micron head.

I examined the surface morphology of the untreated P-55 pitch-based carbon fiber at various magnifications and later used the images as a basis for comparison with the treated fibers. Figures 2 and 3 show striation marks that run the length of the fiber. These striations form on all the fibers during the extrusion process as the fibers are spun. Figures 4 and 5 show other striation patterns whose orientation are not parallel to the fiber axis. The most common orientation is observed at a 45° angle to the fiber axis. The origin of these patterns is not known with certainty at this time but it is thought that they form because the pitch becomes too hot as it goes through the extruder and begins to flow.

After viewing the untreated P-55 fibers with the STM, the surface of the fibers were altered with various treatments in order to increase the active surface area (ASA), which is composed of sites capable of forming a chemical bond. Such sites on the P-55 fiber surface include edge carbon atoms as well as structural imperfections. With an increase in active surface area, the degree of fiber-matrix interaction should increase as well.

The first batch of P-55 fibers were oxidized in air to a 0.76% weight loss at 550° C. Since oxygen can only remove the edge atoms, preferential attack of

the fiber was expected. The localized pitting and trenches that form are clearly visible in the surface view shown in Figure 6. As the magnification of the "smooth" area in Figure 6 is increased, the pits, which are 3 times as wide as they are deep, become more obvious (Figure 7).

The second batch of P-55 fibers were exposed to low temperature oxygen plasma and experienced a 6% weight loss. Uniform etching of the fiber surface was expected since atomic oxygen can remove any carbon atom, edge or basal plane. Thus, on the micron scale, the surface should look relatively smooth. However, as can be seen in Figure 8, pock-marked regions appeared on the fiber surface. Such preferential oxidation is possibly due to disordered regions. Figure 9 shows one of the pits at a much higher magnification. It is interesting to note that the depth of the pits are 15 times the width which would be expected with catalytic attack but not atomic oxygen. This effect is not completely understood at this time.

A third and fourth batch of P-55 fibers were treated with concentrated nitric acid at room temperature and boiling temperature, respectively. The reaction rate at room temperature is slower than that at boiling temperature. As expected, room temperature nitric acid basically removes only theimpurities off the fiber surface resulting in only a slight change in the active surface area (Figure 10). At boiling temperature, on the other hand, the reaction is much more severe and pitting will occur, as is evidenced in Figure 11.

V. Recommendations

With the development of the STM, it is now possible to view the surface of the graphite fiber non-destructively from the micron scale down to the angstrom scale. However, since the STM operates at such relatively high magnifications,

it is possible to view only a very small fraction of the surface at a time. It is, thus, difficult to determine what structure is actually representative of the fiber surface. The entire length of many fiber samples will need to be investigated in order to determine whether the structure seen is a true representation of the bulk fiber sample or only a local imperfection in a single fiber. The length of the research program did not allow for such an involved investigation.

With regard to operating the STM, I found that at the at the atomic scale, the sample was very susceptible to thermal drift. I would, thus, recommend placing the entire microscope in thermal isolation in order to allow for better temperature stability.

References

1. Hoffman, W.P., H.T. Phan, T.W. Owens, and W.C. Hurley, "An STM Examination of the Surface of a Graphitized Carbon Fiber," *Proc. 19th Biennial Conference on Carbon*, University Park, Pa, June 1989.

2. Hoffman, W.P., V. Elings, G. Gurley, *Carbon* 26, 754 (1988).

FIGURE CAPTIONS

Figure 1. Schematic diagram of the scanning tunnelling microscope.

Figure 2. Striation marks from extrusion process are evident in STM micrograph of P-55 carbon fiber. (Scan size-2200 nm)

Figure 3. A higher magnifcation STM surface view of the striations characteristic of the P-55 carbon fibers. (Scan size-350 nm)

Figure 4. STM surface view shows flow patterns oriented at a 40°angle to the fiber axis. (Scan size-4000 nm)

Figure 5. STM micrograph shows another type of flow pattern. (Scan size-3500 nm)

Figure 6. STM micrograph shows preferential attack of a P-55 carbon fiber that was oxidized in air to a 0.76% weight loss at 550° C. Pit depth is 3× pit width. (Scan size-7000 nm)

Figure 7. The "smooth" area in Fig. 6 is magnified revealing the pits that were not visible at lower magnifications. (Scan size-300 nm)

Figure 8. After 6% weight loss in low temperature oxygen plasma, pock-marked regions appear on P-55 carbon fiber surface in this STM micrograph. (Scan size-3000 nm)

Figure 9. Magnified surface view of one of the pits in Fig. 8. Pit depth is 15× pit width which is similar to catalytic attack. (Scan size-350nm)

Figure 10. STM topview of P-55 carbon fiber that was treated at room temperature with concentrated HNO_3 reveals preferential attack. (Scan size-3000 nm)

Figure 11. STM topview shows the pitting that occurs on a P-55 carbon fiber that was treated with boiling concentrated HNO_3. (Scan size-3200 nm)
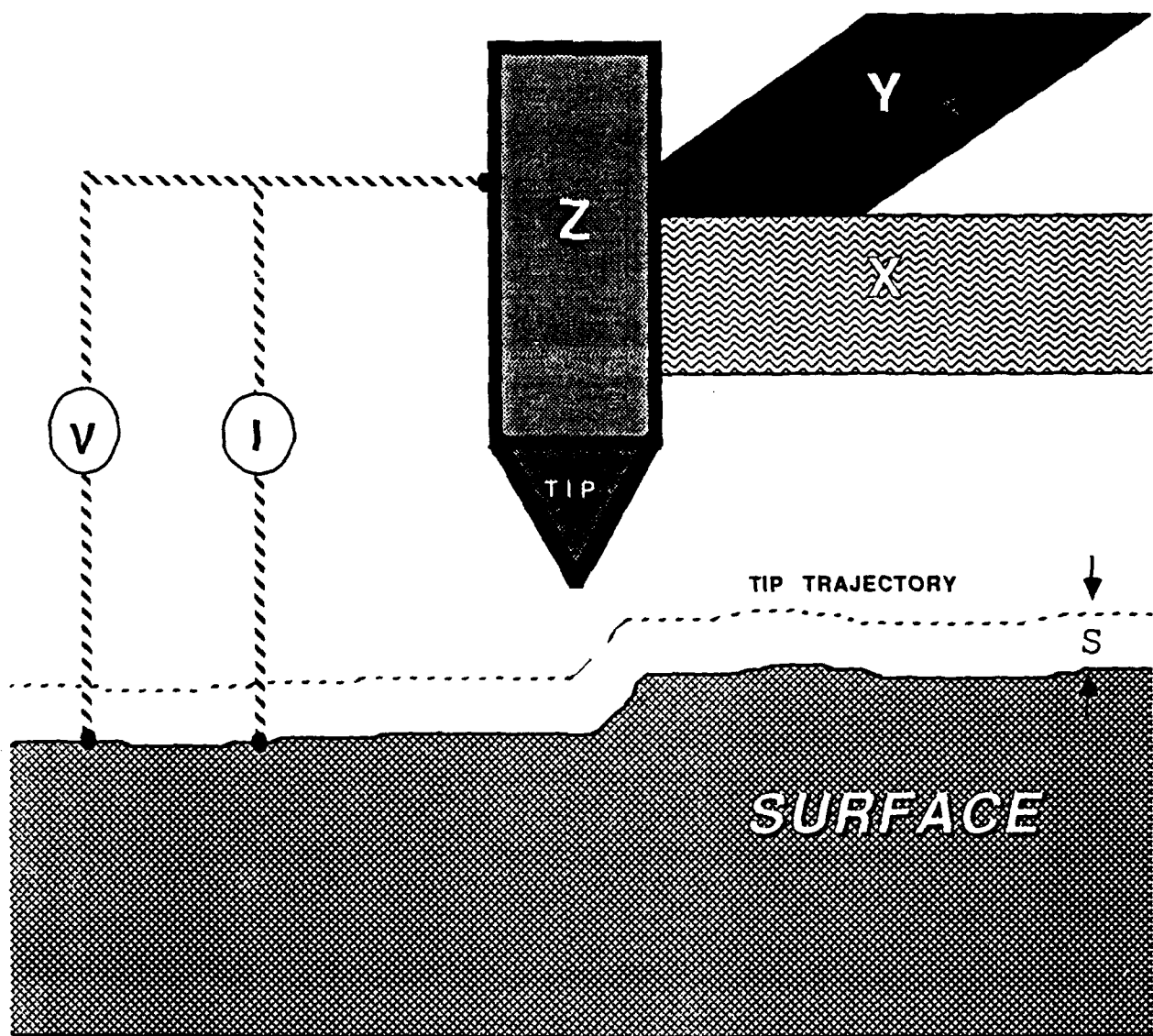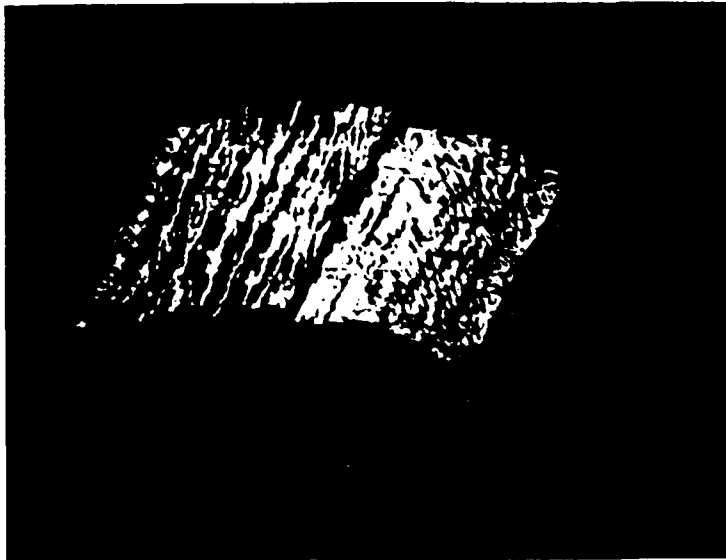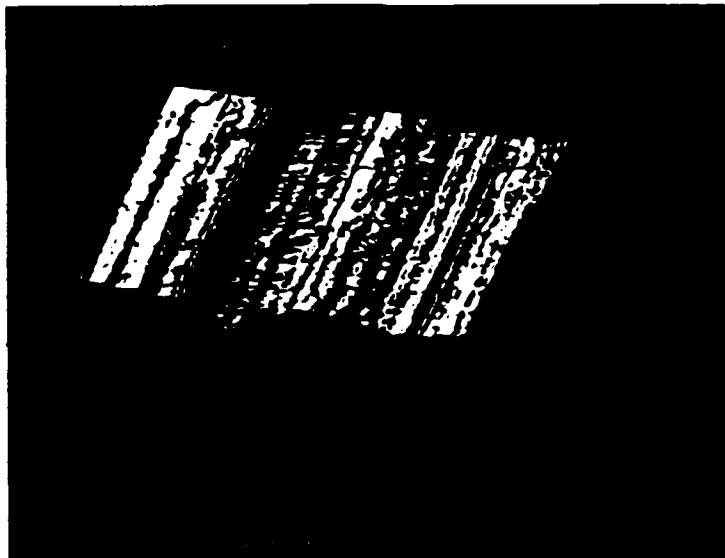
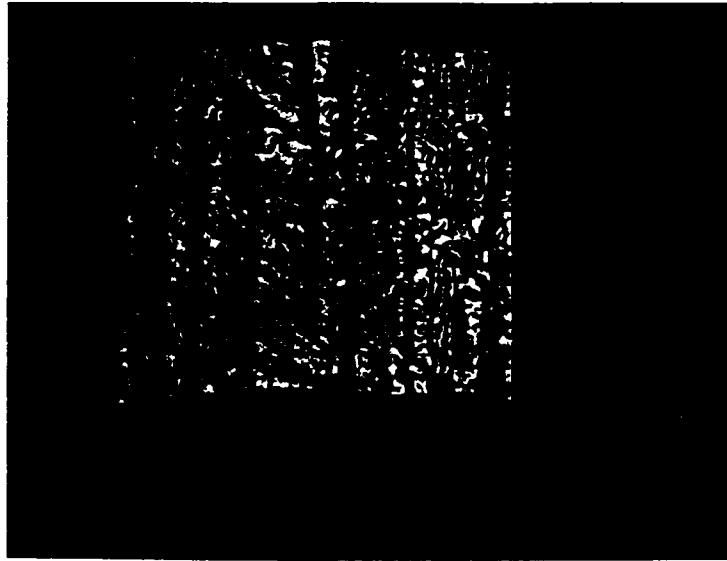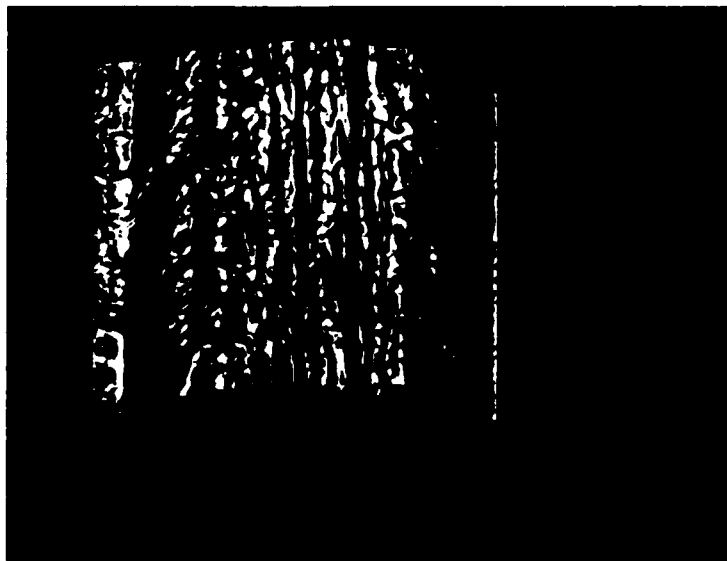# SCANNING TUNNELLING MICROSCOPE

Figure 1.

Figure 2.

Figure 3.

Figure 4.

Figure 5.

Figure 6.
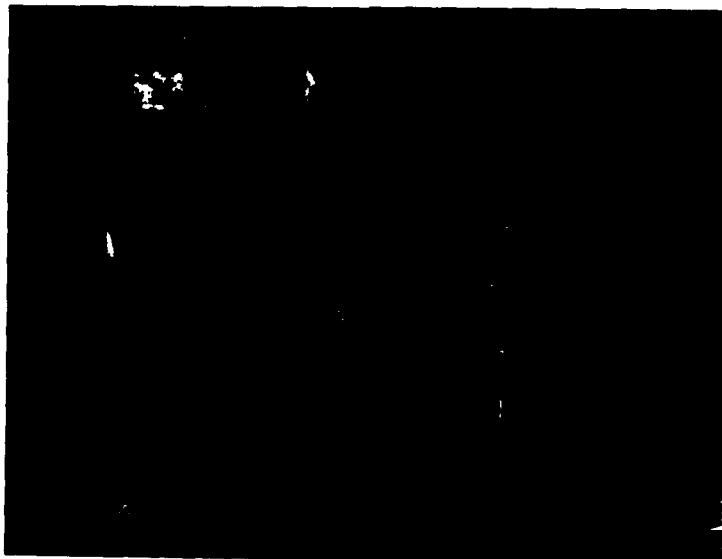
Figure 7.
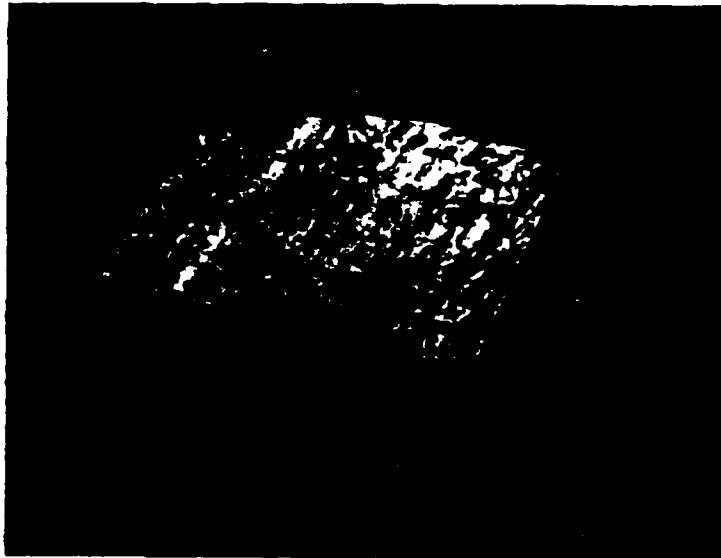
Figure 8.
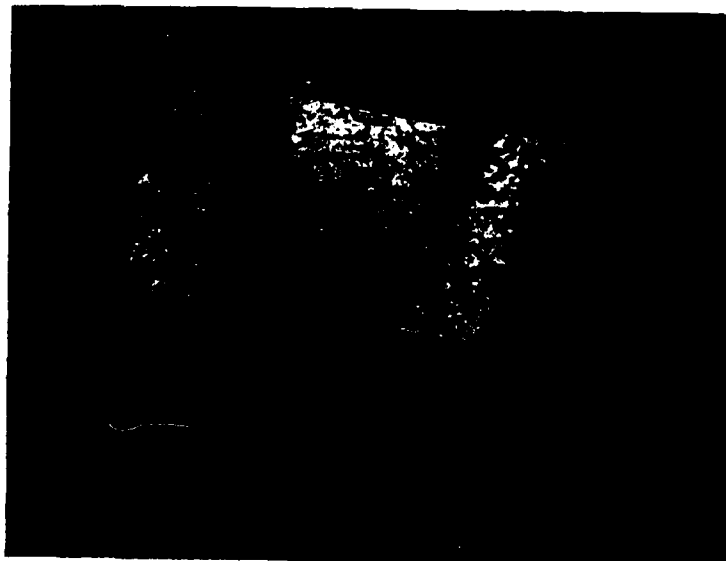
Figure 9.
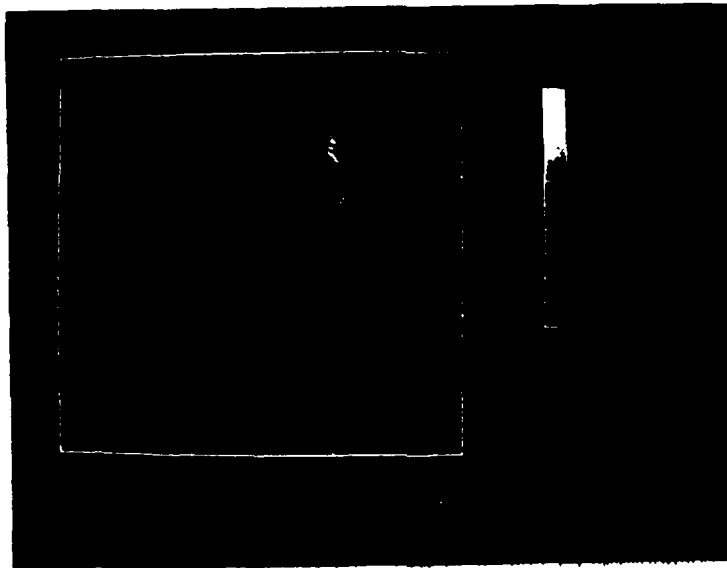
Figure 10.
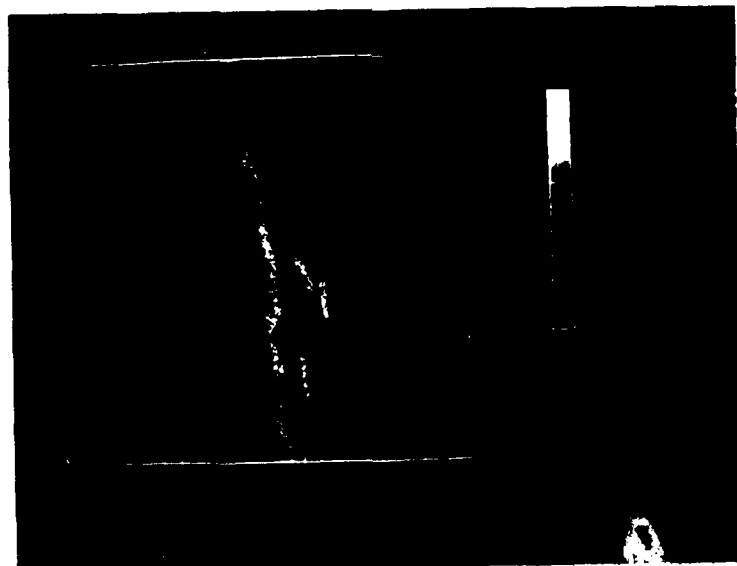
Figure 11.

1989 USAF-UES SUMMER FACULTY RESEARCH PROGRAM/
GRADUATE STUDENT RESEARCH PROGRAM

Sponsored by the
AIR FORCE OFFICE OF SCIENTIFIC RESEARCH

Conducted by the
Universal Energy Systems, Inc.

FINAL REPORT

FINITE ELEMENT MODEL FOR ASTREX.

Prepared by: Randy Trung Quy Nguyen

Academic Rank: Graduate Student

Department and   Mechanical Engineering

University   San Jose State University

Research Location: USAF/AL
                        Astronautics Laboratory
                        Edwards AFB, CA 93523

USAF Researcher: Dr. Alok Das

Date: September 1st , 1989

Contract No: F49620-88-C-0053

Finite Element Model for ASTREX

by
Randy Trung Quy Nguyen

ABSTRACT

To control structure interaction of a big model as ASTREX, one needs to know the initial vibration frequencies of the model due to the gravitational and the thrust forces. This is in essence the project that I devoted my summer to completing. By generating the finite element model, NASTRAN, I came up with all the necessary data results that will help other researchers in the future to understand the concept of the model and make it easier for them to work further along in improving the technology. By using the initial vibrational frequencies of the model, one can see the deformation caused by the bending and movement of the system. These vibrational frequencies can also be used to control the model in rotation and translation to any desired position.

ACKNOWLEDGMENTS

I wish to thank the Air Force Systems Command and the Air Force Office of Scientific Research for their sponsorship which made this research possible. Also, I wish to thank the professional staff of Universal Energy Systems for their support of this research project so I could gain working experience and the opportunity to use my knowledge of mechanical engineering in real life situations.

I greatly appreciate the support of the Astronautics Lab of Edwards Air Force Base. In particular, I wish to thank Dr. Alok Das for securing the necessary information and detail of the project research; Mr. Waid Schlaegel for serving and explaining the requirement of the computer system language and Mr. Joel Berg for helping to the research project. And finally, the research group for making the project much more interesting and enjoyable.

I. INTRODUCTION:

Looking ahead into the future, space systems will need to be much larger than any current spacecraft. These large space systems will be sent into orbit for both economic and defensive needs; therefore, they requite minimum mass. Besides low mass density, the large space system dynamics and control also has to face with the problems of unprecedented size, pointing and shape control, and high modal density. Furthermore, lack of prior experience in modeling control of such systems and large physical size makes ground testing difficult. Because of these problems, the range of technologies being developed for large space system dynamics and control needs more thorough research. The government hires engineers and scientists for testing and uncovering the solutions to all those problems that arise from the increasing needs of the technological world.

During the past 10 weeks, I have been assigned to generate the finite element model for the ASTREX by using NASTRAN software. ASTREX; Advanced Space Structure Technology Research Experiments, is a large space satellite ground system. Its facility is located at the Astronautics Laboratory, Edwards Air Force Base. It is a large space structure composed of 3 mirror beam expander, primary support (tetrahedral space truss), truss struts (graphite/epoxy composite tubes, aluminum joints), tripod metering truss, tertiary mirror simulator (steel, with aluminum struts) and non-structural masses (steel). ASTREX has 253 nodes, 1598 degree of freedom, 305 bar elements, 77 quadrilaterals, and 54 triangulars.

My research interest has been in the area of analyzing the vibration frequencies and the static forces of the model. During study the model ASTREX, my objectives were to learn how to use the NASTRAN language in order to translate the Boeing data file into NASTRAN version, to execute the data file and to analyze the result from the different aspects.

II. OBJECTIVES OF THE RESEARCH EFFORT:

Finite element modelling is one of the most efficient method of solving for the vibration of a structure modal; it can be used in many different ways. My first objective when I first began the research project was to learn how to use NASTRAN. What is NASTRAN? NASTRAN (NAsa STRuctural ANalysis) was conceived and developed by the National Aeronautics and Space Administration (NASA) to fill a need for a universally available finite element program. It is also a system that creates and manipulates a data base to solve problems using matrix structural analysis. The system is composed of a data base, an executive system and modules that perform modeling , data base manipulation and program I/O. How does one get started with NASTRAN? A reasonable approach is to first define the physical problems then worry about the rest of the NASTRAN input card. It thus seems to makes sense to think first about that portion of the data deck called Bulk Data. This is the section of the input deck that is used to define:
- The grid point identification.
- The element connectivity.
- The element properties.
- The material properties.
- The constraints.
- The loads and eigenvalue extraction routines.

a) The grid point identification: Each grid point must have an identification number that is unique among all point identification. Since NASTRAN generates an internal for degrees of freedom by starting at the lowest ID (grid point identification number) and progressing to the highest, the ID's need not form a consecutive numerical sequence.

b) The element connectivity: The finite elements are characterized by a name such as ROD, BAR, or HEXA for truss, beam and solid hexagonal elements. The mnemonic for a connection card is characterized by a 'C' preceding the element type; for example, CROD, CBAR, and CHEXA specify the connectivity data for the truss, beam and solid elements.

c) The element properties: Typical structural systems are generally composed of relatively few materials. Area properties such as plate thickness and beam cross-sectional area moments of inertia tend to be the same. Then, instead of repeating the material

parameters for each element, the appropriate material can be specified by pointing to the correct material set number.

d) The material properties: The mnemonic of the property card is characterized by a 'P' preceding the element mnemonic. For example, PROD, PBAR are property cards for the truss, beam elements. The property card includes all the properties for an element.

e) The constraints: There are 3 types of constraints: permanent, specification and multipoint constraints. The permanent constraint is specified directly into the grid card. It provides a convenient means of removing one or more of the six node point degrees of freedom that are automatically defined by NASTRAN, but that do not physically exist in the mathematical model. The specification of constraint is sufficient to allow the user to specify and linear relationship between degrees of freedom. The multipoint constraint is simply a linear equation that relates the displacement degree of freedom. Relations of this type can be used to model rigid links between node points or to specify constraints that are a linear combination of grid point displacements.

f) The loads: The finite elements that are used to model structural systems include those that exhibit bending, twisting behavior. The forces have a physical interpretation which we can establish the stiffness of an element.

g) Eigenvalue extraction routines: The eigenvalue problem in NASTRAN is defined for the a-set of degrees of freedom. The a-set has a broader meaning for dynamics than it had for statics and may include generalized degrees of freedom as well as physical degrees of freedom.

III

After learning how to operate the NASTRAN, I translated the finite element model of the ASTREX from Boeing to NASTRAN. Despite my background in finite element, I was unfamiliar with the coding style of NASTRAN; therefore, I faced many difficult problems. Initially, I found from the Boeing data file that there were some non-structure mass elements that were not connected to the primary support. The next Boeing version, they connected these non-structure mass elements by rigid card, which showed that the non-structure masses have very stiff bending moments and torsions. For some unknown reasons, NASTRAN could not understand the rigid card. It kept printing out faulty data

results. To remedy that bug, I changed the rigid card to bar card and I also changed the modulus of elasticity higher so that the bending moments and torsions were stiff enough compensate for the exchange to a bar card. The next problem I dealt with was the eigenvalues' result. After setting my frequency range from 0 Hz to 1000 Hz, I wanted to measure only 50 eigenvalues. Unfortunately, these values were much higher than the Boeing result; I then realized the problem was caused by setting the frequency range too high compared to the Boeing frequencies. Finally, I came up with results that are very closer to Boeing as shown in Table 1.

Table 1: The differences for the eigenvalues and the frequencies between our model and Boeing model for the ASTREX.

Mode No.	Our Model		Boeing Model	
	Eigenvalue	Frequency	Eigenvalue	Frequency
01	5.96183E3	1.22888E1	5.970343E3	1.22975E1
02	5.99924E3	1.23273E1	6.049349E3	1.23786E1
03	8.12483E3	1.43458E1	8.374839E3	1.45649E1
04	9.21417E3	1.52773E1	1.097240E4	1.66713E1
05	1.27521E4	1.79726E1	1.405261E4	1.88668E1
06	1.47333E4	1.93183E1	1.470102E4	1.92971E1
07	1.87143E4	2.17724E1	1.906203E4	2.19737E1
08	3.88797E4	3.13820E1	3.875348E4	3.13310E1
09	4.04509E4	3.20099E1	4.086860E4	3.21747E1
10	5.04997E4	3.57655E1	5.047150E4	3.57555E1

From the table above, I reasoned the data file of our model was correct since it differed little from the Boeing model. The next step that concerned the project was the center of mass, since this is a very large structure space model, the changing of the center of mass will cause the actual data to deviate greaty from the expected results. I tested our model through NASTRAN by comparing the center of mass due to the gravitational forces and the thrust forces applied at certain place to observe how much the center of gravity changed. Since the requirement of forces to rotate the ASTREX to a maximum angle is too small compared to the total weight of itself, the changing of the center of mass was as little as .88%.

IV

Although 10 weeks of the research was too short for me to be fully knowledgeable about ASTREX, it was barely enough time to finish my objective: learning how to use NASTRAN and translating the Boeing model into our system, analyzing the static force due to the center of mass in different aspect. As one can see, the data result of NASTRAN that I translated from Boeing data file differed from .14% to 16%. The research team considere the ASTREX model acceptable. Also, since the model of the ASTREX is a large space model, the changing ofthe center of mass due to the variations in temperature and forces applied to the model is only .88%, this tells us our model will survive during actual operations.

V. RECOMMENDATION:

a. From our point of view, the research team considere the NASTRAN model correct due to the vibrational frequencies, but we are still curious about the static forces on each element. Some data results on these static forces are still unexplainable from gravitational forces; We hope to understand more completely about these factors if Boeing send us their result from the analysis of the gravitational forces.

b. Also, Boeing numbers their nodes in a non-consecutive manner, that caused us a lot of memory, cost and time to reexecute our data file in the same format. Average time for each execution was almost two days, this could be reduced to a half of a day or less if Boeing had numbered their nodes consecutively.

REFERENCES

Shigley and Mitchell, <u>Mechanical Engineering Design</u>, McGraw Hill, Inc. , 1983.

William T. Thompson, <u>Theory of Vibration with Applications</u>, Prentice Hall Inc. , 1988.

Donald T. Greenwood, <u>Principles of Dynamics</u>, Prentice Hall Inc. , 1988.

John Van De Vegte, <u>Feedback Control Systems</u>, Prentice Hall Inc. , 1986

1989 USAF-UES SUMMER FACULTY RESEARCH PROGRAM

GRADUATE STUDENT RESEARCH PROGRAM

Sponsored by the

AIR FORCE OFFICE OF SCIENTIFIC RESEARCH

Conducted by the

Universal Energy Systems, Inc.

FINAL REPORT

Modeling of Combustion Instability in
Solid Rocket Motors

Prepared by:	Sonja C. Schillmoeller
Academic Rank:	Graduate Student
Department and	Mechanical Engineering Department
University:	University of Illinois
Research Location:	AL/LSCC
	Edwards AFB
	Edwards AFB, CA 93523
USAF Researcher:	Capt. Joe Cor
Date:	August 11,1989
Contract No:	F49620-88-C-0053

Modeling of Combustion Instability in Solid Rocket Motors

by Sonja C. Schillmoeller

ABSTRACT

Combustion instability is the result of interaction between the combustion processes associated with solid propellant burning in the combustion chamber of a rocket engine and pressure oscillations present within the gaseous phase of the combustion chamber. If this instability becomes too great, it may result in destruction with the final and unwanted outcome of the rocket engine being completely destroyed. Due to the common use of nonsmoke propellants (which are more susceptible to interactive effects) in tactical weaponry, the ability to predict the occurrence of instabilities is of high priority. Through the years, models have become more realistic in their computational efforts therefore enhancing the ability to better predict the onset of combustion instability. Efforts this summer were mainly concerned with enhancing nonsteady combustion modeling. Currently, nonsteady calculations are performed using the PEM (Petite Ensemble Method) which is not the most recent method of calculating solid propellant burn rates. Enhancement, therefore, consisted of performing nonsteady calculations using the COR (Continuous Oxidizer Regression) method, a more up-to-date method of calculating burn rates.

Acknowledgements

I wish to thank the Air Force Systems Command and the Air Force Office of Scientific Research for sponsorship of this research. Universal Energy Systems must be mentioned for their concern and help to me in all administrative and directional aspects of this program. I wish to give special thanks to Capt. Joe Cor for providing technical and directional advice throughout the summer's research.

I. INTRODUCTION:

Capt. Joe Cor, AL/LSCC, has a background of solid propellant combustion modeling and he has been furthering his work in this area while at the Astronautics Laboratory. He has been working with Professor John Renie of the University of Illinois on advancing the combustion model he developed while a graduate student at Illinois, the Continuous Oxidizer Regression (COR) model. This model, in turn, was a refinement of the Petite Ensemble Model (PEM), which Professor Renie helped to develop at Purdue University. The COR model refined the PEM by tracing the entire burning history of a single oxidizer particle, rather than assuming the particle has certain "time averaged" characteristics, as is assumed in the PEM.

Burning rate control and prediction is of prime importance to Air Force planners designing new weapons systems. The PEM, and the COR model, are capable of predicting burn rates. Another major feature of solid propellants which is of great interest to the Air Force is their acoustic (or pressure-coupled) response. The PEM is capable of predicting the acoustic response of propellants; however, the COR model is not yet able to.

I am a graduate student of Professor Renie's at the University of Illinois and am doing my thesis research on the topic of the modeling of solid propellant combustion. It is my goal to refine the COR model so that it can predict the acoustic response of solid propellants. I am doing this work in coordination with Capt. Cor and Professor Renie.

II. OBJECTIVES OF THE RESEARCH EFFORT:

Currently, there has been no incorporation of the COR model into nonsteady calculations of solid propellants. The pressure-coupled response function (hereafter referred to as the

response function) or the parameter which, in a manner of speaking, indicates the severity of combustion instability, is currently obtained through the use of the PEM. This method has several disadvantages which will be mentioned shortly.

My assignment as a participant in the 1989 Summer Research Program was to modify present code so as to perform nonsteady calculations using the COR model. Nonsteady output was to be obtained using two approaches: the Zeldovich/Novozhilov technique and the Small Perturbation, or Hamann technique. Results were then to be compared to experimental data to validate qualitative and hopefully quantitative accuracy of the calculations.

II.

a. LITERATURE REVIEW:

In its simplest form, a solid propellant consists of oxidizer particles (the most common being ammonium perchlorate crystals or AP crystals) dispersed in a fuel binder. The presence of additives, burning rate modifiers, catalysts, and acoustic suppressants mixed into the fuel binder obviously complicates matters. In its simplest form, however, the combustion of solid propellants consists of many processes - some more important than others, of course. The modeling process becomes more complicated due to the fact that there is a multitude of oxidizer particles of different sizes distributed throughout the fuel matrix.

Over the past decades, various analytical combustion models have been developed with the most recent being the Petite Ensemble Model (PEM). This model is basically a refined version of efforts made by Glick (1974) and Beckstead, Derr, and Price (1970), who, in turn, based their models on work performed by Hermance (1966). A major difference

between the PEM and its predecessors is the manner in which the macroscopic flame structure above the burning propellant surface is treated. In the PEM, this flame structure is treated as a collection of different, non-interacting, quasi one-dimensional flames. This idea had previously never been considered. The PEM also treats the surface of the solid propellant as a fuel plane with concave and/or convex oxidizer particles, depending, of course, on individual oxidizer/fuel binder burning characteristics. Also, when calculations are performed, a single mean state oxidizer/fuel geometry is assumed. This assumption is what leads to the differentiation between the PEM and COR model. The latter treats each oxidizer/fuel binder pair as a separate entity where the burning surface is assumed to continually regress; hence COR, or Continuous Oxidizer Regression. With this concept, a surface geometry and an instantaneous burning rate are determined at discrete time intervals during the overall oxidizer/fuel binder pair combustion. Another observation to note is that the PEM assumes the flames occur over a flat surface. The COR model, on the other hand, considers the possibility of a nonplanar oxidizer surface existing beneath the flames.

As previously mentioned, the parameter of primary interest when analyzing unsteady combustion is the response function, the coupling mechanism between the gaseous pressure oscillations and the combustion processes. A solid propellant's pressure-coupled response function, R_p, is defined as

$$R_p = (m'/\underline{m})/(p'/\underline{p}) \tag{1}$$

The objective of nonsteady state combustion modeling is to predict the response function for a particular solid propellant formulation subjected to various external conditions.

The small perturbation technique for calculating the pressure-coupled response function has as its basis a similar subsurface analysis as employed by previous response models, namely, Denison and Baum (1961) and Novozhilov (1973). According to King (1980),

who used as the foundation of his efforts work performed earlier by Hamann (1974), the response function after application of the small perturbation technique is defined as

$$R_p = (C_1'\Lambda + C_2)/(\Lambda + C_3/\Lambda + C_4) \qquad (2)$$

The Zeldovich/Novozhilov, or ZN, approach (1973) employs the same basic assumptions which were made by the small perturbation technique with the addition of one more assumption. According to Condon, Osborn, and Glick (1976), the rate processes in the gas phase and at the propellant surface can be considered quasi-steady in the sense that their characteristic times are short compared to the characteristic time of the pressure transient. If this is indeed true, then it is valid to argue that the differential equations of the quasi-steady gas phase and surface are identical to the differential equations of the steady-state equations. With this argument, there is now the opportunity to relate the nonsteady response of a solid propellant to certain steady-state parameters, these parameters being the steady-state responses of propellant burning rate or surface temperature to either the combustion pressure or the initial propellant temperature. These parameters are defined as follows:

$$d_1 = (\partial \ln r / \partial \ln p)_{T_o = \text{constant}} \qquad (3)$$

$$d_2 = (T_s - T_o)(\partial \ln r / \partial T_o)_{p = \text{constant}} \qquad (4)$$

$$d_3 = \{1/(T_s - T_o)\}\{\partial T_s / \partial \ln p\}_{T_o = \text{constant}} \qquad (5)$$

$$d_4 = (\partial T_s / \partial T_o)_{p = \text{constant}} \qquad (6)$$

For convenience, another parameter $(d_5 = d_1 d_4 - d_2 d_3)$ is defined allowing the ZN pressure-coupled response function to be defined as

$$R_p = \{d_1 + d_5(\Lambda - 1)\}/\{d_4(\Lambda - 1) + (d_2/\Lambda) + (1 - d_2)\} \qquad (7)$$

b. MODIFICATIONS OF THE CODE:

Basically, three methods of calculating pressure-coupled response functions were

incorporated into the code so as to use the COR scenario instead of the PEM. Two of these used the ZN technique and the last used the small perturbation technique. The first ZN technique, when performing calculations, applied all four perturbations to each "chunk" of the oxidizer/fuel binder pair as it continually regressed until either all the fuel or all the oxidizer had burned away. The second technique, on the other hand, performed one perturbation at a time on all chunks of the oxidizer/fuel binder pair until all perturbations had been considered.

c. EXPERIMENTAL COMPARISONS:

One series of propellant formulations, as reported by Miller (1978), was considered when comparing calculated results and experimental data. The propellant formulations considered were constant solid, nonaluminized AP based propellants. Experimental burning rate and pressure exponent data provided for the nonaluminized propellants were used to establish the validity of the baseline COR model. The theoretical burning rate and pressure exponent for each Miller formulation were calculated and compared with these experimental values. In this manner, some of the lesser-known numerical input constants were varied until the best fit to experimental data, both for burning rate and pressure exponent, was obtained. The results of the experimental and theoretical data are presented in Tables 1 and 2. Table 1 presents the comparison between experiment and theory for the burning rate at 6.89 MPa and Table 2 presents the comparison for the pressure exponent, again at a pressure of 6.89 MPa. In each of these tables, the percent error between experiment and theory is listed also. The average error for the burning rate comparison was approximately 5.11 percent while for the pressure exponent comparison it was 29.23 percent. Pressure-coupled response calculations are presented in Graphs 1-6. In these

Table 1. Experimental Versus Theoretical Burning Rate Comparison

Propellant	Rate-theo.	Rate-exp.	Error
1-5(5)	10.16	10.20	-.37
1-6(6)	14.81	17.40	-14.87
1-7(7)	14.89	14.90	-.09

Table 2. Experimental Versus Theoretical Pressure Exponent Comparison

Propellant	Rate-theo.	Rate-exp.	Error
1-5(5)	.37	.33	11.91
1-6(6)	.35	.54	-35.06
1-7(7)	.40	.68	-40.71

graphs, the variation of the real part of the response function with the natural log of the frequency of pressure fluctuation (frequencies in cycles per second) is depicted. Graph 1, Graph 3, and Graph 5 compare only theoretical calculations, these being two of the three nonsteady techniques. The two techniques considered were the small perturbation technique and the ZN technique which performs all perturbations at once on each chunk of the pseudopropellant. Column 3 represents the ZN technique, whereas Column 5 represents the small perturbation technique. Graph 2, Graph 4, and Graph 6 compare theoretical and experimental data in which Column 6 represents the experimental data. Note that for the propellants assuming the highest and lowest experimental burning rate, peaks in the response function occurred at approximately the same frequency for both experimental and theoretical data. After observing these comparisons, quite evident is the fact that the present modeling of the response function can be interpreted only on a qualitative basis.
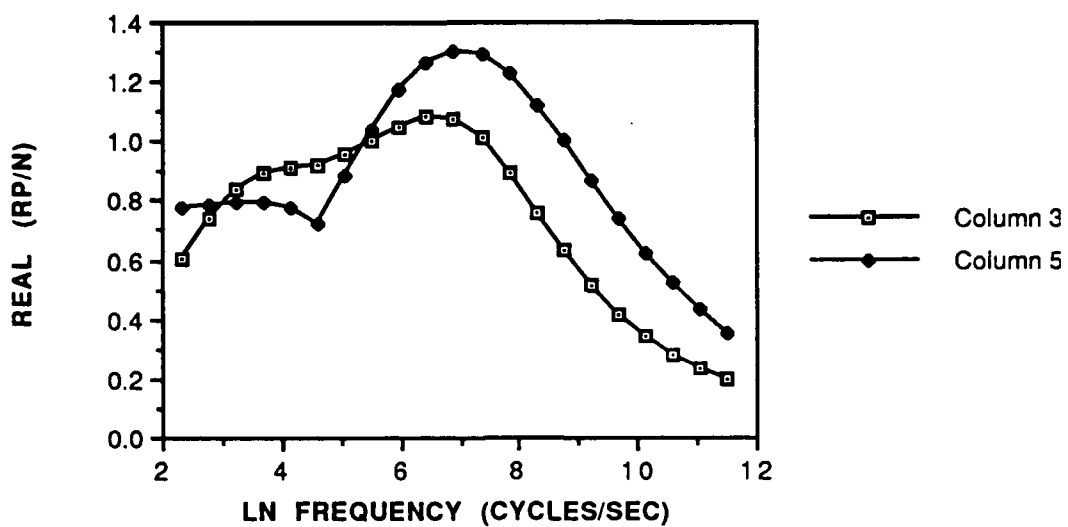
GRAPH 1 PROPELLANT 1-5(5)
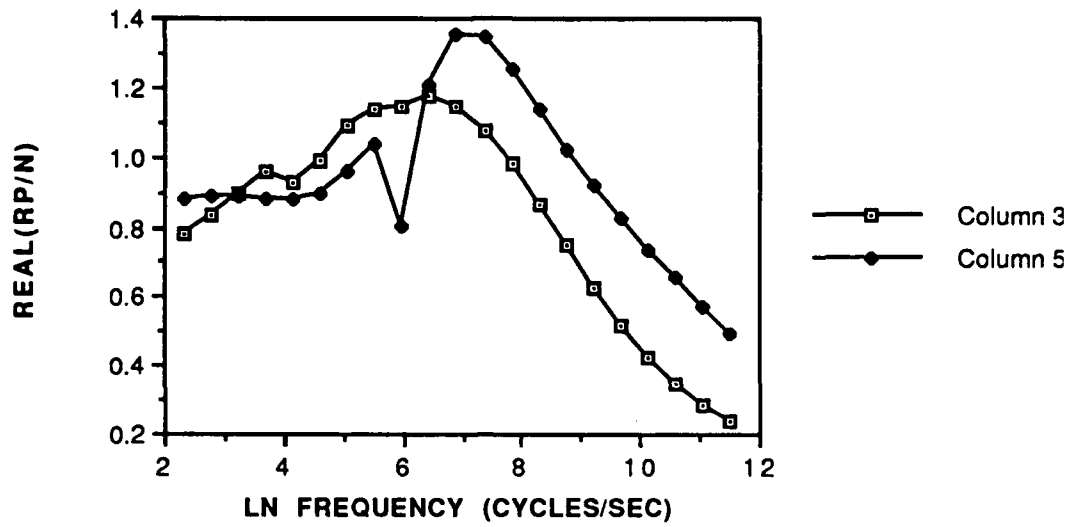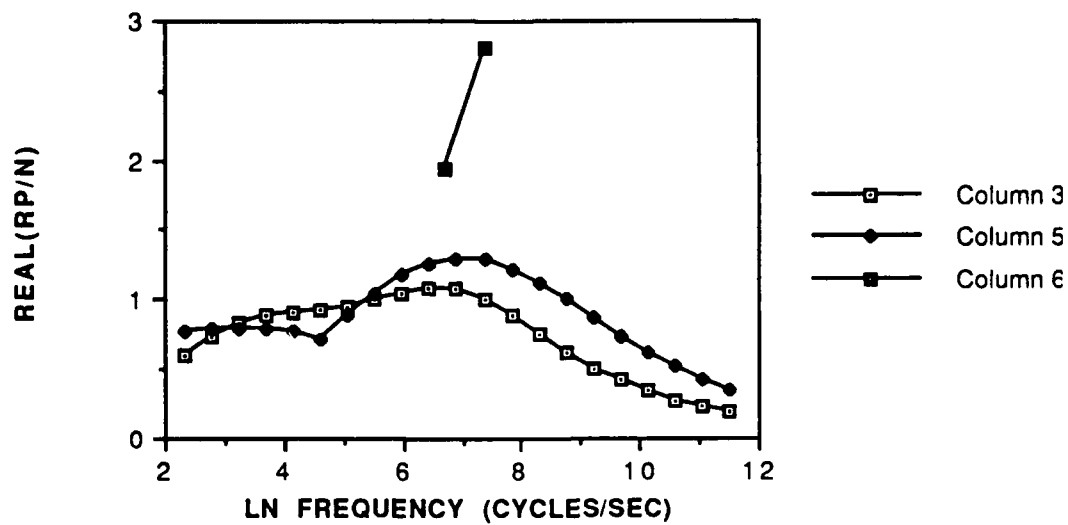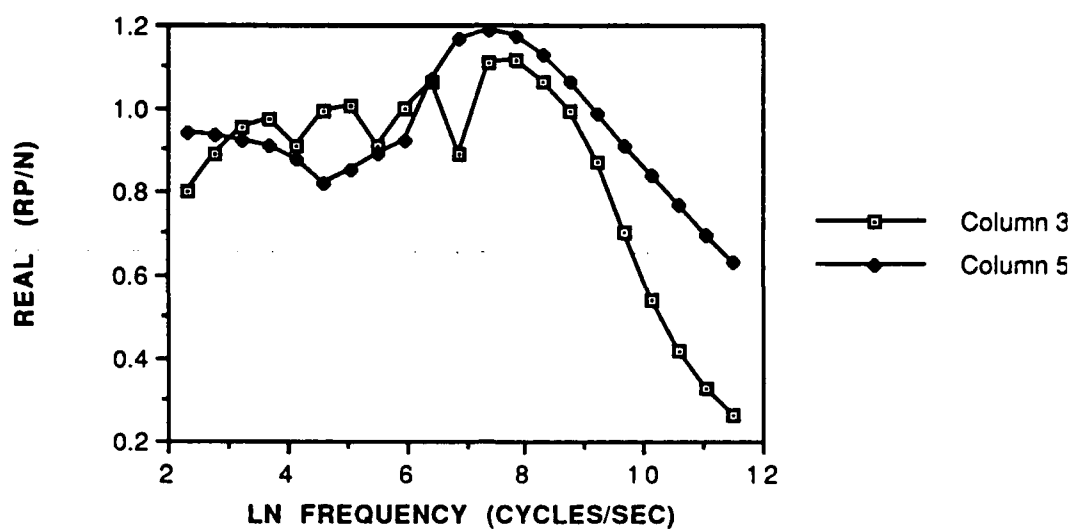

GRAPH 2 PROPELLANT 1-5(5)
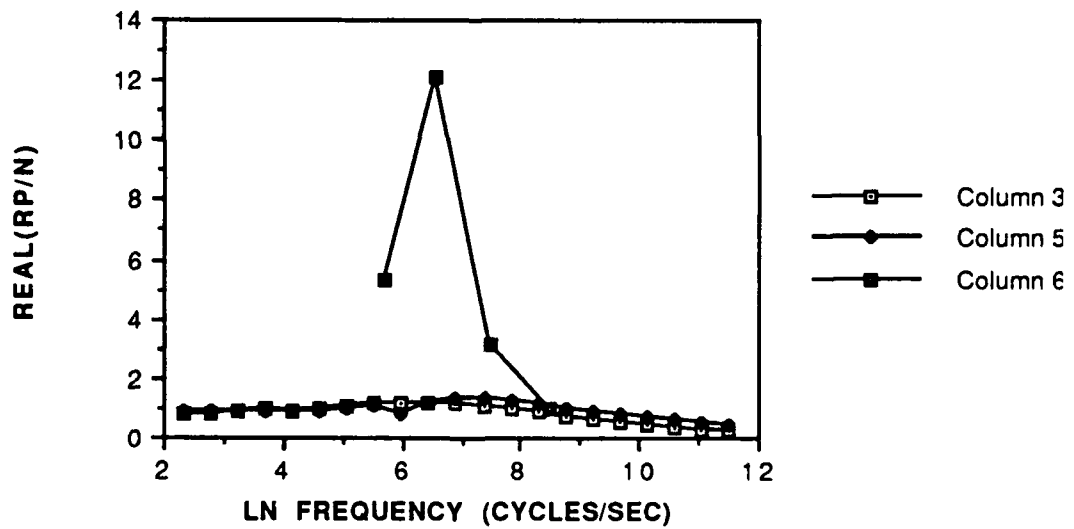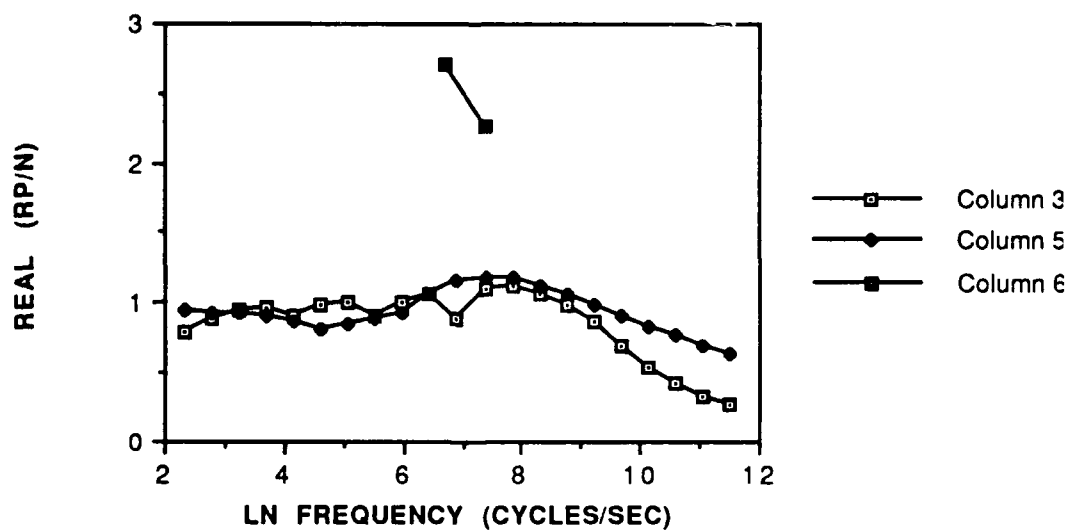
GRAPH 3   PROPELLANT 1-6(6)

GRAPH 4   PROPELLANT 1-6(6)

GRAPH 5   PROPELLANT 1-7(7)

Legend:
- Column 3
- Column 5

GRAPH 6   PROPELLANT 1-7(7)

Legend:
- Column 3
- Column 5
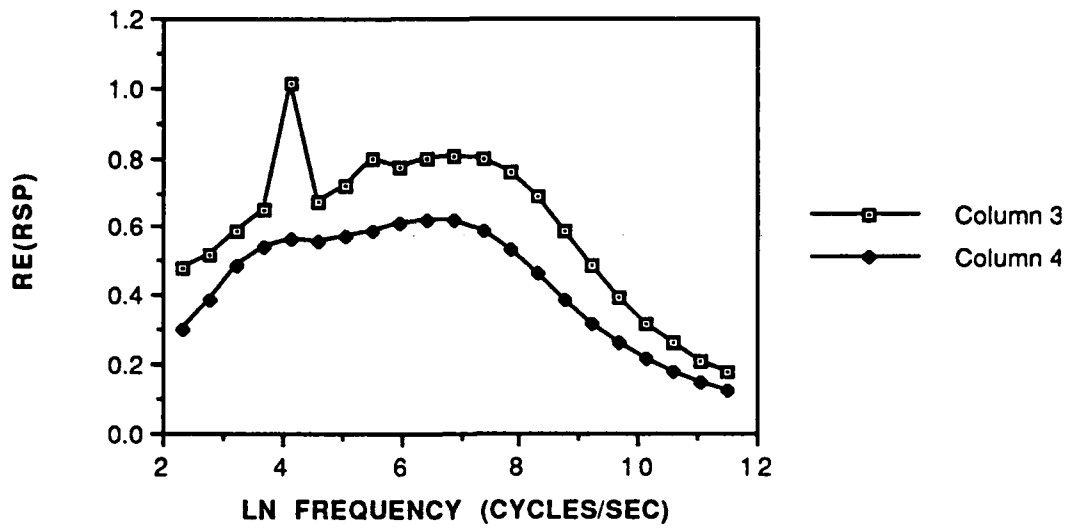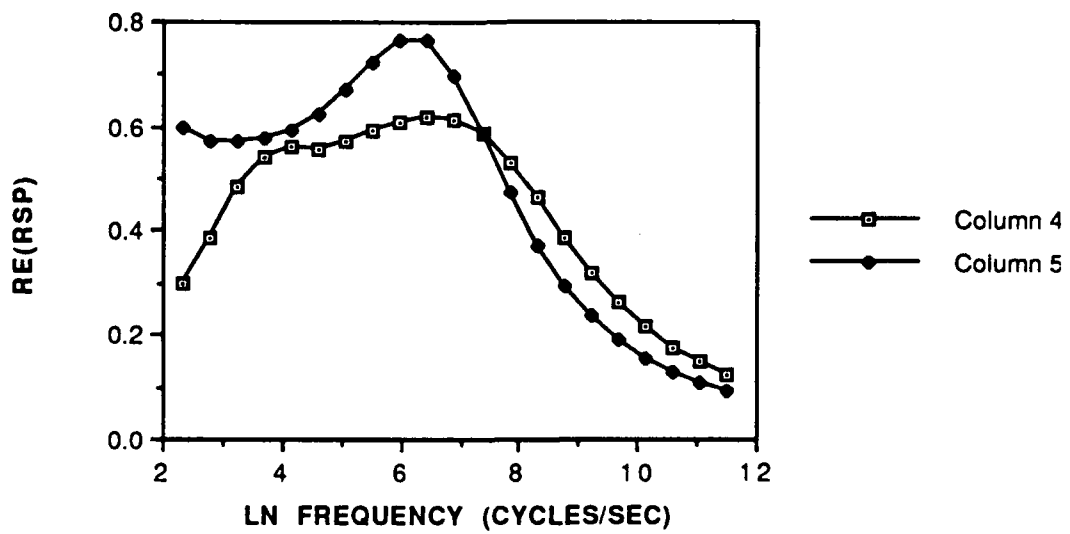- Column 6

d. PARAMETRIC STUDY:

A parametric study was performed to observe how the response function varied with a change in the size of oxidizer particles. Two nonsteady techniques were employed, those being the small perturbation technique and the ZN technique which performs all perturbations at once on each chunk of the oxidizer/fuel binder pair. These results were then compared to theoretical results obtained by Cohen and Strand (1984) to observe whether similar trends prevailed in both models. For this study, calculations were performed at 6.89 MPa with a monomodal AP/HTPB propellant having an oxidizer mass fraction of .88. Such varaiables as activation energies and pre-exponential frequency factors were not varied as they were in the experimental study mentioned earlier. They were not changed since there was no available experimental data of burn rates or pressure exponents to produce a good curve fit. The main concern with this study was to observe if similar trends were produced with both models. Results of response function calculations using the ZN technique are shown in Graphs 7-10. In these graphs, the real part of the response function is plotted against the natural log of the frequency once again. The smaller diameters were always represented by the column possessing the lesser value. Five oxidizer diameters were compared those being 5, 20, 90, 200, and 400 microns. After careful observation of Graph 10, one can see that when diameters are fairly large, practically no change in values of the response function are observed. This contradicts the results of Cohen and Strand's efforts which show, at corresponding diameters, there is a slight increase in response function values as the oxidizer diameter increases. Graph 7 produced similar trends where, at corresponding diameters, and as the oxidizer diameter increased, lower response function values were observed. Graphs 8 and 9 also produced good comparisons in which, as the oxidizer diameter increased, there was at first a general increase and then decrease in response function values with increasing omega. Use of the small perturbation technique basically revealed the same results.

GRAPH 7

Legend:
- □ Column 3
- ◆ Column 4

X-axis: LN FREQUENCY (CYCLES/SEC)
Y-axis: RE(RSP)

GRAPH 8

Legend:
- □ Column 4
- ◆ Column 5

X-axis: LN FREQUENCY (CYCLES/SEC)
Y-axis: RE(RSP)

GRAPH 9

GRAPH 10

16-15
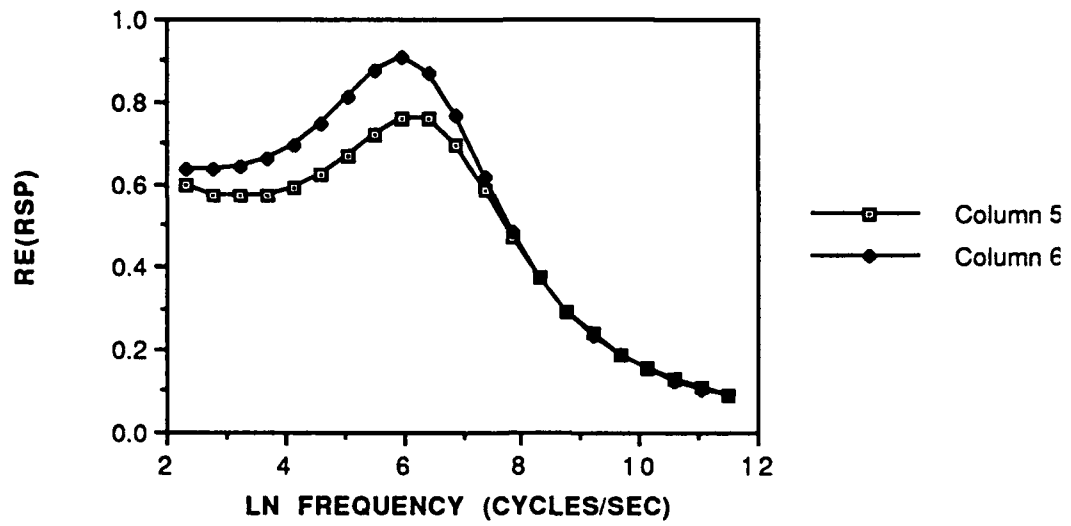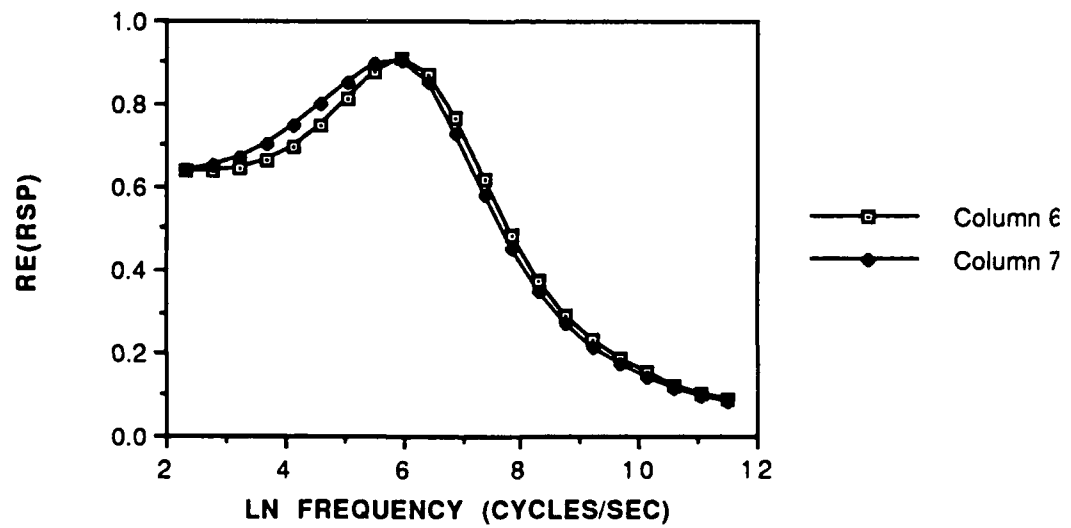
III. RECOMMENDATIONS:

a. Future research includes the further comparison of theoretical results with experimental data. Comparison with experimental data from work performed by Brown (1974), Strand (1979), and Strand (1989) on an A-13 propellant formulation will be completed in the near future.

b. A higher degree of accuracy in terms of quantitative results hopefully will be achieved in the near future. Considerations to take into account when calculating the response function would be:

1) effect of external radiation

2) presence of metallic particles

3) effect of mean crossflow velocity on response function

4) transient effect of ignition

5) better accuracy in terms of steady state burn rates

6) inclusion of the possibility of subsurface reactions

7) exclusion of a quasi-static gas phase assumption

8) presence of additives and/or catalysts

9) effect of compositional fluctuations

10) inclusion of the possibility of oxidizer particles being

released from the propellant surface

11) detailed chemical kinetics

NOMENCLATURE

$C_1 = f_2$

$C_2 = (f_6 f_1 - f_5 f_2)/f_3$

$C_1' = C_1 (p/\underline{m}T)$

$C_2' = C_2 (p/\underline{m}T)$

$C_3 = (f_{42} f_1)/f_3$

$C_4 = (f_{41} f_1 - f_5)/f_3$

$C_{p,s} =$ specific heat of solid oxidizer/fuel mixture

$f_1 = (\partial m/\partial \underline{T}_s)_{p = constant}$

$f_2 = (\partial m/\partial p)_{\underline{T}_s = constant}$

$f_3 = \underline{m} C_{p,s}$

$f_{41} = Q_{sur}$

$f_{42} = C_{p,s}(\underline{T}_s - T_o)$

$f_5 = (\partial \nabla/\partial \underline{T}_s)_{p = constant}$

$f_6 = (\partial \nabla/\partial p)_{\underline{T}_s = constant}$

m'=fluctuation of mass flux at propellant surface

m=mass flux at propellant surface

p'=fluctuation of gas phase combustion pressure

p=gas phase combustion pressure

$Q_f =$ fuel binder heat of pyrolysis

$Q_L =$ oxidizer latent heat of decomposition

$Q_m =$ aluminum latent heat of vaporization

$Q_{sur} =$ net surface energy parameter $= \alpha Q_L + (1 - \alpha - \beta) Q_f + \delta_m \beta Q_m$

$T_o =$ initial solid propellant temperature

$T_s =$ surface temperature

$\alpha =$ propellant oxidizer mass fraction

β=propellant aluminum mass fraction

δ_m=aluminum particle melt parameter

∇=nonsteady state analysis heat feedback parameter

Λ=complex frequency=$.5+\sqrt{.25+i\Omega}$

Ω=nondimensional frequency

Subscripts

- =mean quantity

REFERENCES

Beckstead, M.W., Derr, R.L., and Price, C.F., Combustion Tailoring Criteria for Solid Propellants. AIAA Journal., 1970, Vol. 8, pp. 2200-2207.

Cohen, N.S., Strand, L.D., Combustion Response to Compositional Fluctuations. AIAA Journal., 1984, Vol. 23, pp. 760-767.

Condon, J.A., Osborn, J.R., and Glick, R.L., Statistical Analysis of Polydisperse, Heterogeneous Propellant Combustion - Non-Steady State. CPIA Publication 281., 1976, Vol. II, pp. 209-223.

Denison, M.R. and Baum, E., A Simplified Model of Unstable Burning in Solid Propellants. ARS Journal., 1961, Vol. 31, pp. 1112-1122.

Glick, R.L., On Statistical Analysis of Composite Solid Propellant Combustion. AIAA Journal., 1974, Vol. 12, pp. 384-385.

Hamann, R.J., Three Solid Propellant Combustion Models, A Comparison and Some Application to Non-Steady Cases. Memorandum M-215 Delft University of Technology., 1974.

Hermance, C.E., A Model of Composite Propellant Combustion Including Surface Heterogenity and Heat Generation. AIAA Journal., 1966, Vol. 4, pp. 1629-1637.

King, M.K., Composite Propellant Combustion Modeling. AIAA Paper 80-1124., 1980.

Miller, R. R., Control of Solids Distribution in HTPB Propellants. AFRPL-TR-78-14., 1978.

Novozhilov, B.V., Nonstationary Combustion of Solid Rocket Fuels. Nauka., 1973.

1989 USAF-UES SUMMER FACULTY RESEARCH PROGRAM/

GRADUATE STUDENT RESEARCH PROGRAM

Sponsored by the

AIR FORCE OFFICE OF SCIENTIFIC RESEARCH

Conducted by the

Universal Energy Systems, Inc.

<u>FINAL REPORT</u>

<u>State Variable Control of a Flexible Grid Structure</u>

Prepared by:	Matthew L. Westerheide
Academic Rank:	Graduate Student
Department and	Electrical Engineering Department
University:	University of Missouri-Rolla
Research Location:	Air Force Astronautics Laboratory Edwards AFB, California 93523-5000
USAF Researcher:	Dr. Alok Das
Contract No:	F49620-88-C-0053

State Variable Control of a Flexible Grid Structure

by

Matthew L. Westerheide

Abstract

A finite element model for the structure was developed, tested, and verified. Nastran was used to develop this model in conjunction with a fortran program which calculated the A, B, C, and D matrices for the grid structure, from the Nastran output. A control scheme was then chosen, developed, and finally implemented via a MAX-100 computer.

Acknowledgements

I wish to thank the Air Force Office of Scientific Research for sponsorship of this research. Universal Energy Systems must also be mentioned for their part in the program.

My experience was both rewarding and enriching. Dr. Alok Das and Waid T. Schlaegel gave me initial support. Joel Berg provided a fortran program to determine the A, B, C, D matrices from the Nastran output. Dr. Vittal Rao was very valuable in helping with the theoretical aspects of the project. Last but not least, Angel Cruz and John Ward were very helpful in providing hardware for the project.

1. Introduction:

Control of large space structures is a area of growing interest to the Air Force highlighted by the Space Station Freedom. Large space structures must be made out of light weight material so they can be economically launched into space. The very nature of large light weight structures gives them inherent closely spaced low frequency modes with very light damping ratios (0.5% assumed for the grid structure used at the Astronautics lab at Edwards AFB). These modes must be suppressed for the structural safety of the space station.

My area of research interest lies in the control area. After having graduated from UMR with a BS degree in EE and a Physics minor, I pursued the control area. Having been exposed to different methods of controller/observer design, this project gave me an opportunity to test some of these methods.

The grid (the structure which models many of the same characteristics of a large space structure) is a 2-dimensional aluminum grid structure with dimensions of 5-ft by 5-ft. It is made up of 2-inch wide and 1/8 inch thick 6061-T6 aluminum strips. At every point where the horizontal and vertical strips cross each other, they are connected by four rivets, removing any play at the joints. The grid hangs vertically down cantilevered at the top to a large I-beam which is itself anchored to a wall.

II. Objectives of the Research Effort:

To design a controller for the grid, the first step
is to formulate a mathematical model for the structure.
From the mathematical model, a state variable model needs to
be generated.

The actuator and sensors for the system were
torquers and accelometers respectively. The torquers, which
are nothing more then small permanent magnet dc motors, can
give a rotational twist to the structure at a node point.
The accelometers, on the other hand, measure the local
acceleration at a node point.

The following phase of the project involves choosing
sensor/actuator location.   To maximize the signal-to-noise
ratio, the sensors should be placed where the structure is
most flexible. Also by attaching the sensor/actuator to the
grid, the model will change somewhat for each location. In
this project only placement of the torquers changes the
model because other accelometers or there equivalent mass
were placed at each non-fixed node (the grid has 20
non-fixed nodes plus 5 fixed nodes attached to the I-beam)
of the grid. The torquers should be placed where they can
excite the most modes.

Once a model was found, different
controller/observer methodologies need to be considered to
find out which is most suitable to obtain a desired closed
loop response. Once this is accomplished the controller and
observer are implemented in real time via a Max-100

computer.

III.

a.   The mathematical model of the undamped system is
given by:

$$M \ddot{S} + KS = f(t)$$ (1)

where: M is the mass matrix

        K is the stiffness matrix

        f(t) is the forcing function

Transfering to modal coordinates ($S = Tq$), restricting
the problem to 10 degrees of freedom, and adding damping:

$$\ddot{q} + 2\zeta \omega_n \dot{q} + \omega_n^2 q = T^\tau f$$ (2)

        In   the   above   equation the dimension of T is 75 by
10.   The   first   25 elements of a column correspond to the
eigenvector   associated with translation in the Z-direction.
The second 25 are analogous to rotation about the X-axis and
the   last   25   represent   rotation   about   the   Y-axis.   The
differential   equation   can be represented in state variable
form as:

$$\dot{x} = Ax + Bu$$

$$y = Cx + Du$$ (3)

(4)

where:

$$A = \begin{vmatrix} 0 & I \\ -\omega_n^2 & -2\zeta \omega_n \end{vmatrix} \qquad B = \begin{vmatrix} 0 \\ T^\tau E \end{vmatrix}$$ (5)

Note: E is the controlability influence matrix.

$$C = \begin{bmatrix} O & O \\ O & T \end{bmatrix} A \qquad\qquad D = \begin{bmatrix} O & O \\ O & T \end{bmatrix} B \qquad (6)$$

However since the accelometers are measuring acceleration in a gravitational field, there outputs will be contaminated by a additional factor of g*SIN(theta) or approximately g*theta where theta is the rotation about the x-axis. To account for this, the C matrix must be modified.

$$C = C \quad - g \begin{bmatrix} \begin{bmatrix} 0 \\ T_x \\ 0 \end{bmatrix} & O \\ O & O \end{bmatrix} \qquad (7)$$

The C and D matrices are then premultiplied by a standard unit vector matrix to achieve the desired outputs. Additional adjustments are required to the B, C, and D matrices to account for additional gains such as amplifiers, sensor/actuator gains, etc.

b.   Nastran and a fortran program were used to build a 20th order model for the system. The model could then be reduced using Matrix X to eliminate the uncontrollable/unobservable modes. The gain and phase of the original 20th order SISO model is compared with the experimentally measured gain and phase of the measured modes on the following pages (figures 1 and 2). The phase was determined by measuring the time delay of the grid using an oscilloscope. 360n degrees was then subtracted to line up the plots.
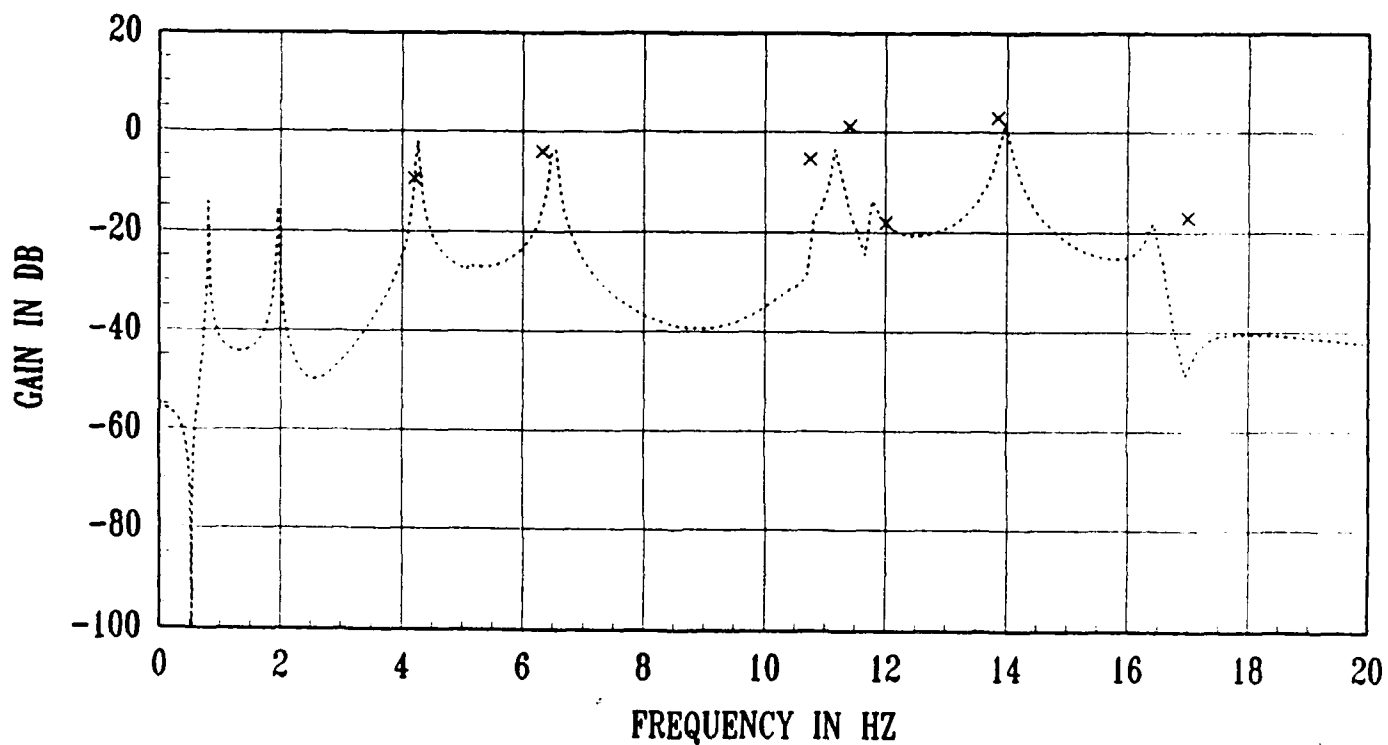
COMPARISON BETWEEN THEORITICAL AND MEASURED GAINS OF SYSTEM
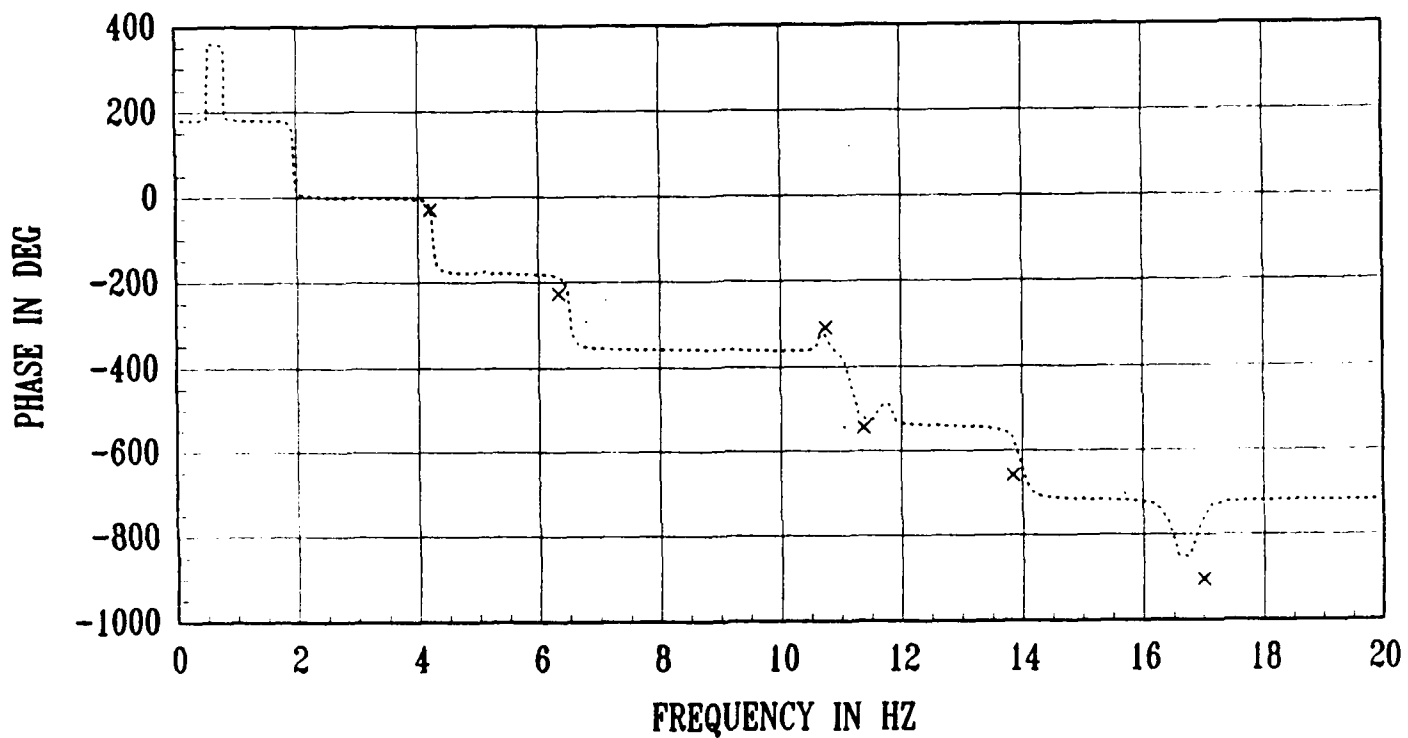
COMPARISON BETWEEN THEORITICAL AND CALCULATED PHASE RESPONSE

IV.

a.   To design a controller/observer for the system, two important aspects need to be considered: (1) How much energy can the observer demand from the sensors with the sensors still behaving linearly. (2) How much energy can the controller output to the actuators before non-linear effects become present. To answer question (1), the sensor outputs were amplified and sampled. Therefore excessive drain on the sensors was impossible. However high demand from the sensors may be undesirable since there is some noise with sensor outputs. To answer question (2) the manufactures specification stated the torquer had a torque sensitivity of 3.64 oz-in/amp and was constant in the range used.

The control methodology used was LQR theory with the observer obtained through controller/observer duality. LQR theory has some practical advantages over other methods such as pole placement techniques for a couple of reasons. First with LQR theory it is possible to set how much control energy you want to supply the actuators. Secondly the desired eigenvalues of the system are determined by how much suppression is desired at each mode which again lends itself towards LQR theory.

The state variable model for the system was put in modal form for modal control with modes 1, 3, 5, 7, 8, and 9 kept for a SISO case and modes 1, 2, 3, 5, 7, 8, and 9 for the MIMO 3-input 3-output case. The weighting matrices for the controller and observer in each case was similar to a

diagonal matrix whose entries are proportional to the square of the mode's frequency (some adjustment was necessary on mode 3 in each case to get desired eigenvalues).

b.   With the previous in mind, experimental plots of open and closed loop response for two modes one using the SISO controller and the other using the MIMO controller are shown on the following pages on figures 3 and 4. From these plots it is apparent the natural damping of the open loop modes in both the SISO and MIMO cases is less than 0.5% (more like 0.3%). However to model the damping correctly for each mode would require to much work for to little benefit.

One problem did occur in the implementation of both the SISO case and MIMO. Mode 9 would become unstable in the closed loop system for reasonable controller signal amplitudes. Only using small amplitudes would the system remain stable. Whether this was a problem do to nonlinearities somewhere in the system, or spillover, or something else remains somewhat uncertain.
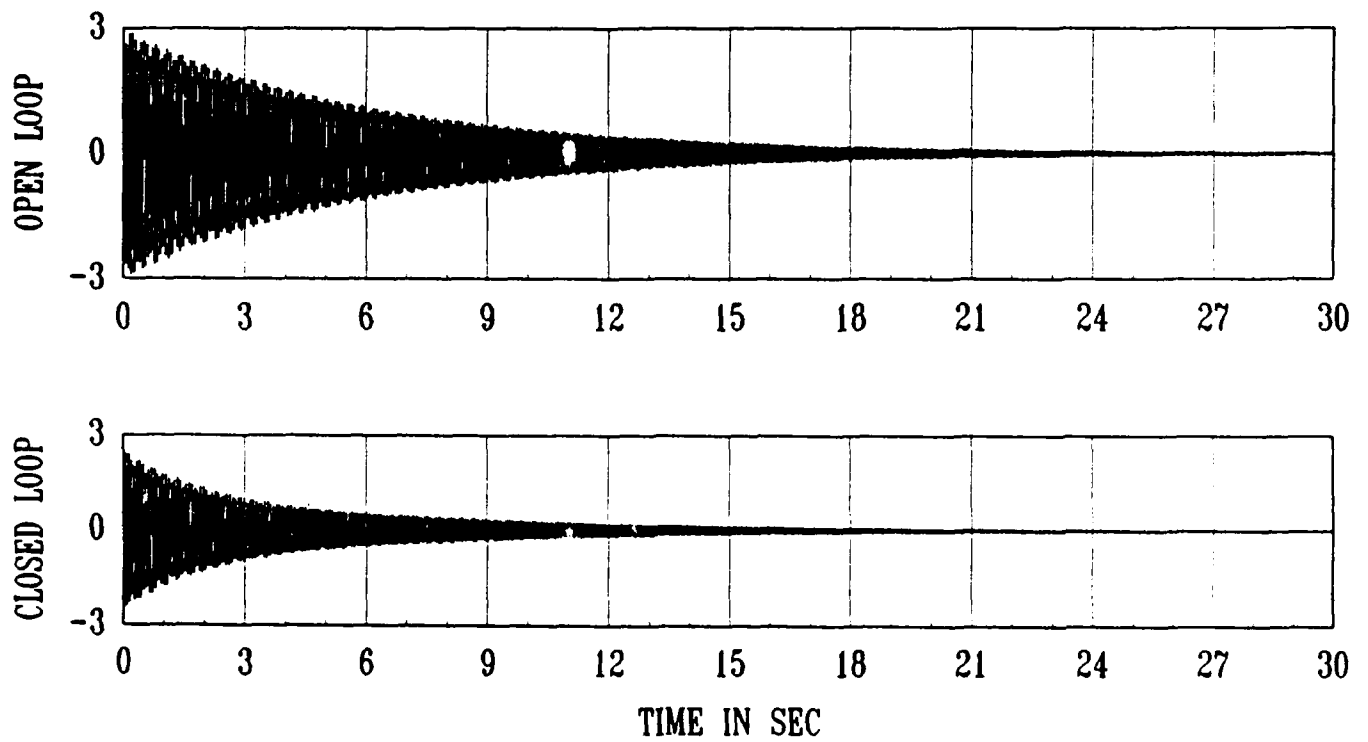
COMPARISON BETWEEN OPEN AND CLOSED LOOP RESP FOR MODE 9
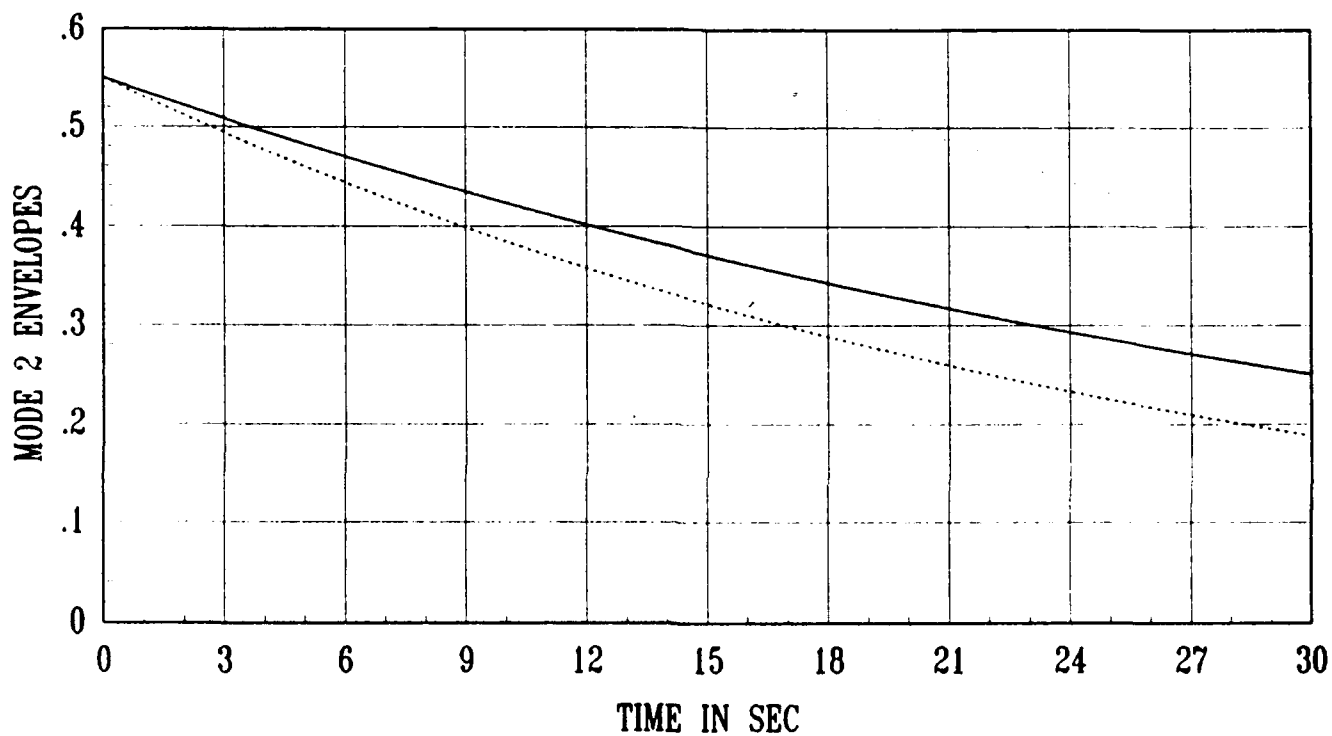
COMPARISON BETWEEN OPEN AND CLOSED LOOP ENVELOPES

Damping Open Loop 2.2×10^{-3}

Closed Loop 3×10^{-3}

MIMO

V. Recommendations:

a.   Since a digital computer (MAX-100) would be used to implement the controller and observer in real time, it is desirable to put the observer in modal form to minimize the number of computations the computer would have to perform to generate the states. With the number of computations minimized, the sampling frequency achievable would be maximized. The controller gain matrix K would then be post multiplied by the transformation matrix relating the old states of the observer to the new states.

b.   To improve the design of the controller, a robust controller should be designed. One very good reason for using a robust controller is the fact that on ground testing of a large space structure is the only type of testing which is economically possible. However when the space structure is lifted into space, its natural modes will be different from those measured on the ground. It would be desirable to design the controller so that these changes don't affect its performance. Also, space is a more hostile environment subject to wide temperature ranges and other changing conditions. As a consequence of this, the space structure will be subject to parameter changes as well.

References

1.   Alok   Das,   Timothy   J.   Strange,   Waid   T.
Schlaegel, John M. Ward, "Experiment in Modeling and
Parameter Estimation of Flexible Structures", <u>Second
NASA/DoD CSI Technology Conference</u>, November 17-19
1987

1989 USAF-UES SUMMER FACULTY RESEARCH PROGRAM

GRADUATE STUDENT RESEARCH PROGRAM

SPONSORED BY THE

AIR FORCE OFFICE OF SCIENTIFIC RESEARCH

CONDUCTED BY

UNIVERSAL ENERGY SYSTEMS, INC.

FINAL REPORT

Carrier Free Radar

Prepared by: Beryl L. Barber, Assistant Professor

                      Electronic Engineering Department

                      Oregon Institute of Technology

                      and Graduate Graduate Engineers

                      Keith Carroll - New Mexico State

                      Douglas Pederson - U C L A

                      George Ramlow - U C L A

Research Location: ESD/Hanscom AFB and RADC/Griffiss AFB

USAF Researchers: Lt. Col. James D. Taylor, USAF

                      Al Dahlgren, ESD

Same Report As
Dr. Beryl Barber
(Report # 32)

1989 USAF-UES SUMMER FACULTY RESEARCH PROGRAM/

GRADUATE STUDENT RESEARCH PROGRAM

Sponsored by the

AIR FORCE OFFICE OF SCIENTIFIC RESEARCH

Conducted by the

Universal Energy Systems, Inc.

FINAL REPORT

Analysis of Testability Concepts and its
Application to RSIP

Prepared by: Dr. S. Natarajan
                      Bradley K. Herman

Academic Rank: Associate Professor
                      Graduate Student

Department and   Electrical Engineering Department

 University: Tennessee Technological University

Research Location: ESD/TCWU
                      Hanscom AFB, MA

USAF Researcher: Major Ken Howes

Date: 18 Aug 89

Contract No: F49620-88-C-0053

Same Report As
Prof. S. Natarajan
(Report # 34)

1989 USAF-UES SUMMER FACULTY RESEARCH PROGRAM

GRADUATE STUDENT RESEARCH PROGRAM

SPONSORED BY THE

AIR FORCE OFFICE OF SCIENTIFIC RESEARCH

CONDUCTED BY

UNIVERSAL ENERGY SYSTEMS, INC.

FINAL REPORT

Carrier Free Radar

Prepared by: Beryl L. Barber, Assistant Professor

                      Electronic Engineering Department

                      Oregon Institute of Technology

                      and Graduate Graduate Engineers

                      Keith Carroll - New Mexico State

                      Douglas Pederson - U C L A

                      George Ramlow - U C L A

Research Location: ESD/Hanscom AFB and RADC/Griffiss AFB

USAF Researchers: _____ USAF

                      Al Dahlgren, ESD

Same Report As
Dr. Beryl Barber
(Report # 32)

1989 USAF-UES SUMMER FACULTY RESEARCH PROGRAM

GRADUATE STUDENT RESEARCH PROGRAM

SPONSORED BY THE

AIR FORCE OFFICE OF SCIENTIFIC RESEARCH

CONDUCTED BY

UNIVERSAL ENERGY SYSTEMS, INC.

FINAL REPORT

Carrier Free Radar

Prepared by: Beryl L. Barber, Assistant Professor

                           Electronic Engineering Department

                           Oregon Institute of Technology

                           and Graduate Graduate Engineers

                           Keith Carroll - New Mexico State

                           Douglas Pederson - U C L A

                           George Ramlow - U C L A

Research Location: ESD/Hanscom AFB and RADC/Griffiss AFB

USAF Researchers: Lt. Col James D. Taylor, USAF

                     Al Dahlgren, ESD

Same Report As
Dr. Beryl Barber
(Report # 32)

1989 USAF-UES GRADUATE STUDENT RESEARCH PROGRAM

Sponsored by the

AIR FORCE OFFICE OF SCIENTIFIC RESEARCH

Conducted by the

Universal Energy Systems, Incorporated

FINAL REPORT

Effects of Jet Aircraft Noise on
Domestic Goats

Prepared by:	Jon D. Zern, B.S.
Academic rank:	Second Year Veterinary Student
Department and	Physiological Sciences
University:	University of Florida
Research Location:	Environics Division (RDV) USAF Engineering and Services Center Tyndall AFB, FL 32403-6001
Faculty Researcher:	E. L. Besch, Ph.D., UES 1989 Summer Fellow
Date:	14 August 1989
Contract No:	F49620-88-C-0053

Effects of Jet Aircraft Noise on Domestic Goats

by

Jon D. Zern

ABSTRACT

Military jet aircraft operations cause unwanted noise pollution and have resulted in numerous complaints from the public. In an effort to deal with this problem, a research protocol was developed by the UES Summer Fellow to evaluate the altered physiology of goats exposed to noise from low-level jet aircraft. The graduate student researcher functioned as the principal assistant to the Summer Fellow in completing project goals. Before the experiment began, about 3-wk of the 10-wk stay at Tyndall AFB were devoted to dealing with processing requisitions, solving logistical problems, arranging for various kinds of project support, and constructing goat pens and shelters. Completion of all preliminary activities, including construction of pens and shelters, required about 4-wk. Baseline animal data collection began at the end of the third week. Collecting vital signs, blood samples, and behavioral observations covered a total of about 7 wk; 2-wk for baseline data and 5-wk for experimental data. Feeding, managing, evaluating, and assisting in project research provided the graduate student researcher a wide variety of meaningful experiences.

Acknowledgements

I wish to thank the Air Force Systems Command, the Air Force Office of Scientific Research, and Universal Energy Systems, Incorporated, for allowing me to participate in the Graduate Student Research Program. The project provided me an excellent opportunity to gain experiences that will enhance my long-term career goals.

Many individuals were responsible for making my stay at Tyndall AFB a memorable occasion. Dr. Joan Scott provided the inspiration that led to the initiation of the "goat study" and was instrumental in identifying names of individuals who contributed significantly to project goals. I also wish to thank the UES Summer Fellow, Dr. E. L. Besch, for his patience, support, leadership, and encouragement. SGT Delwin C. Lovell, U. S. Army, deserves special recognition and thanks for his assistance, comradeship, and other valuable contributions. Other individuals who provided substantive support include Major Michael M. Thompson, USAF, of the Environmental Sciences Branch, AFESC; TSgt Jim B. Whitcomb, Supply Office, Environics Division, AFESC; Bob Bates, Charles Pennington, Paul Vincent, and Regina Register (all from the Office of Natural Resources, Tyndall AFB); Captain Janice Gaska and her Clinical Laboratory Staff at the Tyndall AFB Hospital; and last, but not least, Captain Steven Tobias, Base Veterinarian, for his friendship and professional advice concerning the health maintenance of the goats.

I.   INTRODUCTION:

In fulfillment of its National defense mission and with the expanding inventory of supersonic aircraft, increased flying hours, and other operational considerations, the U. S. Air Force (USAF) must continue to conduct flight operations in current aircraft and in assigned airspaces over private and public land (Public Law 99-606). The advantages of those activities include acquiring basic flight skills, improving mobilization readiness, and meeting mission requirements.   Perhaps the numerous complaints about aircraft noise constitute the major disadvantage (Faber, 1989).   To deal with those complaints, assessments of potentially adverse physiological effects of noise and sonic booms on domestic animal productivity are necessary.   The research project entitled "Effects of Jet Aircraft Noise on Domestic Goats" was designed to provide information to help fill this need.

My interest in participating in this project resulted from a conversation with one of my professors, Dr. E. L. Besch (a 1989 UES Summer Fellow), in the College of Veterinary Medicine, University of Florida, Gainesville.   It was his explanation of the proposed noise research that stimulated me to apply for the Graduate Student Research Progran.   At that time, I believed that my education, interests in environmental physiology, and training uniquely qualified me to provide substantive contributions to the successful completion of project goals.   I also believed that the experiences gained from participating in this project would be valuable to me irrespective of whether I practice veterinary medicine or pursue postdoctoral training after completion of my DVM degree.   Obviously, the events of the past 10 weeks have fulfilled all of my expectations and beliefs.

II. OBJECTIVES

The intensity of noise is an important factor relative to its harmful effects on animals. High intensity sound usually acts as a warning of possible injury to the ear while low intensity sound may cause short-term effects depending upon its acoustic properties. Noise can result in auditory (e.e., hearing loss, nerve damage) and non-auditory (e.g., increased corticosterone, behavioral changes) effects in animals (Borg, 1979).

Noise caused by animals--in the range of 50-60 dB--does not appear to adversely affect an animal but exposures to noise intensities above 90 dB can result in measurable effects (Busnel, 1978). For example, hearing loss has been reported at exposure levels of 85 dB(A) for 8 hr, or equivalent. At intensities of $\geq$ 100 dB(A), temporary or permanent hearing loss may be induced. Jet aircraft at take-off can produce sound intensities of 140 dB (USAF Reg 161-35, 1982).

Comparions of physiological responses of animals exposed to low-level jet aircraft noise (Experimental Group) to animals exposed to typical rural noise levels (Control Group) were proposed as part of this study. In selecting the animal model, several factors were considered: ease of maintenance and management, ready availability, comparative cost, and suitability as a wildlife analog. The obtained data allowed calculation of physiological consequences of exposing domestic goats to jet aircraft noise and prediction of the effects of jet aircraft noise on wildlife ruminant species. At the very least, the information should provide the basis for follow-up experiments utilizing more refined or sensitive measurements to detect effects of similar noise intensities.

Participation in this study offered me the opportunity to not only collaborate with the Summer Fellow but also contribute to the goals and objectives of the project. The majority of the research findings of this study will be described in the FINAL REPORT of the

1989 UES Summer Fellow, Dr. E. L. Besch. My report will be an adjunct to the Summer Fellow's report and will deal primarily with my major role of assisting the Summer Fellow in the project. My specific objectives included purchasing necessary supplies, hay and feed, constructing goat pens and shelters, monitoring vital signs and collecting research data, supervising husbandry practices, observing clinical signs and symptoms, observing behavioral changes, and assisting the Base Veterinarian in health maintenance of the goats.

III. OBJECTIVE A:

Probably the most difficult obstacles that had to be overcome before the project could be initiated involved budget approval and purchase of necessary supplies. Based on two pre-Summer visits to Tyndall AFB and several hours of effort (in Gainesville, FL) developing plans and identifying needed supplies prior to my arrival at the Air Force Engineering and Services Laboratory (AFESC), the UES Summer Fellow developed lists of necessary supplies, associated cost estimates, detailed plans for construction of the goat shelters, feeders, and pens and timelines for the project. Budget approval came quickly but solution of logistical problems, developing the legal instrument for acquiring the goats, and acquisition of supplies required a significant amount of time. Accumulation of baseline animal data began at the end of my 3rd week and construction of goat pens and shelters was completed at the end of my 4th week at the AFESC.

Because of the lack of prior experience in conducting animal experimentation at the Air Force Engineering and Services Laboratory, Tyndall AFB, many logistical problems had to be overcome before the research on the "Effect of Jet Aircraft Noise on Goats" could be initiated. As an example, purchase orders had to be processed through the USAF system, on an expedited basis, after all needed supplies had been identified. These included goat feed and hay, laboratory supplies (e.g., gauze, vacutainer tubes, 20G needles, microscope slides), and materials for constructing the pens and

shelters for the goats. Except for the laboratory supplies, all other items did not have Federal stock numbers so data from private vendors had to be accumulated and itemized before the necessary Form 9s could be processed. Further time was expended in locating vehicles to transport animals, containers to transport water, animal watering devices, storage facilities for feed and hay, and noise measuring devices.

IV. OBJECTIVE B:

Before the project could be initiated at the two Tyndall AFB (TAFB) sites, goat pens, shelters and exercise areas had to be constructed. The design for the pens and shelters (Figure 1) was in accordance with descriptions contained in a Florida Cooperative Extension Booklet entitled "Management Practices, Housing, and Facilities for Goats" (McGowan, 1985; 1986).

Although only about 200 sq ft are required per animal for housing and exercise, that number represents the minimum. A larger area (100 ft X 100 ft = 10,000 sq ft) was planned so as to simulate, as much as possible (and mitigate the potential confinement stressor effects), the space the goats had in their prior habitat as well as provide sufficient exercise area for each animal (Figure 1). Because of the location of the pens and natural predator animals (e.g., coyotes) in the Panama City, Florida, area, the barbed wire fencing was added to the top and bottom of the wire fencing to discourage egress by the goats and ingress by predators.

After purchase of all necessary supplies, the actual construction of the pens, shelters, and exercise ramps was accomplished in about 4 days with the assistance of personnel from the TAFB Division of Natural Resources. The pens and shelters fulfilled their purpose for the entire period of the project. It is anticipated that they will be disassembled soon and the materials recycled for other projects.

V.   OBJECTIVE C:

The early research plan envisioned evaluating the effect of noise on milk production in goats. Unfortunately, excitation of the animal interferes with milk expulsion (Jacobson and McGilliard, 1984) and--together with factors such as the temperament of dairy goats and transportation and environmental stressors--tends to inhibit milk let-down (i.e., the animal becomes dry). More accurate indices of stressor response include blood plasma levels of specific adrenal cortical hormones (e.g., cortisol, corticosterone) and thyroid hormones (e g., triiodothyronine, thyroxine). Glucocorticoids regularly are elevated during "stress" because of the elevated corticotropin releasing hormone (CRH) from the hypothalamus which stimulates the adenohypophysis to release adrenocorticotrophic hormone (ACTH) which stimulates the release of corticosteroids from the adrenal cortex (Granner, 1988).

Periodic collection of blood samples provided plasma for assays of adrenal cortical and thyroid hormones and determination of packed cell volumes, plasma protein concentrations, and differential white blood cell counts. Other serially collected blood samples provided serum in which clinical chemistry values (e.g., glucose, BUN, cholesterol, SGOT) were measured. Respiratory frequencies, body weights and heart rates also were periodically recorded partly because cardiac frequency has been shown to be a predictor of blood cortisol levels (Harlow et al, 1987). The above measurements also will allow for comparisons of stressor response, hydration, growth rate, and general health between the two experimental (6 animals each) and one control (8 animals) groups of goats.

All data will be analyzed with the assistance of the Biostatistics Laboratory of the Health Science Center, University of Florida and the results reported by the UES Summer Fellow.

VI. OBJECTIVE D:

Husbandry of animals includes providing hay and feed, cleaning stalls and sleeping benches, and providing fresh water on a daily basis to minimize the potential for parasitic infections and ultimately maintain a healthful, comfortable environment for the goats. Wet or moldy hay and dirty sleeping benches (i.e., covered with dirt or fecal material) increase the probability of parasitic infections (McGowan, 1985). This can cause a stressor response that could invalidate the data from the individual animal. Lack of pen/stall cleanliness also can increase the incidence of biting flies and mosquitoes both of which can transmit disease (Hibler and Cheney, 1985) or generally make the environment uncomfortable for the animals.

The goats were provided a ration similar to what they received from the owner prior to the beginning of the research project. This consisted of concentrate (1 to 2 lbs per goat per day) and locally obtained hay which was available _ad libitum_. Water also was available _ad libitum_. Preliminary body weight data suggest no differences in the growth rate of the two groups of goats housed at the TAFB sites (i.e., goats exposed to two different jet aircraft noise intensities). In all, there were only three animals that required attention from the veterinarian (Refer to OBJECTIVES E AND G below).

VII. OBJECTIVE E:

Clinical signs and symptoms were monitored regularly because of our concern about the transfer of the two groups of experimental animal to new geographic locations at TAFB. In a new environment, it is not unusual for an animal to acquire new intestinal flora or be exposed to other parasites or other organisms.

During the course of the experiment, gross observations and hematological findings (e.g., eosinophilia) suggested that one goat was

infected with helminths or suffering an allergic response (Swenson, 1984). Because of the diarrhea and associated lethargic behavior, allergic response was tentatively ruled out. A subsequent fecal examination confirmed that the animal was infected with both Bunostomum (i.e., a ruminant hookworm) and coccidia (i.e., a protozoan). Treatment was not initiated immediately because of the continued appetite and firm stools of the animal and because helminths are normal inhabitants of the intestinal tract (Guss, 1977). Further, the presence of coccidia does not necessarily justify treatment (Guss, 1977). Gross observations continued on a daily basis and hematological findings returned to normal in about 2 wk.

VIII. OBJECTIVE F:

The typically reported behavioral signs include startle reflex, avoidance behavior, and vocal repetition rates (Espmark et al, 1974; Ruth, 1976). Because of the project emphasis on the influence of low-level jet aircraft noise of goats, these signs were monitored on a regular (i.e., daily) basis and the results recorded. The rationale was that the animals' behavior would be related to their physiologcal adaptation to the noise stressor and their behavioral signs would diminish as they became "adapted" (Espmark et al, 1974).

In order to be as objective as possible in a field study--where many variables cannot be totally controlled--criteria for behavioral reactions included three defined groups: (1) no reaction, (2) moderate reaction, and (3) strong reaction as detailed in Table 1 (Espmark et al, 1974).

During 80% of the time that the goats were at the two TAFB sites, very little change in routine goat behavioral activity was observed. This is thought to have been due partly to the proximity of goat pens and enclosures to the active jet aircraft runway. When the runway site was chosen at the Northwest end of the northernmost runway ("A" in Figure No. 2), it was assumed that the daily F-15 operations would primarily utilize this runway.

Unfortunately, due to circumstances beyond the control of the research project personnel, the southernmost runway was the only operational runway for 4 of the 5 weeks of this research project. When the aircraft began to utilize the northernmost runway and fly directly over the goat pens (during the last week of the project), strong reactions were observed in the goats' walking, standing and browsing activities.

Table 1.   Behavioral responses of goats under different activities (From Espmark et al, 1974).

Browsing
No reaction
Moderate reaction | 1.   Startle, no interruption of browsing.
2.   Interruption of browsing, raising of head, pricking ears, no locomotion
Strong reaction | Interruption, of browsing, locomotion of up to 10 m

Lying
No reaction
Moderate reaction | 1.   Intentions to get up
2.   Quick raising of head, pricking of ears
Strong reaction | Momentary raising into standing position

Standing
No reaction
Moderate reaction | Startle, transient raising of head, no locomotion
Strong reaction | Startle, transient nodding of head, locomotion

Walking
No reaction
Moderate reaction | Interruption of walking, raising of head, looking around
Strong reaction | Converted walking into running

The goats housed at the Natural Resources site ("B" in Figure 2) showed atypical behavior during the entire 5-wk project period. That is, these goats were apprehensive, easily agitated, and difficult to manage. These responses did not appear to be related to nor influenced by jet aircraft noise. Efforts to identify other potential causes (e.g., existence of natural predators (coyotes) near the site, radar frequencies of nearby transmitters, and sentry dogs trained in the vicinity) of these behavioral responses were unsuccessful. Whether some other, as yet unexplained, factor(s) caused the animals

to appear to be "stressed" must await the results of further analyses of blood plasma for standard indices of stressor response (e.g., elevated cortisol concentrations).

IX.   OBJECTIVE G:

As a second year student enrolled in the professional degree (DVM) program in the College of Veterinary Medicine, University of Florida, Gainesville, I am very interested in the comparative aspects of veterinary medicine in civilian vice military situations. Previously I worked parttime in three different civilian veterinary practices and was eager to learn how my prior experiences would compare to those obtained in a military veterinary clinic.

During my 10-wk stay at TAFB, I was fortunate to be given the opportunity to observe closely the delivery of health care to the military guard dog program, animals that are · affiliated with the Morale, Welfare, and Recreation Division, and companion animals of DOD personnel in the Panama City, Florida area. I also was provided the opportunity to perform venipunctures, fecal and heart worm examinations, and prophylactic procedures (e.g., vaccinations) in addition to providing general day-to-day health care surveillance for the research goats. The latter included procedures on two research goats who exhibited periodic coughing. Examination included collecting blood serum samples for toxoplasmosis titers to be performed off base, attempting to identify other signs (e.g., rales) and symptoms (e.g., coughing), and massaging the trachea to induce the coughing reflex. Based on these examinations, it was determined that the animals' lungs were clear and that they were healthy.

X.   RECOMMENDATIONS:

A.   Because Summer Faculty and Graduate Student Researchers are at Tyndall AFB for only a 10-wk period, it is suggested that special consideration be given to the expeditious processing of purchasing order requests and handling of logistical problems--particularly for

animal research projects--so that the effort of these individuals can be directed solely to data collection/analyses.

B. Data analyses capability should be available at AFESC to the Summer Faculty and Graduate Student Researcher.

C Should animal experimentation be conducted at AFESC in the future, appropriate animal quarters, including feeding and watering devices, should be available in advance of the arrival of the researchers.

D. The Base veterinarian, Captain Steven Tobias, VC, USA, and SGT Delwin C. Lovell, USA, Veterinary Technician, are to be commended for their total dedication, support, and assistance in fulfillment of the research project objectives. The Chief of Natural Resources, Robert Bates, and his staff and Captain Janice Gaska, USAF, Chief of the Clinical Laboratory at Tyndall AFB Hospital and her staff also should receive special recognition for their professionalism, total cooperation, and "can do" attitude.

XI. REFERENCES:

1. Borg, E. Physiological aspects of the effects of sound on man and animals," Acta Otolaryngal Suppl, 1979, Vol 360, pp 80-85.

2. Busnel, R. G., Introduction, In: Effects of Noise on Wildlife, J. L. Fletcher and R. G. Busnel, Eds., New York, Academic Press, 1978, pp 7-22.

3. Espmark, Y., L. Falt, and B. Falt, "Behavioural responses in cattle and sheep exposed to sonic booms and low-altitude sub-sonic flight noise," The Veterinary Record, 1974, Vol 94, pp 106-113.

4. Faber, H. "Agency protests flights over Adirondack Park," New York, New York Times, 19 Feb 89, p. 58.

5.   Granner, D. K., "Pituitary and hypothalamic hormones," Chapter 45, In: Harper's Biochemistry, 21st Edition, San Mateo, California, Appleton & Lange, 1988, pp 482-483.

6.   Guss, S. B., Management and Diseases of Dairy Goats, Scottsdale, Arizona, Dairy Goat Journal Publ Corp., 1977, pp. 102-144.

7.   Harlow, H. J., E. T. Thorne, E. S. Williams, E. L. Belden, and W. A. Gern, "Cardiac frequency: a potential predictor of blood cortisol levels during acute and chronic stress exposure in Rocky Mountain bighorn sheep (Ovis canadensis canadensis)," Can J Zool, 1987, Vol 65, pp 2028-2034.

8.   Hibler, C. P. and J. M. Cheney, "Parasitology and public health," Chapter 5, In: Clinical Textbook for Veterinary Technicians, D. M. McCurnin, Ed., Philadelphia, Pennsylvania, W. B. Saunders Company, 1985, pp 81-109.

9.   Jacobson, N. L. and A. D. McGilliard. "The mammary gland and lactation," Chapter 52, Duke's Physiology of Domestic Animals, 10th ed., M. J. Swenson, Ed., Ithaca, New York, Cornell Univ Press, 1984, pp. 869-870.

10.   McGowan, C. H., "Raising a small flock of goats for meat and milk: selection, breeding practices and feeding the herd goat," Florida Cooperative Extension Service, Florida A&M University-University of Florida, 1985, Circular 643, 13p.

11.   McGowan, C. H., "Raising a small flock of goats for meat and milk: management practices, housing and facilities," Florida Cooperative Extension Service, Florida A&M University-University of Florida, 1986, Circular 644, 12 p.

12.   Public Law 99-606, "Withdrawals of Public Lands for Military Purposes," 100 Stat 3457, 6 Nov 86.

13. Riegle, G. D., F. Przekop, and J. E. Nellor, "Changes in adrenocortical responsiveness to ACTH infusion in aging goats," J Gerontol, 1968, Vol 23, pp 187-190.

14. Ruth, J. S., "Reaction of arctic wildlife to gas pipeline related noise," J Acoust Soc Am, 1976, Vol 60 (Suppl 1), S67 (Abstract).

15. Swenson, M. J., "Blood circulation and the cardiovascular system," Chapter 2, In: Duke's Physiology of Domestic Animals, 10th ed., M. J. Swenson, Ed., Ithaca, New York, Cornell Univ Press, 1984, p. 29.

16. USAF Regulation 161-35, Hazardous Noise Exposure, Washington, DC, U. S. Air Force, OPR, Surgeon General (SGPA), April, 1982.
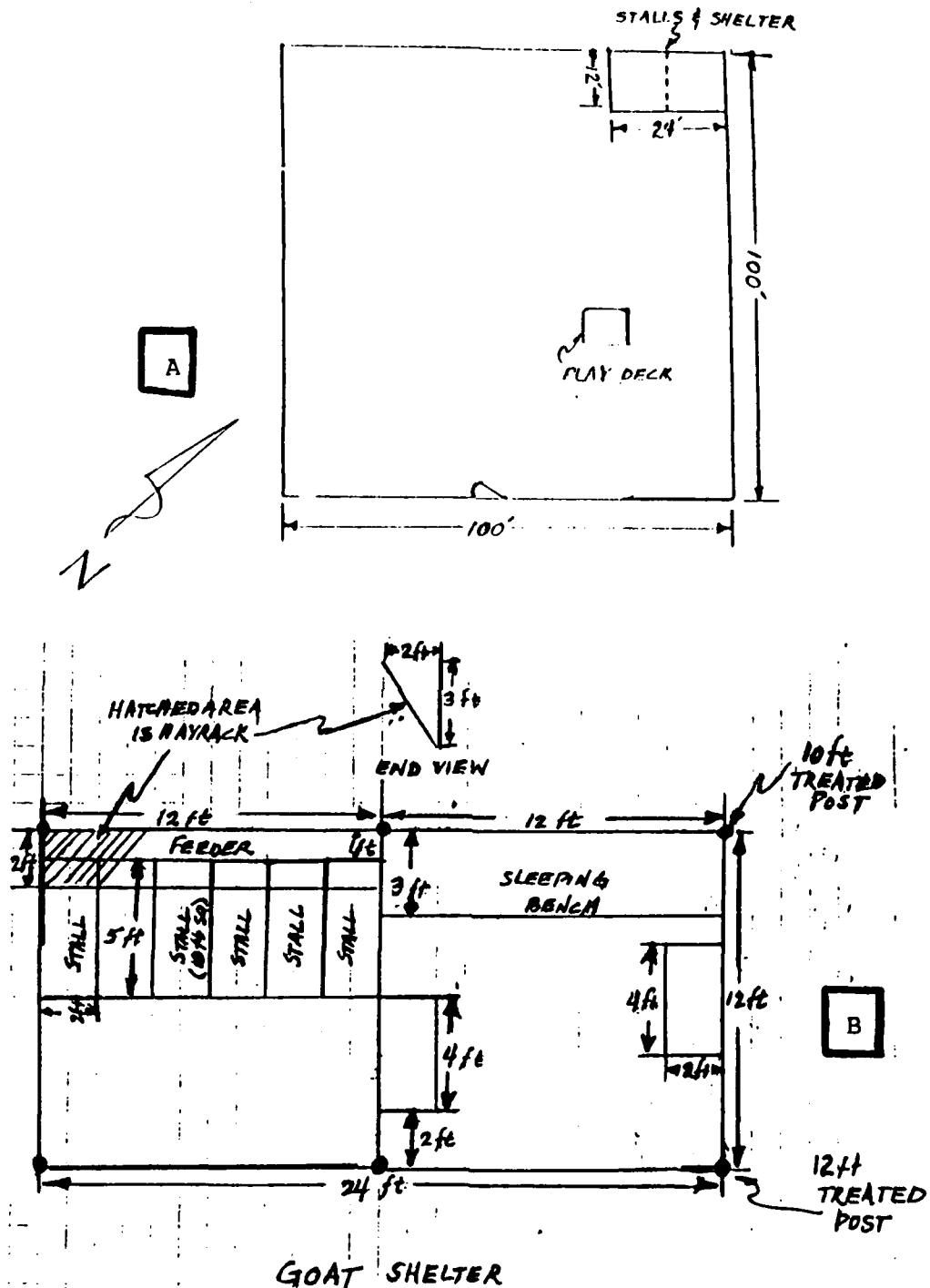
Figure 1. Schematics of goat pens ("A" above) and shelters ("B" above) as described by McGowan (1986).
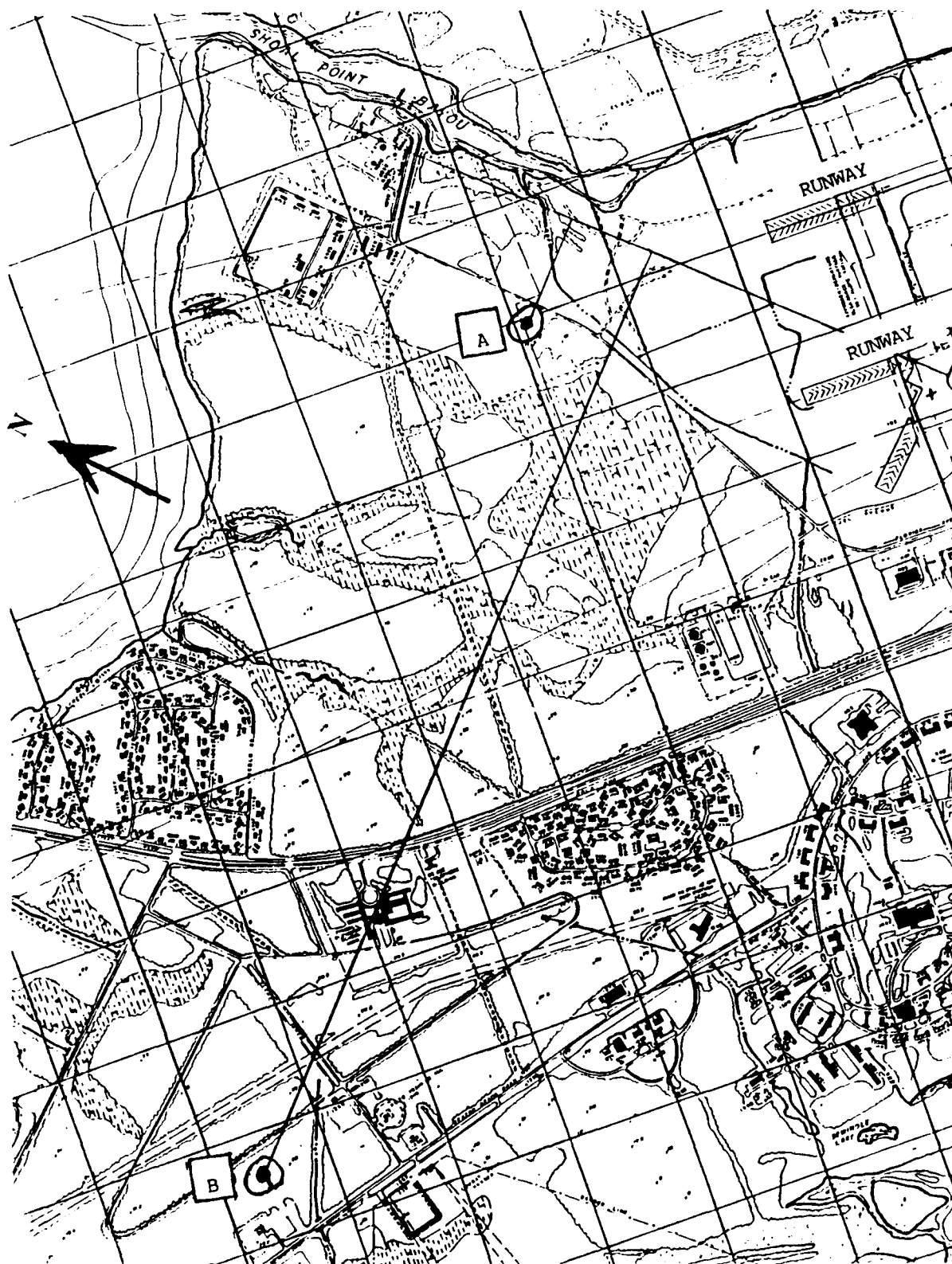
Figure 2. Grid map showing the location of the two goat pen areas and aircraft runways at Tyndall AFB. Location A is the Runway Site and B is the Natural Resources Site.

22-17

1989 USAF-UES SUMMER FACULTY RESEARCH PROGRAM

GRADUATE STUDENT RESEARCH PROGRAM

Sponsored by the

AIR FORCE OFFICE OF SCIENTIFIC RESEARCH

Conducted by the

Universal Energy Systems, Inc.

CONTAMINANT FLUX REDUCTION THROUGH
IN SITU SOLUBILITY MODIFICATION

Prepared by: *Kirk Hatfield*, Ph.D. and Joseph Ziegler

Academic Rank: Assistant Professor,   Graduate Student

Department and   Civil Engineering

  University   University of Florida

Research Location: Engineering and Services Center
                      Tyndall AFB FL 32403-6001

USAF Researcher: Thomas B. Stauffer, Ph.D.

Date: 24 Jul 89

Contract No: F49620-88-C-0053

Same Report As
Prof. Kirk Hatfield
(Report # 41)

1989 USAF-UES SUMMER FACULTY RESEARCH PROGRAM/ GRADUATE STUDENT RESEARCH PROGRAM

Sponsored by the

AIR FORCE OFFICE OF SCIENTIFIC RESEARCH

Conducted by the

Universal Energy Systems, Inc.

FINAL REPORT

AN INVESTIGATION OF DYNAMIC STALL VORTEX CHARACTERISTICS

Prepared by: J.A. Albertson and T.R. Troutt

Department and
University: Department of Mechanical and Materials Engineering
Washington State University

Research Location: Frank J. Seiler Research Laboratory
Aerospace Mechanics Division
United States Air Force Academy, CO

USAF Researcher: Major Robert F. Reilman, Jr.

Date: September 29, 1989

Contract Number: F49620-88-C-0053

Same Report As
Prof. Timothy Troutt
(Report # 51)

1989 USAF-UES SUMMER FACULTY RESEARCH PROGRAM/

GRADUATE STUDENT RESEARCH PROGRAM

Sponsored by the

AIR FORCE OFFICE OF SCIENTIFIC RESEARCH

Conducted by the

Universal Energy Systems, Inc.

<u>FINAL REPORT</u>

<u>SECOND HARMONIC GENERATION IN OPTICAL FIBERS</u>

Prepared by: Lloyd W. Hillman, Ph.D.

Academic Rank: Assistant Professor

Department and   Department of Physics

  University   University of Alabama in Huntsville

And by: Stephen McClain, Graduate Student

                    <u>Mojdeh Anderson</u>, Graduate Student

Department and   School of Electrical Engineering

  University   Cornell University

Research Location: Frank J. Seiler Research Laboratory

                    USAF Academy, CO 80840

USAF Researcher: Maj Jim Rotgé

Date: 15 Oct. 89

Contract No: F49620-88-C-0053

Same Report As
Prof. Lloyd Hillman
(Report # 47)

1989 USAF-UES SUMMER FACULTY RESEARCH PROGRAM

GRADUATE STUDENT RESEARCH PROGRAM

Sponsored by the

AIR FORCE OFFICE OF SCIENTIFIC RESEARCH

Conducted by the

Universal Energy Systems, Inc.

<u>FINAL</u> <u>REPORT</u>

Transition State Analysis: Gluconolactone by MOPAC

Prepared by:	Brad S. Combs
Academic Rank:	Doctoral Student
Department and	Chemistry Department
University:	Wichita State University
Research Location:	Frank J. Seiler Research Lab USAF ACADEMY Colorado Springs, CO 80840
USAF Researcher:	Dr John S. Wilkes
Date:	18 August 89
Contract No:	F49620-88-C-0053

Transition State Analysis: Gluconolactone by MOPAC

by

Brad S Combs

ABSTRACT

MNDO and MNDO/PM3 transition states for the non-enzymatic hydrolysis of 1,5-gluconolactone and 6-deoxy-6-fluoro-1,5-gluconolactone are presented. Initial results indicate that hydrolysis at Carbon 1 (carbonyl carbon) proceeds with a *lower heat of formation* than hydrolysis at Carbon 5. Optimized geometries for associated products and reactants (MNDO and MNDO/PM3) are also reported. The synthetic routes for 6-deoxy-6-fluoro-β-D-glucose and 6-deoxy-6-fluoro-1,5-gluconolactone (chemical probes suitable for NMR work) are described. The results from this study provides useful information concerning the mechanism of hydrolysis of 1,5-gluconolactone.

Acknowledgements

I. INTRODUCTION:

At present, there is very little information on the mecha-
nism for hydrolysis of 1,5-gluconolactone. Gluconolactone
represents an ideal compound for modeling of hydrolysis
transition states in general and information derived from
this will be of use as applied to other, more complex sys-
tems. Gluconolactone is also of biochemical importance in
the metabolism of β-D-glucose. The hepatic enzyme Glucose
Dehydrogenase (E.C.1.1.1.47) produces 1,5-gluconolactone
from β-D-glucose. This cyclic lactone is a potent inhibi-
tor of glycosidases and phosphorylase. Hence, the cellular
levels of 1,5-gluconolactone regulate the breakdown of
glycogen and associated glycoproteins. There is a gradual
hydrolysis of gluconolactone to gluconic acid, however it
appears that the majority of lactone hydrolysis is accom-
plished enzymatically.

My research interests lie in the areas of computer modeling
of transition states, NMR spectroscopy and the kinetic
modeling of hydride transfer reactions. The overall signi-
ficane of this work is its general application (for the
Electrochemistry Section at the Frank J. Seiler Research
Laboratory) to molecular complexes of all types.

II. OBJECTIVES OF THE RESEARCH EFFORT:

The mechanism for hydrolysis of 1,5-gluconolactone has not been studied extensively and remaining to be answered is at what ring position does the hydrolysis attack occur. The hydrolysis of 1,5-gluconolactone can also be effected enzymatically (Brodie, 1955) by the cytosolic enzyme gluconolactonase (E.C.1.1.17), the product of both rections being gluconic acid. The atoms in the lactone most susceptable to ring opening are carbons 1 & 5 (Figure 1.). In an effort to elucidate more information about this process, molecular orbital calculations (MO) were performed to predict the transition states for both processes.

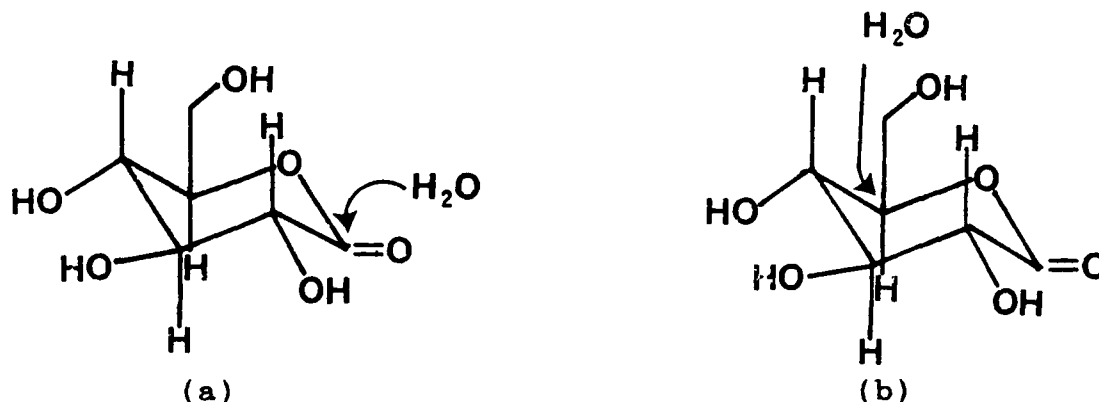(a)   (b)

Figure 1. Hydrolysis of 1,5-gluconolactone via water attack at Carbon 1 (a) and Carbon 5 (b).

All calculations were performed with MOPAC v.5.0 (Stewart, 1983) using either the MNDO or the MNDO/PM3 method. Table 1. contains the optimized heats of formation for the struc-

tures of interest. Saddle calculations were performed (in cartesian coordinates) with the first geometry being the lactone and the associated H_2O molecule (C-1 or C-5) and the second geometry being the corresponding gluconic acid.

Table 1. ΔH_f of compounds and transition states studied.

COMPOUND	MNDO	MNDO-PM3
β-D-Glucose	-268.7	-268.3
Gluconolactone	-255.3	-256.0
D-Gluconic acid	-310.7	-313.1
6-deoxy-6-fluoro-β-D-glucose	-267.6	-269.7
6-deoxy-6-fluoro-gluconolactone	-256.9	-256.9
6-deoxy-6-fluoro-D-gluconic acid	-313.0	-314.4
H_2O	-60.9	-53.4

TRANSITION STATES

Gluconolactone (C-1 Attack)	-220.5	-238.9
Gluconolactone (C-5 Attack	-196.6	-223.7
6-deoxy-6-fluoro-gluconolactone (C-1 Attack)	-225.1	-244.1

The saddle calculations were executed until the saddle point had been passed, as indicated by a reversal of the gradient direction vector (normally ca. 0.4 to 0.8, becoming ca. -0.4 to -0.8) and a abrupt change in energy. The saddle geometry at this point (gradient norm at a minimum and direction cosine switching signs) was selected for the non-linear least squares gradient minimization routine (NLLSQ). The derivative of ΔH_f with respect to the coordinates (gradient norm) was minimized until an acceptable value was obtained (typically <4) at which this stationary point was tested to determine if it actually corresponds to the transition

state. To do this, the final geometry resulting from the NLLSQ (.ARC) file was used and a data file with the keyword FORCE was created. The FORCE calculation gives the frequencies of the vibrations of the transition state and if the stationary point is a valid transition state, there will be only one vibrational mode with a negative frequency. The results from the FORCE calculations are presented in Table 2. Although the transition states for a,e and f (Table 2.) contain 2 vibrational modes with negative frequencies, these were considered to represent true transition states since the second mode with a negative frequency was less than 1-2.2% of the first mode. The data in Table 2. b,c,d cannot be considered true transition states, however the ΔH_f of this "pseudo" transition state does represent a maximum value and with further refinement may be lowered. This preliminary data (Table 2. b,c,d) can be used with caution, however futher refinement is necessary to be able to make valid assumptions regarding the preferred site of attack for H_2O. Using the ΔH_f from the optimized geometries of the products and reactants, with the ΔH_f of the intervening transition state, energy profiles for the hydrolysis reactions have been constructed, Figures 2 - 5. Figures 6 - 9 contain the optimized geometries for some of the PM3 optimized transition states and other compounds studied.

TABLE 2. Frequencies of negative vibrational modes from FORCE.

Compound		Method	1	2	3	4
a) lactone	C-1	MNDO	-2154.0	-30.8	N/A	N/A
b) lactone	C-1	PM3	-1894.9	-175.7	-73.0	-51.6
c) lactone	C-5	MNDO	-340.9	-76.5	-48.9	N/A
d) lactone	C-5	PM3	-572.5	-181.4	-115.1	-27.8

(6-deoxy-6-fluoro)

e) lactone	C-1	MNDO	-2173.6	-47.4	N/A	N/A
f) lactone	C-1	PM3	-2094.3	-19.8	N/A	N/A

III.

A. Synthesis of 1,2:5,6-Di-O-isopropylidene-D-glucofuranose

The method used was essentially that of Glen, Meyers and
Grant (1951, 1954) as modified by Blakley (1954). D-glucose
(150 g) was suspended in 1-L acetone, with efficient stir-
ring. To this suspension was added anhydrous $ZnCl_2$ (120 g)
followed by 85% phosphoric acid (4.4 ml). This mixture was
allowed to stir for 30 hrs. at 20°C, at which point the
undissolved glucose (83.5 g) was filtered off and washed
with acetone. The filtrate and washings were cooled on ice
and neutralized with approximately 72 ml of 25 M NaOH, to a
pH of 7.05. The insoluble inorganic material was removed by
filtration and washed with acetone. The filtrate and wash-
ings were concentrated to dryness under vacuum, at 39°C.
The solid residue was recrystallized from petroleum ether
(60-80°C b.p.) and gave 43 grams of product, (Figure 10. II)
(44.8% yield based on glucose utilized) m.p. 105-106°C
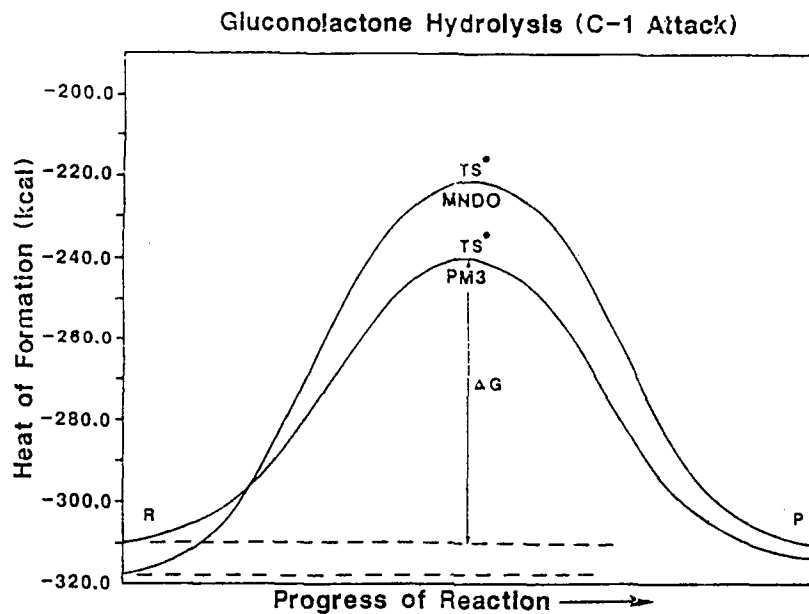(reported m.p. 110 °C).

Gluconolactone Hydrolysis (C-1 Attack)

Figure 2. Reaction profile for gluconolactone hydrolysis (C-1 attack) as calculated by MNDO & MNDO/PM3. (R=lactone & water, P=gluconic acid).
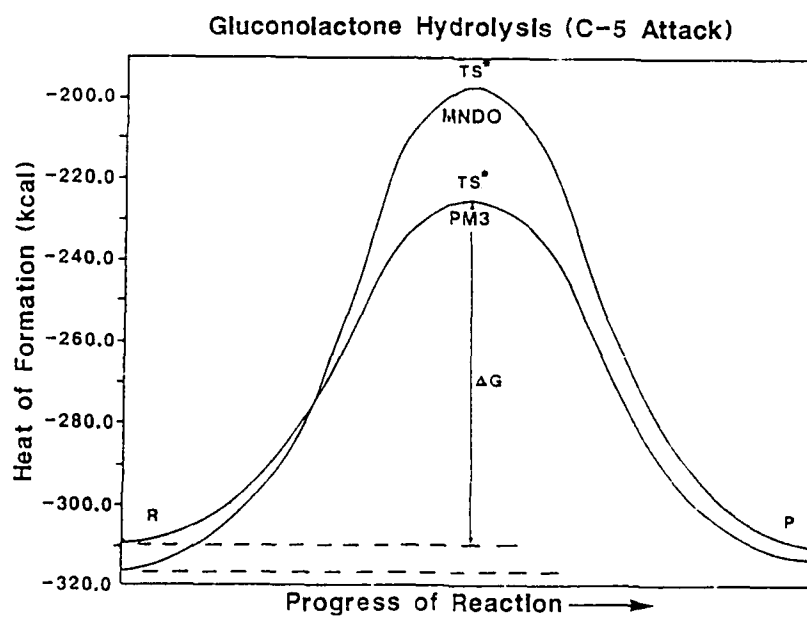
Gluconolactone Hydrolysis (C-5 Attack)

Figure 3. Reaction profile for gluconolactone hydrolysis (C-5 attack) as calculated by MNDO & MNDO/PM3. (R=lactone & water, P=gluconic acid).
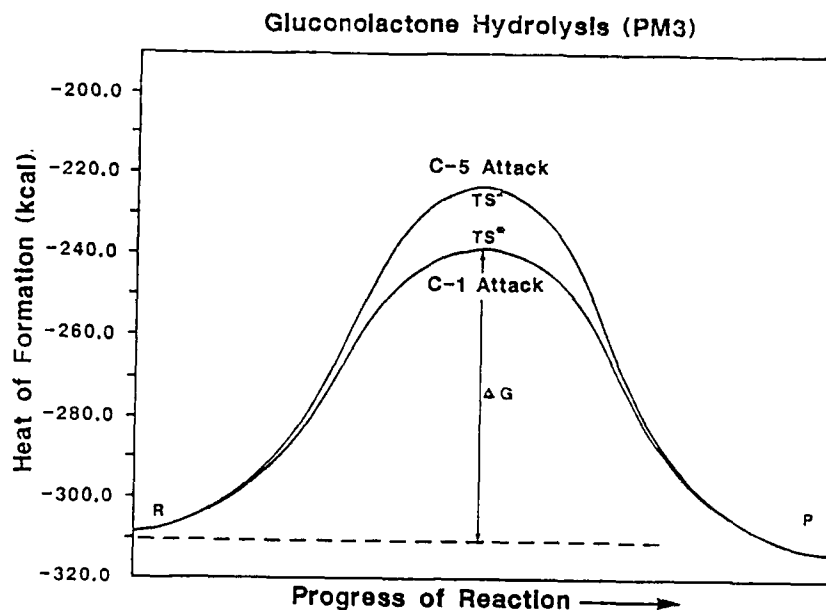
Gluconolactone Hydrolysis (PM3)

Figure 4. Comparison of PM3 results for gluconolactone hydrolysis at Carbons 1 & 5. Difference between transition states is 15.2 kcal.

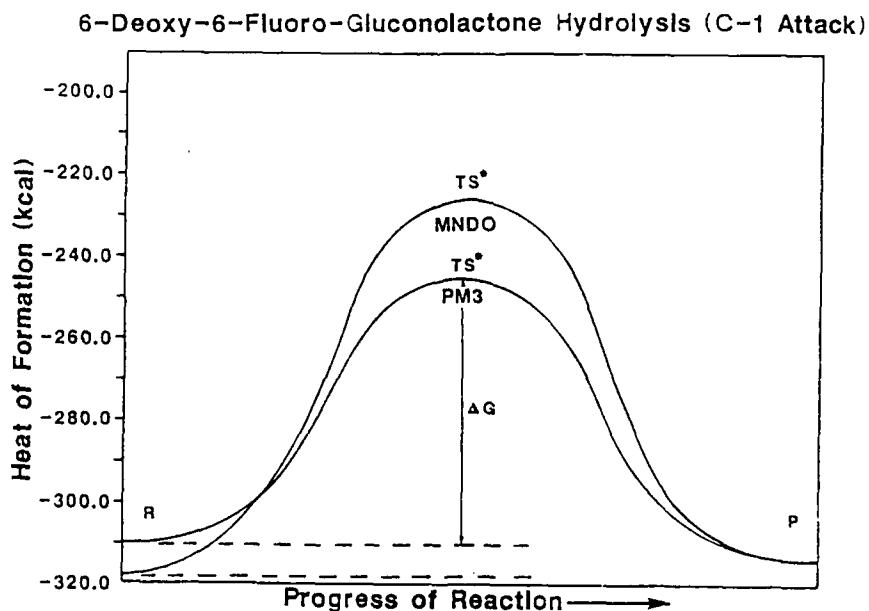**6-Deoxy-6-Fluoro-Gluconolactone Hydrolysis (C-1 Attack)**

Figure 5. Camparison of MNDO & MNDO/PM3 results for hydrolysis of 6-deoxy-6-fluoro-gluconolactone at Carbon 1. Difference between transition states is 19.0 kcal.

Figure 6. PM3 optimized geometry of C-1 transition state and first vibrational mode with a negative frequency, for gluconolactone. Bond lengths in angstroms.
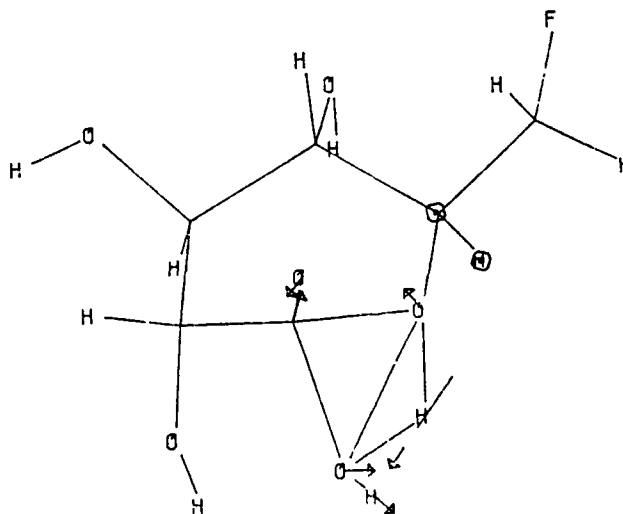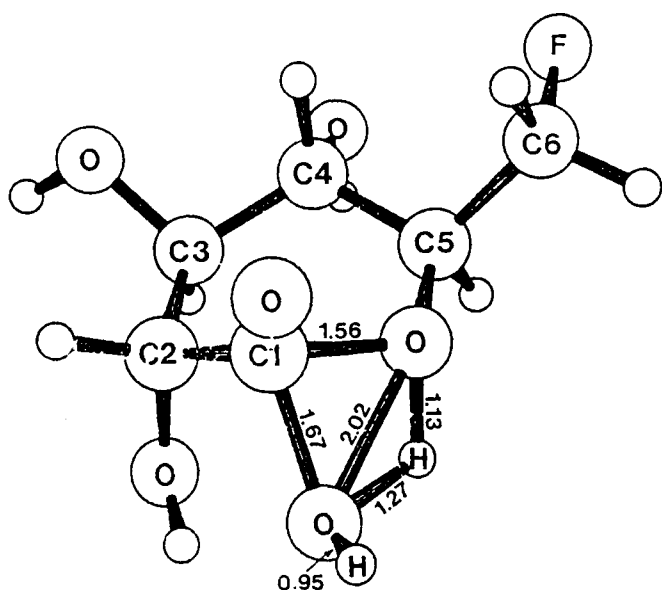
Figure 7. PM3 optimized geometry for C-1 transition state & first vibrational mode with a negative frequency, for 6-deoxy-6-fluoro-gluconolactone. Bond lengths in angstroms.
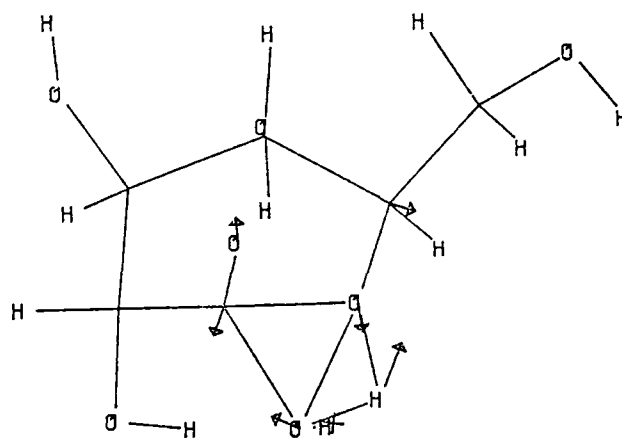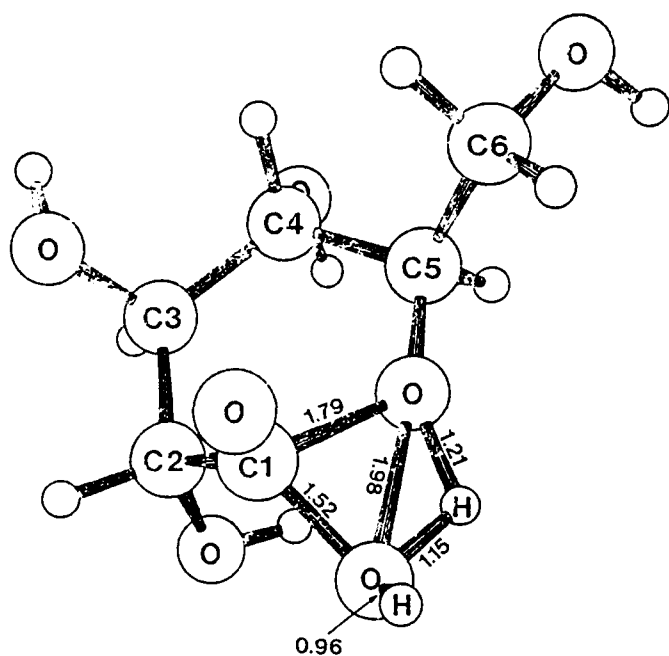
26-11
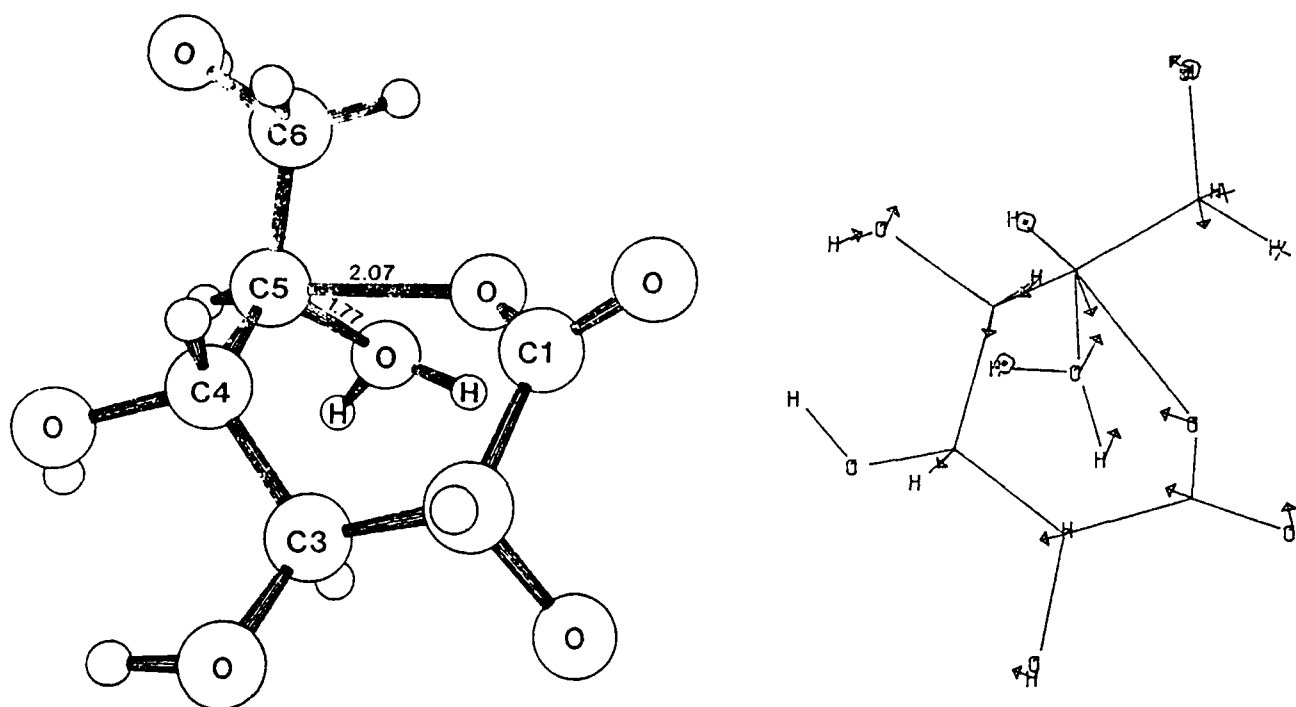
Figure 8. PM3 optimized geometry of C-5 transition state and first vibrational mode with a negative frequency, for gluconolactone. Bond lengths in angstroms.
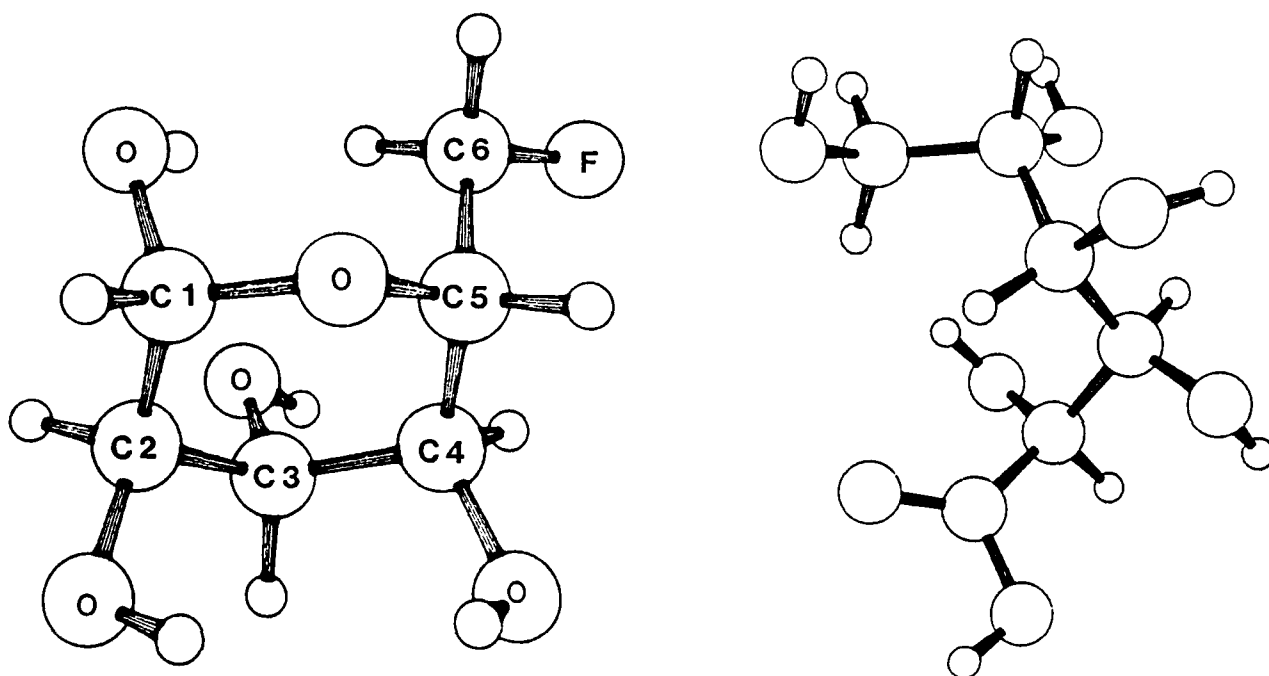
Figure 9. PM3 optimized geometries for 6-deoxy-6-fluoro--D-glucose and D-gluconic acid.
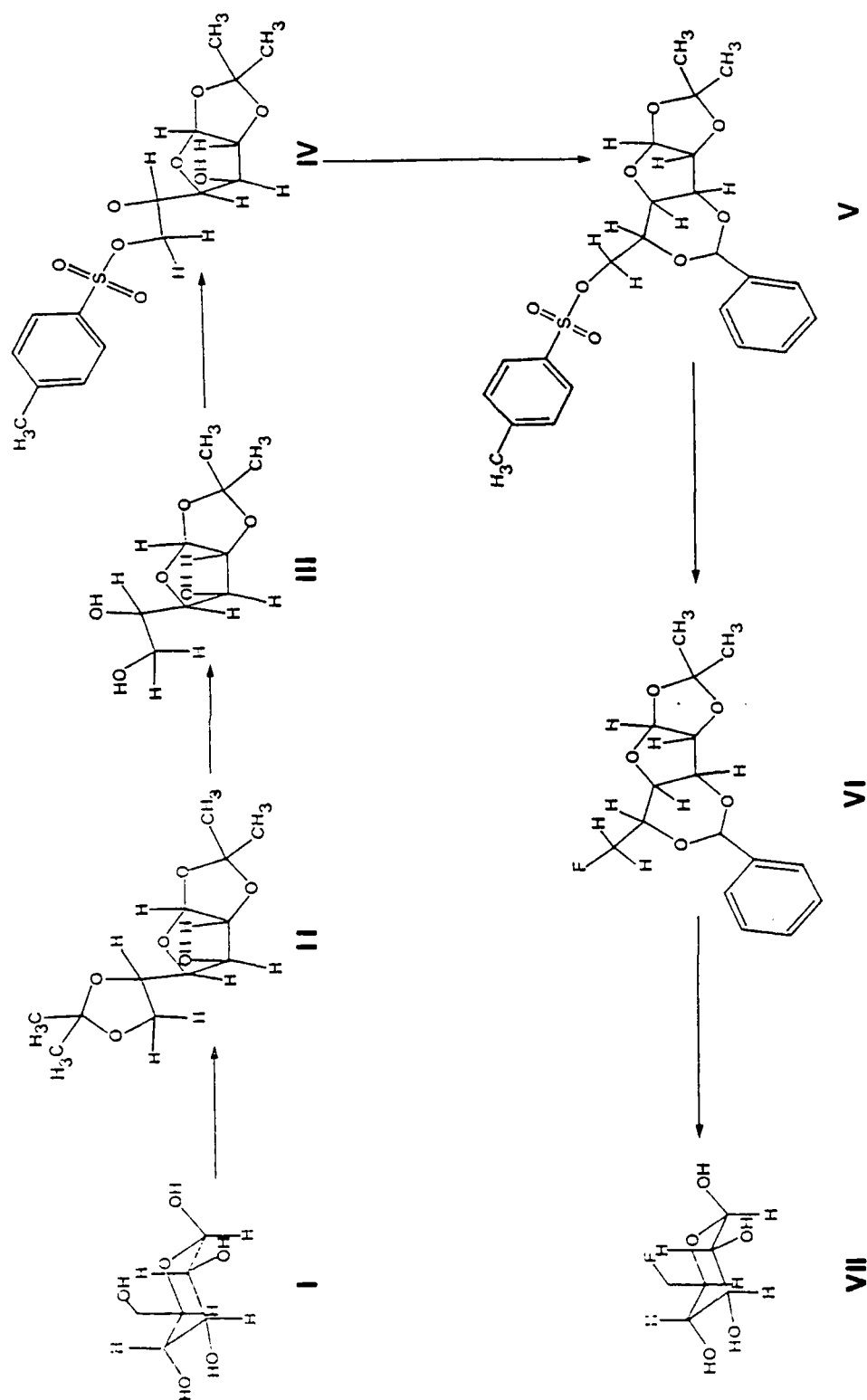
Figure 10. Synthetic route for 6-deoxy-6-fluoro-β-D-Glucose. (I=D-Glucose, II=1,2:5,6-Di-O-isopropylidene-D-glucofuranose, III=1,2-O-isopropylidene-D-glucofuranose, IV=1,2-O-isopropylidene-6-O-tosyl-D-glucofuranose, V=1,2-O-isopropylidene-3,5-benzylidene-6-O-tosyl-D-glucofuranose, VI=1,2-O-isopropyl-idene-3,5-benzylidene-6-fluoro-D-glucofuranose, VII=6-deoxy-6-fluoro-Glucose).

26-13

B. Synthesis of 1,2-O-isopropylidene-D-glucofuranose

The procedure used was essentially that of Meyer and Reichstein (1946). 1,2:5,6-di-O-isopropylidene-D-glucofuranose (80 g) was dissolved in methanol (400 ml), water (336 ml) and 1 N H_2SO_4 4 (64 ml). The solution was allowed to stir at 20°C for approximately 16 hrs. or until the optical rotation had become constant, as shown in Figure 11. The pH of the

Formation of 1,2-O-isopropylidene-D-glucofuranose
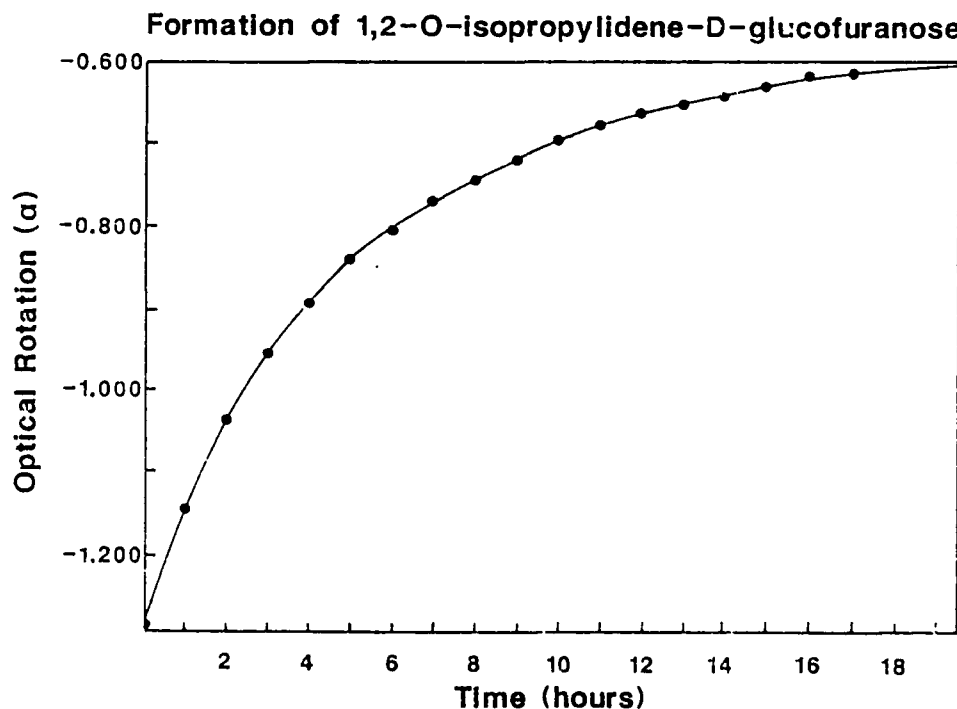
Figure 11. The formation of 1,2-O-isopropylidene-D-glucofuranose versus time, as monitored by optical rotation.

solution was adjusted from 1.7 to 6.9 with $BaCo_3$, and filtered with the aid of Celite 545. The filtrate was evaporated to drynes under vacuum, at 45-50°C. The product was recrystallized from water giving 21.5 grams, 31.8% of theo-

ry, (Figure 10. III), m.p. 158-159°C (reported 160-162°C).

C. Synthesis of 1,2-O-isopropylidene-6-O-tosyl-glucofuranose

The procedure used was essentially that of Ohle and Dick-
hauser (1925) as modified by Meyer and Reichstein (1946) and
Blakley (1954). For this synthesis, p-Toluene sulfonyl
chloride was purified to eliminate tosic acid, by the method
of Pelletier (1953).

50.0 g of dry 1,2-O-isopropylidiene-D-glucofuranose was
dissolved in pyridine (150 ml) with slight warming. The
mixture was cooled to 15°C and a solution of tosyl chloride
(30 g) in chloroform (200 ml) was slowly added under anhy-
drous conditions to maintain the temperature between 15-
20°C. This mixture was allowed to stir for 16 1/2 hrs. at
about 20°C. The mixture was concentrated to about 150 ml by
removing the chloroform, in vacuo at 43°C. The resulting
solution was slowly mixed with 3 M HCl (550 ml) and extract-
ed 10X with a total of 2 L diethyl ether. The ether layer
was washed with 3 M HCl (150 ml), saturated Na_2CO_3 (200 ml)
and water (200 ml). The ether extracts were dried over
Na_2SO_4 and the evaporated under vacuum to a viscous residue
(approx. 50 ml). The residue was dissolved in hot ether
(100 ml) and crystallized by adding minimal amounts of dry
pet. ether (b.p. 44-60°C). The white crystals were collect-
ed by vacuum filtration. The yield was 42 % (30.23 g), m.p.

98-100°C, reported 101-102°C, (Figure 10. IV).

D.   Synthesis of 1,2-O-isopropylidene-3,5-benzylidene-6-O-
tosyl-D-glucofuranose

The method used was that of Blakley (1954), using unfused
$ZnCl_2$ as the condensation agent.   30 grams of dry 1,2-O-
isopropylidene-6-tosyl-D-glucofuranose was mixed with 21.8 g
of anhydrous $ZnCl_2$ and   42.3 ml of freshly distilled ben-
zaldehyde.   This mixture was stirred for 4 hrs. at room
temperature.   The mixture had become a very thick, viscous
amber colored liquid, with some undissolved $ZnCl_2$.   The
product was isolated by extraction with benzene (3 x 100 ml)
and washing the benzene solution with water (4 x 30 ml) to
remove any traces of zinc ion.   The water extracts were
added to the residue remaining after the benzene extraction.
This aqueous solution was extracted with benzene (3 x 50 ml)
and the benzene extract was washed with water until free of
zinc ion.   The benzene extracts were combined and mixed with
an equal volume of water and evaporated to dryness under
vacuum at 60°C.   Water was added and removed as above (9 X)
until no odor of benzaldehyde could be detected.   The crys-
talline residue was recrystallized twice from abs. ethanol
giving 15.8 g (42.6%) of white crystalline product, m.p.
119-120°C, reported 120-121°C, (Figure 10. V).

E.   Synthesis of 1,2-O-isopropylidene-3,5-O-benzylidene-6-Fluoro-6-deoxy-D-glucofuranose

The method used was that of Helferich and Gnuchtel (1941) as modified by Blakley (1954).   Purified 1,2-O-isopropylidene-3,5-O-benzylidene-6-tosyl-D-glucofuranose (5 g) was suspended in abs. methanol (40 ml) and to this mixture was added KF $2H_2O$ (4 g).   This mixture was heated in a combustion tube by steam, for 16 hrs.   As the mixture was heated, the reactants went into solution, which upon cooling yielded crystals of potassium tosylate.   The potassium tosylate was filtered off and washed with minimal amounts of methanol and ether.   The potassium tosylate recovered was 0.75 g (33% theory).   The methanol/ether solution was evaporated to dryness via a stream of dry air.   The resulting "crystals" were washed with water (200 ml).   The crude product was recrystallized several times from abs. methanol.   The isolated product was observed to melt over a range of 104-119°C.   The melting points of the starting material and the expected product are 120-121°C and 104-105°C, respectively.   In view of this and the low yield, it was apparent that the reaction had not gone to completion.   To check this possibility, ^{1}H and ^{19}F NMR spectra were obtained for the reaction mixture which indicated that the reaction mixture contained both 1,2-O-isopropylidene-3,5-O-benzylidene-6-tosyl-D-glucofuranose and the corresponding fluorinated derivative.   The apparent

cause for this is that at the altitude of FJSRL, a steam bath is not at 100°C but rather 94°C, which is apparently critical for driving the reaction in the alloted time. In an effort to complete the reaction and recover the product, the reaction mixture from above was reacted as before, in an oven at 100°C. Upon cooling, no crystals of potassium tosylate were observed, but a small amount of residue was obtained upon evaporation of the solvent. This residue was recrystallized several times from abs. methanol and the isolated product was observed to melt over a range of 69 - 85°C, indicating that the reactants had degraded to a mixture of other compounds. Attempts to salvage the reaction mixture were unsuccessful and the synthesis was terminated at this point.

IV. RECOMMENDATIONS:

A.   In order to further refine the three transition states that had more than one vibrational mode with a negative frequency, it would be necessary to redo the saddle calculation near the transition point. Before the transition point is reached, I would decrease the rate at which the distance between the two geometries is reduced. This is accomplished by the keyword BAR. By reducing the rate of reduction between the two geometries, one could slowly work up to the transition state, monitoring the calculation and making compensations as needed. Once a more refined transition

state geometry is reached, NLLSQ and FORCE calculations can be performed as previously indicated.

B. The general synthetic scheme for 6-deoxy-6-fluoro- -D-glucose seemed to proceed very well, except for the displacement of the tosyl protecting group. In an effort to correct problems encountered during this step, I would simply use a pressure bomb in a oven, regulated to 100°C. A Parr acid digestion bomb with a Teflon insert would be suitable for this.

C. Finally, to obtain 6-deoxy-6-fluoro-1,5-gluconolactone, I feel that the easiest route is enzymatically. I had planned, and would recommend the use of glucose dehydrogenase to stereospecifically convert the 6-deoxy-6-fluoro- -D-glucose, synthsized as outlined, to the corresponding lactone. This is a single step reaction that can be monitored via the formation of NADH at 340 nm, is complete in less than a minute and the product is easily isolated from the enzyme and coenzyme.

REFERENCES

Blakley, E.R., The Synthesis of 6-deoxy-6-fluoro-D-Glucose and a study of its metabolic effects. PhD thesis, University of Minnesota, 1954.

Brodie, A.F. and Lipmann, F. J. Biol. Chem., 1955 Vol.212, pp. 677-685.

Glen, W.L., Meyers, G.S. and Grant, G.A., Monoalkyl Hexoses: Improved Procedures for the Preparation of 1- and 3-Methyl Ethers of Fructose, and of 3-Alkyl Ethers of Glucose. J. Chem. Soc., 1951, pp. 2568-2572.

Helferich, B. and Gnuchtel, A., Glucose-6-Fluorohydrin and some of its derivatives. Ber. 1941, Vol. 74, pp.1035-1039.

Meyer, A.S. and Reichstein, T., 1-Idomethylose. Helv. Chim. Acta. 1946, Vol. 29, pp.139-153.

Ohle, H. and Dickhauser, E., On the joining of acetone to sugar and its derivatives: Other acyl-derivatives of mono-acetone glucose. Ber. 1925, Vol. 61, pp. 2593-2606.

Pelletier, S.W., p-Toluenesulfonyl chloride (Tosyl chloride) purification. Chem. Ind. 1953, p. 1034.

Stewart, J.J.P., MOPAC: A Semiempirical Molecular Orbital Package. Quantum Chemistry Program Exchange No. 455, 1983, Latest update version 5.00.

1989 USAF-UES SUMMER FACULTY RESEARCH PROGRAM/

GRADUATE STUDENT RESEARCH PROGRAM

Sponsored by the

AIR FORCE OFFICE OF SCIENTIFIC RESEARCH

Conducted by the

Universal Energy Systems, Inc.

FINAL REPORT

SECOND HARMONIC GENERATION IN OPTICAL FIBERS

Prepared by: Lloyd W. Hillman, Ph.D.

Academic Rank: Assistant Professor

Department and   Department of Physics

  University   University of Alabama in Huntsville

And by: Stephen McClain, Graduate Student

                    Mojdeh Anderson, Graduate Student

Department and   School of Electrical Engineering

  University   Cornell University

Research Location: Frank J. Seiler Research Laboratory

                    USAF Academy, CO   80840

USAF Researcher: Maj Jim Rotgé

Date: 15 Oct. 89

Contract No: F49620-88-C-0053

Same Report As
Prof. Lloyd Hillman
(Report # 47)

.   .

.

1989 USAF–UES SUMMER FACULTY RESEARCH PROGRAM

GRADUATE STUDENT RESEARCH PROGRAM

Sponsored by the

AIR FORCE OFFICE OF SCIENTIFIC RESEARCH

Conducted by the

Universal Energy Systems, Inc.

<u>FINAL REPORT</u>

<u>MODELING OF A STRUCTURE–ACTUATOR SYSTEM WITH STRUCTURE–BORNE REACTION–MASS ACTUATORS AND OPTIMAL DESIGN OF PASSIVE VIBRATION ABSORBERS</u>

Prepared by:	Hung V. Vu, PhD, Assistant Professor
	<u>Hao Q. Pham</u>, Graduate Student
Department and	Mechanical Engineering
University:	California State University, Long Beach CA 90840
Research Location:	Frank J. Seiler Research Laboratory
	United States Air Force Academy CO 80840–6528
USAF Researchers:	Major John P. Duke
	Dr William L. Hallauer, Jr.
	Captain Jeff Turcotte
	Captain Steven G. Webb
Date:	15 August 1989
Contract No.:	F49620–88–C–0053

Same Report As
Prof. Hung Vu
(Report # 52)

1989 USAF-UES SUMMER FACULTY RESEARCH PROGRAM

GRADUATE STUDENT RESEARCH PROGRAM

Sponsored by the

AIR FORCE OFFICE OF SCIENTIFIC RESEARCH

Conducted by the

Universal Energy Systems, Inc.

FINAL REPORT

Adaptation of the Axisymmetric TASS Model for Hurricane Simulations

Prepared by: Pat Fitzpatrick

Academic Rank: Graduate Student

Department and   Meteorology Department

  University: Texas A&M University

Research Location: Geophysics Laboratory

                      Hanscom AFB

                      Boston, MA 01731

USAF Researcher: Dr. Phanindramohan Das

Adaptation of the Axisymmetric TASS Model for Hurricane Simulations

by

Pat Fitzpatrick

ABSTRACT

In the numerical modelling of tropical cyclones, one may utilize a three dimensional version for real case studies, or utilize an axisymmetric version to study the physical and dynamical processes, despite their lack of realism. Usually the latter is chosen for computational purposes. Furthermore, the nonhydrostatic models with ice microphysics currently represent the hurricane's interactions best. The goal of the study was to develop a scheme that would incorporate a nonhydrostatic domain near the center of the tropical cyclone, and superimpose it on a larger scale, hydrostatic domain that includes the outer fringes of the storm. The Terminal Area Systems Simulator (TASS) model, a nonhydrostatic, compressible computer program complete with ice microphysics, was chosen for the study, since it simulates winds and physical processes of cumulus convection reasonably well.

Most of the research was focused on altering TASS so that it could simulate a hurricane eyewall. The main features that needed changing were some microphysical parameters, the boundary layer fluxes from the sea, and the initialization procedure for the genesis of the tropical cyclone. The fluxes were computed using aerodynamic bulk formulas, and the formation mechanisms included installation of a region of low-level vorticity, sea temperature, a convectively unstable lapse rate, and a moist mid-layer. Furthermore, the model's scaling assumptions needed altering, and this aspect of the research is still taking place. The implications of the research are that hydrostatic and nonhydrostatic interactions can be investigated, and that the development of this type of model may reduce the high computation time currently required for these models.

ACKNOWLEDGEMENTS

I wish to thank the Air Force Systems Command, Air Force Office of Scientific Research, and Universal Energy Systems for sponsoring the Graduate Student Research Program, and for allowing me to participate as a Summer Fellow. Furthermore, my appreciation goes out to the Geophysics Laboratory at Hanscom AFB for providing me with a comfortable and efficient research environment.

This summer was made quite enriching, both educationally and spiritually, due to many people. Artie Jackson and Stu Meunsch provided good advice on computers and forecasting. Tom Kleespies helped me learn the VAX system in the meteorology branch, along with a painful lesson on machine language. Tim Roache was a good friend every step of the way, and not a bad fisherman either. Bob Neal and Rick O'Donald were very kind, and provided many warm and happy memories. Don Chislolm and Don Norquist offered support and understanding for the peculiarities of numerical modelling. Finally, I offer my deepest gratitude to Phanindramohan Das for bringing this program to my attention, and for being so helpful in every aspect of my research.

I. INTRODUCTION:

In the numerical modelling of the development of tropical cyclones, two
approaches are taken. In one approach the goal is to predict the
behavior of real hurricanes so that a three-dimensional model is needed.
In the other, the aim is to study the role of the various dynamical and
physical processes. Since the computational effort required to model
tropical cyclones with two dimensional models is more than an order less
than that required for three dimensional models, high-resolution
axisymmetric models with elaborate representation of such processes are
found to be convenient, in spite of their lack of realism.

In the area of axisymmetric models, again, two different approaches are
used. In the first, the hydrostatic dynamics is assumed and
nonhydrostatic (convective) processes are parameterized or implied.
Yamasaki (1977) and Rosenthal (1978) first utilized this approach, in
which cloud-scale motions are explicitly calculated, and the closure
involves in-cloud turbulence and cloud physics. So, latent heat release
and convection are now calculated on the resolvable scales. The model
results demonstrate the formation of squall lines in the early stage,
and the formation of a tropical cyclone in the later stages. The
following sequence occurs on the order of 4 to 6 days:

(a) Initially, features which resemble squall lines develop. These
     convective systems produce evaporation and unsaturated downdrafts.
(b) The squall lines do not directly intensify the vortex, but their
     cumulative effect is to alter the relative humidity and

temperature structure of the system. The convection starts moving inward.

(c)   As the middle layers become more moist, nonpropagating clouds form near the center (the eye wall). Subsidence occurs in the center (the eye). 'Rows' of clouds form outside the eye wall (cloud or spiral bands).

(d)   Once the eye has formed, intensification proceeds rapidly.

In the second, and currently rather popular, approach, the field of the cyclone is treated as nonhydrostatic and compressible. Thus, this approach is somewhat more realistic in a hurricane than the previous method, especially near the eyewall. The sequence of development of the storm is similar to the outline previously mentioned. One of the pioneers of the nonhydrostatic method, Hugh Willoughby of the Hurricane Research Division in Miami, recently included ice-phase microphysics along with the standard water-phase relationships involving rain and water vapor. This ice microphysics, which includes ice, snow, and graupel was neglected in previous studies (Willoughby, 1984).

When these are included in the model, many more convective rings (spiral bands) develop than with just the water phase. The speculated reasons are that there is greater convective instability and more active, stronger moist downdrafts. Furthermore, the simulated vortex grows slower and the downdrafts appear horizontally coherent, as they often originate at the melting level. Low-level convergence due to horizontal spreading of downdraft air appears to be a significant forcing mechanism for the convective rings outside the eyewall.

This nonhydrostatic approach offers many dynamical and physical research possibilities. However, models based on this approach require much computer time because of the water/ice-microphysics calculations. Furthermore, the horizontal grid increments must be small enough to resolve the features of the eye and eyewall (which averages 5 to 20 km), yet must include the large spatial domain of the storm (1500 km). Even with a stretched grid, the computation time is enormous. Finally, since the model is incompressible, acoustic waves can be generated and totally distort the model output unless a reasonably small time step is chosen. As can be seen, the computational time is a great obstacle in hurricane modelling research.

My research interests are in mesoscale and synoptic meteorology, and the numerical modelling of the atmosphere on these scales. More specifically, tropical phenomena, such as tropical cyclones, intrigue me. Several synoptic and numerical methods courses, as well as a tropical meteorology class, contributed to my acceptance to the Graduate Student Research Program.

II. OBJECTIVES OF THE RESEARCH EFFORT:

As previously mentioned, the tropical cyclone as a whole can be treated as a hydrostatic system, since vertical accelerations and the Coriolis Force are usually three to four times order of magnitude less than the vertical pressure gradient. However, some nonhydrostatic interplay is involved, since all vertical motions in the hurricane, regardless of scale, are produced by imbalances among the forces, in particular around

the eyewall. No model thus far tries to incorporate both of these concepts.

My assignment as a participant in the 1989 Graduate Student Research Program (GSRP) is to develop a scheme that would incorporate a nonhydrostatic domain within a larger-scale hydrostatic model. It was determined that the Terminal Area Simulation System (TASS) mesoscale model, a nonhydrostatic program complete with ice microphysics, would be used for the study. TASS is formulated for the general purpose of studying the physical-dynamical character of convective clouds and storms (Proctor, 1988). It is capable of realistic simulations of convective clouds ranging from nonprecipitating cumulus to intense, long-lasting supercell hailstorms that produce tornadoes and microbursts . (Trapp, 1989). This model would be altered so that it simulated the eyewall--the core of the storm. Thus, most of the research effort was focused on methods to rewrite the code for this purpose.

Once some preliminary changes were incorporated into the model, initial runs were attempted to simulate the eyewall of the storm the final few weeks. However, sound waves were generated. Research into this problem, as well as a full tropical cyclone model that is nonhydrostatic around the eyewall region and hydrostatic away from the center, will continue at the University of Texas A&M. While such a model has its obvious appeal of convenience, because it can potentially reduce the computational time, it also is likely to provide a glimpse into the interplay of hydrostatic and nonhydrostatic processes in the spin-up of a tropical cyclone.

III.

a.   The first task at hand was choosing a nonhydrostatic, mesoscale
model with ice physics, and TASS met these conditions. In addition,
this axisymmetric model has some other nice features. The primitive
equations are divided into two parts. Since the model assumes the
atmosphere is compressible, it generates acoustic waves, which requires
very small time steps to solve or the model becomes unstable. A routine
developed by Klemp and Wilhelmson works around this problem by dividing
the equations into acoustic and advective, or nonacoustic, parts and
integrating separately. In other words, a short time step is used for
the acoustically active terms, while a larger and more efficient time
step is used for the remaining terms (Klemp and Wilhelmson, 1978).

The equations of motion are standard, except that there are six coupled
equations for continuity of water substance (vapor, nonprecipitating
cloud droplets and ice crystals, rain, snow, and hail). The variables
are placed on a staggered grid, and time integration is done using the
Adams-Bashforth method. The model also includes a conventional first-
order closure for subgrid turbulence; a diagnostic surface boundary
layer based on Monin-Obukhov similarity theory; and open lateral
boundary conditions. The lateral boundaries use a radiation boundary
scheme modified Orlanski scheme, except that these equations also are
solved using Adams-Bashforth (Orlanski, 1976).

Microphysical interactions are parameterized assuming integrated
exponential distributions. For example, these include the evaporation

of rain, the melting of snow and hail, the accretion of rain by snow and hail, etc. The terminal velocity for rain and hail are computed locally as mean-weighted values.

A simulation was run by reading in a sounding from a region where a severe storm with a microburst was known to have occurred previously, then initiating a downburst centered along the models vertical axis by prescribing a distribution of precipitation at the top boundary in a manner similar as Eskridge and Das (1976). As precipitation and hail falls into the domain, the mass and density of the air are effectively increased. A negative buoyancy force results from the mass loading, which is further enhanced by microphysical cooling. Then, the downburst was initiated by imposing precipitation and rotation as well, in a manner similar to Trapp. Ultimately, this led to a comparatively stronger downdraft and outflow speeds. Overall, the vertical, tangential, and radial winds, as well as the physical aspects of the storm were reasonably simulated.

b. Once the model was chosen, and the internal structure of the program was understood, attempts were made to change the model from a thunderstorm simulation to an eyewall simulation. The main features that needed alteration were some microphysical parameters, the boundary layer fluxes/sea interactions, and the initialization procedure of the tropical cyclone.

The microphysical processes are parameterized with a bulk method as mentioned previously. Diameters of precipitating particles are assumed

to be distributed exponentially with constant intercept parameters. These values were the same as before, except that the density of hail was changed to 300 kg/m**3, and the intercept parameter for rain is changed to 2.2E7/m**4. According to Willoughby, these values represent hurricane conditions better, but nevertheless are arbitrary.

Of more immediate concern is the air-sea interaction. TASS assumes no heat or moisture flux from the ground unless a millimeter of rain falls. However, these fluxes are the primary reason hurricanes can form and perpetuate themselves under proper conditions. Thus, TASS, which was formulated for storms that occur over the continents, must be coded so that it can simulate oceanic transfers. The normal procedure to represent these fluxes is to use bulk aerodynamic formulas, where some sort of empirical exchange coefficient, and reference temperatures and mixing ratios for the sea and the air immediately above the ocean are used (Anthes, 1982). Furthermore, TASS assumes a constant roughness length of 0.1 m. However, the roughness length over the ocean (the waves) is a function of wind speed. Thus, Charnock's relation is used instead so that the roughness length is an array.

Finally, one must somehow cause a tropical cyclone to form in the first place. However, the transformation of a disturbance to a cyclone has yet to be realistically modelled. Usually, all tropical cyclones are initialized by a Rankine vortex, in which tangential winds increase linearly out to a certain critical radius (constant vorticity), then the tangential winds decrease exponentially past that radius (angular momentum is conserved, or zero vorticity). Unfortunately, this never

deals with how the vortex was formed in the first place. Nevertheless, we shall follow this conventional procedure. It has been found that all tropical cyclones form in a region of low-level cyclonic vorticity (such as in regions where the ITCZ has been displaced poleward from the equator, like over Africa and Central America), and the Rankine vortex roughly approximates this. Thus, for the eyewall simulation, we impose solid rotation that linearly increases from the eye to a maximum of 8 m/s at r - 75 km for the initialization.

Other climatological genesis parameters must also be included. For instance, disturbances rarely form within 5 degrees of the equator, which implies that the Coriolis Force is important in the spin-up of these systems. Thus, the latitude variable in the program is set at 12 degrees. One of the remarkable relationships is the existence of a threshold sea-surface temperature below which tropical cyclones do not form (26.5 degrees C). Why this happens is not immediately clear, but perhaps the exponential variation of saturation vapor pressure with temperature is part of the reason. So, we set the sea temperature 28 degrees C in the bulk formula to meet this requirement. Finally, the middle tropospheric relative humidity must be high, and the temperature profile must be convectively unstable (Gray, 1978). To meet these requirements, we use Jordan's (1958) mean tropical sounding during the 'hurricane months' of July - September, which has a moist mid-layer and the proper lapse rate.

One of the main drawbacks of these procedures was that to meet these requirements, the staggered grid had to be shifted upwards one-half a

grid increment. Furthermore, since the model was written for a thunderstorm, it assumed the vertical and horizontal grid sizes to be equal, and the equation were simplified. Thus, much of the equations needed to be rewritten, since the horizontal scale of a hurricane is much larger than its vertical scale. This postponed the model runs, because during the revision process the dreaded acoustic waves appeared in the output. So, the model's code still needs work. Nevertheless, the theory for the transition of the TASS model from a mesoscale thunderstorm to a hurricane eyewall appears sound.

IV. RECOMMENDATIONS

a.   The axisymmetric TASS model appears to represent the thermodynamic and dynamic aspects fairly well. In addition, a three dimensional version also exists. An interested party may consider simulating a tropical cyclone's wind structure and genesis parameters more closely and realistically, or perhaps even investigate steering currents if a moving grid is superimposed. This will undoubtedly require a Cray supercomputer, however.

b.   The ideas for modification of the TASS model to a hurricane eyewall appears sound. However, a few 'bugs' in the code needs attention. Once this is achieved, we wish to incorporate this nonhydrostatic eyewall into a larger hydrostatic domain of the entire storm. Therefore, we can investigate the interactions of forces that cause vertical motion between the two.

c.   This research can potentially reduce the high computational time needed to model these tropical systems. Just as the primitive equations

can be solved using a time-splitting scheme, one can develop a 'space-splitting scheme,' in which the nonhydrostatic structure is solved for several iterations using fine resolution and relatively small time steps. Then, using a coarser grid outside the eyewall, the hydrostatic features are solved using a longer time step.

Furthermore, different types of primitive equations can be used for comparison, or for 'space-splitting.' In particular, a set of governing equations based on non-Archimedian theory may be substituted. The advantage of this method is that density perturbations are implied in the horizontal equation of motion, and also there is no need for a specific reference density, as needed in the conventional formulation (Das, 1979).

REFERENCES

Anthes, R. A., Tropical Cyclones: Their Evolution, Structure, and Effects. *Meteror. Monographs, Vol. 19* 1982, American Meteor. Soc., Boston, (ISBN 0-022876-54-8) 208 pp.

Das, P., A Non-Archimedian Approach to the Equations of Convective Dynamics. *J. Atmos. Sci*. 1797, Vol. 36, pp. 2183-2190.

Eskridge, R. E., and P. Das, Effect of a Precipitation-driven downdraft on a Rotating Wind Field: A Possible Trigger Mechanism for Tornadoes? *J. Atmos. Sci*. 1976, Vol. 33, pp. 70-84.

Gray, W. M., Hurricanes: Their Formation, Structure, and Likely Role in the Tropical Circulation. *Meteorology Over the Tropical Oceans*. 1979, D. B. Shaw, Ed., Roy. Meteor. Soc., pp. 155-218.

Jordan, C. L., Mean Soundings for the West Indies Area. *J. Atmos. Sci*. 1958, Vol. 15, pp. 91-97.

Klemp, J. B., and R. B. Wilhelmson, The Simulation of Three-dimensional Convective Storm Dynamics. *J. Atmos. Sci*. 1978, Vol. 35, pp. 1070-1096.

Orlanski, I., A Simple Boundary Condition for Unbounded Hyperbolic Flows. *J. Computat. Phys*. 1976, Vol. 21, pp. 251-269.

Orville, H. D. and F. J. Kopp, Numerical Simulation of the History of a Hailstorm. J. Atmos. Sci. 1977, Vol. 34, pp. 1596-1618.

Proctor, F. H., The Terminal Area Simulation System. Volume I: Theoretical Formulation. NASA Contractor Rep. 4046 1987, NASA, Washington, D.C., 176 pp.

Rosenthal, S. L., Numerical Simulation of Tropical Cyclone Development with Latent Heat by the REsolvable Scales I: Model Description and Preliminary Results. J. Atmos. Sci. 1978, Vol. 35, pp. 258-271.

Trapp, J. R., The Effects of Cloud Base Rotation on Microburst Dynamics - A Numerical Investigation. Thesis, 1989, Texas A&M University, 122 pp.

Willoughby, H. E., H.-L. Jin, S. J. Lord and J. M. Piotrowicz, Hurricane Structure and Evolution as Simulated by an Axisymmetric, Nonhydrostatic Numerical Model. J. Atmos. Sci. 1984, Vol. 41, pp. 1169-1186.

Yamasaki, M., A Preliminary Experiment of the Tropical Cyclone Without Parameterizing the Effects of Cumulus Convection. J. Meteor. Soc. Japan 1977, Vol. 55, pp. 11-31.

1989 USAF-UES SUMMER FACULTY RESEARCH PROGRAM
GRADUATE STUDENT RESEARCH PROGRAM

Sponsored by the
AIR FORCE OFFICE OF SCIENTIFIC RESEARCH
Conducted by the
Universal Energy Systems, Inc.

FINAL REPORT

Estimating Characteristics of Chemical Explosions in New England and
Eastern Kazakhstan Using Local and Regional Seismic Data

Prepared by:	Alan L. Kafka, Ph.D. ; Matthew Jacobson-Carroll
Academic Rank:	Associate Professor ; Graduate Student
Department and	Geology and Geophysics
University	Boston College
Research Location:	GL/LWH
	Hanscom AFB
	Bedford, MA 01731
USAF Researcher:	Dr. John Cipar
Date:	30 September 1989
Contract No:	F49620-88-C-0053

Same Report As
Prof. Alan Kafka
(Report # 56)

1988 USAF-UES SUMMER FACULTY RESEARCH PROGRAM/

GRADUATE STUDENT RESEARCH PROGRAM

Sponsored by the

AIR FORCE OFFICE OF SCIENTIFIC RESEARCH

Conducted by the

Universal Energy Systems, Inc.

FINAL REPORT

FINAL SUMMARY OF RESEARCH EFFORT

Prepared by: Thomas E. Kimble

Academic Rank: Graduate Student

Department and University: Center for Space Sciences

                                University of Texas at Dallas

Research Location: AFGL/Hanscom AFB, Space Physics, PHP

USAF Researcher: Dr. Susan Gussenhoven

Date: January 27, 1989

Contract No: F49620-88-C-0053

FINAL SUMMARY OF RESEARCH EFFORT

Structure in plasma density may be produced locally by particle precipitation or non-locally by ion transport effects. To explore these complex relationships at high latitudes, it was essential to separate polar cap and auroral regions in the ion drift and concentration data by using observations from the DMSP SSJ 4 particle detector. Three different types of data (ion density, drift, and precipitating electron fluxes) were collected in order to describe the effects of particle precipitation and ion transport on the same spatial scales. Several sets of data were examined both visually and quantitatively to determine the dependence of plasma structure on IMF, magnetic activity, hemisphere, and position along the satellite track. The relationships still remain unclear.

In addition, it seemed to be quite useful to reconcile observations with theoretical predictions of what to expect. In particular, theoretical calculations were performed to determine ionization rates and the time required for ions to be transported along field lines. Most of these calculations were based on a code developed at AFGL that solves an equation for electron transport under the assumption that no role is played by electron or ion temperatures. This lack of temperature dependence proved to be a serious limitation. Inasmuch as temperature changes enter into the problem both linearly in the computation of neutral densities and non-linearly, in solving the electron transport equation, theoretical calculations were not tractable during the short time spent in the Summer Research Program, and it was preferable to continue this research at UTD.

An understanding of these phenomena is important to my research at UTD on mid and high latitude plasma structure. By comparing observations from both the DMSP and DE-2 satellites it was thought possible to describe, as fully as possible, the spectral characteristics of number density with scales sizes both greater than and less than 80 km and at altitudes above and below 800 km at the

auroral zone. Although the project as originally conceived did not reach a publishable stage, it seems fruitful to continue to explore these relationships using the DE-2 data available at UTD.

1989 USAF-UES SUMMER FACULTY RESEARCH PROGRAM

GRADUATE STUDENT RESEARCH PROGRAM

Sponsored by the

AIR FORCE OFFICE OF SCIENTIFIC RESEARCH

Conducted by the

Universal Energy Systems, Inc.

Comparative Analysis of Various Atmospheric Modelling Techniques

<u>FINAL REPORT</u>

Prepared by:	David C. Sanborn, M.S.,M.S.E.E
Academic Rank:	Graduate Student
Department:	Electrical Engineering
University:	University of Lowell
Research Location:	Geophysics Laboratory (AFSC) GL/LY Hanscom Field Bedford, Mass. 01731
USAF Researcher:	Kenneth Champion, Ph.D
Date:	18 September 1989
Contract No:	F49620-88-0053

Comparative Analysis of Various Atmospheric

Modelling Techniques

by

David C. Sanborn

ABSTRACT

A comparative analysis of various atmospheric models
developed by international and national bodies such as
the International Council of Scientific Unions (ICSU),
Committee on Space Research (COSPAR), the Geophysics
Laboratory (GL) of the United States Air Force Systems
Command, and the Middle Atmospheric Program (MAP) was done
over the summer of 1989. Existing models of the atmosphere
from various sources specify properties from data sets
obtained from different platforms (rockets, satellites, and
balloons). There are also variabilities such as those
due to latitude, longitude, and time of day/year to be
considered.

ACKNOWLEDGMENTS

I wish to thank the Air Force Systems Command and
the Air Force Office of Scientific Research for sponsor-
ship of this research. Universal Energy Systems is to
be commended for administrativesupport and guidance
during the program. My experience at the Geophysics
Laboratory (GL) was rewarding and enriching. Especially
important was the support, encouragement, and congenial
working atmosphere provided by Dr. Kenneth Champion,
Senior Scientist, Atmospheric Sciences Division. The
magnificent GL research library and staff was invaluable
in providing technical resources for my work. Also,
many people, too numerous to mention, provided inform-
ation on sources for my work as well as opportunities for
working for the USAF as a civilian scientist.

I. INTRODUCTION:

My research interests are in the areas of geophysics concerning the application of physics to problems involving the lower and middle atmosphere (0-100 km). My academic background at the University of Lowell consists of an M.S. degree in radiological sciences (with several meteorological courses, as well as graduate level physics courses), an M.S. degree in electrical engineering, specializing in electromagnetic theory, wave propogation, space physics, and ionospheric physics. My interests in the Summer Graduate Student Research Program co-incided with much of what the Geophysics Laboratory, Atmospheric Sciences Division is working on. The Atmospheric Sciences Division is concerned with all aspects of the physics and meteorology of the lower and middle atmosphere which affect worldwide USAF operations. My work here closely co-incided with that of the Atmospheric Sciences Division which is continously refining and improving the modelling of the atmosphere.

II. OBJECTIVES OF THE RESEARCH EFFORT

The objective of this research was to evaluate present models of the lower and middle atmosphere (0-100 km). A comparative analysis of eight different properties of these models was tabulated and reviewed during the summer spent at the Geophysics Laboratory.

III. APPROACH

The task was to extensively review existing models dating from 1976-1988. The models reviewed were the following:

a.) Air Force Reference Atmospheres, 1978

b.) Middle Atmosphere Temperature Reference Model From Satellite Measurements, Adv. Sp. Res.,1985

c.) Middle Atmosphere Reference Model Derived From Satellite Data, MAP HBK. 16, 1985

d.) Global Reference Atmosphere From 18-80 km,AFGL, 1985

e.) Monthly Mean Global Climatology of Temperature, Wind, Geopotential Height, and Pressure For 0-125 km,1988

f.) NASA/MSFC Global Reference Atmosphere (GRAM-88), 1988

Tables compiled for each of the above sources had eight categories: temperature, density, pressure, height profiles, data sources, modelling, wind and comments.

IV.   a.)   BASIC PHYSICS OF THE ATMOSPHERE

The atmosphere consists primarily of O_2 and N_2 with various minor constituents. Just identifying the major and minor components is not sufficient. The real atmosphere is not a static medium. This medium is governed by changes in temperature, pressure, density, chemistry and solar radiation. Its behavior is largely governed by dynamic processes. These processes include advection, convection, and dispersive diffusion. In dealing with atmospheric data one must allow for measured quantities to undergo sizeable random fluctuations, and periodic variations such as diurnal or seasonal changes. Over a period of 30 years empirical atmospheric modelling based on dry air, perfect gas, and hydrostatic equilibrium has been refined by gathering data from local to global scales. However, processes such as convection, radiation transport, circulation and fluid dynamics have not been included. Standard nomenclature has been adopted by international convention to distinguish different altitude regimes. The troposphere is the region nearest to the Earth (to about 11 kilometers) where temperature decreases with height (lapse rate is typically $-6.5°K/km$). The tropopause is not fixed but adjusts to meteorological conditions within an altitude range of 10 to 20 km. The next region is the stratosphere where the temperature rises to reach a peak at the stratopause (about 50 km). Above this is the mesosphere where temperature declines to a minimum of about $180°K$ at

the mesopause (80-90 km). The highest part of the at-
mosphere is the thermosphere which has no well defined
upper boundary. In the thermosphere the temperature
increases to about 500°K to 2000°K above 300 kilometers,
but this varies widely with solar activity. My project
is concerned with heights up to 100 kilometers.

Because the global energy budget of the atmosphere
is balanced by outgoing infrared radiation two processes
are important for the vertical transfer of heat. These
processes are absorption and re-emission of thermal rad-
iation and dynamical atmospheric processes. Optically
active atmospheric components include H_2O, CO_2, and O_3.
N_2 and O_2 are inactive because they cannot emit dipole
radiation, so they do not participate in the thermal bud-
get. Vertical atmospheric transport occurs at all alti-
tudes and is very large above 100 km during geomagnetic
storms. At pressures and temperatures prevailing in the
lower and middle atmosphere the ideal gas law approxim-
ation is good. Dynamical processes are important at all
altitudes.

Atmospheric motions are laminar, turbulent, and
wavelike. Turbulence results because of shear stresses.
Small vortices or eddies occur which carry heat, momen-
tum, atmospheric gas, and trace materials in all direct-
ions. Turbulent mixing is based on Fickian diffusion
where the flux is derived from the gradient of a mixing
ratio. Molecular diffusion, which occurs with laminar

flow, is determined by the mean free path between collisions of molecules, which is inversely proportional to pressure. About 100 kilometers and above this is the dominant process. On the global scale one can consider material transport across a number of reservoirs. The slow rate of transport at the Interhemispheric Tropical Convergence Zone (ITCZ) naturally subdivides the troposphere into Northern and Southern hemispheric components. One can consider the stratosphere and troposphere as separate reservoirs with the tropopause serving as a common boundary. Vertical and horizontal mixing in the troposphere is faster than the transport of air across the ITCZ. The stratosphere is not an ideal reservoir because it is not well defined. The rate of exchange between the stratosphere and troposphere will reflect the degree of transport through the tropOpause. General atmospheric circulation theory indicates that tropospheric air passes into the stratosphere over equatorial regions where it moves northward and sinks back into the troposphere at higher latitudes. In a General Circulation Model (GCM) the air mass exchange involves a four box model of the atmosphere where common boundaries are the tropopause and the ITCZ. The rate of air exchange between individual reservoirs is expressed in terms of exchange coefficients and air mass content of the donor reservoir.

b.)   DATA COLLECTION

Various methods of measurement are used to obtain
·the data for the models examined. These include meteor-
ological sounding balloons (radiosondes) for 0-30 km ,
Meteorological Rocket Network (MRN) rockets and rockets
equipped with pressure gauges, falling spheres, and
grenades for altitudes of 25-90 kilometers. True global
coverage was accomplished by satellites using specialized
radiometers (SCR,PMR,SAMS, and LIMS). The techniques of
satellite atmosphere sounding involve three categories:
occultation, scattering, and emission. In occultation
one measures the changes that the atmosphere impinges on a
signal of known characteristics. The geometry corresponds
to limb sounding. In scattering,the approach is to
measure the characteristics of the scattered radiation.
In emission, the radiation source is the atmosphere and
the sensor measures the spectral characteristics and inten-
sity of the radiation itself. In temperature sounding the
radiation distribution emitted by gases is well known,
so radiance can be used to derive temperature. To obtain
an accurate temperature profile, the emission band should
have the following properties:

a.) the emitting constituents have a known
     mixing ratio

b.) the emission band should not overlap the
     bands of other constituents

c.) local thermodynamic equilibrium (LTE)
     should prevail so the Planck emission
     is followed

d.) the wavelength should be long enough so
scattered radiation is insignificant
compared to thermal radiation

Atmospheric constituents are identified by the
presence of spectral lines or bands. The line strength
is related to the number density of the molecules. The
PMR (pressure modulator radiometer) uses gas correlation
spectroscopy to measure radiation from the emission lines
of specific radiatively active atmospheric constituents
with a very high spectral resolution. This allows
the observation of radiation from very close to the center
of the lines, thus allowing sounding of high altitude
layers. In a PMR sensor collected radiation passes
through a cell containing the same gas. The pressure
in the cell is modulated at an angular frequency which
leads to the modulation of cell transmission T. The
depth of modulation of T is a function of optical frequency.
The change in T depends upon the cell pressure
modulation and the specific spectral line which allows
for the measurement of incident radiation intensity.
Spectral lines are not infinitely narrow. Line broadening
results from three main sources: excited state life-
times, pressure induced collisions, and thermal motion.
The thermal motion of a molecule during emission or ab-
sorption gives rise to the Doppler effect. This thermal
motion is a random process and induces broadening of the
spectral line. The Doppler line width is related to gas
temperature and dominates at high altitudes. Pressure

32-10

induced collisions give rise to the Lorentz shape function. The Lorentz width is related to the mean time between collisions which is inversely proportional to pressure. Lorentz broadening dominates at high pressure and is important at low altitudes. From the Doppler shift of the center of the line one can measure wind velocities in the atmosphere at all altitudes.

V.   MODELS

a.)   The Air Force Reference Atmospheres (Cole and Kantor, 1978) were developed to provide information on seasonal, latitudinal, longitudinal, and day to day variability of the thermodynamic properties of the atmosphere for altitudes of 0-90 kilometers. This model has monthly atmospheres defined in temperature altitude profiles where the vertical gradients of temperature are linear with respect to geopotential altitude. Tables are given in geometric height. The atmospheric model assumes the air is dry, in hydrostatic equilibrium, and behaves as a perfect gas. The molecular weight of the atmosphere is assumed to be constant to 80 km. It follows from this that the molecular scale temperatures and kinetic temperatures are identical to 80 km. Height profiles are given in geometric heights 0-90 km , except 0-54 km. at $90°N$; and $60°N$ for $10°W$, $100°W$, and $140°W$, respectively. At $75°N$ the height profiles are given for

10°W and 140°W. Mean monthly temperatures, pressures, and densities are tabulated. Data were collected for the Northernhemisphere only. Pressure, density, and temperature measurements for 0-30 km are from radiosondes, while for 30-90 km the MRN (Meteorological Rocket Network) rockets using thermistors, and rockets using grenades, gauges, and falling spheres take over. There are no wind measurements. Summer longitudinal variations in the structure of the atmosphere are small at all latitudes and all altitudes above 20 km. In winter, changes with longitude remain small at low latitudes but become important at high latitudes. At high latitudes the warmings and coolings of the winter stratosphere and mesosphere induce large changes in the vertical and horizontal structure of the atmosphere. The magnitudes of these variations (temperature, density, and pressure) have been prepared using models A,B,C, and D. Models A(warm), B(warm), C(warm), and D(cold) profiles are based on observations from radiosondes, meteorological rockets, and rockets using grenades, falling spheres, and pressure gauges.

b.)   A Middle Atmosphere Temperature Reference Model From Satellite Measurements (Barnett and Corney, Adv. Space Res.,1985) contains no algorithms or tables. The model is basically of temperature, with some pressure in-

formation. It is represented only as contours on figures. Data were obtained globally from Nimbus satellites equipped with SCR,PMR,SAMS, or LIMS sensors. The data cover different latitude and height ranges and different times during the 1973-83 period. The prime inputs for the model were from the SCR and PMR data which were combined using the method of weighted means. Initial input values were used from CIRA 1972 for the mesosphere and upper stratosphere and from Newell (private communication, 1977) for the lower and mid stratosphere. Zonal mean temperatures are given for January for all latitudes, and longitudinal wave numbers 1 and 2 for January for the Northern hemisphere. Wave number 1 is also given for the winter months for the Northern hemisphere. Amplitudes and phases of the annual and semi-annual waves are given as a function of latitude. The major advance was the inclusion of longitudinal variations in the model.

c.)   The Middle Atmosphere Reference Model Derived From Satellite Data (Barnett and Corney, MAP HBK., 1985) has a global coverage using data from SCR, PMR, SAMS, and LIMS radiometers. It is an extension of the model in section b.). Zonal mean monthly temperatures, geopotential heights, and geostrophic winds are tabulated using pressure scale heights (and pressure equivalents) as vertical co-ordinates in Table I. Zonal mean monthly temperatures, pressures,

and densities are tabulated with geometric height as the
vertical co-ordinates in Table II. This model has zonal
mean monthly climatology, latitudinal variability, geo-
potential heights, and geostrophic winds up to 80 km.
Values for the wind above 60 km are not accurate due to
effects of tides and gravity waves. Wind values near
equatorial latitudes are omitted because the large Cor-
iolis force there results in lack of accuracy. This model
contains no algorithms and is based on empirical analysis
of satellite data.

d.)   A Global Reference Atmosphere From 18-80 km
(Groves, 1985) has tables of global zonal mean monthly
temperatures, pressures, densities, number densities,
pressure scale heights, and geostrophic winds 18-80 km
and 80°S - 80°N. For modelling purposes there is seasonal,
latitudinal, and longitudinal variability. Pressure,
density, and temperature profiles assume the perfect gas
law and the hydrostatic equation. Gloval coverage is
achieved using SCR, PMR, SAMS, and LIMS satellite data
as in models b.) and c.). What makes these models unique
and different from models unique and different from models
b.) and c.), which are based solely on global satellite
remote sounding data, is that data from radiosondes,
rocketsondes and rocketborne gauges, grenades and falling
spheres (from both Southern and Northernhemispheres) are
compared with the satellite data and used to determine
empirical corrections to the profiles obtained from the

satellite data. For that reason all the values in this model (except the longitudinal terms) are different from those in models b.) and c.) in that they are based on both satellite remote sounding and in situ measurement data.

e.)   The Monthly Mean Global Climatology of Temperature, Wind, Geopotential Height, and Pressure for 0-120 km (Fleming, Chandra, Shoeberl, and Barnett, 1988) is modelled using data from Global Atmospheric Circulation Statistics (Oort, 1983) for 0-20 km. The Middle Atmosphere Reference Model (MAP HBK. 16) for 20-80 km , and MSIS 86 (Hedin, 1987) for 86-120 km.   The MSIS 86 provides empirical models of the thermosphere globally for 86 km and above. Geometric height profiles are tabulated globally for temperature (0-120 km), and pressure (20-120 km). Zonal mean monthly temperature, geopotential height, and geostrophic wind are tabulated as functions of pressure and geometric height (0-122.5 km). The given values for geostrophic winds above 60-80 km are not accurate due to the effects of tides and gravity waves. Numerous satellite and ground based measurements provide relatively complete spatial and temporal data coverage below 80 km (on a global monthly mean basis). Nevertheless, many atmospheric phenomena remain in question, such as the polar latitudinal temperature maximum of the winter polar stratopause and the relationship of the temperature and wind fields to the annual springtime

depletion of ozone over the Antarctic Knowledge of the
upper mesosphere and lower thermosphere is limited due to
the relative sparsity of data, and complex forcing mech-
anisms such as gravity waves and tides. The development
of a global distribution of radar systesm is providing
a substantial array of direct wind measurementsfor the
60-110 km region.

f.)   The NASA/MSFC Global Reference Atmosphere Model
(GRAM-88) uses a series of modelling techniques. From
0-25 km the "4D" meteorological model is used. From
25-90 km a modified Groves (1971) model is used. From
90-115 km an empirical transistion approximation is used
to join to the Jacchia model. Above 115 km the Jacchia
(1970) model is used. The Southern and Northern hemisphere
data sets for pressure, temperature, and density undergo
seasonal shifts. The quasibiennial oscillation (QBO) in
density, temperature and wind fields is also included in
the model. The QBO has a period of 870 days. GRAM-88 allows
for the simulation of random perturbation profiles about
mean conditions. Wind fields at 0-25 km and 90-120 km
are computed from pressure measurements using the geo-
strophic wind relation. From 25-90 km winds are given
by global spherical harmonic functions empirically derived
from upper atmosphere wind data. This model does not
predict parameters in the sense of a forecast model. It

provides estimates of the mean values and statistically realistic perturbations about mean conditions. This model has no tables.

The climatology of several atmospheric parameters are obtained by using current data sources for 0-120 km. This climatology provides accurate representation of zonally averaged atmospheric states and some information on longitudinal variations.

VI.   RECOMMENDATIONS

All the models examined used static modelling techniques:dry air, perfect gas, and hydrostatic equilibrium. However, later models start to include some dynamical processes on a limited scale. Dynamic models should be developed as an extension of the General Circulation Models (GCM) used for meteorological forecasting in the troposphere. GCM's are being developed for the stratosphere, mesosphere, and thermosphere. It is recommended that the analysis of additional data for the Lower to Middle Atmosphere from radiosondes, rocketsondes, Robin balloons, and radars and Lidars from U.S. and French sources be done. Upper atmospheric data taken from radars and on-board accelerometers taken during the re-entry of the Space Shuttle can be analyzed. Rocket and ground based studies of the mesosphere show waves are very important in the dynamics of this region. These waves manifest themselves in wind, temperature, density, pressure, ionization, and airglow

fluctuations in the 60-120 km range. Tidal waves are solar and latitudinal dependent. A new technique, Rayleigh lidar Sounding, has been developed to probe the Middle Atmosphere to obtain density and temperature profiles 30-90 km. It has been limited to ground based measurements, but it could be expanded to a space-borne platform. It has excellent spatial and temporal resolution, not available from present global data. The laser beam propogates in the atmosphere and two principal processes provide a backscattered signal: Rayleigh scattering for atmospheric molecules and Mie scattering by aerosols. A profile of density is obtained by the echo. Gravity waves are localized and have been detected using lidars. It is assumed that these oscillations are caused by acoustic gravity waves whose normal modes are forced in the lower atmosphere. Temperature and density fluctuations induced by gravity waves for the height region 60-120 km are not well known. Energy density decays with height indicate that the gravity waves are saturating (breaking) producing eddies (turbulence) or they are being externally damped by molecular processes. Work is being done on the coupling of wave energy between the stratosphere and ionosphere and it should be continued. Considerably more observations are required before the structure and roles of atmospheric waves in the 60-100 km region can

be fully elucidated. The components of the wavelength and phase velocity of internal gravity waves needs to be worked on. Dissipating and saturating gravity waves contribute to the momentum budget of the mesosphere. Radar measurements from Kyoto (Japan) and Adelaide (Austra lia) delineate strongly asymmetric tidal behavior in diurnal and semidiurnal components in the 80-100 km region. Is the asymmetric forcing due to insolation absorption by O_3 or H_2O? Semidiurnal tidal components have been observed in the 100-130 km region. Theoretical studies of the Middle Atmosphere tidal phenomena have considered physical processes beyond classical tidal theory. This includes molecular and eddy diffusion of heat and momentum, Newtonian cooling, electrodynamic forces, and the interaction of background winds and meridional temperature gradients. Excitation of tidal oscillations via absorption of EUV and UV radiation in the stratosphere and mesosphere, H_2O insolation, absorption in the troposphere and lower stratosphere, and O_3 insolation absorption in the stratosphere and mesosphere have also been examined in the new models. Further work on all of this needs to be continued.

Another new technique is the development of the MST (Mesosphere-Stratosphere-Troposphere) radar which is usable in all weather. MST radars make use of scattering from small-scale structures in the atmospheric refraction index, of the order of half a radar wavelength. In the mesosphere

turbulent echoes are observable. MST radars measure echo strength, Doppler shift, and Doppler width. A network of MST's has been proposed. MST radars can be used to study gravity waves, turbulence, convection, atmospheric tides, and atmospheric kinetic energy distributions.

The incoherent scatter radar technique measures charged particle characteristics. Energy deposition at high latitudes modulates global scale dynamics, energetics, and composition of the Earth's upper atmosphere. A data base established at NCAR needs to be analyzed.

A global program using a variety of observing and modelling techniques, called the International Geosphere-Biosphere Program (IGBP), is being planned. It will desribe and seek to understand the interactive physical, chemical, and biological processes that regulate the total Earth system. It will focus on the interdisciplinary character of these interactive processes.

1989 USAF-UES SUMMER FACULTY RESEARCH PROGRAM /

GRADUATE STUDENT RESEARCH PROGRAM

Sponsored by the

AIR FORCE OFFICE OF SCIENTIFIC RESEARCH

Conducted by

Universal Energy Systems, Inc.

<u>FINAL REPORT</u>

<u>Characterization Of A Spatial Light Modulator For Optical Filtering</u>

Prepared by:	Scott W. Coffin
Academic Rank:	Graduate Student
Department and	Electrical Engineering
University:	University of Oklahoma
Research Location:	RADC/OP/AOP Griffiss AFB Rome, NY 13441
USAF Researcher:	Andrew Pirich
Date:	28 July 1989
Contract No.:	F49620-88-C-0053

Characterization Of A Spatial Light Modulator For Optical Filtering

by

Scott W. Coffin

ABSTRACT

The Semetex Sight-Mod spatial light modulators offer the possibility of real time optical filtering capabilities. Here a 128x128 Semetex Sight-Mod spatial light modulator (SLM) is viewed with an eye toward phase-only correlation filtering. Computer software was developed to allow graphics drawn on a computer drawing program to be displayed on the SLM. These frames can then be chained into multiple frame files for sequential display. This software was developed to aid in characterization of the Sight-Mod device and for use in its operation in a filter set up. Then several important characteristics of the device are both predicted and measured, the results of which are given in this report.

ACKNOWLEDGEMENTS

There are indeed many who deserve my thanks. First of all I would like to express my appreciation to the Air Force Systems Command and the Air Force Office of Scientific Research for their sponsorship of this research. Universal Energy Systems certainly must be thanked for the administration of the Graduate Student Research Program.

At the Photonics Laboratories I wish to state my thanks to Don Hansen and Andrew Pirich for their support. Dr. Samuel Kozaitis and Dr. Kenneth Teegarden certainly deserve thanks for their direction and encouragement. Lt. Michael Ward should not go without mention for his help. I am also in debt to Dr. William Kuriger for his aid and influence.

I. INTRODUCTION:

The advancements made within the last decade have brought two dimensional spatial light modulators to a new high point in the possibilities for applications such as impressing information onto optical signals, optical recognition systems, and the continuing research into optical computing.

The Photonics Laboratories of the Rome Air Development Center at Griffiss Air Force Base have an active interest in the filtering of optical signals and are especially interested in how spatial light modulators can be used in amplitude and phase filtering systems. In order to facilitate the application of our SLM, computer software had to be developed and tested. Then characteristics of the device had to be determined.

My interests have been in the areas of digital electronics, quantum and semiconductor physics, solid state electronics, and more recently in the opto-electronics area. My combined backgrounds in physics and electrical engineering and work on an optically detected pressure sensor project contributed to my

assignment to the Analog Optical Processing group of the Photonics

Laboratories under my professor, Dr. William Kuriger.

II. OBJECTIVES OF THE RESEARCH:

My objective as a participant in the 1989 Graduate Student

Research Program (GSRP) was to aid in the evaluation of the

current technologies of spatial light modulators.

The Semetex Corporation of Torrence, California markets Sight-

Mod (Semetex Iron Garnet H-Triggered Magneto-Optic Device) SLMs

in a number of array sizes from one single pixel to 256x256 two

dimensional arrays. Our model was a 128x128 SLM with standard

equipment non-anti-reflective coated optics and dichroic sheet

polarizers (1).

Computer programs that allow the setting and resetting of

selected individual pixels and sets of pixels on the SLM were

desired. In addition a method of drawing a frame of pixels and then

being capable of taking this picture and putting it in a form that was

able to be displayed on the SLM was needed. Then it was desired to

be able to chain individual frames together into a single file of

several frames that can then be displayed on the SLM sequentially. These computer programs aided in the evaluation of the SLM characteristics during my research period. Also helpful in the longer time frame than characterization would be a program that allows individual frame files to be displayed at random as the end result of decisions made within a controller on the basis of the output of a correlation filter.

The characteristics that were measured were factors such as the amount of Faraday rotation of the device and its transmittance. The properties of the standard equipment polarizers. The measured contrast ratio and determination of points of possible phase-only operation. Finally the Semetex SLM was used to successfully duplicate a filtering experiment currently conducted at the Photonics Laboratories. Previously the experiment was performed with filters physically cut into sheets of opaque material and then moved or changed by hand to position it properly for the filtering out the desired characteristics of the input image that were wished to be filtered out.

III.

a.   The first step in developing a software package for the purpose of assisting in the characterization of the SLM was to develop and implement an algorithm to convert frames from a readily available format to one that can be displayed on the SLM. The Semetex Corporation supplied a demo program with the SLM device that was capable of displaying files with one or more frames. These frames would be displayed by that program in the sequence that the frames existed in a file, much like a strip of motion picture film. We had an existing program for the Apple Mac II that allowed one to draw any desired image in a 128x128 pixel structure and store it as a binary file. This program was very handy because it also allowed one to take the FFT of that image. The Mac II was fitted with an IBM compatible internal board so that the binary files could be written to a 5 1/4 inch IBM format disk and then used as input to the SLM via the IBM compatible machine that was fitted with the Semetex SLM driver board. The problem to be solved lay in that the manner in which the FFT program stored the bits representing the image did not match the manner in which the SLM

accepted the data bits representing the image. Therefore, the

methodic analysis of ordered images produced by the FFT program

and other images given as part of the demo program from the

Semetex Corp. was employed to arrive at an algorithm to rearrange

the individual bits which represented pixels to the proper order such

that the image drawn on the Mac II was displayed properly on the

SLM. A relatively simple program was then written to chain

converted frames together such that they could be displayed in

sequence by the demo file.

In preparation for using the SLM in an automated filtering set up a

program was developed that could use the common 'bload' statement

to very quickly move a file from disk to a specific memory location,

then be displayed on the SLM. The idea was that a controller could

analyse a correlation and make an intelligent guess about what

frame to display in the filter next and use this loading scheme to do

so randomly. An algorithm was then devised to convert the regular

two kilobyte frame files into the bsave/bload format.

b.   The result of the software development stage delivered

programs which were capable of performing all of the above criteria.

The conversion from the format written by the FFT program to the format read by the SLM was the only stage to present any road blocks. But, they were soon overcome. The process involved the rearrangement of individual bits because the FFT program stored the horizontal bytes of the image in sequence row by row. However, the SLM read the image by reading the first byte of the data and that byte became the first pixels of the first eight rows and so forth across the screen. Then the 129th byte read became the first pixels in the ninth through the sixteenth rows, and so on.

Another result of the software development was a program that could write individual pixels, columns, and/or rows on demand.. The basic algorithm was supplied by a fellow researcher within the Photonics Laboratories and it was then adapted to our particular needs and SLM array size.

IV.

a.   To characterize the Semetex SLM an important starting place is the amount of Faraday rotation given by the device. When a pixel is in the on state it rotates the incoming linearly polarized light by

the Faraday rotation angle in one direction and when the pixel is in the off state it rotates the polarization by the Faraday rotation angle in the other direction (2). Therefore, an angle that is twice the Faraday rotation can be measured by focusing the light of a laser through a single pixel and measuring the angle that a good polarizer must be rotated to obtain minimum transmission when that pixel is changed from one state to the other state. The minimum transmission is determined by focusing the output of the SLM onto an optical power meter and finding the minimum reading.

The maximum amount of light transmitted by the SLM was determined by measuring the intensity of the light just before the SLM and measuring the maximum intensity of light passed by the device and it's polarizers. This was also the method used for measuring the transmittance, or fraction of light passed, by the dichroic polarizers of the SLM by themselves.

The contrast between the intensities of light transmitted by the pixels in the on state and the off state was determined by setting the input polarizer in alignment with the polarization of the highly polarizer laser, for maximum transmission through the input

polarizer, then focusing the laser through a single pixel. Measurements of the intensity of light focused on a detector at the output of the SLM were taken for the on or open state and the off or closed state over the output polarizer span of zero to 180 degrees. The contrast ratio or modulation depth was calculated by the difference in intensities divided by the sum of the intensities for a particular setting of the output polarizer.

To predict the values that may be obtained for the intensity of light transmitted as a fraction of the maximum the following formulas were used,

$$\cos(A-B)^2 \qquad (1)$$

for the open state, and

$$\cos(A+B)^2 \qquad (2)$$

for the closed state. Where A is the position of the output or analyzing polarizer, from here on just called the polarizer (assuming that when A is zero the output polarizer is in alignment with the input polarizer), and B is the amount of Faraday rotation. The contrast ratio can then be predicted by using

$$\frac{INTdifference}{INTsum} = \frac{\cos(A-B)^2 - \cos(A+B)^2}{\cos(A-B)^2 + \cos(A+B)^2} \qquad (3)$$

as defined like Ross, Psaltis, and Anderson (1983). The possible points for phase-only operation would be identified by points of zero contrast and where when viewing the diffraction pattern of the device there is also the presence of the diffraction pattern of an image displayed on the SLM in addition to the diffraction pattern of the pixel structure itself, (Psaltis, Paek, and Venkatesh, 1984).

b.   The Semetex Corp. has claimed that the model of SLM that we have offers five degrees of Faraday rotation (1). However, using the procedure outlined above, A difference of twelve degrees between the open and closed states was obtained which gives a Faraday rotation of six degrees. The predicted transmission as a function of polarizer orientation can then be found for both pixel states using equations one and two, see figure one. The actual measured transmission is shown in figure two. The two graphs compare quite nicely except for the last two of three data points of the measured transmission, which are believed to be in error. Next, the right side of equation three was used to predict the contrast ratio as a function of polarizer orientation and the left side was used to calculate the actual contrast ratio from the measured intensities.

Figure three shows both and they agree fairly well. However, when contrast ratio is expressed as intensity maximum divided by intensity minimum Semetex claims a ratio of 2900:1 can be obtained (1). Our data only gives forth a 66:1 ratio when represented in that form.

Using the Malus law (Hecht and Zajac, 1979), and realizing that transmittance will be at its best if the Faraday rotation is ninety degrees, we can predict the transmittance by the sine squared of the Faraday rotation. This yields a transmittance maximum of about one percent, which does not account for factors such as reflectance, loss due to addressing wires, etc.. The Semetex Corp. claims their device offers a transmittance of nine tenths of a percent (1). I was able to gather as much as six percent of the input intensity at the output for a beam that spread over an area much larger than one pixel with polarizers set for maximum transmission. I do not know whether or not Semetex's measurements were for maximum or average transmission with respect to polarizer orientation.

The individual polarizers of the SLM were measured for

transmittance and extinction ratio. Each polarizer was found to be only about sixty two percent transmissive at full open and provided and an extinction ratio (maximum transmitted intensity divided by minimum transmitted intensity) of about 11248:1. The polarizer on the input side of the semetex was found to be five degrees off in it's markings. The measurements performed on this polarizer showed that it gave maximum transmission when markings on the face showed five degrees from the know angle of incoming polarized light from a highly linearly polarized laser.

For phase-only operation obviously the contrast ratio must be zero. This happens at three points of polarizer orientation. Namely zero, ninety, and one hundred and eighty degree settings of the polarizer. Unfortunately only the ninety degree point fulfilled the requirements set forth above for phase-only operation. This is unfortunate because the transmission is so low at this point, approximately .01% of input power.

V.

    a.   Here at the Photonics Laboratories an experiment has been

used to demonstrate spatial filtering. This experiment consists of shining a collimated laser beam through a 35mm slide that has the images of two airplanes on it. One airplane is drawn entirely with vertical lines and the other entirely with horizontal lines and the two images are superimposed. Admittedly this is not a real world situation but it simplifies the Fourier transform of the airplanes enough that alignment is no longer a difficult problem. The simplicity of the image of the airplanes allows the entirety of the transform of each airplane to be at right angles to each other The Fourier transform of the airplanes is then taken by a lens and an opaque sheet with a slit in it is placed in the Fourier plane. The Fourier plane is, of coarse, at the focal point at the output side of the lens. This filter slit has a opaque area in the very center to block the zeroth order of the transform. This zero order block is important because no information about an individual plane can be drawn from that diffraction spot, the information that is desired is in the higher orders. Now when everything is centered and the slit is oriented horizontally it will only pass the transform of the airplane composed of vertical lines, which has a purely horizontal transform, and only the image of that airplane is seen in the output image plane.

When the slit is oriented vertically only the image of the airplane composed of horizontal lines is viewed in the output plane because it's transform is purely vertical.

b.   This experiment was successfully duplicated using the SLM in the Fourier plane as the filter. The slit images were drawn using the FFT program mention previously and then converted to SLM format with the conversion program developed here. The SLM driver computer was then capable of switching the slits automatically and allowing the image of either plane to be viewed just by changing the frame displayed by the SLM. The alignment of the SLM was trickier than with the physical slits because of the discreet nature of the pixel structure on the SLM. The image of the airplanes in the output was also slightly more distorted than using the physical slits. This is also due to the nature and size of the SLM pixel structure. This latter effect will decrease with the advent of higher resolution SLMs, but the difficulty in alignment will increase as the size of the SLM pixels is reduced. Photographs of the output for each airplane are shown in figure four.

This is one way to demonstrate how the SLM can be used to

simplify the end use of a spatial filtering system and even produce

automated spatial filters. Automated object recognition is an

excellent example of where such a method could be well employed.

VI. RECOMMENDATIONS:

In tne light of the research that I have been involved with here at

the Photonics Laboratories I think that it would be very wise to

continue the research into using spatial light modulators in optical

correlation systems. Because of the limited availability of

equipment at the time I performed my research, I would suggest that

characterization of the Semetex Sight-Mod be repeated and

continued as well as investigations into other spatial light

modulators that may be or may soon be on the market. I believe that

further research into this particular SLM under more ideal

circumstances may indeed yield measured characteristics closer to

those predicted than I was able to obtain. Characterization of an

anti-reflective coated SLM may also prove worthwhile. In my

opinion the potential advantages of such a device, especially as it's

qualities improve, would serve Air Force as well as many other

industrial applications well.
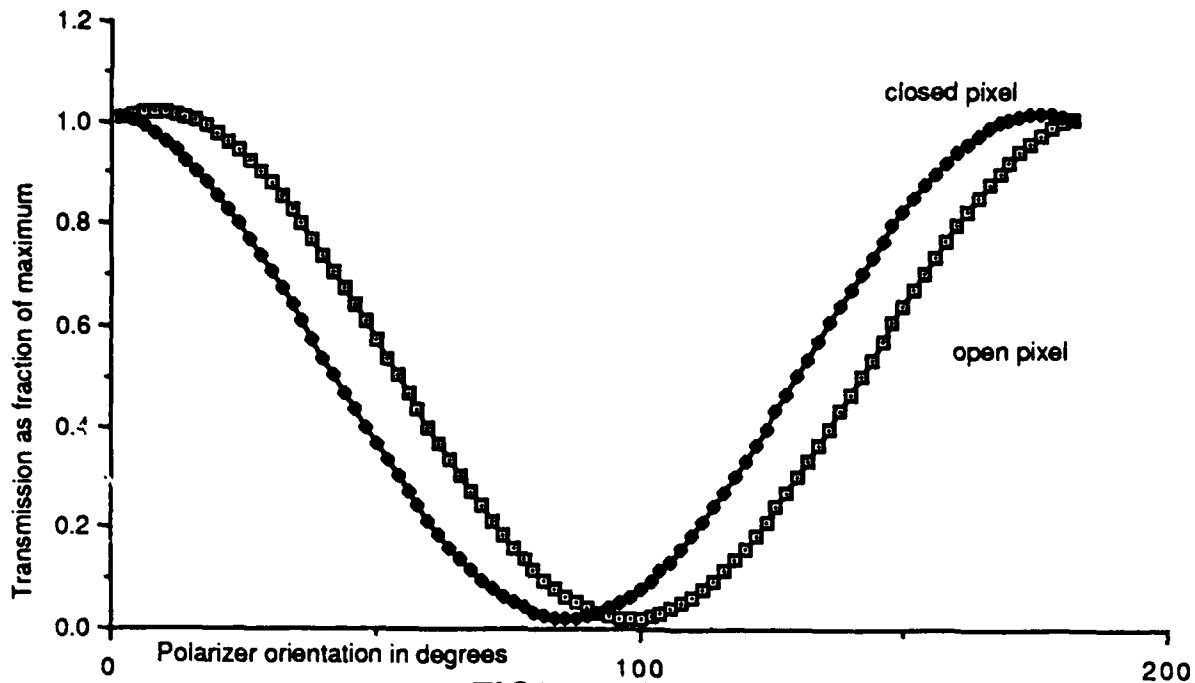
FIGURE ONE
Predicted transmission as function of polarizer orientation
for six degrees Faraday rotation
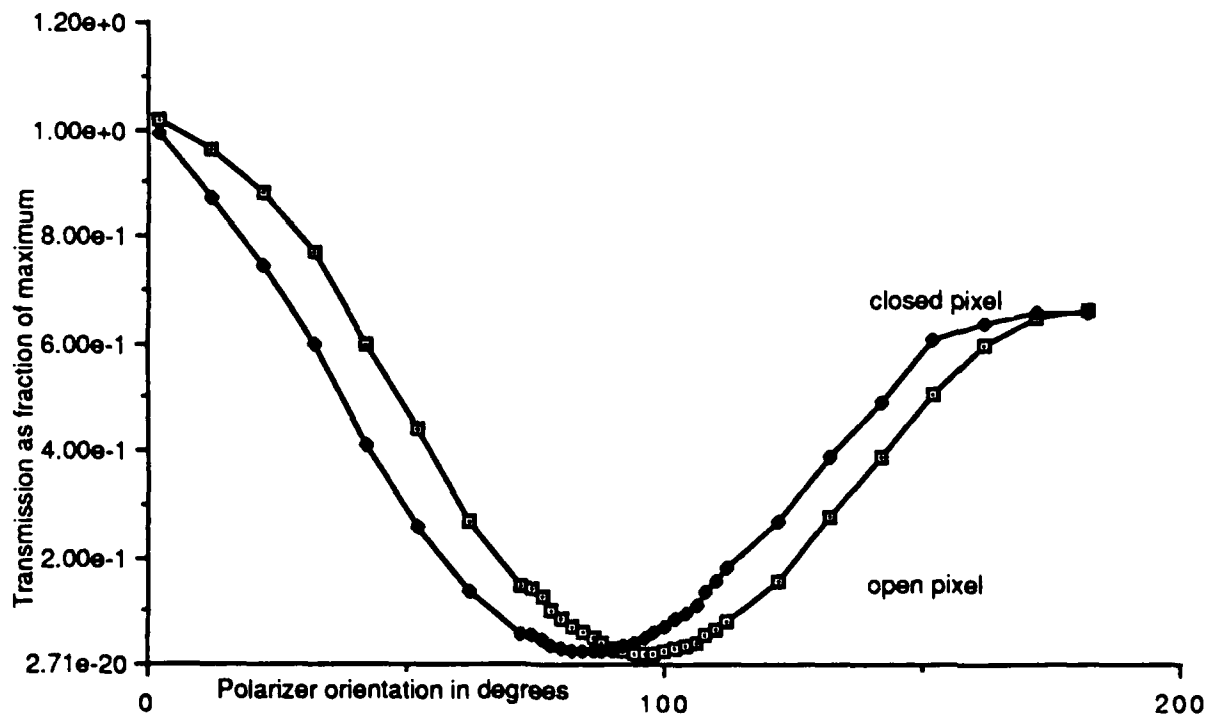
FIGURE TWO
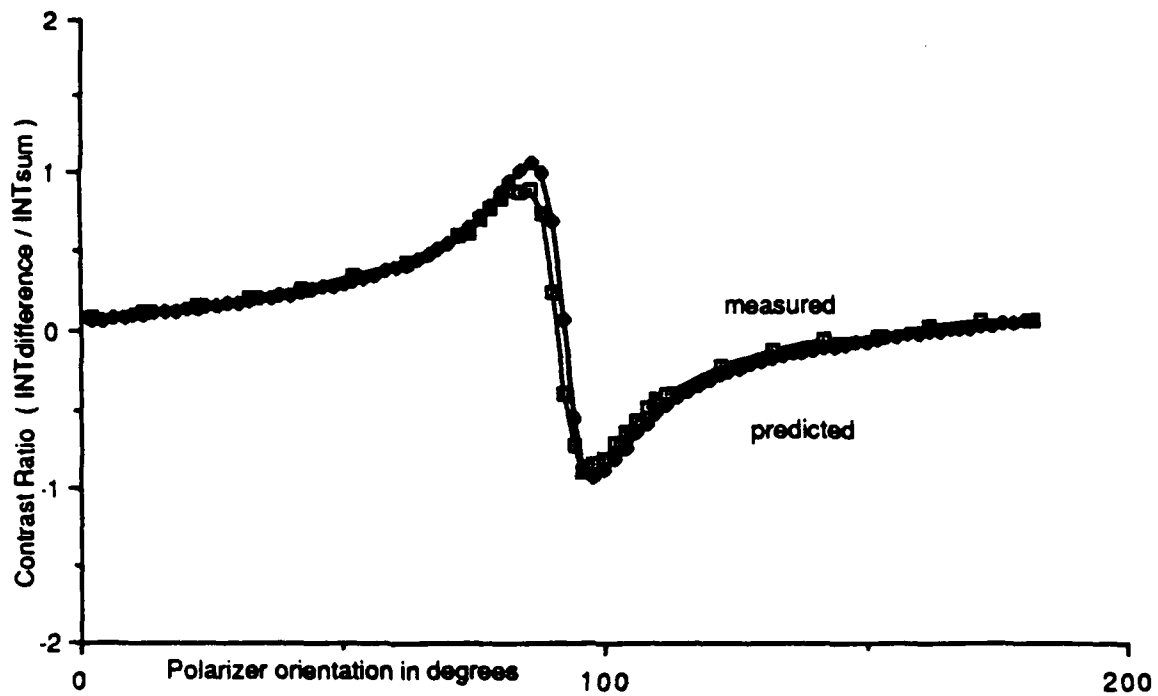**Measured Transmission as function of polarizer orientation**

FIGURE THREE
Predicted and measured Contrast Ratio
as function of polarizer orientation

FIGURE FOUR
Photographs of filtered output for plane recognition

REFERENCES

1. Specifications And Performance Updates, Semetex Corporation, Torrence, California, November, 1988, p. 11-13.

2. Ibid, p. 2.

3. Ross, William E., Demetri Psaltis, and Robert H. Anderson, Two-dimensional magneto-optic spatial light modulator for signal processing. Optical Engineering, 1983, Vol. 22, p. 488.

4. Psaltis, Demetri, Eung G. Paek, Santosh S. Venkatesh, Optical image correlation with a binary spatial light modulator. Optical Engineering, 1984, Vol. 23, pp. 698-699.

5. Hecht, Eugene and Alfred Zajac, Optics, Reading, Mass., Addison-Wesley Publishing, 1979, pp. 225-226.

1989 USAF-UES SUMMER FACULTY RESEARCH PROGRAM/

GRADUATE STUDENT RESEARCH PROGRAM

Sponsored by the

AIR FORCE OFFICE OF SCIENTIFIC RESEARCH

Conducted by the

Universal Energy Systems, Inc.

FINAL REPORT

ADAPTIVE BEAMFORMING SOFTWARE FOR

THE DIGITAL BEAM STEERING ANTENNA

Prepared by: Randal L. N. Mandock

Academic Rank: Student

Department and   School of Geophysical Sciences

  University: Georgia Institute of Technology

Research Location: USAFRADC/EEAA
                   Ipswich EM Measurement Site
                   12 Skytop Rd., Ipswich, MA 01938

USAF Researcher: Jeffrey S. Herd

Date: 29 Sep 89

Contract No: F49620-88-C-0053

ADAPTIVE BEAMFORMING SOFTWARE FOR THE DIGITAL BEAM STEERING ANTENNA

by

Randal L. N. Mandock

ABSTRACT

Theoretical beam patterns were investigated with conventional and adaptive nulling models. The Applebaum adaptive beamforming algorithm was used to study the effects of random system errors and of strong interference sources located within the half-power beamwidth of the main beam. Figures 1 through 8 show that increasing the level of element channel errors results in beam broadening, beam squint, increasing sidelobe levels, and the filling in of nulls. Figures 9 through 15 illustrate the change in Applebaum pattern produced by varying the look angle in the absence of element channel errors. For look angles greater than one-half the half-power beamwidth, the effect of the jammer is barely recognized on the main lobe and the adaptive pattern is well-behaved. Within the half-power beamwidth the nulling algorithm splits the main beam and is essentially ineffective for jammers located there. As shown by Figures 16 through 22, the same conclusions are derived with inclusion of real system errors.

ACKNOWLEDGEMENTS

I. INTRODUCTION:

A topic of interest to the Antennas and Components Division (EEA) of the Rome Air Development Center (RADC) is adaptive beamforming with phased array radars. Steyskal (1987) listed six applications for digital beamforming which are advantageous for the receive mode. In an attempt to satisfy both my research interests and those of RADC, my USAF research colleague, Jeff Herd, recommended that I pursue the first of Steyskal's applications, improved adaptive pattern nulling. The objective of adaptive pattern nulling is to align angular regions of low array sensitivity with the directions of sources of strong or jamming interference.

The basis for my assignment to EEA was to facilitate the transfer of software technology between the Antenna Technology Branch (EEAA) and the Ipswich Electromagnetics Measurement Site. Digital beamforming software comprises one of the cornerstones of my thesis research in remote sensing of the atmosphere by sound; therefore software research in adaptive beamforming was chosen as an appropriate bridge between my current research interest and that of EEA.

The elements of my background which have proven valuable for the summer effort include several years experience in scientific computing, digital signal analysis, and wave propagation through various media. Prior experience in software development on Hewlett Packard computing systems also contributed to the success of the effort.

II. OBJECTIVES OF THE RESEARCH EFFORT:

The preliminary objectives of the research effort were broad, but focused primarily on the investigation of several adaptive algorithms for digital beamforming. These goals were optimistic and included modeling the pattern of a planar array, investigating the sensitivity of the model to various sources of error and uncertainty, and verifying the model with the Ipswich 32-element array antenna. Shortly after my

arrival at the Ipswich Site these goals were refined to allow for deficiencies in my background.

The revised goals consisted of adapting existing software to function on the Ipswich computers. The final objectives were to:

1. Model the far field of a planar array with an array pattern program from the literature.
2. Translate the RADC ADERR program from FORTRAN to HPBASIC. Incorporate ADERR as a subroutine to the main digital beamforming program.
3. Test and verify the subroutine with real and synthetic data.

III. THE ARRPAT PROGRAM:

a.   The ARRPAT program found in Appendix G of Stutzman and Thiele (1981) is used to compute the complete radiation pattern of an arbitrary antenna array. It was chosen to satisfy the first objective because of its flexibility and tutorial structure. The program was modified to allow faster execution, then tested against published array patterns to verify its performance. The final FORTRAN version is on file at the Ipswich Site as a stand-alone program.

b.   Preliminary results of experiments with ARRPAT indicate that the program is an effective tool for predicting theoretical array patterns for sparse planar arrays. ARRPAT was used to examine several array configurations that I had proposed for my thesis research. On the basis of these results, the final array configuration will most likely not conform to any of those proposed.

IV. ADERR REVISED:

a.   ADERR is an RADC adaptive beamforming program which can be used to steer pattern nulls in up to four directions. Modifications were made to ADERR which allow it to run on the Hewlett Packard computers at the Ipswich site. An HPBASIC random number generator was added as an option

to replace the random number file used by RADC. An interactive plotting subroutine was added and is automatically called when the pattern values have been computed. The final versions are optimized stand-alone programs in FORTRAN and HPBASIC.

b.   Due to the limited duration of the summer effort, ADERR was not incorporated as a subroutine to the main digital beamforming program. However, the stand-alone version was found to be adequate for analyzing synthetic data. For a 24-element array the final HPBASIC version executes more than five times faster than the RADC version running on an IBM PC Compatible system, while the revised FORTRAN version executes two times faster than the RADC version.

V.   VERIFICATION AND TESTING OF ADERR II (REVISED ADERR) PROGRAM WITH
      SYNTHETIC DATA:

a.   The approach taken to verify ADERR II was to compare synthetic pattern values with patterns generated by RADC. Other tests included verifying null locations, sidelobe levels, effects of random errors, and performance in the absence of errors. The number and positions of jamming sources were varied to analyze their effect on the main beam and sidelobes.

b.   The significant features of selected array patterns generated by RADC with synthetic data were reproduced by ADERR II. Additionally, in the absence of random errors in the amplitude and phase of the antenna channels (element channel errors), the Frost and Applebaum patterns computed by the program were found to agree.

Figures 1 through 8 indicate the effects of varying the level of element channel errors from 0 to 2 Pi, as predicted by the Applebaum algorithm. A target that produces unit amplitude excitation at each element of a linear 24-element array is located at broadside, while a fixed source of jamming interference is located at 17 degrees from broadside. The element spacing is half-wavelength. The power level at each element due to the jammer is 1000 times that produced by the target. The receiver

noise level is fixed at a constant value 10 dB below the received target power level. The figures show that increasing the level of element channel errors results in beam broadening, beam squint (off-axis position of main beam maximum), increasing sidelobe levels, and the filling in of nulls. However, although the position of the main beam is altered by introducing channel errors, the adaptive null remains exactly at 17 degrees throughout. Several of the curves are shifted downward to align the main beam maximum with 0 dB.

Figures 9 through 15 illustrate the change in Applebaum pattern produced by varying the look angle in the absence of element channel errors. The target, jammer, and receiver noise power levels are identical to those for Figures 1 through 8. For look angles greater than 2 degrees (one-half the half-power beamwidth), the effect of the jammer is barely recognized on the main lobe and the adaptive pattern is well-behaved. Within the half-power beamwidth the nulling algorithm splits the main beam and is essentially ineffective for jammers located there. As shown by Figures 16 through 22, the same conclusions are derived with inclusion of real system errors.

VI. RECOMMENDATIONS:

a. The results of ADERR II modeling will be utilized as a baseline database to be compared with experimental results obtained at the Ipswich Site. ADERR II can also be used to perform parametric studies of the adaptive nulling algorithms with multiple system variables such as receiver noise figures, channel-to-channel errors, signal to jamming noise ratios, and location and number of jammers.

b. Suggested follow-on research is a series of modifications to the ADERR II code. The first suggestion is to modify ADERR II to allow for more sophisticated modeling elements. Other suggested modifications are to include algorithms to accomodate the following:

1. Finite word size for antenna signal data.
2. Mutual coupling between antenna elements.

3. Effects of failed antenna elements.

c.   In order to satisfy the third objective of incorporating experimental data into the model, ADERR II must be modified to accept a time series of antenna data signals and to compute the covariance matrix elements from these series rather than from the constant antenna element values which are used in its present form.   This will require the addition of a short subroutine which performs complex multiplies and adds.

REFERENCES

Steyskal, H., 'Digital Beamforming Antennas: An Introduction,' Microwave J., 1987, Vol. 30, pp. 107-124.

Stutzman, W.L. and G.A. Thiele, Antenna Theory and Design, New York, NY, John Wiley & Sons, 1981, pp. 572-575.
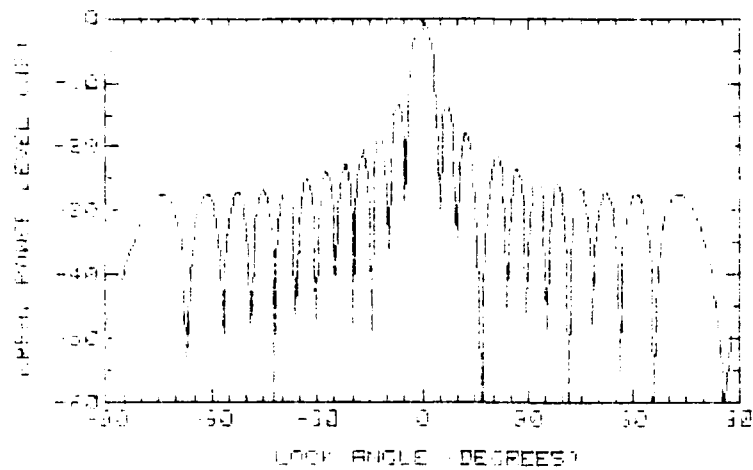
FIG. 1. CHANNEL ERROR IS 0. JAMMER AT 10 DEG.
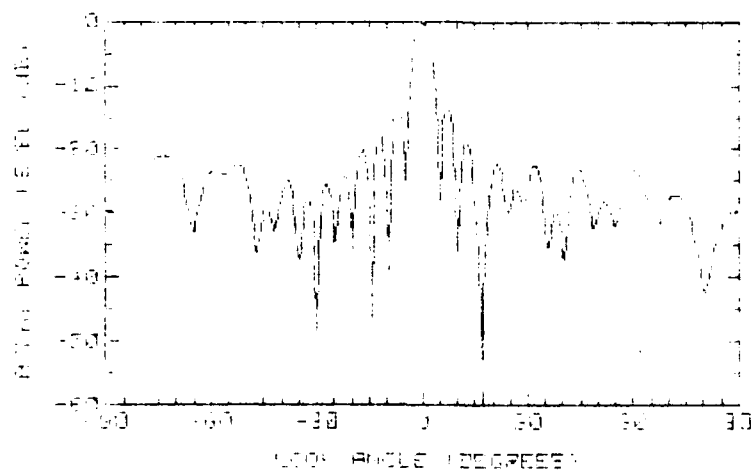
FIG. 2. CHANNEL ERROR IS 0.1. JAMMER AT 10 DEG.
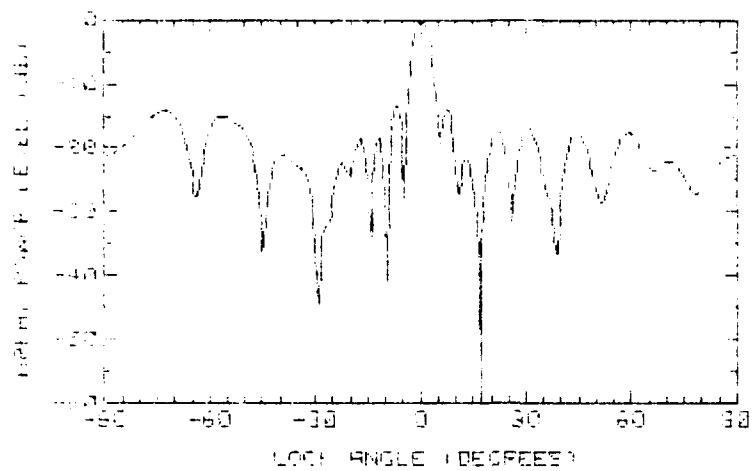POWER LEVEL CURVE SHIFTED DOWNWARD BY 0.813 dB.

FIG. 3. CHANNEL ERROR IS 0.3. JAMMER AT 17 DEG.
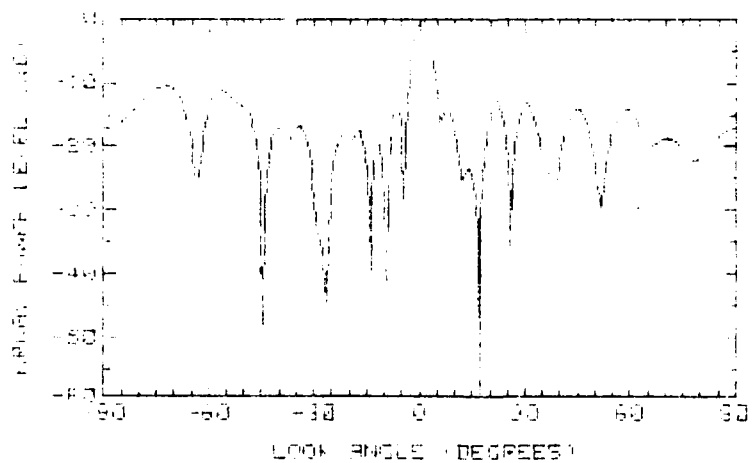POWER LEVEL CURVE SHIFTED DOWNWARD BY 0.193 dB.

FIG. 4. CHANNEL ERROR IS 0.5. JAMMER AT 17 DEG.
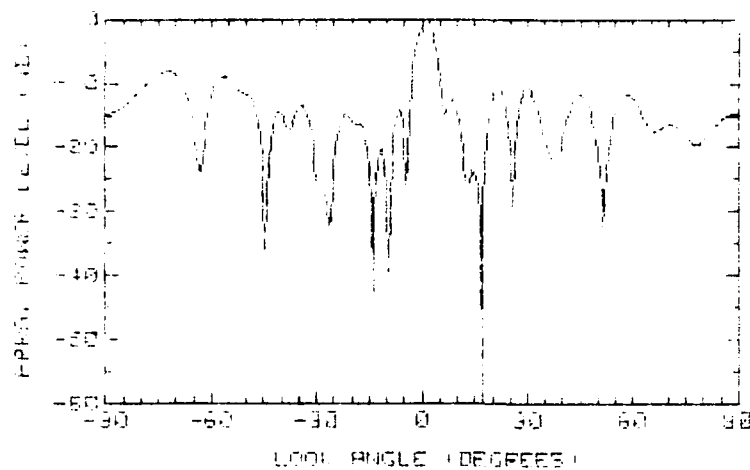POWER LEVEL CURVE SHIFTED DOWNWARD BY 0.414 dB.

FIG. 5. CHANNEL ERROR IS 0.7. JAMMER AT 17 DEG.
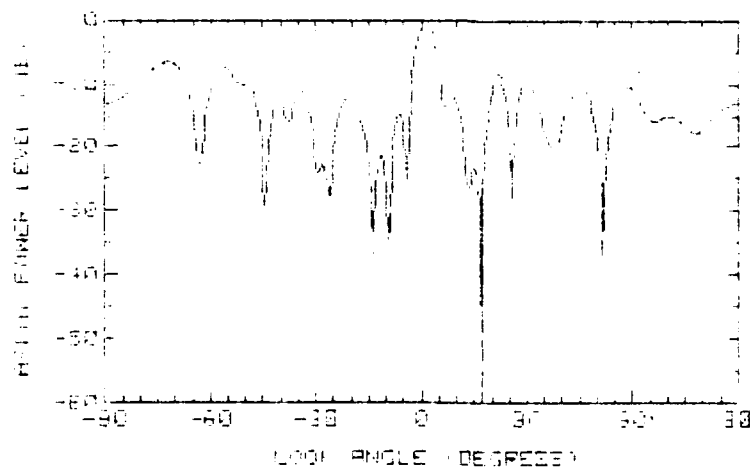POWER LEVEL CURVE SHIFTED DOWNWARD BY 0.875 dB.

FIG. 6. CHANNEL ERROR IS 0.9. JAMMER AT 17 DEG.
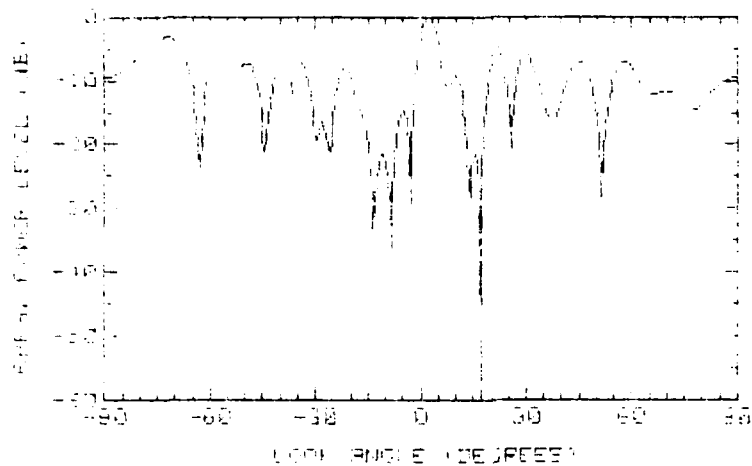POWER LEVEL CURVE SHIFTED DOWNWARD BY 1.343 dB.

FIG. 7. CHANNEL ERROR IS 3.3. TRIMMED AT 17 DEG.
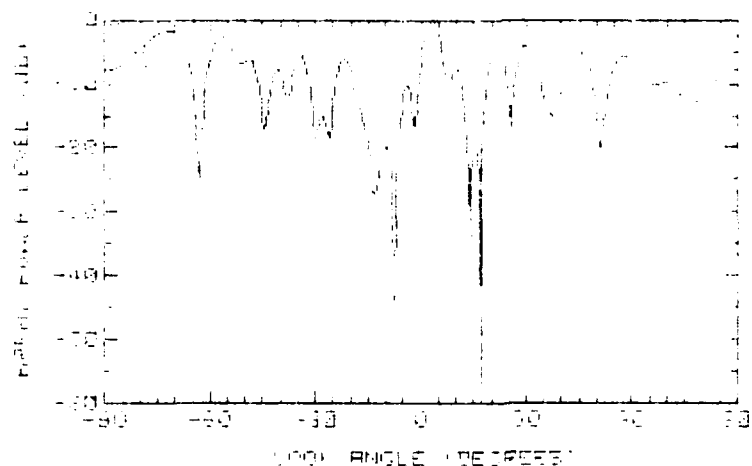POWER LEVEL CURVE SHIFTED DOWNWARD BY 4.742 dB.

FIG. 8. CHANNEL ERROR IS 0 PI. TRIMMED AT 17 DEG.
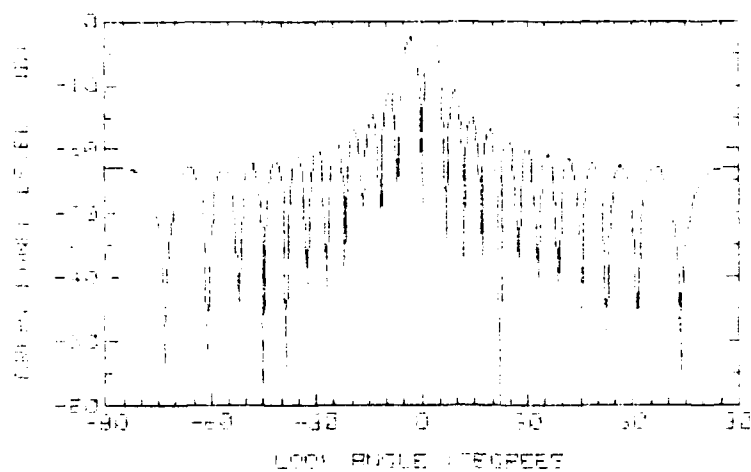POWER LEVEL CURVE SHIFTED DOWNWARD BY 13.069 dB

FIG. 9. CHANNEL ERROR IS 0. JAMMER AT 0.1 DEG.

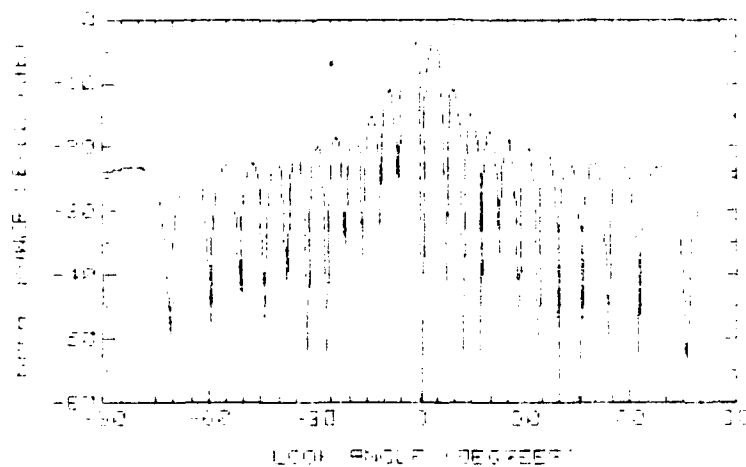

FIG. 10. CHANNEL ERROR IS 0. JAMMER AT 1 DEG.
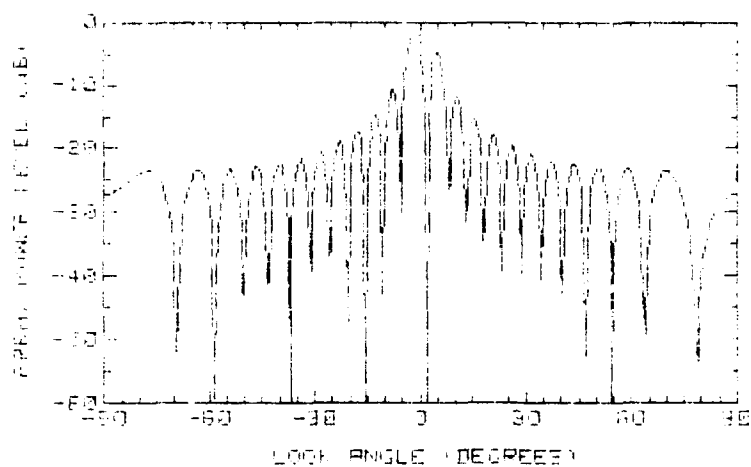
FIG. 11. CHANNEL ERROR 0. JAMMER AT 0 DEG.
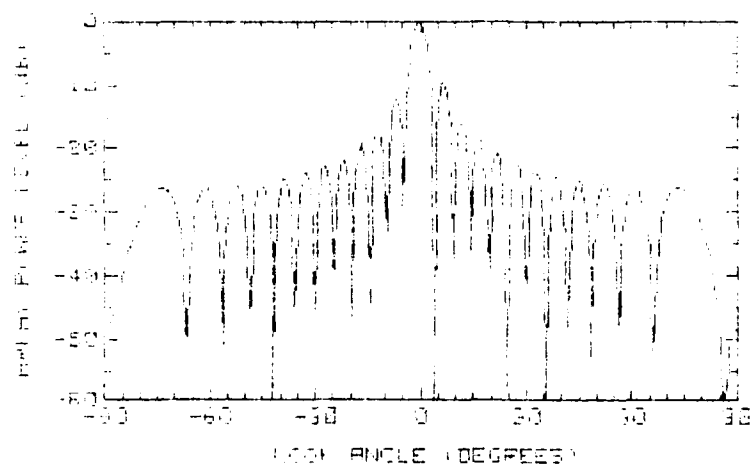
FIG. 12. CHANNEL ERROR 25 0. JAMMER AT 0 DEG.

FIG. 17. CHANNEL DEPTH IS 0. JAMMER AT 0 DEG

FIG. 18. CHANNEL DEPTH IS 0. JAMMER AT 0 DEG.

FIG. 15. CHANNEL ERROR IS 0, JAMMER AT 10 DEG.
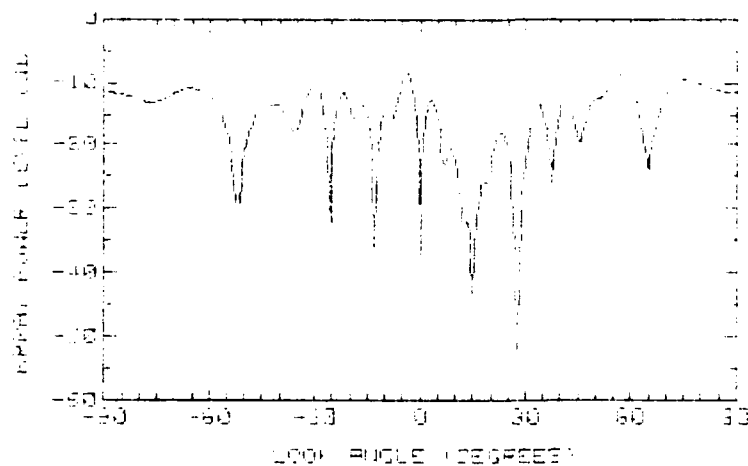
FIG. 16. CHANNEL ERROR IS 0.25, JAMMER AT 0.1 DEG.
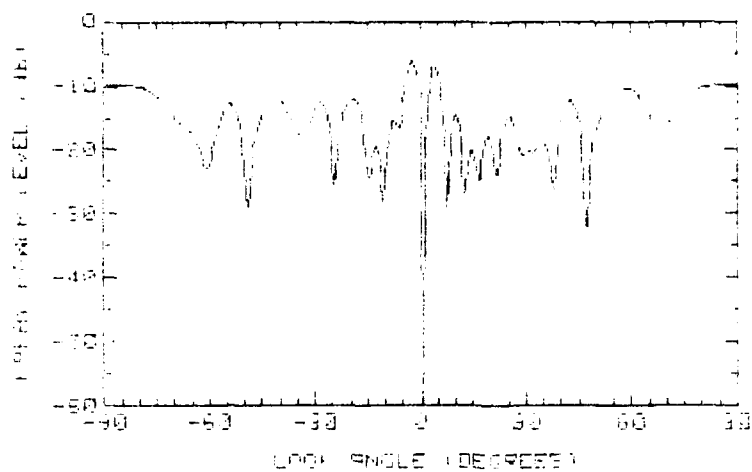
FIG. 17. CHANNEL ERROR IS 0.15. JAMMER AT 1.0 DEG.
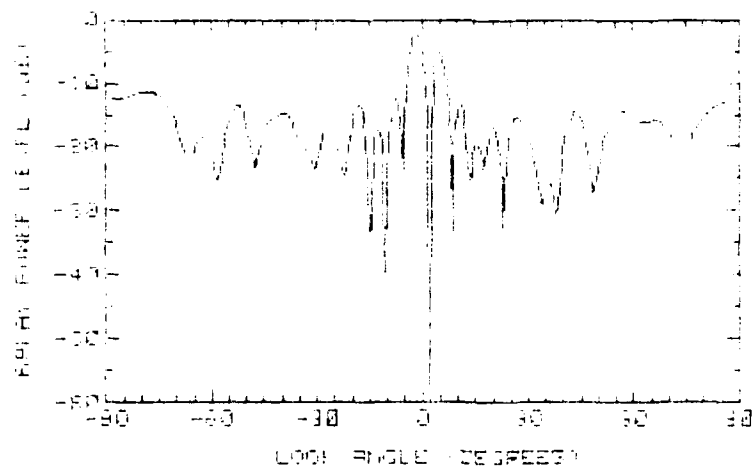
FIG. 18. CHANNEL ERROR IS 0.15. JAMMER AT 2 DEG.
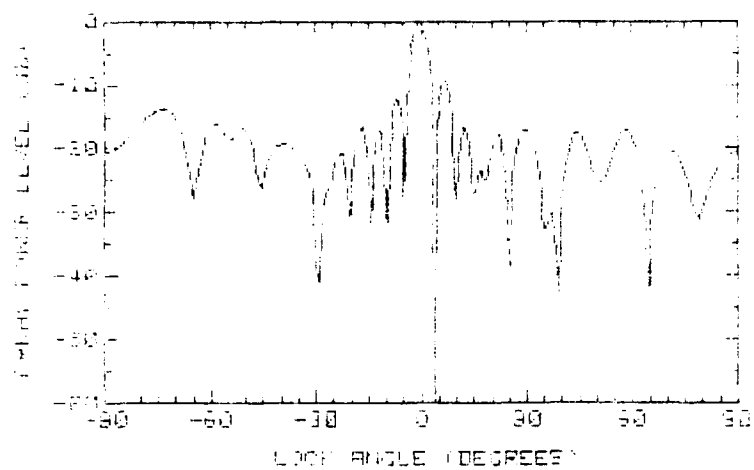
FIG. 19. CHANNEL ERROR IS 0.25. JAMMER AT 4 DEG.
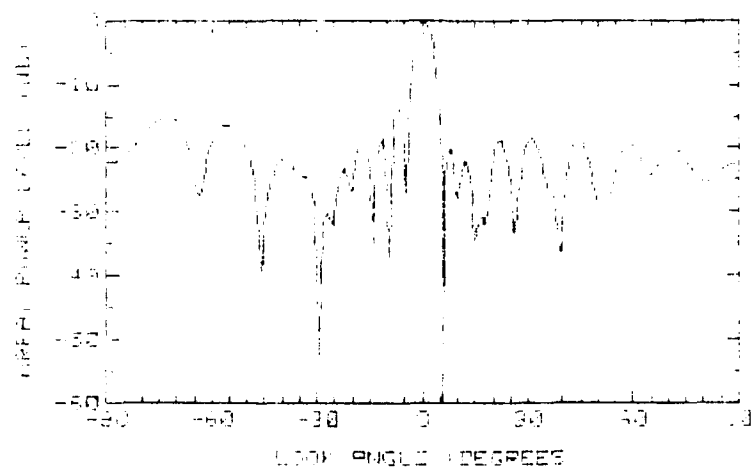
FIG. 20. CHANNEL ERROR IS 0.25. JAMMER AT 6 DEG.
POWER LEVEL CURVE SHIFTED DOWNWARD BY 0.868 dB.
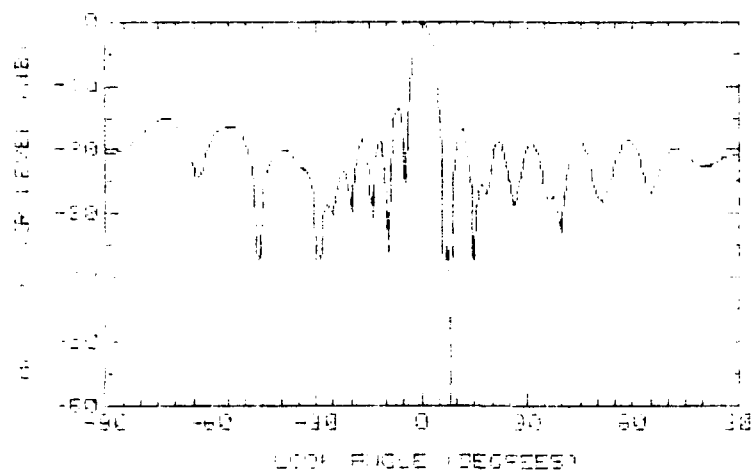
FIG. 31. CHANNEL ERROR IS 0.35. JAMMER AT 9 DEG
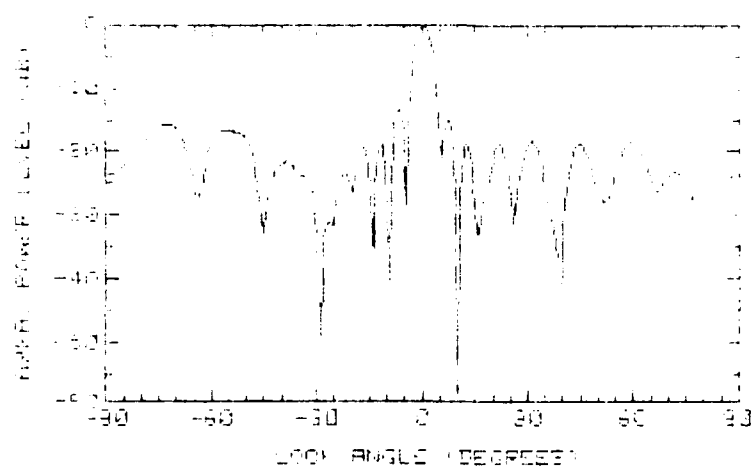
FIG. 32. CHANNEL ERROR IS 0.35. JAMMER AT 10 DEG.
POWER LEVEL CURVE SHIFTED DOWNWARD BY 0.104 dB.

FINAL REPORT

1989 USAF-UES SUMMER FACULTY RESEARCH PROGRAM

GRADUATE STUDENT RESEARCH PROGRAM

Sponsored by the

AIR FORCE OFFICE OF SCIENTIFIC RESEARCH

Conducted by the

Universal Energy Systems, Inc.

A STUDY OF INTERACTING TUNNELING UNITS

WITH POSSIBLE APPLICATION TO HIGH TEMPERATURE SUPERCONDUCTORS

Prepared by: Michael W. Klein[*]

Academic Rank: Professor

Department: Physics Department

University: Worcester Polytechnic Institute

Research Location: Rome Air Development Center
                      Hanscom Air Force Base, MA 01731

USAF Researcher: Alfred Kahan

Date: July 24, 1989

Contract No: F49620-88-C-0053

Project No: 210

[*] This is a joint report by **Michael W. Klein**, Summer Faculty

Research Fellow and **Timothy P. Mavor**, Graduate Student.

Same Report As
Prof. Michael Klein
(Report # 71)

1989 USAF-UES SUMMER FACULTY RESEARCH PROGRAM

GRADUATE STUDENT RESEARCH PROGRAM

Sponsored by the

AIR FORCE OFFICE OF SCIENTIFIC RESEARCH

Conducted by the

Universal Energy Systems, Inc.

FINAL REPORT

A Simplified Method of Determining Noise Parameters of High Frequency MESFET's

Prepared by:	William Patience
Academic Rank:	Graduate Student
Department and	Electrical and Computer Engineering Department
University:	Ohio University
Research Location:	USAF/RADC-EEAC Hanscom AFB Bedford, MA 01731
USAF Researcher:	Richard Webster
Date:	Sept. 6, 1989
Contract No:	F49620-88-C-0053

A Simplified Method of Determining Noise

Parameters of High Frequency MESFET's

by

William Patience

ABSTRACT

Using established circuit analysis techniques and linear, noisy two-port theory, an expression for noise figure is derived. S-parameter and noise figure measurements are taken over appropriate frequency ranges at a constant source impedance and used to determine all unknown parameters in the noise figure expression. At a particular operating frequency, noise figure is now expressible in terms of a single variable, source impedance. The procedure outlined by Lane [1] can be readily applied, with no additional measurements required.

Acknowledgements

I. INTRODUCTION:

One of the major considerations in the design of microwave and millimeter-wave amplifiers is their noise performance. The noise properties of an amplifier can be completely characterized by four parameters; minimum noise figure (F_{min}), optimum source admittance ($G_{opt} + jB_{opt}$), and noise resistance (r_n). These parameters are used to create constant noise figure circles on the Smith chart.

The Monolithic Microwave Integrated Circuits (MMIC) team at RADC/EEAC, Hanscom Air Force Base is very interested in optimizing amplifier noise performance at high frequencies. Thus an efficient and accurate method of noise measurement is essential.

My research interest in low noise microwave design along with my current work towards an M.S. degree in this area contributed to my assignment at RADC/EEAC.

II. OBJECTIVES OF THE RESEARCH EFFORT:

The standard technique for determining noise parameters requires tuning of the circuit and optimizing generator impedance. Unfortunately, this procedure is inconvenient, time consuming and must be entirely repeated at each frequency of interest. Several papers have been published recently on the determination of noise parameters using more convenient techniques [2]-[5]. These approaches, however, are limited to applications below approximately 20 GHz.

My assignment for the summer was to develop an efficient technique for measuring noise parameters at millimeter-wave frequencies.

III. ANALYSIS

The noise equivalent circuit model used in our analysis, similar to the model proposed by Heinrich [8], is shown in Fig. One. The two noise current sources, i_{nd} and i_{ng}, represent the noise in the drain and gate, respectively. They can be expressed as [9]

$$\overline{\left|i_{nd}\right|}^2 = 4kT\Delta f\, g_m\, P$$

$$\overline{\left|i_{ng}\right|}^2 = 4kT\Delta f\, C_{GS}^2\, w^2 \tfrac{1}{g_m}\, R \qquad (1)$$

where R and P are dimensionless noise coefficients. These two sources are correlated; thus a complex correlation coefficient is needed. In accordance with [7], [8], this correlation is assumed to be purely imaginary.

$$jC = \frac{\overline{\left|i_{ng}\right|}\ \overline{\left|i_{nd}^*\right|}}{\sqrt{\overline{\left|i_{ng}\right|}^2\ \overline{\left|i_{nd}\right|}^2}} \qquad (2)$$

The extrinsic thermal noise sources e_{ng}, e_{nd}, and e_{ns} are characterized by their Nyquist formulas,

$$\overline{|e_{ng}|}^2 = 4kT\Delta f R_G$$

$$\overline{|e_{nd}|}^2 = 4kT\Delta f R_D \qquad (3)$$

$$\overline{|e_{ns}|}^2 = 4kT\Delta f R_S$$

where k is the Boltzmann constant, T is the absolute temperature, Δf is the frequency bandwidth.

The equivalent circuit of Fig. One can be configured as a simplified two port, as shown in Fig. Two, and then transformed into a noiseless two port preceeded by a noisy network [6], [7], shown in Fig. Three. The new noise sources, e and i, are given by

$$e = N_1 i_{ng} + N_2 i_{nd} + N_3 e_{ns} \qquad (4)$$

$$i = N_4 i_{ng} + N_5 i_{nd} + N_6 e_{ns} + e_{nd}/z_{21}$$

where N_i (i=1 to 6) are coefficients depending on circuit parameters. Noise figure can now be written as

$$F = \frac{\overline{|V_{gen} + e_{ng} + e + i Z_{11}|}^2}{\overline{|V_{gen}|}^2} \qquad (5)$$

Using equations (1-4), noise figure is expressed as

$$F = 1 + \frac{R_G + R_S|N_3 + N_6 Z_+|^2 + R_D \left|\frac{Z_+}{Z_{21}}\right|^2}{R_{gen}}$$

$$+ |N_1 + N_4 Z_+|^2 \frac{w^2 C_{GS}^2}{R_{gen}\, g_m} R \qquad (6)$$

$$+ |N_2 + N_5 Z_+|^2 \frac{g_m}{R_{gen}} P$$

$$- \frac{2}{R_{gen}} Re\left[(N_1 + N_4 Z_+)(N_2 + N_5 Z_+)^* jw C_{GS}\right] C\sqrt{RP}$$

36-6

Noise figure is thus expressed as a function of circuit model parameters, source impedance, frequency, and three dimensionless noise coefficients. These coefficients, P, R, and C, are dependent upon device geometry and bias, as well as operating frequency. In the millimeter-wave range, however, they vary minimally with respect to frequency and are assumed constant in our analysis. To minimize error arising from noise coefficient inaccuracy, the measurrements should be conducted over a limited frequency range. At lower frequencies this assumption becomes questionable and may cause the analysis to fail.

The circuit parameters for a given dc bias are obtained by a least squares fit of measured S parameters. Keeping the same bias, the noise figure of the device is now measured over a range of frequencies at a constant source impedance. The value of source impedance is arbitrary and is usually chosen at 50 ohms, which is a convenient resistance for these measurements. The noise coefficients P, R, and C are evaluated by once again using the method of least squares to fit the noise figure data with equation (6).

The noise coefficients are now defined over a frequency range selected for a given investigation. Choosing any frequency of operation within this range, noise figure is now a function of source impedance alone. This provides a distinct advantage over standard techniques, that require an entire new set of measurements for each frequency. Choosing a set of source impedances well distributed on the Smith chart [11], the corresponding noise figures are determined

from equation (6). Thus no additional measurements are required. The noise parameters (F_{min}, R_n, and Y_{opt}) can be found by performing a least square fit of this data and the well known noise figure equation.

$$ F = F_{min} + \frac{R_n}{G_{gen}} \left| Y_{gen} - Y_{opt} \right|^2 \qquad (7) $$

IV. SUMMARY

Unfortunately, our analysis could not be tested in the millimeter wave range. The only data available was that of an NEC710 series low noise GaAs FET from 2GHz to 18GHz. A comparison of F_{min} from the data sheet and our analysis is shown in Graph One. In general the degree of accuracy increases steadily as frequency increases. Accuracy also seems to increase when the data range is limited to higher frequencies. When the input data range was restricted to low frequencies (2-10GHz), the analysis produced results without physical meaning. The best results were obtained at 18GHz, using a data range from 12 - 18GHz.

The results tend to imply that at even higher frequencies, up into the millimeter-wave range, greater accuracy will be obtained. However, further testing is needed to substantiate these implications.

V. RECOMMENDATIONS:

The accuracy of this procedure in the millimeter-wave range is still uncertain. Extensive testing should be conducted to determine the validity of the assumptions, the frequency range where the procedure is accurate and the degree of accuracy that can be obtained. Improving the circuit model by adding the additional elements suggested by Heinrich [8] may lead to greater accuracy.

Currently, this procedure is useful in predicting noise parameters only at room temperature. The analysis should be extended to allow predictions even at cryogenic temperatures. The ability of this procedure to predict the noise performance of HEMT's should also be examined.
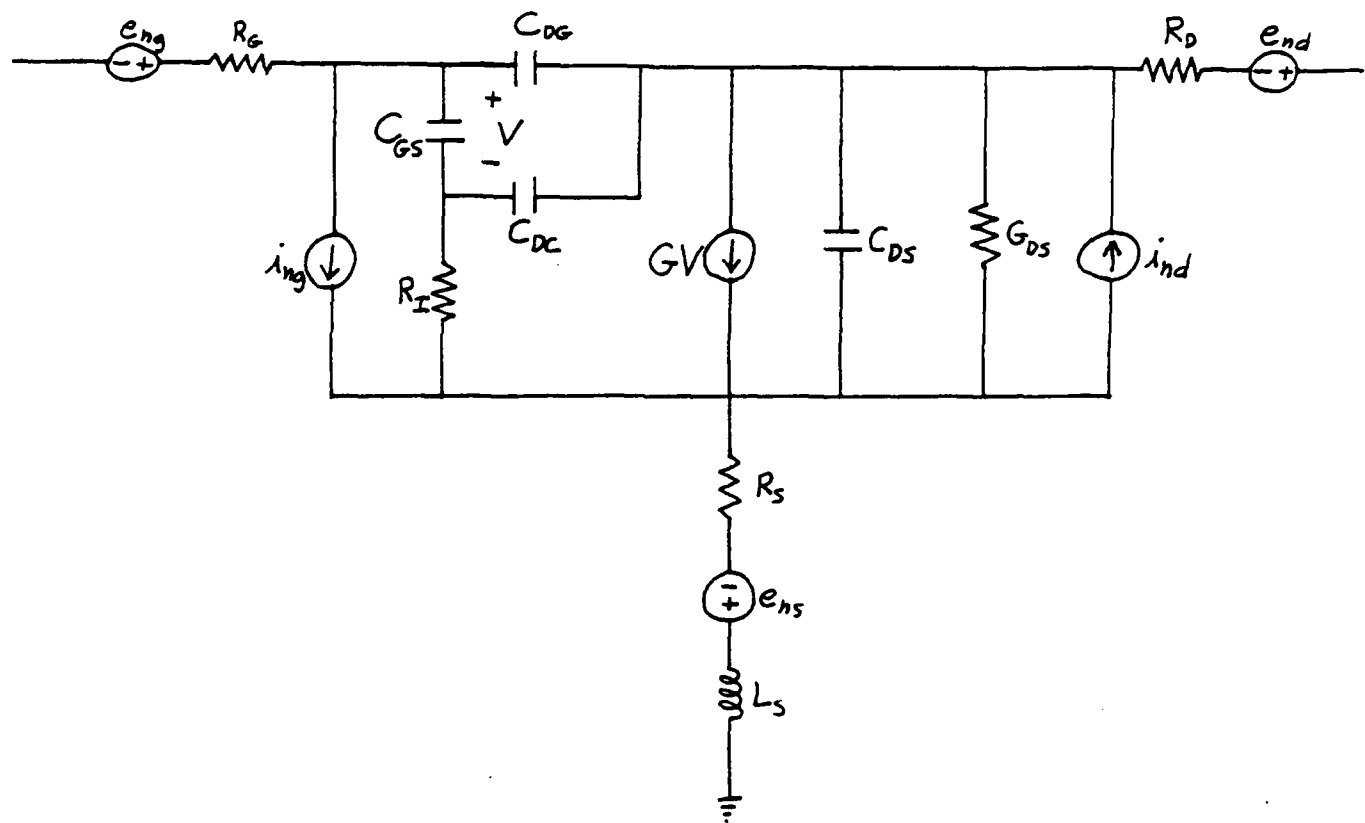
Fig. One
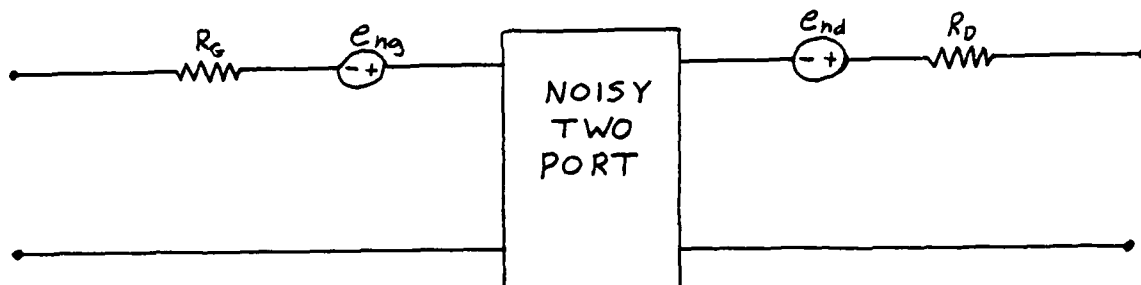
Fig. Two
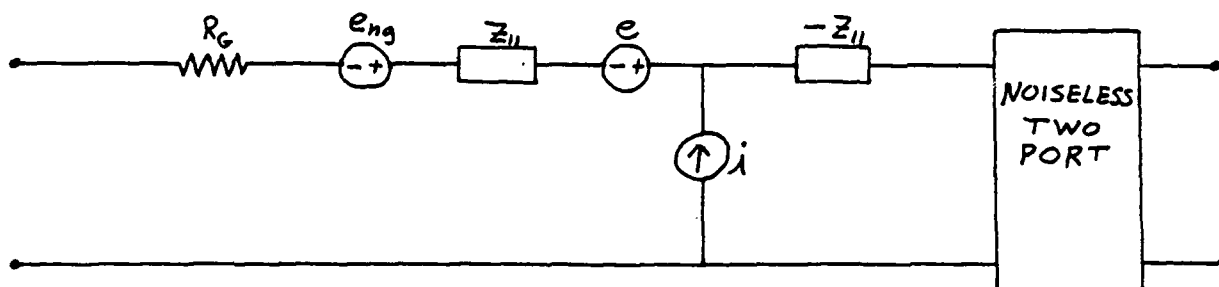
Fig. Three

Comparison of F_{min} from NEC data sheet
with F_{min} found using our analysis.

F_{min}
(ratio)

1.8

1.7

1.6

1.5

1.4

1.3

1.2

1.1

Blue – F_{min} from data sheet.

Green – F_{min} found using our analysis.
      Data range 2 – 18GHz.

Red – F_{min} found using our analysis.
      Data range 12 – 18GHz.

2   4   6   8   10   12   14   16   18   Freq. (GHz)

36-12
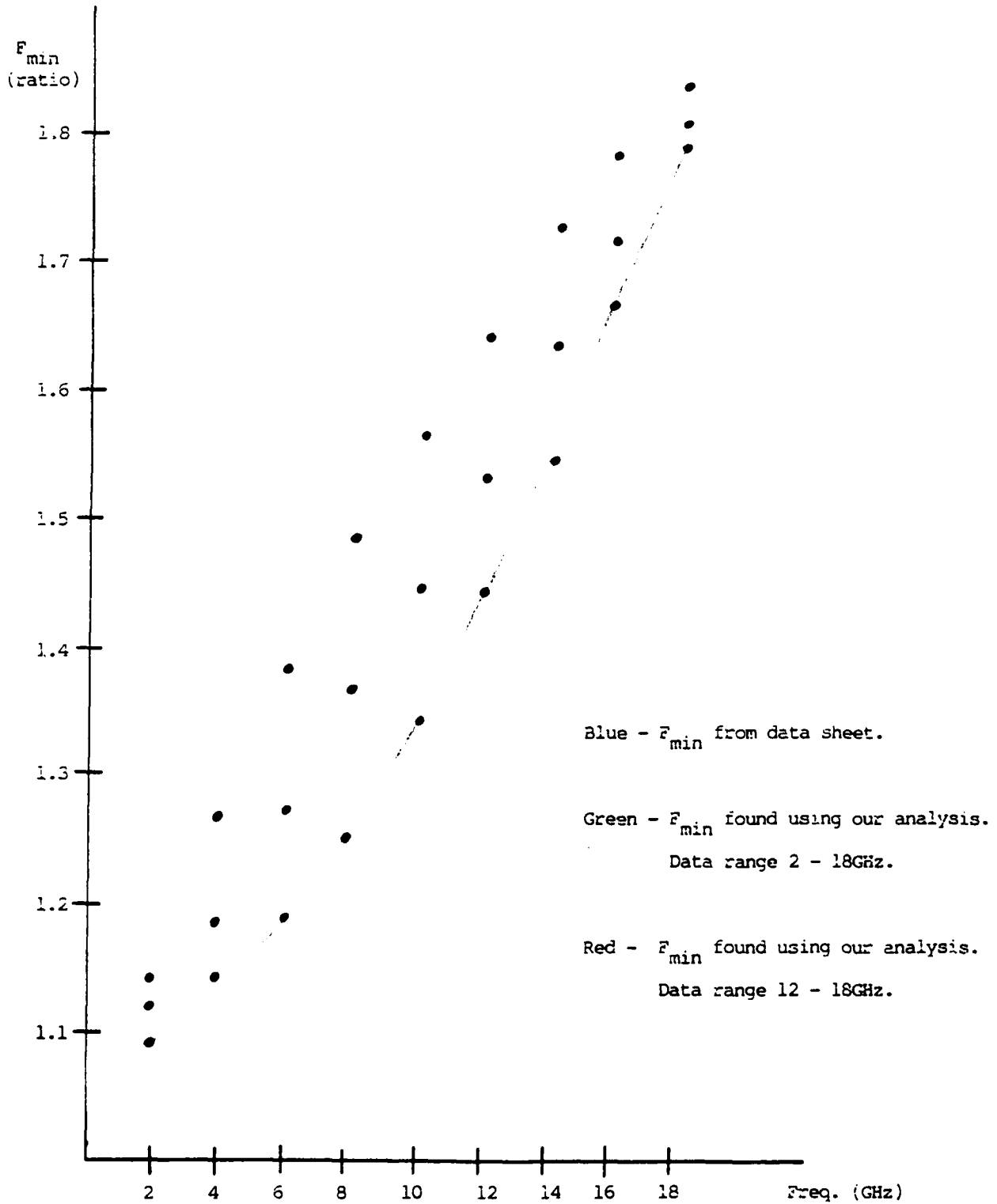
TABLE ONE

Frequency	F_{min} from NEC Data Sheet	F_{min} found using our analysis		
		Data Range: 2-18 GHz	Data Range: 10-18 GHz	Data Range: 12-18 GHz
2.0 GHz	.55 dB	.58 dB	.44 dB	.39 dB
4.0	.60	1.03	.83	.74
6.0	.80	1.40	1.18	1.06
8.0	1.00	1.70	1.49	1.35
10.0	1.30	1.95	1.76	1.62
12.0	1.60	2.16	2.01	1.86
14.0	1.90	2.34	2.24	2.09
16.0	2.20	2.50	2.45	2.30
18.0	2.50	2.65	2.63	2.49

REFERENCES

1. Lane, R. Q., "The Determination of Device Noise Parameters", Proc. IEEE, vol. 57, pp. 1461-1462, 1969.

2. Pospieszalski, M. W., "Modelling of Noise Parameters of MESFET's and MODFET's and Their Frequency and Temperature Dependence," IEEE Trans. Microwave Theory Tech., vol. MTT-37, pp. 1340-1350, Sept. 1989.

3. Gupta, M. S., O. Pitzalis, Jr., S. E. Rosenbaum, and P. T. Greiling, "Microwave Noise Characterization of GaAs MESFET's: Evaluation by On-Wafer Low Frequency Output Noise Current Measurement," IEEE Trans. Microwave Theory Tech., vol. MTT-35, pp. 1208-1218, Dec. 1987.

4. Gupta, M. S., and P. T. Greiling, "Microwave Noise Characterization of GaAs MESFET's: Determination of Extrinsic Noise Parameters," IEEE Trans. Microwave Theory Tech., vol. MTT-36, pp. 745-751, April, 1988.

5. Robertson, R. C., and T. Ha, "Optimum Noise Source Impedance Determination for GaAs FET's at Room and Cryogenic Temperatures," Int. Journal of Electronics, vol. 63, pp. 359-369, 1987.

6. Rothe, H., and W. Dahlke, "Theory of Noisy Fourpoles," Proc. IRE, vol. 44, pp. 811-818, 1956.

7. Pucel, R. A., H. A. Haus, and H. Statz, "Signal and Noise Properties of Galium Arsenide Field Effect Transistors," Advances Electron. Electron Phys., vol. 38, pp. 195-265, 1974.

8. Heinrich, W., "High Frequency MESFET Noise Modeling," IEEE Trans. Microwave Theory Tech., vol. MTT-37, pp. 836-842, May, 1989.

9. Van der Ziel, A., "Gate Noise in Field Effect Transistors at Moderately High Frequencies," Proc. IRE, pp. 461-467, Mar., 1963.

10. Cappy, A., and W. Heinrich, "High Frequency FET Noise Performance: A New Approach," IEEE Trans. Electron Devices, vol. 36, pp. 403-409, Feb., 1989.

11. Davidson, A., B. Leake, and E. Strid, "Accuracy Factors in Microwave Noise Parameter Measurements," 1989 International Microwave Symposium, vol. 2, pp. 827-830.

1989 USAF-UES SUMMER FACULTY RESEARCH PROGRAM

GRADUATE STUDENT RESEARCH PROGRAM

Sponsored by the

AIR FORCE OFFICE OF SCIENTIFIC RESEARCH

Conducted by the

Universal Energy System, Inc.

FINAL REPORT

Study of a Communication Receiver for Spread Spectrum Signals

Prepared by:	Donald R. Ucci, Ph.D. / Ernest Rho
Academic Rank:	Associate Professor / Graduate Student
Department and	Electrical and Computer Engineering Department
University:	Illinois Institute of Technology
Research Location:	RADC/DCCD
	Griffiss Air Force Base
	Rome, NY 13441
USAF Researchers:	Mr. John P. Patti and Mr. Stephen C. Tyler
Date:	September 28, 1989
Contract No:	F49620-88-C-0053

Same Report As
Prof. Donald Ucci
(Report # 77)

1989 USAF-UES Summer Faculty Research Program/
Graduate Student Research Program

Sponsored by the
AIR FORCE OFFICE OF SCIENTIFIC RESEARCH
Conducted by the
Universal Energy Systems, Inc.

FINAL REPORT

A Computer Model for Temporal Frequency Spectrum
of Vegetation Clutter Return

Prepared by: Jay K. Lee / Lynda Tomlinson
Academic Rank: Assist. Professor / Grad. Student
Department and   Electrical and Computer Engineering
University: Syracuse University
Research Location: Rome Air Development Center
                    Griffis AFB
                    Rome, NY 13441
USAF Researcher: Michael Wicks
Date: August 15, 1989
Contract No: F49620-88-C-0053

Same Report As
Prof. Jay Lee
(Report # 73)

1989 USAF-UES SUMMER FACULTY RESEARCH PROGRAM/

GRADUATE STUDENT RESEARCH PROGRAM

Sponsored by the

AIR FORCE OFFICE OF SCIENTIFIC RESEARCH

Conducted by the

UNIVERSAL ENERGY SYSTEMS, INC.

FINAL REPORT

NEURAL NETWORKS AND PARALLEL COMPUTATION OF FOURIER TRANSFORMS

Prepared By: John Wagnon

Academic Rank: Graduate Student

Department and   Electrical Engineering

  University: Oklahoma State University

Research Location:Rome Air Development Center
                  Griffiss Air Force Base, New York

USAF Researcher: Capt. Buzz Szarek

Date: September 1989

Contract No.:   F49620-88-C-0053

NEURAL NETWORKS AND PARALLEL COMPUTATION

OF FOURIER TRANSFORMS

by John Wagnon

Summer Graduate Fellow RADC/IRRA

Abstract

Computation of the Fourier Transform is a very common
preprocessing scheme in signal processing systems. An
implementation of the Discrete Fourier Transform based on
neural network design principles would take advantage of the
networks analog behavior and massive parallelism to compute the
transform in times one would expect to be orders of magnitude
faster than most conventional implementations. This paper
examines a neural design based on the error backpropagation
training rule, two based upon Hopfield network design
principles, and a final, direct form, design based intuitively
on the definition of the Discrete Fourier Transform. Only the
last two designs are deemed satisfactory upon close examination
and recommendations are made for comparing them. Finally, this
research clearly illustrates that not every problem is suitable
for a neural network solution.

Introduction

The Discrete Fourier Transform in some way forms the basis for the vast majority of digital signal processing schemes. Its importance to digital speech processing cannot be overestimated and, along with polar transformations, the discrete Fourier transform is a standard preprocessing scheme in many image processing systems. Because the number of computations required to calculate the Fourier transform increases as the square of the number of points in the transform, several algorithms for fast computation of the Fourier transform have been devised, the most popular of which is the Cooley-Tukey Fast Fourier Transform.

A parallel implementation of the Fourier transform would not suffer from the same time restrictions as sequential computation. If the implementation were completely parallel, the size of the transform would make little or no difference in the time required for computation. This paper discusses four massively parallel implementations of the discrete Fourier transform based on neural network design principles. This overview should serve as an initial resource for anyone considering an actual parallel hardware implementation of the discrete Fourier transform.

After summarizing the four neural designs, criticisms and recommendations for future research will be offered.

I. The Discrete Fourier Transform

The Discrete Fourier Transform (DFT) , F(k), of a discrete time signal, f(n), of length N samples is defined as

$$(I.1) \qquad F(k) = \sum_{n=0}^{N-1} f(n)e^{-j2\pi nk/N} ,$$

with the inverse transform defined as

$$(I.2) \qquad f(n) = 1/N \sum_{k=0}^{N-1} F(k)e^{j2\pi nk/N} .$$

The transform is a periodic sequence of complex numbers with period N that represents the frequency content of the discrete time signal. Converting the sequence to polar form reveals the magnitude and phase shift of each complex exponential frequency component. For many applications, only the magnitude data is retained. Another important aspect of the Fourier transform is that no new information is contained in F(k) beyond k = N / 2 as a consequence of the Nyquist sampling theorem. Therefore only the first N / 2 complex coefficients need to be calculated. When designing a system to compute the Fourier transform, whether in hardware or software, this bit of information allows the designer to save half the space or half the time required for the system.

Finally, by converting the complex exponential in the transform equation to rectangular form, the transform can be

converted into two transforms for the real and imaginary parts of F(k) as shown below in equation I.3.

$$(I.3) \qquad F(k) = \sum_{n=0}^{N-1} f(n)\cos(2\pi nk/N) - j \sum_{n=0}^{N-1} f(n)\sin(2\pi nk/N)$$

II. Learning Fourier Transforms by Error Backpropagation

Multi-layer feedforward networks trained by the error backpropagation algorithm suggested by Rumelhart et al. have been a watershed of adaptive neural networks research for the past few years. These networks learn what their outputs should be, given a certain input, by cyclically presenting a training set of sample input and output pairs and adjusting the weights based on the errors so that a gradient descent of the error surface is performed in weight space.

It has been shown that these adaptive networks are useful for pattern classification or recognitions and that, given certain constraints on the architecture of the network, they can be trained to approximate any continuous function in the range $[0,1]^m$ to any desired degree of accuracy.

Therefore, one approach to a neural implementation of the discrete Fourier transform would be to scale the coefficients between zero and one and train a net via error backpropagation.

To investigate the feasibility or desirability of such a scheme, a computer program was written in Turbo C to simulate an error backpropagation system. The program used a slightly

modified learning algorithm suggested by Vogl et al. that dynamically varies the learning parameters of the network based on how quickly the network learns the training set. This modified error backpropagation algorithm proved to be capable of learning functions from five to thirty times faster than the conventional backpropagation algorithm.

Several miscellaneous functions were devised to test the program including exclusive-or, a standard test for learning algorithms, the T-C-L-X identification problem, in which the network learns to identify rotated versions of the four letters, and a few other pattern classification problems. The networks learned all of these functions quickly, verifying the usefulness of the error backpropagation algorithm.

A program generated random 16 point DFT training sets consisting of 40, 60, and 80 examples. Only the 40 and 60 example training sets were used because of computer memory limitations (the simulations were being run on an AT compatible machine). These training sets were presented to single and double layer networks.

The single layer network learned to respond to the training set to within .067 rms error in 30 iterations through the training set, but another 280 iterations succeeded only in bringing the rms error down to .064. When presented with waveforms not represented in the training set, the rms error shot back up to .22. Using larger training sets resulted in no improvement and the single layer network was abandoned in favor of a double layer network chosen to satisfy the requirements

for a network to learn to approximate a function to any desired accuracy.

The double layered network fared slightly better and also exhibited some interesting properties. After 250 iterations through the 40 waveform training set, the rms error was down to .05. When presented with a different 40 waveform training set, the network's rms error increased immediately to .21 like the single layer network but tapered down to .02 at 650 iterations. When presented with still a different training set with 60 waveforms, the error again increased but this time only to .14 before training brought it down to .052 again after 150 iterations.

Subsequent presentations of new training sets resulted in lower and lower initial errors and slightly lower finishing errors after the same amount of training time. This leads one to speculate that a reasonably accurate discrete Fourier transform could be achieved using error backpropagation if a large enough training set were used or if enough different training sets were used subsequently. However, although there is no theoretical lower limit on how close a net can be trained to approximate a function, the error curve appears to be exponential decay. Graphical analysis corroborates this hypothesis. Hence the question becomes not how close can the network be trained but how long do you have to train the network. Once the initial knee of the learning curve has been passed, another thousand iterations may buy only a minute fraction more accuracy.

At this point it seems appropriate to make a few
observations about the effort to train a network to perform a
Fourier transform. Firstly, it isn't clear that an
implementation of a network trained by error backpropagation
could perform as accurately or as quickly as a conventional
Fast Fourier Transform (in hardware that is--a software
simulation is obviously inferior to the FFT). Secondly, the
amount of time required to train a hardware implementation of
the back propagation algorithm to perform a Fourier transform
could be prohibitive. And lastly, the actual computations
required to perform a DFT are well known, whereas back
propagation is often used in situations where no analytic
relationship between inputs and outputs of a function are
obvious or easily expressed.

These observations, when considered with the limited
results summarized above, make it seem that better results may
be achieved by approaching this problem analytically. The
following sections summarize three designs implementable using
analog electronics.

III. Fourier Transforms Using Hopfield Optimization Circuits

Dr. John Hopfield of CalTech has investigated certain
classes of neural systems and circuits since the early 1980's.
These networks, named for him, usually have one layer of fully
interconnected neurons. Dr. Hopfield found that certain cases
of these networks behaved according to Liapounov functions with

well defined local minima. Although much of his work

concentrates on using these networks as associative memories, a

1986 paper he published with David W. Tank of AT&T Bell

Laboratories discusses mapping optimization problems onto his

fully interconnected neural networks.

The Liapounov function the networks obey is a second order

function of the outputs and inputs of the network. If an

optimization problem can be expressed as a second order

minimization, then perhaps, after some rearrangement, the

optimization problem can be mapped onto the weights of a neural

network which will then function as an analog computer to solve

the problem. In their 1986 paper, Tank and Hopfield discuss

three applications of this technique: an A/D converter, a

signal decision circuit, and a linear programming circuit.

The first two examples involve translating the problem

into a least squared error minimization problem from which the

weights for the neural network can easily be determined by

analogy between the least squared error equation that must be

minimized and the Liapounov function which the network will

minimize.

In the final example, the topology of the network is

changed slightly, resulting in a new Liapounov function which,

it is shown, makes the network suitable for solving linear

programming problems where the inputs to the network are the

variables and constraints, the weights represent the cost

function to be optimized, and the outputs are the independent

variables which are to be adjusted so that the cost function is

'optimal'.

These analog optimization circuits may be useful for neural computation of the discrete Fourier transform. In the 1986 Hopfield and Tank paper, a discussion of the signal decision circuit addresses just that problem. The signal decision network will, given an analog input vector, provide a binary output vector where each bit corresponds to the presence of a certain waveform or pulse shape. The input weights are determined by the functions themselves and the interconnection weights are determined by the dot products of the functions of interest with each other. In this way the network determines not only how well the inputs match certain functions but how much better one subset of the basis functions will work than another subset.

The network will function for orthogonal or nonorthogonal basis functions, but, interestingly enough, for orthogonal basis functions (such as those used for calculating the Fourier transform of a sequence) the feedback connections disappear and the input weights reduced to the basis functions. This reduces the network to a thresholded transform. The inputs to the neurons are the dot product of the basis functions with the input sequence and each neuron thresholds this value so that if a certain component has a great enough magnitude, the corresponding output bit goes high.

One may implement this circuit using standard analog electronics (transistors, capacitors, resistors), making this an attractive alternative to the feedforward net discussed

above. It isn't even apparent that the backpropagation

training algorithm is easily implementable in hardware, while

the component values for this circuit are determined

analytically a priori. However, Hopfield's signal decision

circuit does not perform a Fourier transform, it merely

indicates which frequencies are present in a waveform. In a

sense, it is thresholded, or clipped, Fourier transform.

The Linear Programming Network, also described in Hopfield

and Tank's 1986 paper, may also be applied to the neural

transform problem. Culhane, Peckerar, and Marrian propose

using the network to optimize the cost function

(III.3) $E = (\alpha/2) |Dv - b|^2 + (1/\beta R)|v|^2$,

where D is the inverse transformation matrix, v is the output

vector, and b is the input vector, and the other factors are

constants. The first term will go to zero if the correct

transformation is performed and the second term represents the

error intrinsic to this network.

Culhane et al. report some interesting properties of this

circuit. Both the convergence time and the error decrease as

the size of the transform increases, and convergence is always

guaranteed as long as the amplifiers used meet a loose speed

criteria. See the original paper for a discussion of that

requirement. They also address some of the problems that will

be encountered when actually fabricating the connection matrix

needed for the circuit.

However, they totally ignore the amplifier design, assuming the amplifiers all to be linear, also, unlike most Hopfield nets, the connection matrix is not a matrix of conductances, but actually a matrix of multiplicative weights. These, they suggested be implemented using the familiar inverting summer op-amp configuration, doubling the number of yet undesigned amplifiers needed for the circuit. Finally, they designed the optimization network to perform the Hartley transform with the intent to use a bank of adders to derive the Fourier transform from it, adding another layer of amplifiers to the circuit.

While the computer simulation results reported by Culhane et al. verify thei· design's performance and its improvement as the size of the transform is increased, it seems that the complexity and cost (not to mention inconvenience--the input to the circuit is a vector of currents, probably requiring a layer of preprocessing to convert from sampled voltage to current) should buy something more than an approximation of the desired transform, albeit a very close one.

III. An Alternative Design and Recommendations.

A simple alternative to these designs could be realized in analog electronics easily. If one remembers that the Discrete Fourier Transform is a linear transformation (in rectangular form) it seems obvious that a single bank of summers could be used to implement the transform directly. While this circuit

would suffer from the same limitations on the connection matrix

as the previously described designs, it would not have the

limitations imposed by mapping the linear transformation onto a

highly nonlinear neural network. Although the convenient

inverting summer configuration would result in the negative of

the Fourier transform, this could be compensated for by

whatever system is using the Fourier information.

The next step in this effort would be to compare the

performance of the direct form realization of the DFT described

above to the Linear Programming Circuit implementation

described in the previous section. These two circuits seem

closest to actually usable designs and they also come closest

to performing the correct transformation. A circuit analysis

software package such as SPICE would be necessary for this

comparison and things such as parameter variation, defective

components, power consumption, cost in terms of chip space, and

noise must be taken into account. Lastly, some thought must be

given to what type of circuitry must be created to drive the

DFT circuit and also what kind of computer or device is the DFT

circuit going to drive. It may very well be that the speed of

the A/D converters likely to be used on the output of the DFT

circuit would make the speed up provided by parallelism a

wasted effort.

IV. Conclusions

Upon reviewing the efforts to design a neural network to perform a Discrete Fourier Transform described above, it might be useful to remember the qualities that make neural networks of interest. In general, neural networks perform rough, massively parallel, analog computation. They are expected to be very noise, error, and damage tolerant and to exhibit associative, or inductive, human-like qualities. Since they take their inspiration from biological neurons, it makes sense to expect them to perform well in those areas that biological neurons perform well.

It isn't at all apparent that even a well trained signal processing expert could look at a raw signal and do more than indicate roughly which harmonic components are present. Even the eyes and ears which routinely distinguish between different frequencies of light and sound employ what amount to filter banks to put the sensory data into a more manageable form. It seems strange therefore to expect artificial neural systems to be able to compute the DFT of a signal any better than conventional systems, if even that well. The only advantage a neural network would have over a conventional algorithm would be that the neural network would be completely parallel and therefore much faster. Of course, if a neural DFT system was to feed a sequential machine, the speed advantage gained by implementing the transform in parallel could very well be wasted by the amount of time it takes the cascaded machine to

process or even retrieve the information.

So, in conclusion, the result, or moral, of this research seems to be that the form of the Fourier transform is a well known, linear computation while neural systems seem best suited for ambiguous and highly non-linear problems. If a parallel implementation of a Fourier transform is desired, then one should simply implement the transform in parallel and not complicate the issue by searching for a solution among a class of systems not at all suited to the problem.

While artificial neural systems are very interesting and appear to be very useful as solution to problems in pattern recognition and other, similar arenas where noise and error tolerance and associative behavior is important, one must remember that they are not good for everything and conventional solutions must always be kept in mind to measure neural systems against.

Acknowledgements

This paper has summarized the results of research
performed in the summer of 1989 at Rome Air Development Center,
Image Systems Division, Griffiss Air Force Base, Rome, New
York. To try to separate my work from that performed by the
rest of the Neural Networks Group and Battlefield Intelligence
Branch would be to denigrate the spirit of cooperation and team
work that developed between us all as the summer advanced.

I would like to personally thank Dr. Jim Wolper of
Hamilton College for his constant encouragement, companionship
and help throughout the research and in particular for his
analysis of the backpropagation error curves my simulations
generated. I also want to recognize and thank Captain William
(Buzz) Szarek for his friendship and for his enthusiastic and
sincere management of the neural networks research effort.

Those also deserving credit here are Major Bob Russell,
who initiated the RADC neural networks effort, Bill McClellan,
who got saddled with us and made the best of it, and David
Froehlich, Scott Shyne, Scott Huse, Ken Taylor, and Lt. Greg
Ahlquist, the rest of the Neural Networks Group, who served as
sounding boards, resources, and friends throughout the summer
research effort.

References

1. Ludeman, Lonnie C., <u>Fundamentals of Digital Signal Processing</u>, New York, NY, Harper & Row, Publishers, Inc., 1986.

2. Rumelhart, D.E., Hinton, G.E., Williams,R.J., "Learning Internal Representations by Error Backpropagation," from Rumelhart, McClelland and the PDP Research Group (eds) <u>Parallel Distributed Processing</u>, vol 1, chap 8, Cambridge, MS, MIT Press, 1986.

3. Hecht-Nielsen, Robert, "Theory of the Backpropagation Neural Network," *presented by invitation* at the September 1988 INNS Annual Meeting.

4. Vogl, T.P., Mangis, J.K., Rigler, A.K., Zink, W.T., and Alkon, D.L., "Accelerating the Convergence of the Back-Propagation Method," <u>Biological Cybernetics</u>, Volume 59, pp. 257-263.

5. Tank, David W., and Hopfield, John J., "Simple 'Neural'
    Optimization Networks: An A/D Converter, Signal Decision
    Circuit, and a Linear Programming Circuit," IEEE Trans. on
    Circuits and Systems, Volume CAS-33, No. 5, May 1986, pp.
    533-541.

6. Culhane, Andrew D., Peckerar, Martin C., Marrian, C.R.K.,
    "A Neural Net Approach to Discrete Hartley and Fourier
    Transforms," IEEE Trans. on Circuits and Systems, Volume
    36, No. 5, May 1989, pp. 695-703.

1989 USAF-UES SUMMER FACULTY RESEARCH PROGRAM/

GRADUATE STUDENT RESEARCH PROGRAM

Sponsored by the

AIR FORCE OFFICE OF SCIENTIFIC RESEARCH

Conducted by the

Universal Energy Systems, Inc.

<u>FINAL REPORT</u>

<u>AN EXPERIMENTAL PROTOCOL FOR LINE-OF-SIGHT SLEWING,</u>

<u>OPTICAL ALIGNMENT AND AFT BODY STATION KEEPING CONTROL EMULATION</u>

Prepared by:	Thomas A. W. Dwyer, III	(1)
	<u>David S. Andreshak</u>	(2)
	Toby B. Martin	(2)
Academic Rank:	Professor	(1)
	Graduate Student	(2)
Department and	Aero/Astro Engineering Department	
University:	University of Illinois	
Research Location:	WL/ARCD Kirtland AFB Albuquerque, NM 87117-6008	
USAF Researcher:	Mr. David Founds	
Date:	4 August 89	
Contract No:	F49620-88-C-0053	

Same Report As
Prof. Thomas Dwyer
(Report # 81)

1989 USAF-UES SUMMER FACULTY RESEARCH PROGRAM

GRADUATE STUDENT RESEARCH PROGRAM

Sponsored by the

AIR FORCE OFFICE OF SCIENTIFIC RESEARCH

Universal Energy Systems, Inc.

FINAL REPORT

SCATTERING OF ELASTIC WAVES IN A RANDOM

INHOMOGENEOUS SOIL MEDIA

Prepared by:	Duane R. Sanders, Ph.D
	Robert W. Bolton, M.S.
Academic Rank:	Assistant Professor
	Lecturer
Department and	Civil Engineering Department
University:	Texas A&M University
Research Location:	WL/NTESG
	Kirtland AFB
	Albuquerque, NM 87117-6008
USAF Researcher:	Dr. Robert Reinke
Date:	12 Aug 89
Contract No:	F49620-88-C-0053

Same Report As
Prof. Duane Sanders
(Report # 86)

1989 USAF-UES SUMMER FACULTY RESEARCH PROGRAM

GRADUATE STUDENT RESEARCH PROGRAM

Sponsored by the

AIR FORCE OFFICE OF SCIENTIFIC RESEARCH

Conducted by

Universal Energy Systems, Inc.

FINAL REPORT

MODELING THE RESPONSE OF PRESSURIZED COMPOSITE CYLINDERS TO LASER DAMAGE

Prepared by: Harry A. Hogan, Ph.D.
                    Stuart J. Harbert, M.S.

Academic Rank: Assistant Professor
                    Graduate Assistant

Department and   Department of Mechanical Engineering

  University: Texas A & M University

Research Location: WL/TALE
                    Kirtland Air Force Base
                    Albuquerque, NM 87117

USAF Researchers: Mr. Jorge Beraun
                    Dr. Pat Vail

Date: 26 July 1989

Contract No: F49620-88-C-0053

Same Report As
Prof. Harry Hogan
(Report # 84)

1989 USAF-UES SUMMER FACULTY RESEARCH PROGRAM/

GRADUATE STUDENT RESEARCH PROGRAM

Sponsored by the

AIR FORCE OFFICE OF SCIENTIFIC RESEARCH

Conducted by the

Universal Energy Systems, Inc.

<u>FINAL REPORT</u>

<u>AN EXPERIMENTAL PROTOCOL FOR LINE-OF-SIGHT SLEWING,</u>

<u>OPTICAL ALIGNMENT AND AFT BODY STATION KEEPING CONTROL EMULATION</u>

Prepared by:	Thomas A. W. Dwyer,III	(1)
	David S. Andreshak	(2)
	<u>Toby B. Martin</u>	(2)
Academic Rank:	Professor	(1)
	Graduate Student	(2)
Department and	Aero/Astro Engineering Department	
University:	University of Illinois	
Research Location:	WL/ARCD Kirtland AFB Albuquerque, NM 87117-6008	
USAF Researcher:	Mr. David Founds	
Date:	4 August 89	
Contract No:	F49620-88-C-0053	

Same Report As
Prof. Thomas Dwyer
(Report # 81)

1989 USAF–UES SUMMER FACULTY RESEARCH PROGRAM

GRADUATE STUDENT RESEARCH PROGRAM

Sponsored by the

AIR FORCE OFFICE OF SCIENTIFIC RESEARCH

Conducted by the

Universal Energy Systems, Inc.

FINAL REPORT

GPS TIME SYNCHRONIZATION

Prepared by:	Walter Cyrus McCarter, M.A.
Academic Rank:	Graduate Student
Department and University:	Department of Mathematics North Carolina State University
Research Location:	WL/AWPP Kirtland AFB Kirtland, NM 87117
USAF Researcher:	Dr. Warner A. Miller
Date:	September 18, 1989
Contract No:	F49620-88-C-0053

GPS TIME SYNCHRONIZATION

by

Walter Cyrus McCarter

ABSTRACT

Precise global clock synchronization is an integral part of the Global Positioning System (GPS) operations. The GPS satellites' clocks are moving with respect to the clocks of the surface stations observers at speeds sufficient to necessitate careful consideration of special relativistic effects on the synchronization of the clocks. At the same time, the GPS satellite orbit radii are large enough to cause a sufficient difference between gravitational potentials at the satellite clocks and at the surface station clocks to produce an effect on the clocks synchronization of the same order of magnitude as the special relativistic effects. A consistent treatment of both effects can be done only in general relativity.

We have performed a general relativistic analysis of the GPS time transfer effects. The expressions obtained for the effects admit an unambiguous physical interpretation of each term, which clarifies the physical origin of effects.

ACKNOWLEDGMENTS

I. INTRODUCTION.

Proper operation of the satellite–based Global Positioning System (GPS) imposes increasingly demanding requirements on global clock synchronization. Such synchronization requires taking into account both special relativistic effects and effects caused by the earth's gravitational field. A consistent treatment of both kinds of effects can be performed only within the framework of general relativity.

Meanwhile, almost all previous attempts to resolve the problem were undertaken within the framework of special relativity. There were also considerable differences in results obtained by different researchers evaluating the special relativistic effects, and some apparent confusion concerning the formulation of the problem.

The Space-Time Physics Group of the Advanced Concept Branch of the USAF Weapons Laboratory at Kirtland Air Force Base recognized that a general relativistic solution of the problem was necessary. They therefore hired Dr. Arkady Kheyfets to do an investigation of the general aspects of the problem. He looked at a simple situation and determined the basic physics involved. Since I have worked on mathematical physics with two of the best relativists in the world, Dr. John A. Wheeler and Dr. Arkady Kheyfets, it was a safe bet that I could do the calculations necessary to extend Dr. Kheyfets' work to the general situation, which, for the most part, I have.

II. OBJECTIVES OF THE RESEARCH EFFORT

The GPS constellation will someday contain 18 clocks (with 3 active spares) moving with respect to each other. The GPS satellites will have near circular orbits of 4 earth radii, with 12–hour periods, which means that the satellite velocity will be ~ 8 times the velocity of the surface station observer. The required precision of clock synchronization necessitates taking into account special relativistic effects on the rate of the clocks. In addition, all aspects of GPS occur in the earth's gravitational field with the positions of the clocks having different gravitational potentials. The gravitational influence of the field on the clocks rate is determined by the parameter $\frac{M_{\oplus}}{r}$ which produces an effect of the same order of magnitude as the second order special relativistic effects. A consistent treatment of both effects together can be done only within the framework of general relativity.

My objectives for the research effort are:

(1) to find the correct general relativistic expression for the Doppler shift in the earth's gravity field up to the second order;

(2) to clearly state the principles involved in the problem of global clock synchronization in the earth's gravitational field;

(3) to formulate and give one solution to the problem of global clock synchronization in the earth's gravitational field, to relevant order;

(4) to discuss the observable parameters needed to carry out the synchronization and the problem of finding a valid measurement procedure for these parameters.

III. DOPPLER SHIFT IN THE SCHWARZSCHILD FIELD.

We use Schwarzschild geometry as the model of the earth's gravitational field. The estimate of the Schwarzschild parameters shows that the effect of $\frac{M_{\oplus}}{r}$ is of the same order as effects of the squares of the relevant velocities. Thus, to discuss the Doppler shift up to the second order in velocity, we can use Schwarzschild geometry

as a model of the earth's gravitational field and, provided that we retain terms proportional to $\frac{M_\otimes}{r}$, we obtain a satisfactory expression for the Doppler correction.

The Schwarzschild geometry is a static spherically symmetric geometry. Its metric in Schwarzschild coordinates is given by the expression[1]

$$ds^2 = -\left(1 - \frac{2M_\otimes}{r}\right) dt^2 + \left(1 - \frac{2M_\otimes}{r}\right)^{-1} dr^2 + r^2 \left(d\theta^2 + \sin\theta d\phi^2\right), \quad (1)$$

where t, r, θ, and ϕ are Schwarzschild coordinates, $M_\otimes$ is the earth mass, and the speed of light and gravitational constant are set equal to unity.

Figure 1 describes the Doppler shift of an electromagnetic signal sent from the transmitting satellite to the surface observer. The free falling satellite has a geodesic world line, whereas the observer, being attached to the earth, does not[2]. A Doppler shift arises since the 4–velocity of the satellite (at the moment of signal transmission) and the 4–velocity the observer (at the moment of receiving) are not parallel. Parallel transport of the satellite 4–velocity along the null geodesic connecting the event of transmitting and the event of receiving does not coincide with the 4–velocity of the observer.

The frequency shift can be expressed in terms of the 4–velocities of the satellite and the observer and the 4–momentum of the photon traveling from the satellite to the observer

$$\mathcal{D} = \frac{\nu_S - \nu_O}{\nu_S} = \frac{{}_S P_\mu V_S^\mu - {}_O P_\mu V_O^\mu}{{}_S P_\mu V_S^\mu}, \quad (2)$$

where V_S^μ, V_O^μ are the 4–velocities of the satellite and the observer and ${}_S P_\mu$, ${}_O P_\mu$ are the photon 4–momentum at the event of transmitting and the event of receiving, respectively. The 4–momentum of the photon is parallel transported along the null geodesic connecting the events of transmitting and receiving and is tangent to the null geodesic at all times.

Let us calculate the Doppler shift up to the second order using the tensor series expansion of the world function[2], developed by J. L. Synge. Following J. L. Synge we introduce new coordinates $(x^\mu)_{\mu=0,1,2,3}$ related to the Schwarzschild coordinates

as follows

$$x^0 = t, \quad x^1 = r \sin\theta\cos\phi, \quad x^2 = r\sin\theta\sin\phi, \quad x^3 = r\cos\theta. \qquad (3)$$

The metric tensor in these coordinates can be expressed as the sum $g_{\mu\nu} = \eta_{\mu\nu} + \gamma_{\mu\nu}$, where $\eta_{\mu\nu} = \text{diag}(-1,1,1,1)$ and $\gamma_{\mu\nu}$ are small and static ($\gamma_{\mu\nu,0} = 0$). Coordinates (x^μ) are very convenient for a pictorial representation of the Doppler shift. In Fig. 2 these coordinates are used as coordinates of a Euclidean space. Of course, in this space the geodesics of the original Schwarzschild space do not always look like straight lines. The world line of the satellite in this picture is geodesic but looks curved. The vertical straight lines are the integral lines of the timelike Killing vector field of the Schwarzschild metric (described by the equations $x^i = \text{const}$, $i = 1,2,3$). The satellite and the observer are moving with respect to Schwarzschild coordinates, so that the 4–velocities V_S, V_O are not parallel to the Killing vectors $\frac{\partial}{\partial t} = \frac{\partial}{\partial x^0}$. The angles between V_S, V_O and Killing vectors $\frac{\partial}{\partial t}$ (directed upward) are different and determined by the satellite and the observer orbital velocities. If the satellite and the observer were at rest with respect to Schwarzschild coordinates (in which case their world lines would be pictured as vertical straight lines), we would get for the Doppler shift

$$\mathcal{D} = \frac{M_\otimes}{R_S} - \frac{M_\otimes}{R_O}. \qquad (4)$$

The right hand side of the (4) is often called the gravitational Doppler shift. It is of the second order and should be expected to appear as one of the terms in the final result.

In fact, the final result for the Doppler shift up to the second order is

$$\mathcal{D} = (V_O^i - V_S^i)\frac{\Delta x^i}{\Delta t} + (V_O^i - V_S^i)\frac{\Delta x^i}{\Delta t}V_S^k\frac{\Delta x^k}{\Delta t} + \left(\frac{M_\otimes}{R_S} - \frac{M_\otimes}{R_O}\right) + \frac{1}{2}(V_S^i V_S^i - V_O^i V_O^i) \quad (5)$$

where $i,k = 1,2,3$, $\Delta x^i = x_O^i - x_S^i$, $\Delta t = x_O^0 - x_S^0$, and summation over repeating indices is assumed.

The first two terms in this expression are the first order Doppler shift and the second order correction to the first order term. The third term is the gravitational

Doppler shift (4). The last term can be called the centrifugal correction term, because, in a classical picture of circular orbits, the term can be thought of as the difference of potentials of centrifugal forces caused by angular velocities of the satellite and the observer orbital motion. The physical origin of the last term in the general case is motion of the satellite and the observer with respect to Schwarzschild coordinates.

IV. GLOBAL CLOCK SYNCHRONIZATION IN SCHWARZSCHILD FIELD

The relation between the clock rates and the Doppler shift is established[1,2] via relation (Fig. 3)

$$\mathcal{D} = \frac{\nu_S - \nu_O}{\nu_S} = 1 - \frac{\nu_O}{\nu_S} = 1 - \frac{d\tau_S}{d\tau_O} \tag{6}$$

or

$$d\tau_S = (1 - \mathcal{D})d\tau_O \tag{7}$$

However, a closer look at this formula and at Fig. 3 makes it obvious that the infinitesimal interval of the satellite and the observer proper times ($d\tau_S$, $d\tau_O$) are measured at different Schwarzschild times. A more precise form of (7) would look as follows

$$(d\tau_S)_{t_t} = (1 - \mathcal{D})(d\tau_O)_{t_r} \tag{8}$$

where t_t and t_r are Schwarzschild times of transmitting and receiving of the signal. The retardation of t_r compared to t_t is reflected in (5) by the structure of the first order term and the second order correction to the first order term.

The above procedure of comparing the proper time rates of two clocks in general relativity is the only one (up to equivalence) that is correct for arbitrary gravitational fields. Generally speaking, it will work only for two clocks (and under some reasonable conditions). In a general enough gravitational field (with no symmetries) it will not provide global synchronization for more than two clocks. This is not a drawback of this particular procedure. In general relativity the global syn-

chronization of clocks in a gravitational field with no symmetries is impossible in principle.

However, our model gravitational field of the earth (Schwarzschild field) is very symmetric (static, spherically symmetric). In this particular case our procedure will do the job. So will many others. The task is to find the simplest one. For instance, one would like to minimize time dependent contributions like the first two terms of (5). It would be good to have all the clocks show Schwarzschild coordinate time, i. e. the time of an observer placed at spatial infinity and resting with respect to Schwarzschild coordinates. Schwarzschild coordinate time is the closest possible analog of ECI time; the special relativistic limit of the Schwarzschild coordinate frame coincides with the ECI frame.

To do this, compare the rates of the clocks of the satellite and the observer with Schwarzschild clocks at the same Schwarzschild time (Fig. 4). Elementary calculations show that, to order $M_\otimes over R$,

$$(d\tau_S)_t = \left(1 - \frac{2M_\otimes}{R_S}\right)^{\frac{1}{2}} \left(1 - V_{S\perp}^2\right)^{\frac{1}{2}} dt \tag{9}$$

$$(d\tau_O)_t = \left(1 - \frac{2M_\otimes}{R_O}\right)^{\frac{1}{2}} \left(1 - V_{O\perp}^2\right)^{\frac{1}{2}} dt \tag{10}$$

where $V_{O\perp}$ ($V_{S\perp}$) is the component of the observer's (satellite's) 4–velocity V_O (V_S) orthogonal to the timelike Killing vector field of the Schwarzschild metric.

First let us look at the case of coplanar circular orbits about the equator. Namely, we assume that R_O, $V_{O\perp}^2$, R_S, $V_{S\perp}^2$ are constant. In this case both $d\tau_O$ and $d\tau_S$ are proportional to dt with constant proportionality coefficients. Thus one can take as fundamental any of them (the different choices are equivalent to the different choices of time units). Dividing (9) by (10), we obtain

$$(d\tau_S)_t = \frac{\left(1 - \frac{2M_\otimes}{R_S}\right)^{\frac{1}{2}} \left(1 - V_{S\perp}^2\right)^{\frac{1}{2}}}{\left(1 - \frac{2M_\otimes}{R_O}\right)^{\frac{1}{2}} \left(1 - V_{O\perp}^2\right)^{\frac{1}{2}}} (d\tau_O)_t \tag{11}$$

or, in the usual second order approximation,

$$(d\tau_S)_t = \left[1 - \left(\frac{M_\otimes}{R_S} - \frac{M_\otimes}{R_O}\right) - \frac{1}{2}\left(V_{S\perp}^2 - V_{O\perp}^2\right)\right](d\tau_O)_t \qquad (12)$$

which is interesting to compare with (5) (note the loss of the terms related to the time delay).

Integration of (11) yields

$$\tau_S = \frac{\left(1 - \frac{2M_\otimes}{R_S}\right)^{\frac{1}{2}}\left(1 - V_{S\perp}^2\right)^{\frac{1}{2}}}{\left(1 - \frac{2M_\otimes}{R_O}\right)^{\frac{1}{2}}\left(1 - V_{O\perp}^2\right)^{\frac{1}{2}}}\tau_O + C \qquad (13)$$

The constant of integration C can be made equal to zero by employing an appropriate choice of the origin for τ_O, τ_S. We will show one way to do it for the particular case of equatorial observer , coplanar equatorial satellite, and the orbit period shorter than the period of earth rotation. Let us suppose now that the ground observer is sending his clock time continuously straight upward along radial null geodesics. Then the Schwarzschild travel time of the signal is

$$\Delta t = R_S - R_O + 2M_\otimes \ln \frac{R_S - 2M_\otimes}{R_O - 2M_\otimes} \qquad (14)$$

Thus, if the satellite receives the ground station message sent at $\tau_O = \tilde{\tau}_O$ and, at the moment of receiving, sets on its clock time

$$\tilde{\tau}_S = \left(1 - \frac{2M_\otimes}{R_S}\right)^{\frac{1}{2}}\left(1 - V_{S\perp}^2\right)^{\frac{1}{2}}\left[\left(1 - \frac{M_\otimes}{R_O}\right)^{-\frac{1}{2}}\left(1 - V_{O\perp}^2\right)^{-\frac{1}{2}}\tilde{\tau}_O + \Delta t\right] \qquad (15)$$

then the event on the world line of the satellite at $\tau_S = 0$ and on the world line of the observer at $\tau_O = 0$ become simultaneous with respect to Schwarzschild time. If we choose as $t = 0$ the Schwarzschild time hypersurface passing through both events, then at any Schwarzschild moment of time t the clock of the observer and the satellite will show

$$\tau_O = \left(1 - \frac{2M_\otimes}{R_O}\right)^{\frac{1}{2}}\left(1 - V_{O\perp}^2\right)^{\frac{1}{2}}t \qquad (16)$$

and

$$\tau_S = \left(1 - \frac{2M_\otimes}{R_S}\right)^{\frac{1}{2}} \left(1 - V_{S\perp}^2\right)^{\frac{1}{2}} t \tag{17}$$

making it possible to tell Schwarzschild time by looking at either clock.

The constant C in (13) thus becomes equal to zero. The described procedure allows us to synchronize to Schwarzschild time as many clocks as one wishes and can be generalized easily to any placement of the observer on earth any satellite orbit inclination (only expression for Δt will become more complicated). We will derive these more complicated expressions in the next section.

V. RATES OF CLOCKS FOR THE GENERAL CASE

Let us go back to eqs. (9) and (10) for the rates of clocks. In the general case of arbitrary but fixed earth observer and an arbitrary elliptical satellite orbit , we need to find expressions for $R_\mathcal{O}(t)$ and $R_S(t)$. Let us use conservation of energy in Schwarzschild form to redefine eqs. (9) and (10).

$$d\tau_\mathcal{O} = dt \left(1 - \frac{2M_\otimes}{R_\mathcal{O}(t)}\right) (\overline{E_\mathcal{O}})^{-1} \tag{18}$$

$$d\tau_S = dt \left(1 - \frac{2M_\otimes}{R_S(t)}\right) (\overline{E_S})^{-1} \tag{19}$$

$$\overline{E} = \left(1 - \frac{2M_\otimes}{R}\right)^{\frac{1}{2}} (E_\mathcal{L}) \tag{20}$$

$\overline{E}$ is a constant called the Schwarzschild "energy at infinity" since it can be related to what a Schwarzschild observer at spatial infinity would measure for the energy of an earth observer or orbiting satellite. $E_\mathcal{L}$ is the energy a local Schwarzschild observer would measure.

For an earth observer at fixed latitude and longitude we find ;

$$R_\mathcal{O}(t) = R_{\text{earth}} = \text{constant} \tag{21}$$

$$\theta_\mathcal{O} = \text{constant} \tag{22}$$

$$\frac{d\phi_{\mathcal{O}}}{dt} = \text{constant} \tag{23}$$

a circular spiral in time.

For a satellite in an elliptical orbit about the equator we find,

$$\theta_S = \frac{\pi}{2} \tag{24}$$

$$R_S(\phi_S) = \frac{(1-e^2)a}{1+e\cos(\phi_S+\varepsilon)} \tag{25}$$

$$t_S(R_S) = \Lambda(R_S) + \Upsilon \sin^{-1}\left[\frac{2(M_\otimes^2 - \overline{L}^2)R_S - 2M_\otimes(1 - 2\overline{E_S}^2)}{(-\omega)^{\frac{1}{2}}}\right] \tag{26}$$

$$\Lambda(R_S) = \frac{\left[-(1-\overline{E_S}^2)R_S^2 - 2M_\otimes(1-2\overline{E_S}^2)R_S + (6M_\otimes^2 - \overline{L}^2)\right]^{\frac{1}{2}}}{6M_\otimes^2 - \overline{L}^2} \tag{27}$$

$$\Upsilon = \frac{M_\otimes(1-2\overline{E_S}^2)(1-\overline{E_S}^2)}{(\overline{L}^2 - 6M_\otimes^2)^{\frac{3}{2}}} - \frac{4M_\otimes\overline{E_S}}{(\overline{L}^2 - 6M_\otimes^2)^{\frac{1}{2}}} \tag{28}$$

$$\omega = -4(6M_\otimes^2 - \overline{L}^2)(1-\overline{E_S}^2) \tag{29}$$

$$a = M_\otimes(2\overline{E_S}^2 - 1)(1-\overline{E_S}^2)^{-1} \tag{30}$$

$$1 - e^2 = \left(\frac{\overline{L}}{M_\otimes}\right)^2 (1-\overline{E_S}^2)\left(1 + 4(1-\overline{E_S}^2) - 6\left(\frac{M_\otimes}{\overline{L}}\right)^2\right) \tag{31}$$

$$\varepsilon = -2\pi\left(\frac{M_\otimes}{\overline{L}}\right)^2 \tag{32}$$

where $\overline{L}$ is a constant representing the Schwarzschild angular momentum as measured by a fixed Schwarzschild observer at spatial infinity. Here e and a are called the Schwarzschild eccentricity and semi–major axis respectively. Inverting (25) would give us $R_S(t)$. To get an arbitrary elliptical satellite orbit we need only rotate the plane of the equatorial orbit to the plane of the desired orbit. The formulas for $R_{\mathcal{O}}(t)$ and $R_S(t)$ could then be substituted into (18) and (19) to determine the rates of the earth observer and satellite clocks as a function of Schwarzschild time.

VI. INITIAL SYNCHRONIZATION FOR THE GENERAL CASE

Global clock synchronization for the case of coplanar equatorial circular orbits was discussed in section IV. covering general principles. The general case is just a matter of using the more complicated expressions for R_O and R_S along with properly propagating a null (light) signal between the earth observer and satellite in a Schwarzschild field. This null signal no longer travels along a radial null geodesic so the propagation is not trivial. However, a propagation procedure can be established and the above principles for synchronization can be carried over completely. The synchronization method itself remains valid, despite the more complicated formulas.

Still, having noncoplanar (with respect to the earth observer) elliptical satellite orbits has brought forth two problems. First, we have not discussed in detail the null signal propagation. For the general case this procedure needs to be developed, and the author can certainly do so, but it is beyond the scope of the present research and the length of this paper. Second, having valid formulas is quite different from using properly measured, general relativistically valid parameters in the formulas. We have a valid synchronization procedure and valid formulas but the parameters being supplied to the theory are not necessarily valid. We will discuss what difficulties this second problem can cause in the next section.

VII. THEORETICAL AND OBSERVABLE PARAMETERS.

In the above sections of this report, the formulas necessary to carry out the determination of the rates of clocks in a Schwarzschild field have been given to order v^2 and $\frac{M_\oplus}{R}$. An initial synchronization method has also been given which is valid to the same order. Schwarzschild coordinates and concepts have been used throughout, since it was necessary to treat the problem general relativistically. The earth observer was easy to treat and will not be discussed here. The satellite orbit was more difficult to obtain, but given the orientation of the orbit and $\overline{E_S}$ and $\overline{L}$

or e and a one could determine it.

What about the parameters $\overline{E_S}$ and $\overline{L}$? They were called the Schwarzschild energy and angular momentum at spatial infinity, i.e. what a fixed Schwarzschild observer at spatial infinity would measure for these parameters. $\overline{E_S}$ and $\overline{L}$ are directly related to their Newtonian counterparts. $\overline{E_S}$ and $\overline{L}$ were also given in terms of the Schwarzschild semi–major axis, a, and the Schwarzschild eccentricity of the orbit, e. We can interpret these as a semi–major axis and an eccentricity again because in the limit $\frac{M_\odot}{R_S} \to 0$ they reduce to their Newtonian counterparts. This is fine for interpretation, but we here on the earth are not fixed observers at spatial infinity. What trouble does this cause us?

Let us simplify the discussion by considering equatorial elliptical orbits. Equation (24) gives the radial coordinate for a satellite in elliptical equatorial orbit in a Schwarzschild field to order $\frac{M_\odot}{R_S}$. The Newtonian approximation would be

$$R_S = (1 - e'^2) \left[1 + e' \cos(\phi_S)\right]^{-1} a' \tag{33}$$

Where e' is the regular eccentricity of the orbit and a' is the semi–major axis of the orbit measured in the usual way. Notice that the Schwarzschild and Newtonian expressions differ by a factor in the cosine term. This is the famous precession term and causes the perihelion of the orbit to shift or precess over time (as with Mercury). This term will not be a problem to interpret. The precession is measured by observing the change in angular coordinates relative to the fixed stars at spatial infinity – our Schwarzschild observer. Thus our earth observer and our Schwarzschild observer can be easily related. Otherwise (33) looks similar, as it should, since it was written this way to show that in the limit as $\frac{M_\odot}{R_S} \to 0$ the parameters e and a can be interpreted as their Newtonian counterparts e' and a'. Rewriting (24) to bring out the differences between Einstein's and Newton's theories[3] we get:

$$R_S = A\left[(1 + \epsilon) + C_1 \cdot \overline{e} \cos(\phi_S + \epsilon \cdot C_2) + \overline{e}\left(C_3 \cdot 2\cos(\phi_S) + C_4 \cdot \overline{e}\right)\epsilon\right]^{-1}. \tag{34}$$

ϵ is a parameter of order $\frac{M_\odot}{R_S}$. C_1, C_2, C_3 and C_4 are constants. A is a constant related to the semi–major axis and $\overline{e}$ a constant related to the eccentricity. One

can see that the precession effect is of order $\frac{M_\otimes}{R_S}$. It is not, however, the only term of order $\frac{M_\otimes}{R_S}$. Even if the orbit were circular, the term $(1 + \epsilon)$ would shift the orbit by a factor of $\frac{M_\otimes}{R_S}$ from the Newtonian one. The orbit would still be a circle, but would be off by the ϵ factor. In the elliptical case, besides the precession, we see a $\cos(2\phi_S)$ wobble in the orbit and constant shift of the orbit by the $\overline{e}^2$ term.

How much difference does this make when we measure e and a or try to synchronize? In our conventional way of measuring, we use Special Relativity. We then interpret our results in a Newtonian way. We are off by a factor of $\frac{M_\otimes}{R_S}$. How does this effect the time of travel of the light ray? We just introduce several errors of order $\frac{M_\otimes}{R_S}$. Can we ignore these errors?

Let us look back at our synchronization procedure. Assume the clocks start out synchronized, with no errors in e, a, initial time T_i, or final time T_f. Looking at (18) and (19) we know that the rates of the clocks for the earth observer and the satellites will vary. Even if they start out synchronized, they will not stay that way. Having the formulas, with no errors, we could just resynchronize a satellite clock relative to the earth observer clock by knowing how much the two clocks had shifted from each other. Now let us assume some error and look at what effect these errors in e and a might have.

Take the circular case for simplicity. Proper time and Schwarzschild time are then related by

$$\tau_S = \int_{T_i}^{T_f} \frac{(1 - 2\frac{M_\otimes}{R_S})}{\overline{E_S}} dt. \tag{35}$$

T_i and T_f are the initial and final times when one last synchronized and when one is about to resynchronize, respectively. R_S and $\overline{E_S}$ are now constants, but these constants have errors in them. How much? If we treat R_S as Newtonian then we have an error of $\frac{M_\otimes}{R_S}$ in its value. How much error does this create for $(1 - 2\frac{M_\otimes}{R_S})$? Assuming no error in $M_\otimes$, for simplicity, we get, to the lowest order,

$$\delta\left(1 - 2\frac{M_\otimes}{R_S}\right) = \left(2\frac{M_\otimes}{R_S}\right)\left(\frac{\delta R_S}{R_S}\right). \tag{36}$$

This error is of order $(\frac{M_\oplus}{R_S})^2$. Looking back to (20), we see that a similar result holds for $\overline{E_S}$. Let

$$\alpha = \frac{(1 - 2\frac{M_\oplus}{R_S})}{\overline{E_S}} \qquad (37)$$

$$\tau_S = t(\alpha + \delta\alpha). \qquad (38)$$

Though $t = (T_f - T_i)$ can get large, $\delta\alpha t$ will not get very large. Note, however, that if we ignored the $2\frac{M_\oplus}{R_S}$ factor entirely in α we could end up with a very large error.

This is not the only error that occurs from treating our measurement procedure Special Relativistically. The time of travel of the signal carrying the resynchronization time shift to the satellite will be off. This has two effects. First, we will add the wrong amount of time to the resynchronization shift we send to our satellite clock. Second, we will have used the wrong values for the initial time T_i and final time T_f used in the integral to determine the amount of the resynchronization shift we are sending. The amount of resynchronization shift error for the circular case would make (38) look like

$$\tau_S = (t + \delta t)(\alpha + \delta\alpha) \qquad (39)$$

where δt is the error in time, of order $\frac{M_\oplus}{R_S}$, due to our mismeasurement of T_i and T_f. (Here $t \sim \frac{R_S}{c}$ and since R_S is off by $\frac{M_\oplus}{R_S}$ so is t.) $\delta t \delta \alpha$ is of order $(\frac{M_\oplus}{R_S})^3$ and can be ignored. $\alpha \delta t$ is of order $(\frac{M_\oplus}{R_S})$ and technically should be kept.

VIII. RECOMMENDATIONS.

The general relativistic analysis of the Doppler shift, the rates of clocks and the global synchronization problems in the Schwarzschild field to order $\frac{M_\oplus}{R}$ and v^2 leads us to the following recommendations and conclusions:

(1) the formula for the Doppler shift and rates of clocks has been determined for arbitrary fixed earth observer and elliptical, equatorial satellite orbit. The more general formulas are only a matter of inversion and rotation and do not effect the physics discussed in this report;

(2) for the Schwarzschild model of the earth's gravitational field, more than one global synchronization scheme can be suggested. The synchronization scheme of Sect. IV is much simpler than the one based on the Doppler shift, Sect. III. This simplicity is achieved by maximal use of the Schwarzschild metric symmetries and by eliminating the terms in the Doppler shift caused by time delay;

(3) general orbits and earth observers do not change the synchronization scheme, just make the formulas more complicated;

(4) General Relativity should be used in the formula for clock rates since the error resulting from not doing so accumulates with time and can be very large;

(5) mismeasurement of the orbital parameters, i.e. R_S, e, a, etc., by using special relativity to compute the shape of the orbit can also accumulate with time, but are of the next higher order. There is a small error in the initial and final synchronization times of relevant order, but this does not accumulate;

(6) Using Newtonian parameters in the General Relativistic synchronization scheme is valid to order $\frac{M_\oplus}{R}$. This means that using the Newtonian formula for elliptical orbits with time of travel, velocities and energies measured using Special Relativity will work for the time being[4].

a. It is recommended that a proper general relativistic propagation of a null signal be considered. This is used in the (re)synchronization process, the measurement of parameters, as well as space–time ranging. This will allow us to estimate the errors caused by this procedure and, if necessary, modify the procedure[5].

b. It is recommended that resynchronization occur fairly often, say once or twice a year[5], and before doing so that the orbital parameters be remeasured. This will bring the system back to within $\frac{M_\oplus}{R}$ error each time and inhibit the accumulation of error with time.

REFERENCES.

1. C. W. Misner, K. S. Thorne, J. A. Wheeler: "Gravitation", W. H. Freeman and Co., San Francisco, 1971.

2. J. L. Synge: "Relativity: The General Theory", North–Holland Publishing Co., Amsterdam, 1966.

3. R. Adler, M. Bazin, M. Schiffer: "Introduction to General Relativity", McGraw–Hill Book Co., N.Y., 1975.

4. L. R. Gibson: "A Derivation of Relativistic Effects in Satellite Tracking", Report NSWC TR 83–55, April, 1983.

5. A. Kheyfets: "Relativistic Effects in GPS Time Transfer", Report 1989 USAF-UES Research Initiation Program, to be published.
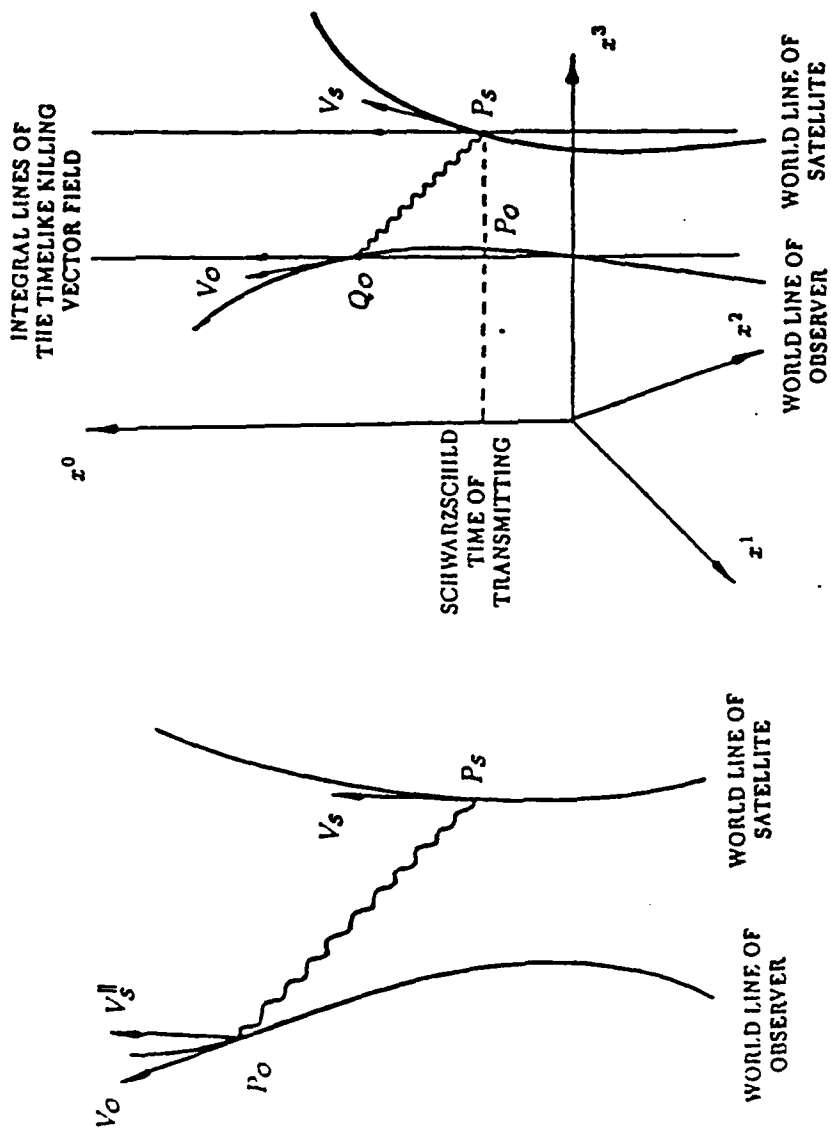
Fig. 1. Geometry of the Doppler shift. Vector $V_s^{\parallel}$ is the result of parallel transport of V_s along the null geodesic $P_s P_o$. Doppler shift is caused by $V_o \neq V_s^{\parallel}$.

Fig. 2. The Doppler shift and its main contributing factors as viewed by observers resting with respect to Schwarzschild coordinates.
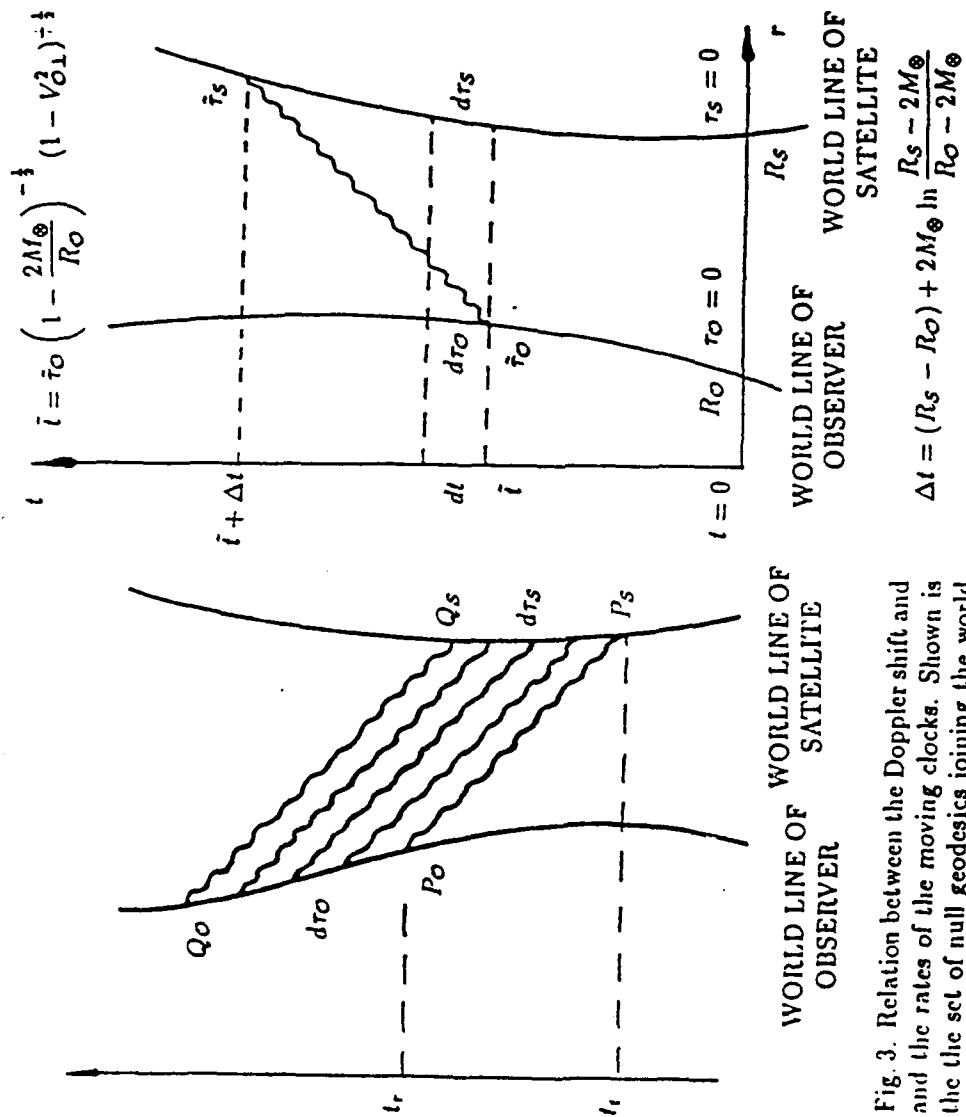
$$\tilde{t} = \tilde{\tau}_O\left(1 - \frac{2M_\oplus}{R_O}\right)^{-\frac{1}{2}}(1 - V_{O\perp}^2)^{\pm\frac{1}{2}}$$

WORLD LINE OF SATELLITE

WORLD LINE OF OBSERVER

$\tilde{\tau}_S$

dr_S

$r_S = 0$

R_S

R_O $r_O = 0$

dr_O

$\tilde{\tau}_O$

r

t

$\tilde{t} + \Delta t$

dt

$\tilde{t}$

$t = 0$

$$\Delta t = (R_S - R_O) + 2M_\oplus \ln \frac{R_S - 2M_\oplus}{R_O - 2M_\oplus}$$

Fig. 4. Relation between the satellite and the observer clock rates in a Schwarzschild simultaneity band and initial clock syncronization procedure.

WORLD LINE OF SATELLITE

WORLD LINE OF OBSERVER

Q_S

$d\tau_S$

P_S

Q_O

dr_O

P_O

t_r

t_i

Fig. 3. Relation between the Doppler shift and and the rates of the moving clocks. Shown is the the set of null geodesics joining the world lines of the satellite and the observer. Each geodesic represents a wave crest. If there are n such crests and $d\tau_S$, $d\tau_O$ are the clock-measures of P_SQ_S and P_OQ_O respectively, then $n = \nu_S d\tau_S = \nu_O d\tau_O$.

1989 USAF-UES SUMMER FACULTY RESEARCH PROGRAM/

GRADUATE STUDENT RESEARCH PROGRAM

Sponsored by the

AIR FORCE OFFICE OF SCIENTIFIC RESEARCH

Conducted by the

Universal Energy Systems, Inc.

FINAL REPORT

PRELIMINARY GUIDELINES ON TUNABLE DIODE LASER USE

Prepared by: Mary Jane Nickels

Academic Rank: Graduate Student

Department and   Chemistry department

  University: University of New Mexico

Research Location: Weapons Laboratory, Kirtland AFB, ARDJ

USAF Researcher: Dr. E. Dorko

Date: August 31, 1989

Contract No: F49620-88-C-0053

PRELIMINARY GUIDELINES ON TUNABLE DIODE LASER USE

By

Mary Jane Nickels

ABSTRACT

Tunable diode lasers are state-of-the-art technology. This final report encompasses the progress made in getting this instrument operational and guidelines for operating this instrument.

Acknowledgements

I wish to thank the Air Force Systems Command and the Air Force Office of Scientific Research for sponsorship of this research. Universal Energy systems must be mentioned for their concern and help to me in all administrative and directional aspects of this program.

I would also like to sincerely thank Dr. Ernest Dorko, Dr. Mike McAuliffe, Lt. Ralph Tate and Dr. Ed Walters for their support encouragement, and guidance.

I. Introduction

This summer I had the opportunity to work with a tunable diode laser (TDL). A TDL can be tuned over a range of 2-40 um. The TDL output can be pulsed, modulated, cw, or computer controlled. This system contained four diode lasers each with a spectral range of 30 cm^{-1} and with multimode power of 1 mW. The general set-up consisted of two cold-heads; one for the laser cavity, one for the detector cavity containing three IR detectors, Helium compressor- refrigerator system, mode selection monochrometer assembly, transfer optics assembly, etalon and electronics to support these systems.

II. Chronological Summer Progress

It was apparent when I began working with the TDL there was a problem. The detected signal was 1st derivative-like, and not square wave (as it should have been). The detector cavity was disassembled to see if there was anything that could be remedied at the site. The problem was discovered in the cold-head electrical connections. The process of cooling down and warming up the cold-head had caused the enamel on the electrical connections to chip off causing them to short-out. The assembly was returned to the manufacturer (Laser Photonics, Inc.) for repair. The connections were replaced and the detector/cold-head assembly was returned. After the assembly was installed in the TDL, it was apparent there was still a problem. The detector assembly was unable to cool down to the optimum operating temperature of 14-18K, but only cooled down to 22K. It was now possible to detect the signal, but the strength of the signal was diminished. This problem was attributed to the helium compressor-refrigerator system. The helium compressor has surpassed 30,000 hours of use, and was due to be rebuilt. Because of this, it

was unable to adequately cool down both cold-heads. This required the purchase of an additional helium compressor, one for each cold-head. During this time I was able to operate the TDL and learn the mechanics of operating the instrument. I was able to get an absorption spectrum of ammonia. (FIG. 1) This spectrum correlated exactly with an ammonia spectrum collected by Dr. Dolson using the TDL. Absorption peak assignments were made from his work. Following this, I attempted to get the rest of the instrument operational, specifically, the etalon. The etalon is used to generate the calibration fringes necessary to make accurate wavenumber assignments. The etalon was aligned (using the factory alignment slits) and I was unable to detect HeNe or IR fringes through the etalon. It was thought this was caused by improper alignment of the transfer assembly optics. I proceeded to make accurate templates for each type of mirror. The HeNe alignment beam was then centered on each of these mirrors. The etalon was then aligned in the path of the HeNe and still there were no fringes produced. The etalon was disassembled and the problem was discovered. The scanner plate was 90 degrees out of alignment. This can occur when the scanner plate driver is kept in an extreme position. This problem was easily corrected but other problems occured (which will be treated later on in this report). The etalon will now generate IR and HeNe fringes with the "right alignment". The factory alignment slits will not be useable until re-alignment is accomplished (see below). The details of the experiment will be expounded upon in the following sections.

III. Operating the TDL

Included in this report is the general outline on how to get the

the range of interest and turning on the heater. The heater warms up slow enough to observe the effects on the oscilloscope. To detect the laser output intensity, chop the signal using the mechanical chopper, and connect the output of the detector pre-amp to the scope input. The chopper is the reference. Adjustments to maximize this signal are made by adjusting the parabolic mirror and the focusing mirror in front of the detector. The transfer optics should already be aligned, but the IR beam diverges from the path of the HeNe used to align the optics.

A. Connections

The proper connections of the diode laser electronic components are as follows: (See fig. 2.2- 3 Channel Collect program reference manual, ignore all other diagrams involving these connections).

To observe absorptions on oscilloscope:

Reference LCM- from lock-in amplifier (LIA) J12 to J7 reference (LCM)

External trigger from oscilloscope to reference out (LCM)

AC output (LIA) J7 to oscilloscope

LIA J11 to DC output from computer BNC board

BNC board DAC 2 to external in J6 (LCM)

Modulation on positive sawtooth modulation, mechanical chopper off

Connect detector pre-amp output to J10 (LIA)

J8 (LIA) Reference connect to oscilloscope, displays locked signal

Signal J7 (LIA) AC output to oscilloscope, displays modulated signal and absorptions on scope.

To collect data:

The key is that the LCM (J7) be disconnected and connected to the mechanical chopper. To collect data using the 3 Channel Collect program the signal must be referenced from the mechanical chopper.

The modulation should now be turned off. Deflection of the LIA sensitivity must be maximized, but not topped out. Absorptions can be seen by deflection toward the center of the sensitivity scale, or by a decrease in the strength of the chopped signal on the oscilloscope, when turning the fine current control of the LCM. The range of this control is approximately 200 ma.

When using computer controlled scanning to collect data, be aware that when accessing the system the current values change. Note the current reading before accessing the program so you can return it to its previous value. This is where you had observed absorptions on the oscilloscope. Since the signal is being chopped you are no longer able to observe them on the oscilloscope. When using the 3 Channel Collect program it is important to input the command "Spint".
This command has been written into the autoexec.bat routine, but the user should be aware of its importance. If it is not inputted, the program will not collect data. The commands necessary to use this program are very straightforward. Experimentation of the input values will lead to the best spectrum plot. To access any of the various parameter tables, simply input the parameter of interest, then re-input the command with the appropriate value. The data sensitivity value is read directly from the LIA setting.

I would assume that the electronic connections for the reference spectrum are identical to those of the sample spectrum electronics. The etalon electronic connections are more involved.

B. Alignment

Align the transfer optics with the HeNe beam using the templates. The HeNe beam should be centered on each mirror with a deviation of 1-2 mm. Since the instrument housing vibrates,(due to

the motion of the cold-head) alignment must be performed daily. After aligning the optics, check and tighten each of the bases. Horizontal alignment will loosen the bases. Alignment is best accomplished in consecutive order of beam path. Centering the beam on the second turning mirror is sometimes impossible, but centering the beam on the next mirror is easily done.

C. Etalon

The etalon is used to generate a fringe pattern that is used for accurate wavenumber calculation of unknown sample absorption peaks. IR and HeNe fringe patterns can be generated using the etalon. Use only the revised etalon manual. The frequency stabilized (f.s) HeNe is used to generate HeNe fringes. The HeNe (f.s) beam must be co-aligned with the alignment HeNe beam after the pellicle splitter to the path through the etalon. Co-alignment throughout the instrument is not possible due to the different angles of incidence of the two HeNe beams. Adjustments after the beams are co-aligned, to align the beams through the etalon, are made using the horizontal and vertical adjustment knobs on the beam splitter. The etalon is under a pressure of one torr of dry nitrogen. The pellicle beam splitter within the etalon is very hygroscopic. In correcting the scanner plate orientation problem (earlier described) the pellicle beam splitter became very wrinkled due to the uptake of water when the etalon was opened. The repercussions of this are that the factory alignment slits are no longer useful. A portion of the pellicle beam splitter not damaged must be used. The correct positioning of the etalon is determined by maximizing the fringe signal detected and viewed on the oscilloscope. To monitor the contrast of the HeNe fringes the correct back reflection from the etalon must be directed

back to the visible photodiode detector. This is no easy task. (Reference p.10 etalon manual) Determining which reflected beam to direct to the photodiode detector is difficult. The two strongest back reflections are parasite window reflections. The correct beam is modulated and does not move when turning the zero knob of the scanner driver. Currently, the etalon will produce IR and HeNe fringe patterns. The windows to the etalon are constantly heated to prevent fogging. If the etalon is moved, this should be taken into consideration. The etalon will be sent to Laser Photonics, Inc. to have the pellicle beam splitter replaced and have the scanner plate accurately aligned.
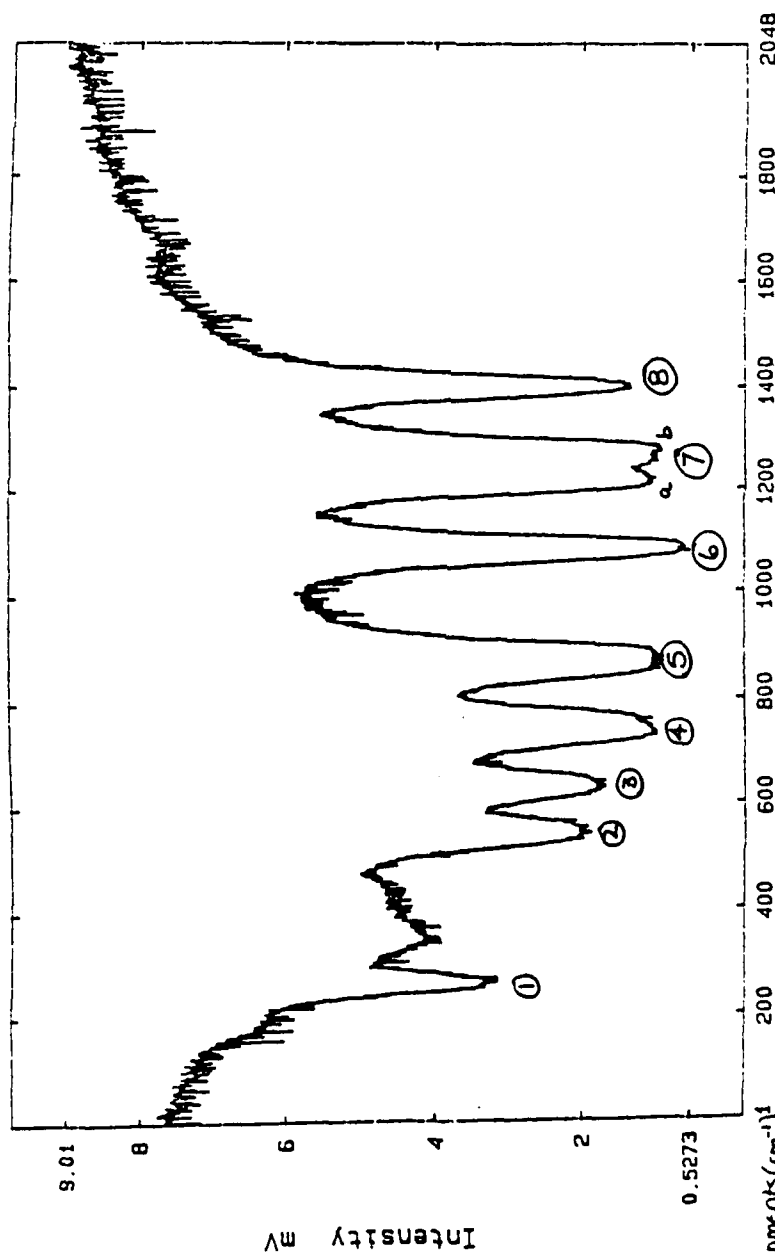
D. Miscellaneous Information

The scanner driver takes four hours to stabilize. It is recommended that this be left on at all times. The scanner driver contains two fuses; one external, one internal. The KRS-5 window to detector 3 needs to be replaced. It is cloudy and may be interfering with signal detection. KRS-5 windows are poisonous and care should be taken not to touch them. Pellicle beam splitters are extremely fragile and care should be exercised with them, also. The electronic connections to the etalon are believed correct, but have never been tested. A string level aids in horizontally aligning the etalon. The etalon should be centered within its cavity. The center has been marked on the housing and etalon. The TDL is currently set-up to collect sample and reference spectrums as well as etalon fringe patterns.

IV. Recommendations

My experience with the TDL will definitely benefit my future research since I will be working with a diode laser.. The information within this final report precedes the information available in John E. McCords (1988 UES Summer fellow) final report. It is recommended that those interested access Mr. McCords report for information on collecting complete spectra use the TDL.

Thank-you.

Ammonia Spectrum (Fig.1)

Intensity mV

9.01
8
6
4
2
0.5273

200 400 600 800 1000 1200 1400 1600 1800 2048

assignments (cm⁻¹)
① 1122.05508
② 1122.09359
③ 1122.10392
④ 1122.11778
⑤ 1122.13310
⑥ 1122.15975

⑦ a - 1122.17719
   b - 1122.18766
⑧ 1122.20354

INDEX
20mA scan

Instrument
Conditions
T= 1.1087 V
I = 0.5657 Amps
Monochromator reading 5101

Ammonia Pressure
~ 100 mTorr

* The NH₃ reference lines are 5,6,7,8; p.169 Rao
①=5, ②,③,④,⑤,⑥= 6 ⑦a&b=7 ⑧=8

H.J.NICKELS 7/25/89

OPERATION OF DIODE LASER SP5800

1. Make sure the lasers are cooled down as per instructions for replacement, evacuation, and cool down.

2. Turn on power switch to SP 5720 CTS (Cryogenic Temperature Stabilizer). Check temperature of cold head and lasers.

3. Make sure heater switch on SP5720 is off.

4. Initial control settings on SP 5820 LCM (Laser Control Module):

    Power: off
    Current control: Completely counterclockwise
    Limiting Current: Set to specs for laser to be used
    Polarity Switch: Set to pos or neg according to specs for laser to be used (VERY CRITICAL)
    Modulation: off
    Laser Power: off
    Sweep: off

5. Set temperature with set point button and coarse and fine controls on the SP5720 CTS to the temperature spec for the laser that is being used.

6. Turn on the heater switch and wait until the temperature stablizes at the set temperature.

7. Turn power on to SP5820 LCM (POWER SWITCH)

8. Turn laser on (LASER ON BUTTON)

9. Set current on laser to specs. Use coarse and fine controlls and observe current on the laser ampers readout (NOTE: THE COARSE CONTROL AND THE LIMIT CONTROL READ ONE HALF THE ACTUAL CURRENT)

10. Once all readings are stable then the laser beam can be alligned into the detectors for maximum output.

    a. Turn on power switch and chopper switch on front of optics cavity of laser, turn on detectors (NOTE; MAKE SURE DETECTORS ARE COOLED IF NECESSARY WITH LIQUID NITROGEN), and connect signal from back of optics cavity to trigger scope (for test purposes). Connect output from detector amplifier to input signal port of scope (for test purposes).

    b. If beam strongly out of allignment, then turn on HeNe laser beam and allign parabolic mirror in front of diodes and if necessary allign the optics from diodes into detecctor. Use scope signal to maximize power output.

    c. Turn HeNe off and maximize scope signal from the diode by adjustments of the parabaloic mirror (NOTE: MAKE SURE MIRROR DIRECTLY IN FRONT OF LASER BEING USED). Hint: Move horizontal adjustment a notch and attempt adjustment with vertical and translation. Continue making small incremental changes until signal maximized (NOTE: MAKE INITIAL TRAVERSE OF MIRROR MANUALLY TO OBSERVE ROUGH LOCATION OF SIGNAL)

11. Remove shorting mirrors from beam path and set grating drum adjustment to correspond to the rated frequency for the laser. Maximize power out from the beam at this frequency by small adjustments of the grating and by use of the parabolic mirror adjustments.

12. THE LASER IS READY TO BE USED ON AN EXPERIMENT

13. To shut down:

    a. Turn amperage to laser down to zero (Counterclockwise on coarse control)

    b. Turn laser off (LASER OFF BUTTON)

    c. Shut 5820 LCM power switch off.

    d. Shut heater switch on SP5720 CTS off

    e. Observe temperature drop to lowest temperature of refrigerator.

    f. Shut off chopper and power switch on optics cavity of laser

    g. Place laser in observation mode until ready to use again. Continue to monitor temperature, pressure, operation time, etc